PRESSURE DEPENDENT MAGNETIC INVESTIGATION OF TETRACYANOETHYLENE-BASED MOLECULE-BASED MAGNETS AND THEIR ANALOGUES

by

Jack Guy DaSilva

A dissertation submitted to the faculty of
The University of Utah
in partial fulfillment of the requirements for the degree of

Doctor of Philosophy

Department of Chemistry

University of Utah

August 2013

The University of Utah Graduate School

STATEMENT OF DISSERTATION APPROVAL

The dissertation of **Jack Guy DaSilva**

has been approved by the following supervisory committee members:

Joel S. Miller	, Chair	**4/18/2013** Date Approved
Peter B. Armentrout	, Member	**4/18/2013** Date Approved
John C. Conboy	, Member	**4/18/2013** Date Approved
Valeria Molinero	, Member	**4/18/2013** Date Approved
Mike Scarpulla	, Member	**4/18/2013** Date Approved

and by **Henry S. White**, Chair of the Department of **Chemistry**

and by Donna M. White, Interim Dean of The Graduate School.

ABSTRACT

Several metal-tetracyanoethylene (TCNE) compounds, including the [bis(pentamethylcyclopentadienyl)iron(III)]$^{+}$[tetracyanoethylene]$^{-}$, [FeCp*$_2$][TCNE], family of molecule-based magnets and two cyanide based MBMs were investigated by pressure dependent DC magnetic measurements. The 0-D electron transfer salts: [FeCp*$_2$][TCNE], ferromagnetic [FeCp*$_2$][TCNQ] (TCNQ = 7,7,8,8-tetracyanoquinodimethane), metamagnetic [FeCp*$_2$][TCNQ], [FeCp*$_2$][HCBD] (HCBD = hexacyanobutadiene), and [FeCp*$_2$][DDQ] (DDQ = 2,3-dichloro-5,6-dicyano-*p*-benzoquinone) exhibited an array of magnetic behavior both at ambient and applied pressure. [FeCp*$_2$][TCNE] and [FeCp*$_2$][HCBD] exhibited weak ferromagnetism above 4.2 and 3.1 kbar, respectively. The ferromagnetic polymorph of [FeCp*$_2$][TCNQ] displayed linear increase to the critical temperature, T_c, and the bifurcation temperature, T_b, reaching 5.01 and 5.46 K, respectively at 10.3 kbar. The coercive field, H_{cr}, displayed exponential-like increase, reaching 550 Oe at 10.3 kbar. The metamagnetic polymorph of [FeCp*$_2$][TCNQ] displayed linear increase of the T_c at low applied pressure, reaching 2.90 at 2.9 kbar, then transitioned to a paramagnetic state at further applied pressure. [FeCp*$_2$][HCBD] transitioned from a paramagnetic state at ambient pressure to a weak ferromagnetic state at 3.1 kbar with a T_c, H_{cr}, and H_c of 2.46 K, 25 Oe, and 2,200 Oe, respectively. The T_c and H_c then increased linearly

with further applied pressure to 4.80 K and 10,000 Oe, while the H_{cr} increased exponentially to 795 Oe, at 11.4 kbar. [$FeCp^*_2$][DDQ] exhibited paramagnetic behavior at ambient and applied pressures up to 9.2 kbar. The structurally related 2-D $Mn^{II}(TCNE)I(H_2O)$ and 3-D $Mn^{II}(TCNE)_{3/2}(I_3)_{1/2}$, showed significant increases to the T_c, T_b, and H_{cr} with applied pressure. A high- and low-pressure regions were observed for $Mn^{II}(TCNE)I(H_2O)$. 2-D $[Ru_2(O_2CBu^t)_4][M(CN)_6]\bullet H_2O$ (M = Fe, Cr) displayed suppression of hysteretic properties at high applied pressure and irreversibility of the suppression. A Mean Field (MF) analysis of three structurally related non-cubic Prussian blue analogues (PBA) was performed to assess the intensity of their coupling modes. These values were framed by the reinvestigation of several known cubic PBAs and comparing the coupling intensities, as well as evaluating the MF theory in the context of these structures as several had been evaluated by other means.

TABLE OF CONTENTS

LIST OF TABLES

LIST OF FIGURES

LIST OF SYMBOLS AND ABBREVIATIONS

LED	light emitting diode
OLED	organic light emitting diode
MBM	molecule-based magnet
3-D	three-dimensional
1-D	one-dimensional
2-D	two-dimensional
0-D	zero-dimensional
T_c	critical temperature
H_{cr}	coercive field
PBA	Prussian blue analogue
TCNE	tetracyanoethylene
M	magnetization
E	molar energy
H	applied field
n	principle quantum number
μ_n	microscopic magnetization
N_A	Avogadro's number
k_B	Boltzmann's constant
χ	molar magnetic susceptibility

T	temperature
C	Curie constant
g_e	Landé g-factor
S	total spin
θ	Weiss constant
H_c	critical field
CAF	canted antiferromagnetic state
i	spin bearing moiety index number
j	spin bearing moiety index number
J	magnetic coupling energy
D_{ij}	Dzyaloshinski-Moriya canting energy
z	number of nearest spin bearing neighbors
T_N	Néel temperature
RKKY	Ruderman-Kittel-Kasuya-Yosida
MF	Mean Field
M_{ZFC}	zero-field cooled magnetization
M_{FC}	field cooled magnetization
M_r	remnant magnetization
Oe	Oersted
T_b	bifurcation temperature
B	Brillouin function
M_s	saturation magnetization
ω	magnetic field oscillation frequency

AC	alternating current
DC	direct current
χ'	in-phase AC susceptibility
χ''	out-of-phase AC susceptibility
φ	phase shift
Cp*	pentamethylcyclopentadiene
E_A	electron affinity
TCNQ	7,7,8,8-tetracyanoquinodimethane
DDQ	2,3-dichloro-5,6-dicyano-p-benzoquinone
$TCNQF_4$	2,3,5,6-tetrafluoro-7,7,8,8-tetracyanoquinodimethane
HCBD	hexacyanobutadiene
emu	electromagnetic unit
mol	mole
K	Kelvin
MM	metamagnetic
FO	ferromagnetic
C_p	specific heat
IR	infrared
cm^{-1}	wave number
QD	Quantum Design
PPMS	Physical Property Measurement System
SQUID	Superconducting Quantum Interference Device

MPMS	Magnetic Property Measurement System
T	Tesla
DCNQ	2,3-dicyano-1,4-naphthoquinone
mg	milligram
T_{sc}	superconducting critical temperature
x	digital sensor readout
P	pressure
2σ	standard deviation
χ^2	variance
hfac	hexafluoroacetyacetonate
BBA	1,3-bis-*N*-*t*-butylaminoxyl
OBM	organic-based magnet
THF	tetrahydrofuran
Hz	frequency
ND	neutron diffraction
T_1	metamagnetic-like peak temperature
ϕ	frequency shift of T_f
Bu^t	*tert*-butyl
T_f	freezing temperature
TPP	tetraphenylporphyrin
DCNQI	dimethyl-*N*,*N*'-dicyanoquinonediiminide
NCMe	acetonitrile

eV	electron volt
OEP	octaethylporphyrin
Å	Ångström
SOMO	singly occupied molecular orbital
Me	methyl
fcc	face centered cubic
HS	high-spin
LS	low-spin
FI	ferrimagnetic
AF	antiferromagnetic
S_M	total spin of M
$S_{M'}$	total spin of M'
D	anisotropy
K	interlayer coupling
$M1$	average spin on Mn^{HS}
$M2$	average spin on Mn^{LS}
H_{eff}	effective field
$\hat{H}$	effective Hamiltonian
PXRD	powder X-ray diffraction

ACKNOWLEDGMENTS

At the pinnacle of my graduate career two contradictory phrases come to mind: the first from John Donne, "No man is an island, entire of itself." and the second from John L. Parker Jr., "That's why I'm going to let you do them by yourself, just the way people do everything that's important." I reconcile the truth of both these statements by recognizing those who assisted me during this educational process and through the understanding that it was still I who performed the tasks described herein.

Ironically, perhaps the most important entities to thank are the state of Utah and the close friends I found within it. My sanity and drive were maintained through the unparalleled access to the outdoors I experienced in Salt Lake City and those I enjoyed it with: Jorge de Freitas, Tim Lane, Alaric Champine, Brian Michaels, Travis Haussener and Jason Boyle.

My next great escape came from my family, for always welcoming me home or anywhere else with open arms. Thank you Mom, Papa, and Kurt.

Academically, I was supported and instructed by every member of the Miller Research Group: Dr. Amber C. McConnell, Dr. Chris Kareis, Dr. Bretni Kennon, Dr. William W. Shum, Dr. Jordan L. Arthur, Dr. Endrit Shurdha, Mr. Preston, Ms. Hoa-Lan Vo, Mr. Casey Hawkins, Josh Sussman, Andrew Simonson, Royce A. Davidson, Adora Baldwin, and the late Mr. Josh D. Bell. Additionally Dr. Ryan Steele was of special assistance in understanding the proposal, which I selected. During the rush of first-year classes so long ago now I helped and was in turn aided by Dave Bell, Brandon McMann, and especially Jessica Johnston.

Last, thank you to the University of Utah for providing me with an opportunity to pursue a doctoral degree in their Chemistry department, to my committee members for the time counseling they have offered, and the Department of Energy (Grant No. DE-FG0293ER45504).

CHAPTER 1

MAGNETIC MATERIALS, INTRODUCTION TO MAGNETISM, AND ORGANIC ELECTRON ACCEPTORS

Magnetic Materials

Magnetic materials have numerous utilities and applications, such as, the compass and the iPhone, and have progressed human technologies from antiquity into the modern age. Currently magnets serve a pivotal role in the devices that humans rely upon: electrical transformation, [1] binary memory storage, [2] sound production, [3] microwave emission,[4] and transportation.[5] Magnets in use today are termed traditional and typically composed of metals or metal oxides. Much research of the past decades has centered about the discovery and manipulation of organic-based analogs of metallic and metalloid functional materials, such as light emitting diodes (LED), steel, aluminum, and magnets. The analogs of the former three materials have proven to be flexible in the case of organic light emitting diodes (OLED) and lightweight in the case of carbon fiber. A possible alternative to the aforementioned traditional magnets, and focus of this research, are molecule-based magnets (MBM) synthesized from discrete molecular building blocks.

MBMs contrast sharply with traditional magnets: traditional magnets require energetically intensive metallurgical processes for synthesis; form hard, brittle, 3-D network solids, but have greater magnetic density. MBMs can be synthesized at room temperature through solution chemistry and form extended network structures of 1-D,[6] 2-D,[7] and 3-D connectivity,[8] as well as electron transfer salts of 0-D connectivity.[9,10,11] This variety of magnetic and chemical architecture exemplifies the potential for synthetic tunability, as the connectivity is wholly dependent on the synthetic technique

or ligand choice.[12] The use of organic ligand subunits increases the degrees of freedom in the structure of MBMs giving rise to tunable magnetic characteristics: magnetization onset temperature or critical temperature (T_c),[13] magnetic hardness/softness or coercivity (H_{cr}),[14] optical transparency,[15] ferroelectricity,[16] magneto resistivity,[17] and photomagnetism.[18] MBMs harbor the potential to harness both of these advantages over traditional metal and metal oxide magnets. Currently the greatest challenge in organic-based magnetochemistry is achievement of room temperature T_c's, as most MBMs have a sub-room temperature T_c; two notable exceptions are a Prussian blue analogue (PBA) $KV^{II}[Cr^{III}(CN)_6]$ T_c = 376K[19] and $V(TCNE)_x$ T_c > 400K (TCNE = tetracyanoethenide).[13] Furthering our understanding of the magnetic properties and their dependencies in these systems will hopefully lead to the development of more prevalent and finely tuned MBMs.

Introduction to Magnetism

Magnetism is expressed as an energetic response to an applied magnetic field. A diamagnetic substance contains an even number of electrons, which are paired in their orbits about a given nucleus or nuclei. Paired electrons repel applied magnetic fields, resulting in lower magnetic flux in the region of a given substance. If a substance contains unpaired electrons, the unpaired electrons attract an applied magnetic field resulting in greater magnetic flux in the region of a given substance. It should be noted that the core electrons of paramagnetic substances are diamagnetic due to their paired ground state, but the repellent force of the paired core electrons is orders of magnitude less than the corresponding attraction resultant of a single unpaired electron yielding a net paramagnetic behavior.[20]

Curie-Weiss law. For the purpose of measurement, the change in magnetization resultant to an applied magnetic field is measured. This perturbation, when framed in by classical mechanics is the magnetization, M, and is written as

$$M = \frac{-dE}{dH}, \tag{1.1}$$

where M is the molar magnetization, E is the molar energy, and H is the applied field. E may be indexed by the principle quantum number, n, and termed E_n, which allows a quantum mechanical description of the microscopic magnetization, μ_n,[21] where eqn. (1.1) transforms to

$$\mu_n = \frac{-dE_n}{dH} . \tag{1.2}$$

Through application of the Boltzmann distribution law[21] the macroscopic magnetization can be described as the summation of a population-weighted average of the macroscopic magnetization for all n, yielding

$$M = \frac{N_A \sum_n \left(-\frac{\partial E_n}{\partial H}\right) e^{\left(-\frac{E_n}{k_B T}\right)}}{\sum_n e^{\left(-\frac{E_n}{k_B T}\right)}}, \tag{1.3}$$

where N_A is Avogadro's number and k_B is the Boltzmann constant. This allows determination of the molar magnetic susceptibility as

$$\chi = \frac{dM}{dH} .^{21} \tag{1.4}$$

A result of Pierre Curie's 1895 doctoral thesis was the finding that χ was inversely proportional to T,

$$\chi = \frac{C}{T} \tag{1.5}$$

and the proportionality constant was termed the Curie constant, C,[22a]

$$C = \frac{N_A g_e^2 \mu_B^2 S(S+1)}{3k_B}, \quad [20] \tag{1.6}$$

where g_e is the Landé g-factor, μ_B is , and S is total spin. Ideal paramagnets are composed of magnetically isolated spins (each spin is oriented independently of any neighboring spin), which are oriented randomly in a Boltzmann distribution due to thermal energy and follow Curie Law at all temperatures. More commonly short-range interactions exist between electrons causing a tendency to align relative to neighboring spins.

Curie-Weiss Law was introduced to account for this non-ideal behavior,

$$\chi = \frac{C}{T - \theta}, \tag{1.7}$$

where θ is the Weiss constant and its signs delineates the type of magnetic interaction in a given material.[20] These interactions are facilely represented through a plot of $\chi^{-1}(T)$ (Figure 1.1), where paramagnetic materials exhibit a linear temperature dependence and the temperature axis intercept is θ. A negative θ indicates antiparallel alignment of neighboring spins, termed antiferromagnetic, and a positive θ indicates parallel alignment, termed ferromagnetic. These alignments are limited to short ranges, tens or hundreds of neighboring spin loci.

Magnetic ordering. When short-range spin correlation becomes uniform or quasi-uniform throughout a magnetic domain a lowering of energy for the system is achieved through the establishment of long-range order and the material is said to magnetically order. The phenomenon of long-range magnetic order in a bulk material arises from the exchange term displayed in "bra" "ket" form (adapted from ref. 22b)

$$\langle a(1)b(2)|H_{12}|a(2)b(1)\rangle, \tag{1.8}$$

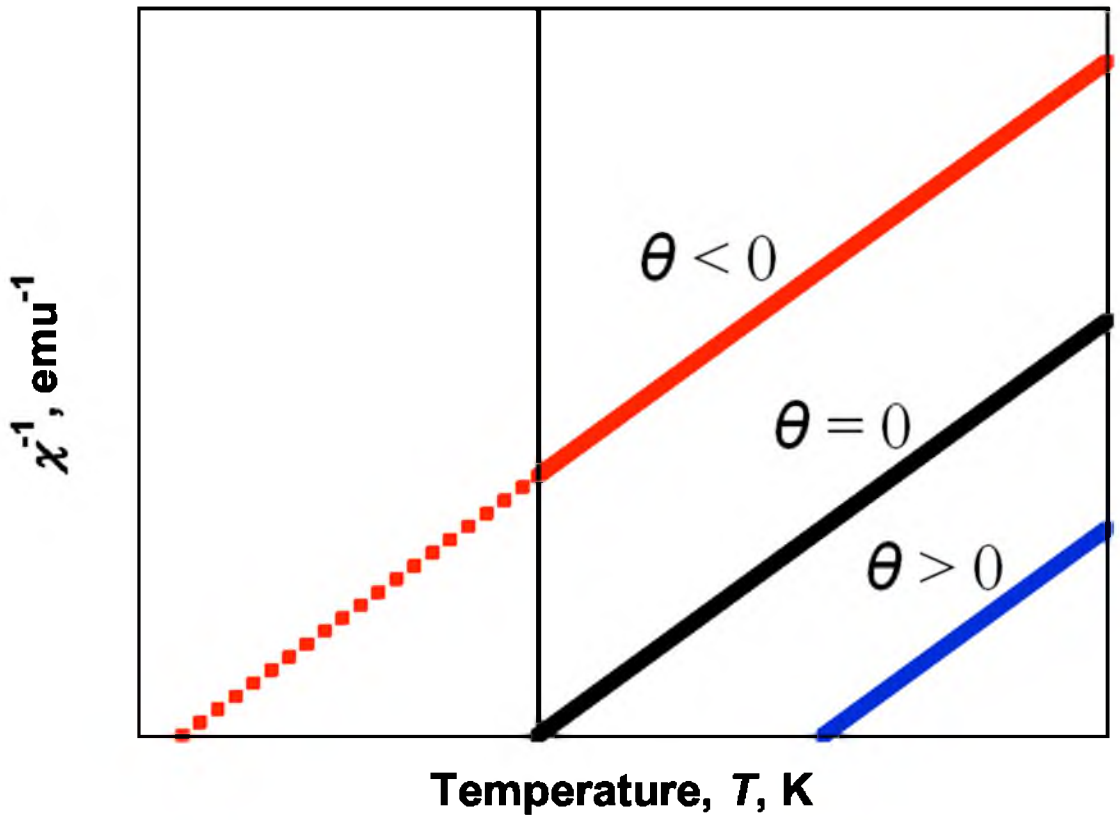

Figure 1.1. Idealized plot of $\chi^{-1}(T)$ diagraming the effect of spin coupling in paramagnets.

where *a* and *b* index orbitals, 1 and 2 index electrons occupying those orbitals and

$$H_{12} = \frac{e^2}{4\pi\varepsilon_0 r_{12}}. \tag{1.9}$$

The two previously described spin coupling modes, antiferromagnetic and ferromagnetic, lead to different magnetic ordering motifs. Some of the most often encountered motifs are (1) ferromagnetism, (2) antiferromagnetism, (3) ferrimagnetism, and (4) metamagnetism. Ferromagnetism arises from parallel alignment of spins, resulting in a spontaneous net magnetic moment at absolute zero. Antiferromagnetism by contrast arises from antiparallel alignment of spins, resulting in the net cancellation of individual magnetic moments and thus, zero magnetic moment at absolute zero for the bulk single crystals. Ferrimagnetism may be classified as a subset of antiferromagnetism arising from the coupling of inequivalent magnetic moments. These materials exhibit long-range antiparallel ordering of magnetic moments, yielding a spontaneous net magnetic moment at absolute zero. Metamagnetism is a result of the complex interaction of ferro- and antiferromagnetic coupling, resulting in a field dependent behavior; at low field metamagnets behave as antiferromagnets, while at fields above the critical field, H_c, ferromagnetic behavior is exhibited.[23] These types of magnetism, as well as several others, and their relation to one another are illustrated by Figure 1.2.[24]

Of special note in Figure 1.2 is canted antiferromagnetism, CAF, also termed weak ferromagnetism. CAF is believed to arise from spin-orbit coupling in crystal structures with appropriate symmetry.[25] While the normal exchange that arises from ferro- and antiferromagnetic coupling is described by the symmetric Heisenberg Hamiltonian,

$$H = -2\sum_{i \neq j} JS_iS_j, \tag{1.10}$$

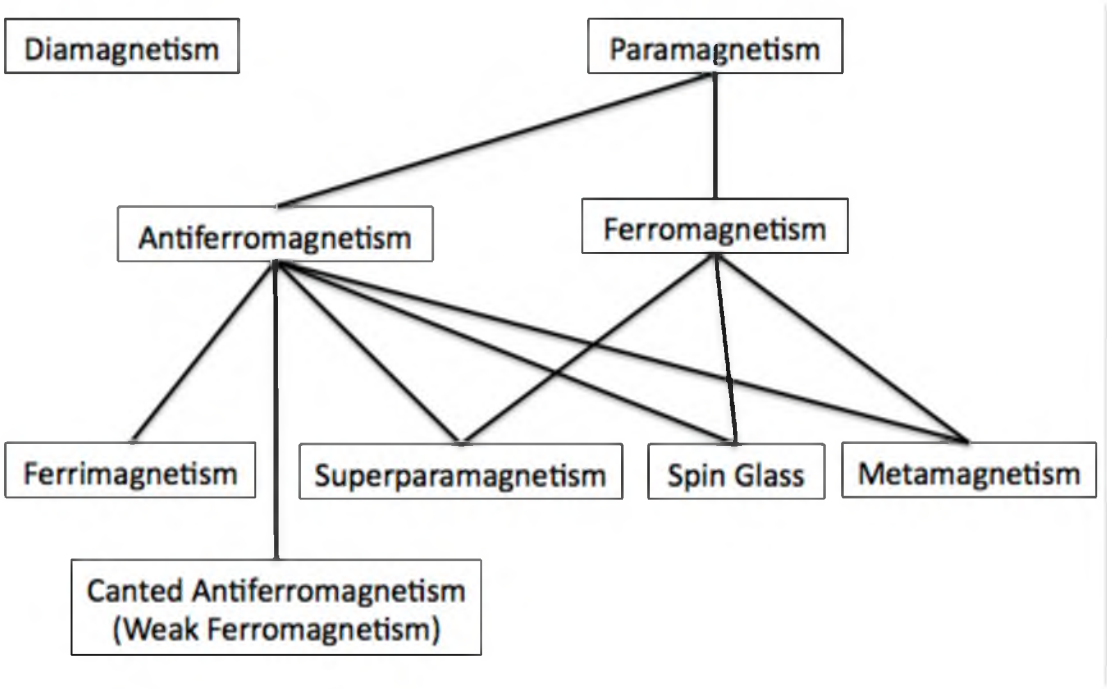

Figure 1.2. Schematic depiction of magnetic behavior (adapted from ref. 24).

where *i* and *j* are spin bearing moieties, *S* is the total spin, and *J* is the exchange energy. The Dzyaloshinski-Moriya Hamiltonian, H_{DM}, by contrast is antisymmetric and requires the absence of inversion symmetry between neighboring spin bearing moieties,

$$H_{DM} = D_{ij} \bullet \left[S_i \times S_j \right]. \tag{1.11}$$

In equation 1.11 D_{ij} is a constant proportional to (g-2)/g, such that the more anisotropic an ion the more canting will be exhibited by a complex.[25]

CAF has the effect of imparting some characteristics of ferromagnets onto an antiferromagnetic system. This is due to the nature of the interaction between neighboring spin sites derived from equation 1.11. The result of the cross product of two spin momenta that are aligned mostly or somewhat antiparallel is a net spin momentum directed orthogonal to the parent momenta, Figure 1.3. Much like ferrimagnetism, CAF derives its ferromagnetic-like behavior from this net spin momentum.

Magnetic behavior arises from the ordered orientation of electron spin momenta, and thereby is in opposition to temperature driven entropy. The magnetic coupling energy, *J*, is a constant value intrinsic to the structural and electronic characteristics of a given compound, while the thermal energy, $k_B T$, varies linearly with temperature. Thus, at low temperatures $J >> k_B T$ is common for a magnetic material and magnet order is achieved. Conversely, at significantly high temperatures $J << k_B T$ is true and the magnetic material is in its random paramagnetic state. A magnetic phase transition occurs at the critical temperature, T_c, where *J* is proportional to $k_B T$. This proportionality is illustrated by the Mean Field theory expression for T_c,

$$T_c = \frac{JzS(S+1)}{3k_B} \tag{1.12}$$

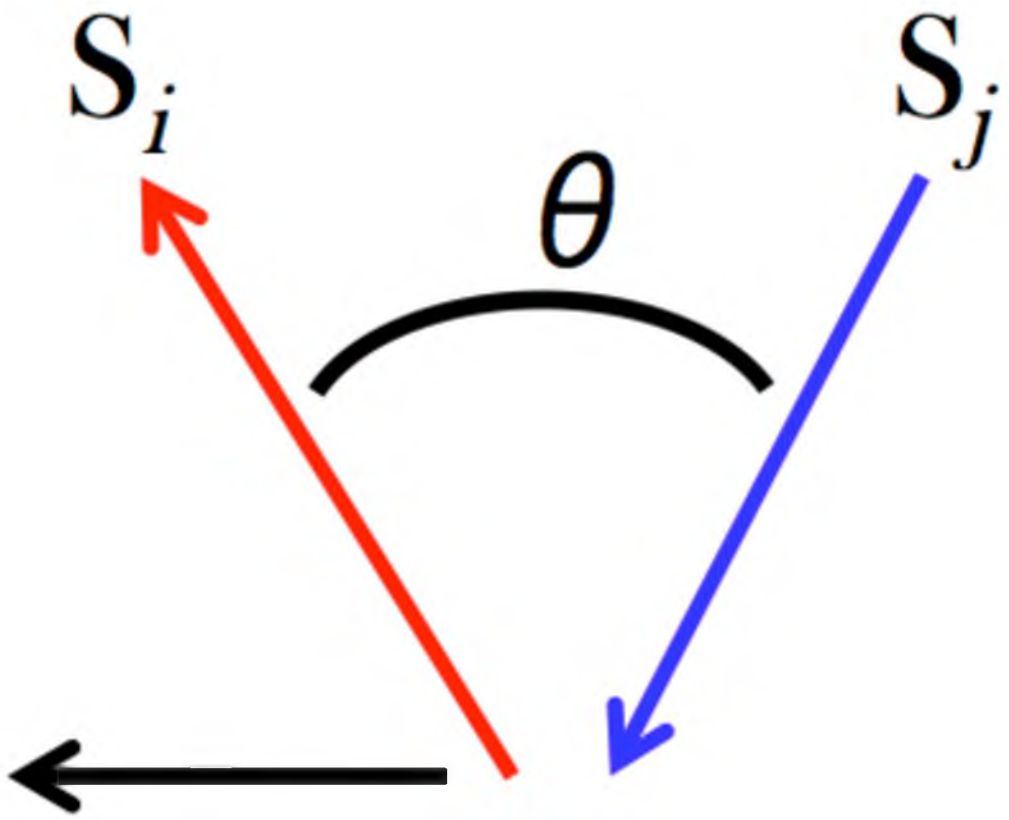

Figure 1.3. The canting angle, θ, between the spin momenta *i* and *j* is shown and a resulting orthogonal net spin momentum is depicted as the black arrow. The depicted orientation is restricted to the plane of the page, which is not true for some crystal structures.

where z is the number of nearest neighbor moieties containing a nonzero amount of spin momenta. The transition temperature may also be termed the Néel temperature, T_N, in the case of antiferromagnets and metamagnets.[22c]

A variety of interactions may lead to magnetic order. Exchange of the magnetic momenta is achieved through pathways that are dependent on the structural and electronic properties of a given material. Magnetic orbitals, defined as orbitals on a species containing unpaired electrons, which have significant overlap with one another allow their respective electrons to interact. This type of orbital interaction is strongest and termed a direct exchange pathway, where two spin carrying moieties are adjacent and, in the case of MBMs bonded to one another. The Pauli exclusion principle and coulombic repulsion, with respect to the nature of the overlap between magnetic orbitals, govern the specifics of the interactions. Orthogonal overlap allows the unpaired electrons to align parallel due to the Pauli exclusion principle, while nonorthogonal overlap requires the spin momenta to align antiparallel due to coulombic repulsion.[26]

A weaker type of exchange pathway is superexchange, in which the magnetic orbitals of spin carriers have significant overlap with a diamagnetic species that is bonded to both spin carriers. Oxide and cyanide are common diamagnetic entities that facilitate superexchange due to their oxidative bonding, small size and diamagnetic nature. In much the same manner that direct exchange arises from overlap of magnetic orbitals, superexchange arises from significant overlap of a magnetic orbital and a valence $2p$ or π orbital of the diamagnetic linker.[26] However, the diamagnetic linker, by virtue of satisfying energetic restrictions arising from coulombic repulsion has both a spin up and spin down electron, which become polarized by the unpaired electron(s) in the neighboring magnetic orbital. Thus, the electrons of the diamagnetic species tend to reside in respective valence orbital lobes and align parallel or antiparallel depending on the nature of orbital overlap, as discussed above. The antiparallel case is most facilely depicted, Figure 1.4.

The weakest, although nontrivial, type of exchange pathway that occurs is the indirect exchange interaction, which propagates through space in the absence of a chemical bond. The dipole-dipole, or dipolar, interaction is common among MBMs, which frequently are composed of 0-D isolated spin carries, 1-D chains, and 2-D

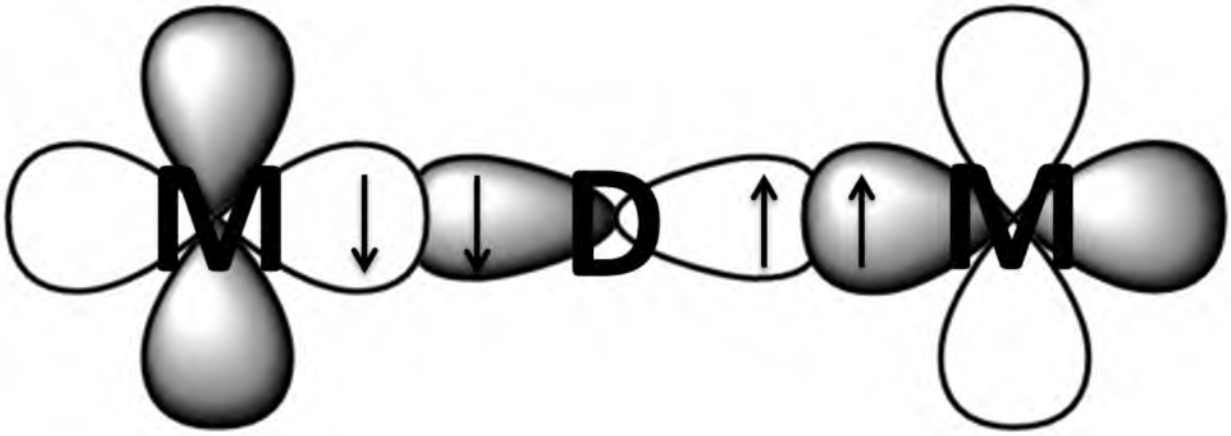

Figure 1.4. A simplified representation of unpaired spins in two metal *d*-orbitals, **M**, interacting with a diamagnetic linker's, **D**, paired electrons in a *p* or π symmetry orbital.

layers.[6,7,11] This type of interaction is typically orders of magnitude weaker than direct exchange and, thus, is challenging to evaluate experimentally in the presence of any other type of exchange pathway. Another example of indirect exchange is the Ruderman-Kittel-Kasuya-Yosida (RKKY) interaction, which operates through the mediation of spin-spin interactions via polarization of electrons in the conduction band. This allows dilute spin carriers to couple over microscopically large distances and induce magnetic order.[27]

The coupling constant, *J*, may be evaluated through modeling experimental *M*(*T*) data with numerical approximations, explicit physical expressions, or spin-only approximations. Numerical approximations have been used to simplify the application of mathematically tedious expressions and are limited to 1-D and 2-D magnetic motifs. For 1-D systems the Fisher-Bonner 1-D chain expression is frequently implemented,[28] and a numerical Padé approximation has been modeled to replicate well-known systems, thereby establishing the appropriate leading coefficients.[29,30] For 2-D systems the Heisenberg and Ising models are typically used.[31] For 3-D systems there exists no explicitly solved physical expression. However, Mean Field, MF, theory has been implemented and is more extensively described in Chapter 7.[32]

Magnetic Measurements

Magnetically ordered systems display a significantly larger degree of complexity and variation in magnetic response compared to paramagnetic systems with regard to temperature, field, field history, and field intensity. This variation may be diagnostic, as is the case for antiferromagnets and ferromagnets, Figure 1.5. This complexity necessarily requires a correspondingly more diverse array of measurements. Paramagnetic compounds and ordered magnets behave similarly at high temperatures (100-400 K for most MBMs) and may be probed through measurement of magnetization in response to an applied magnetic field as a function of temperature. This temperature dependent measurement is termed, *M*(*T*), and is performed by cooling a sample in a magnetometer at zero applied field to approximately 5 K (may vary depending on the material of interest), applying a 1000 Oe field and measuring the magnetization of the sample on warming.

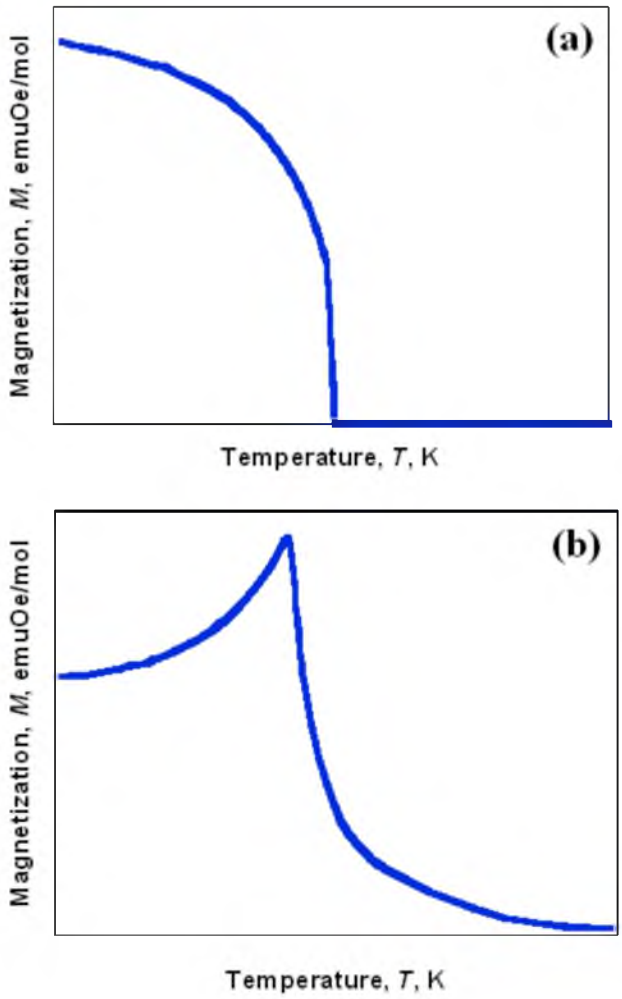

Figure 1.5. Idealized examples of an $M(T)$ for a polycrystalline ferromagnet (a) and a polycrystalline antiferromagnet (b).

For most compounds of interest the aforementioned magnetic field is diminutive enough to allow eqn. 1.4 to be simplified to

$$M = \chi H \ , \tag{1.13}$$

which causes the M to be linearly proportional to the χ. In the high temperature regime the unpaired spins reach a thermal equilibrium and are effectively isolated from one another. Through manipulation of the χ to the χT, from eqns. 1.5 and 1.6, the spin of a given system may evaluated as

$$\chi T = \frac{N_A g_e^2 \mu_B^2 S(S+1)}{3k_B}, \tag{1.14}$$

which is useful for structure confirmation and purity determination of novel materials.[20] It must be noted that equation 1.14 is only for single ions where spin-orbit coupling and zero field splitting are not significant.

The behavior of ordered magnetic compounds is investigated through temperature, $M(T)$, and field, $M(H)$, dependent measurements. The three principal temperature dependent measurements utilized to evaluate magnetic behavior are the zero-field cooled, $M_{ZFC}(T)$, field cooled, $M_{FC}(T)$, and remnant magnetizations, $M_r(T)$. The $M_{ZFC}(T)$ and $M_{FC}(T)$ are typically performed in series by cooling a sample in zero field (± 0.001 Oe), applying a 5 Oe field, measuring the magnetization upon warming, then cooling in the 5 Oe applied field and again measuring the magnetization upon warming. By contrast the $M_r(T)$ is performed by cooling a sample in a 5 Oe field, upon the system stabilizing at low temperature the field is reduced to zero and the magnetization is also measured upon warming. The divergence of the $M_{ZFC}(T)$ and $M_{FC}(T)$ data occurs at the bifurcation temperature, T_b, and is representative of the temperature below which a material exhibits magnetic memory, Figure 1.6. Extrapolation of the most linear portion of the $M_r(T)$ to zero is used to determine the T_c, Figure 1.7.

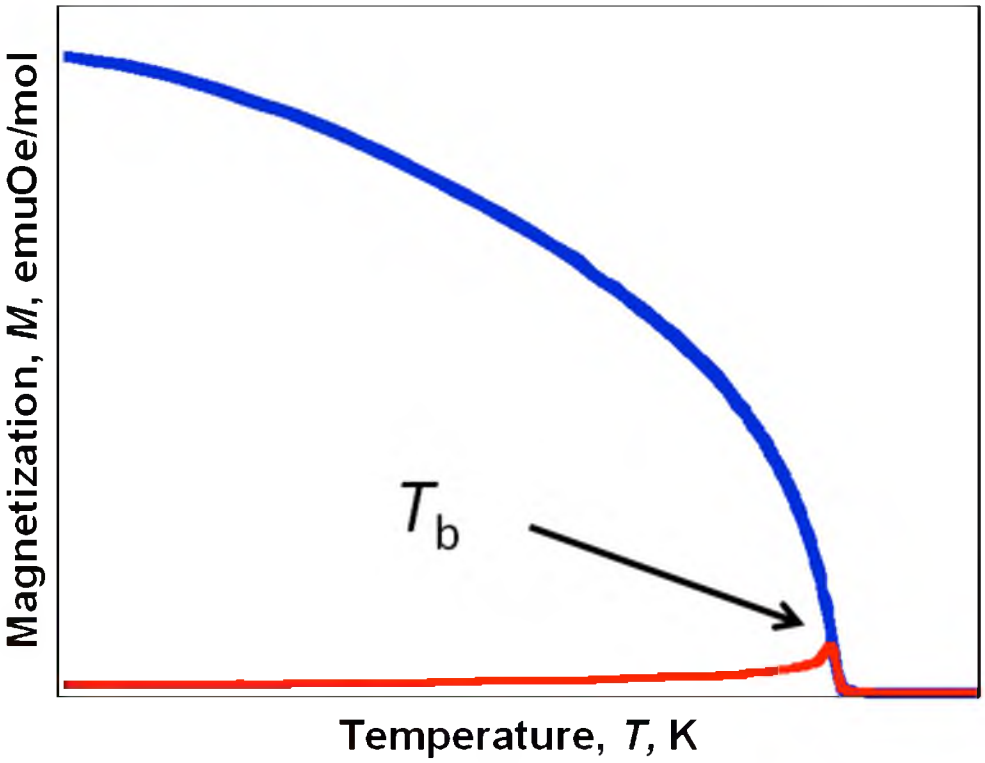

Figure 1.6. Example of a $M_{ZFC}(T)$ (red) and a $M_{FC}(T)$ (blue) for a ferro- or ferrimagnet with the point of bifurcation depicted, T_b.

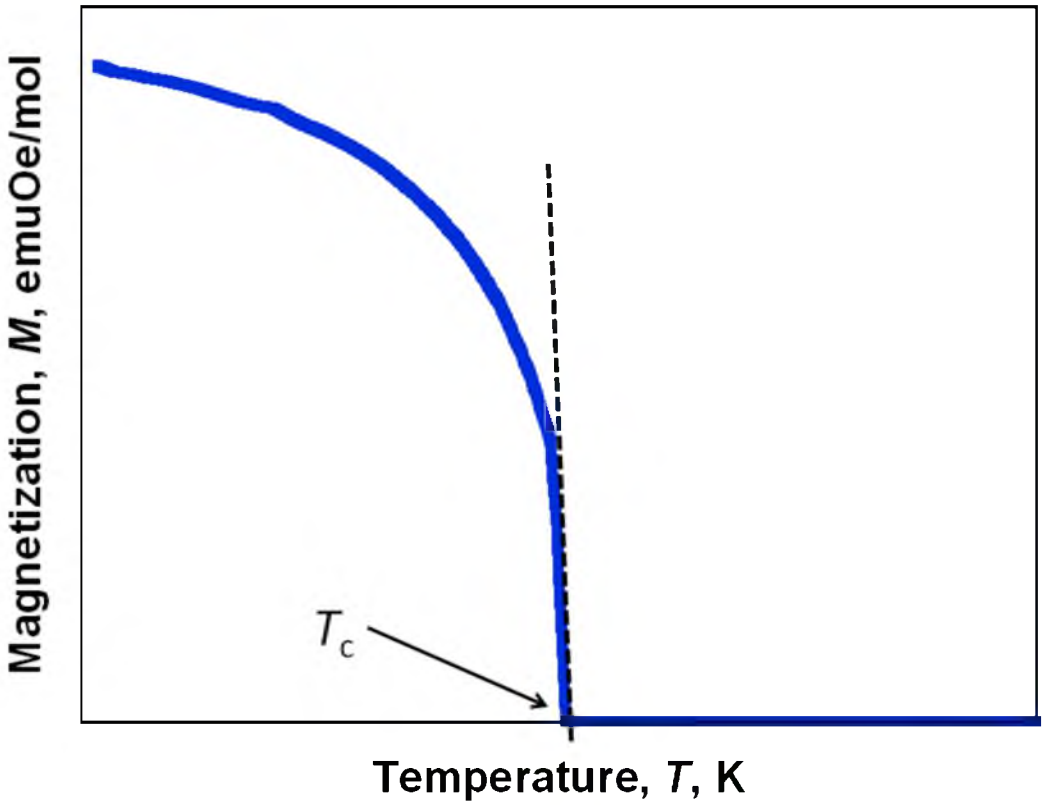

Figure 1.7. Example of a *M*r(*T*) plot (blue) with the linear extrapolation (dashed line) of the T_c depicted.

There exist many evaluation methods of isothermal field dependent measurements, $M(H)$, but this discussion will be limited to the goal of assessing the spin moieties of a paramagnetic compound and determining the existence of a field dependent hysteresis and magnetic phase transition in an ordered magnetic material. A first quadrant $M(H)$ is performed by cooling (or heating) a sample in zero applied field to a desired temperature (frequently the lowest achievable), then increasing the field to the maximum achievable. A hysteretic $M(H)$ is performed in the same manner as a first quadrant $M(H)$, but upon reaching the maximum achievable field, the field is then reduced to the maximum achievable negative value, and finally increased to the maximum achievable field.

For paramagnets the first quadrant $M(H)$ can be modeled using

$$M = N_A g_e \mu_B S B, \tag{1.15}$$

where B is the Brillouin function,[21]

$$B = \frac{2S+1}{2S}\coth\left(\frac{2S+1}{2S}x\right) - \frac{1}{2S}\coth\left(\frac{x}{2S}\right) \text{ and } x = \frac{g_e \mu_B S H}{k_B(T-\theta)}. \tag{1.16}$$

The first quadrant $M(H)$ is also useful for the identification and evaluation of metamagnetic behavior. Metamagnets are characterized by the absence of field dependent hysteresis and the presence of a field dependent transition from an antiferromagnetic ground state to a ferromagnetic ground state.

Field dependent hysteresis arises only for ordered magnetic material, i.e., at temperatures below the T_c. There are three characteristic values used to describe a compound's hysteretic behavior, Figure 1.8: (1) the saturation magnetization, M_s, which is the maximum achievable magnetization of a compound corresponding to complete alignment of all spins and domains; (2) the remnant magnetization, M_r, which is the magnetization exhibited by a compound upon removal of an applied field sufficient to

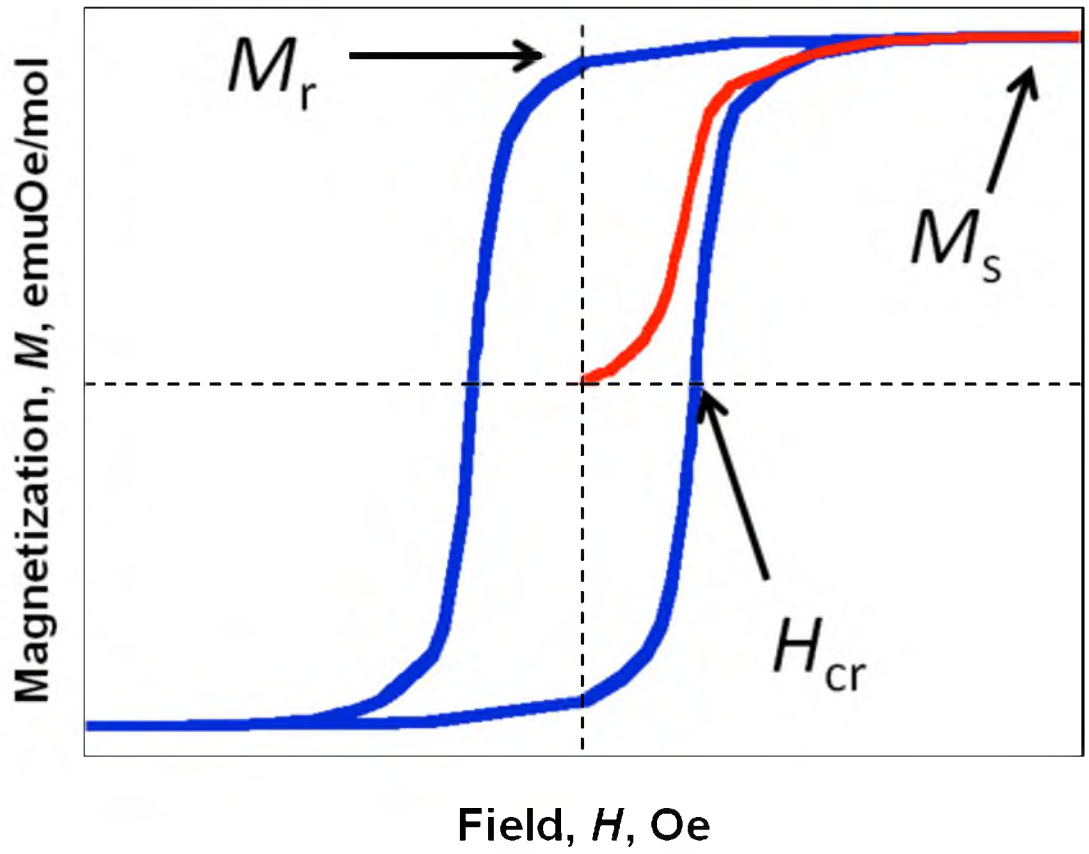

Figure 1.8. Depiction of a $M(H)$ measurement exhibiting hysteresis, the virgin curve (red) marks the beginning of the measurement cycle at the origin, the hysteresis loop (blue) begins at the confluence of the virgin curve, labeled M_s and proceeds to negative fields through the point labeled M_r, upon returning to positive fields the H_{cr} is labeled.

magnetically saturate that compound; (3) the coercive field, H_{cr}, which is the applied field required to demagnetize a compound, i.e. $M_r = 0$. The magnitude of the H_{cr} is indicated by the terms hard and soft magnet, referring to magnets with an $H_{cr} > \sim 100$ Oe or $H_{cr} < \sim 10$ Oe, respectively. The commercial application of a magnet is most often determined by its hardness or softness: one utility of soft magnets is voltage transformation,[1] while hard magnets are often used in memory storage devices.[2]

An AC susceptibility measurement is performed through the application of an alternating current to induce an alternating magnetic field that is superimposed on a constant magnetic field, whereas the previously described measurements utilized a direct current and a constant magnetic field. Alternation of the magnetic field from equivalent positive to negative values results in a time-dependent moment experienced by the sample, Figure 1.9. The induced magnetic moment is described as

$$M_{AC} = \left(\frac{dM}{dH}\right) H_{AC} \sin(\omega t), \tag{1.17}$$

where ω is the magnetic field oscillation frequency and dM/dH is the slope of the isothermal field dependent response, commonly termed susceptibility because of the term's dependence on the instantaneous slope of the magnetization, analogous to equation 1.4.[33] In the limit of magnetic field oscillation approaching zero, AC magnetometry approximates DC magnetometry. Even in this limit, AC techniques retain a greater sensitivity to changes in the magnetic response of a sample to the measurements' dependence on the slope of the magnetization, as opposed to the absolute value as is the case for DC techniques.[33]

Other magnetic properties may be observed as the magnetic field oscillation frequency is increased, arising from the time dependent response of a sample as the induced magnetization lags behind the rate of oscillation. These time dependent behaviors are observed through the comparison of two measured quantities: the in-phase real component, χ', and the out-of-phase imaginary component, χ''. The dependence of these quantities on the magnitude of the susceptibility, χ, and the phase shift, φ, follow the relationships described by eqns. 1.18-1.21.[33]

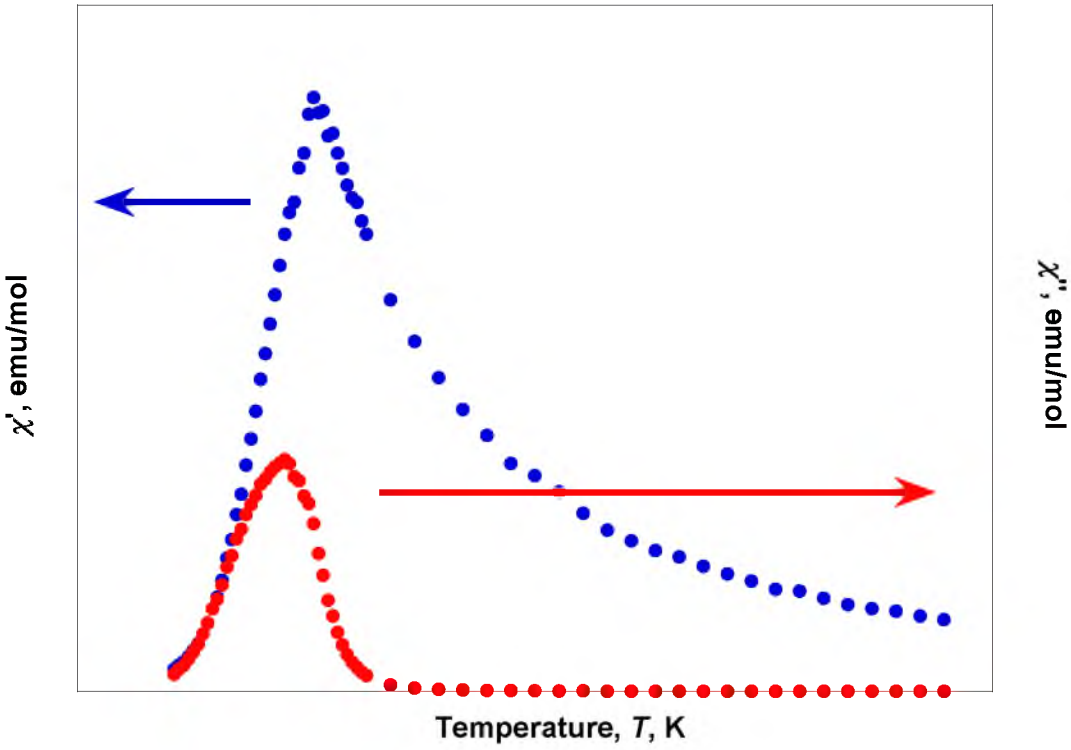

Figure 1.9. Example plot of the $\chi'(T)$ and $\chi''(T)$ from AC measurements of a ferromagnetic material.

$$\chi' = \chi \cos\varphi \tag{1.18}$$

$$\chi'' = \chi \sin\varphi \tag{1.19}$$

$$\chi = \sqrt{\chi'^2 + \chi''^2} \tag{1.20}$$

$$\varphi = \arctan\left(\frac{\chi'}{\chi''}\right) \tag{1.21}$$

The observance of χ'' is indicative of memory, or irreversible behavior of a sample due to the dissipation of internal energies. This dissipation may occur as a result of spin glass properties or, in the case of a ferro- or ferrimagnetically ordered material, the resistance of domain walls to spin reorientation. This allows the observance or absence of χ'' to be a qualitative indicator of a sample's bulk magnetic behavior. The T_c may be determined from AC measurements as the onset temperature of the initial rise in χ'' on cooling; alternatively, for antiferromagnets or any sample exhibiting an absence of χ'' the T_c is taken as the peak in the χ'.

Organic Electron Acceptors

MBMs have been targeted as alternatives to current metal alloy and metal oxide magnets. The viability of MBMs in this capacity was realized through the synthesis of the first MBM bis(pentamethylcyclopentyldienide)iron^{III} tetracyanoethenide, $[Fe^{III}Cp_2^*]^{\bullet+}[TCNE]^{\bullet-}$, in 1986.[9] This has led to the utilization of TCNE and analogous organic ligands in conjunction with primarily first row transition metals, although cations from nearly every group of the periodic table have been utilized, to form coordination polymers. Selection of TCNE and its analogues has been based on several critical criteria: symmetry, electron affinity (E_A), conjugation, and accessible stable radical forms.

The symmetry exhibited by TCNE (D_{2h}) and four peripheral cyano groups with terminal nitrogen allow a vast array of bonding motifs, which maintain significant

symmetry to propagate throughout the extended crystal structures formed. Several structures have been reported containing μ- and μ_4-TCNE, while a large variety have been envisioned and are anticipated, Figure 1.10.[34] The most prominent analogues of TCNE exhibit the same or very similar bonding motifs, as may be inferred from their structure and symmetry, Figure 1.11.

The following dissertation presents the application of Mean Field theory as a theoretical tool to investigate the nature of coupling in coordination polymers and the experimental investigation of several TCNE and TCNE analogue containing structures in an effort to elucidate the structural components of $V(TCNE)_x$, a room temperature MBM with an unknown structure due to its amorphous synthesis.[13]

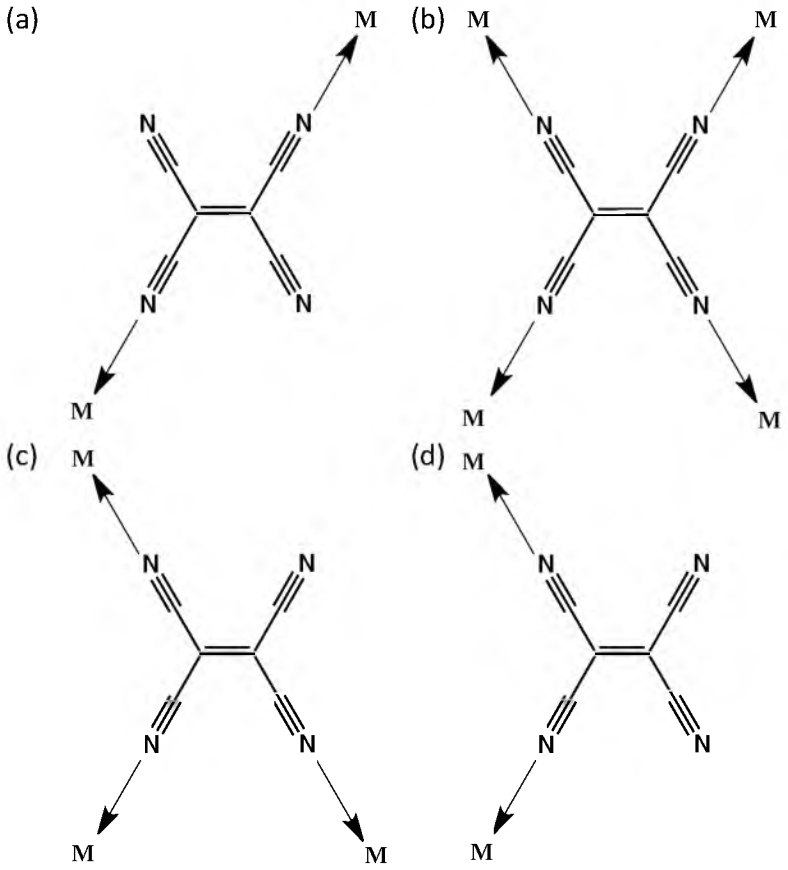

Figure 1.10. Bonding motifs of TCNE. (a) *Trans*-μ-TCNE bonding motif. (b) μ_4-TCNE bonding motif. (c) Proposed μ_3-TCNE bonding motif. (d) *Cis*-μ-TCNE bonding motif.

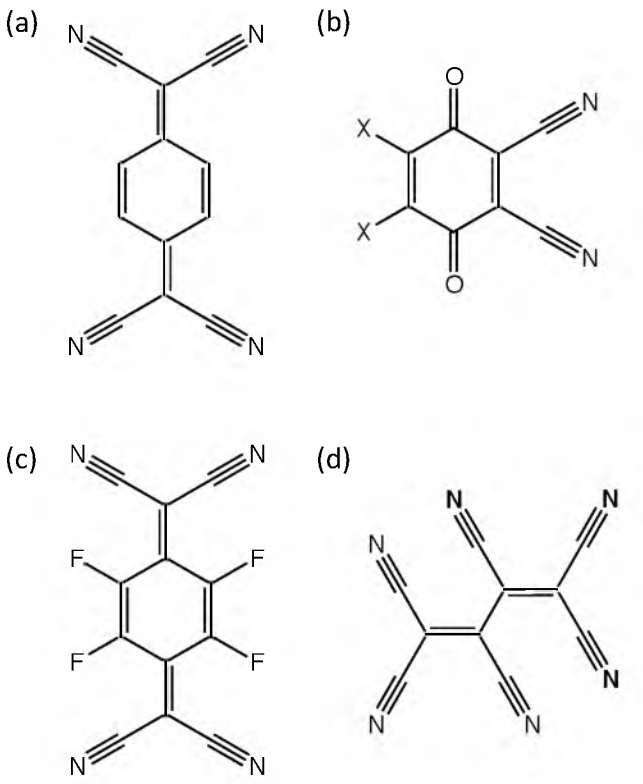

Figure 1.11. TCNE analogues. (a) 7,7,8,8-tetracyanoquinodimethane, TCNQ, D_{2h} symmetry. (b) 2,3-dihalo-5,6-dicyano-p-benzoquinone, DDQ, C_{2v} symmetry (X = Cl, Br, I). (c) 2,3,5,6-tetrafluoro-7,7,8,8-tetracyanoquinodimethane, $TCNQF_4$, D_{2h} symmetry. (d) Hexacyanobutadiene, HCBD, S_{2v} symmetry.

References

(1) Poyser, A. W. *Magnetism and Electricity: A Manual for Students in Advanced Classes, 1*; Longmans, Green, & Co.: London and New York, 1892; pp.285.

(2) Tand, D. D.; Lee, Y.-J. Field-Write Mode MRAMs. *Magnetic Memory*, 1; Cambridge University Press: Cambridge, 2010; pp. 91-92.

(3) Traylor, J. G. Recording Transducers. *Physics of Stereo/Quad Sound*, First Edition; Iowa State University Press: Ames, 1977; pp. 25-26.

(4) Collins, G. B. *Microwave Magnetrons*; McGraw-Hill Book Company: New York, 1948, pp. 1-46.

(5) Werfel, F. N.; Floegel-Delor, U.; Rothfeld, R.; Riedel, T.; Goebel, B.; Wippich, D.; Schirrmeister, P. *Supercond. Sci. Technol.* **2012**, *25*, 014007.

(6) Arthur, J. L.; Lapidus, S. H.; Stephens, P. W.; Miller, J. S. *Science China Chemistry* **2012**, *55*, 987-996.

(7) Pokhodnya, K. I.; Bonner, M.; Her, J.-H.; Stephens, P. W.; Miller, J. S. *J. Am. Chem. Soc.* **2006**, *128*, 15592-15593.

(8) McConnell, A. C.; Shurdha, E.; Bell, J. D.; Miller, J. S. *J. Phys. Chem. C* **2012**, *116*, 18952-18957.

(9) Miller, J. S.; Calabrese, J. C.; Epstein, A. J.; Bigelow, R. W.; Zhang, J. H.; Reiff, W. M. *J. Chem. Soc., Chem. Commun.* **1986**, 1026.

(10) J. S. Miller, J. C. Calabrese, H. Rommelmann, S. R. Chittipeddi, J. H. Zhang, W. M. Reiff, A. J. Epstein, *J. Am. Chem. Soc.* **1987**, *109*, 769.

(11) Miller, J. S. *J. Mater. Chem.* **2010**, *20*, 1846.

(12) Kareis, C. M.; Her, J.-H.; Stephens, P. W.; Moore, J. G.; Miller, J. S. *Chem. Eur.-J.* **2012**, *18*, 9281-9288.

(13) Miller, J. S.; Epstein, A. J. *Coordin. Chem. Rev.* **2000**, *206-207*, 651-660.

(14) Rittenberg, D. K.; Miller, J. S. *Inorg. Chem.* **1999**, *38*, 4838-4848.

(15) Coey, J. M. D. *Curr. Opin. Solid St. M* **2006**, *10*, 83-92.

(16) Martin, L. W.; Chu, Y.-H.; Ramesh, R. *Mat. Sci. Eng. R* **2010**, *68*, 89-133.

(17) Chien, C. L. *Mat. Sci. Eng. B-Solid* **1995**, *B31(1-2)*, 127-131.

(18) Han, J.; Meng, J.-B. *J. Photoch. Photobio. C* **2009**, *10*, 141-147.

(19) Verdaguer, M.; Girolami, G. Magnetic Prussian Blue Analogs. In *Magnetism: Molecules to Materials V*; Miller, J. S., Drillon, M., Eds.; Wiley-VCH: Weinheim, 2004; *5*, pp. 283-341.

(20) Drago, R. S. *Physical Methods for Chemists*; Surfside Scientific Publishers: Gainesville, 1992, pp. 469-476.

(21) Kahn, O. *Molecular Magnetism*; VCH Publisher: New York, 1993, pp. 1-29.

(22) (a) Morrish, A. H. *The Physical Principles of Magnetism*, John Wiley & Sons, Inc., New York 1965; pp. 46-47. (b) Morrish, A. H. *The Physical Principles of Magnetism*; John Wiley & Sons, Inc.: New York, 1965, pp 275-284. (c) Morrish, A. H. *The Physical Principles of Magnetism*; John Wiley & Sons, Inc.: New York, 1965, pp 432-485.

(23) Carlin, R. L. *Magnetochemistry*, Springer, New York 1986, pp. 202-206.

(24) Hurd, C. M. *Contemp. Phys.* **1982**, *23*, 469.

(25) Weng, D.-F.; Wang, Z.-M.; Gao, S. *Chem. Soc. Rev.* **2011**, *40*, 3157-3181.

(26) Mattis, D. C. *The Theory of Magnetism Made Simple*; World Scientific Publishing Co. Pte. Ltd.: Singapore, 2006, pp. 53-69.

(27) Watson, R. E.; Freeman, A. J. *Phys. Rev.* **1966**, *152*, 566-578.

(28) Bonner, J. C.; Fisher, M. E. *Phys. Rev.* A **1964**, *135*, A640.

(29) Estes, W. E.; Gavel, D. P.; Hatfield, W. E.; Hodgson, D. J. *Inorg. Chem.* **1978**, *17*, 1415.

(30) Baker, G. A.; Rushbrooke, G. S.; Gilbert, H. *Phys. Rev. A* **1964**, *135*, A1272.

(31) *Magnetic Properties of Layered Transition Metal Compounds*, de Jongh, L. J., Ed.: Kluwer Academic Publishers: Dordrecht, 1990.

(32) (a) Kittel, C. *Introduction to Solid State Physics. 6th Ed.*; John Wiley and Sons, Inc.: New York, 1986, pp. 421-428. (b) Smart, J. S. *Am. J. Phys.* **1955**, *23*, 356.

(33) Martien, D. Quantum Design Technical Resources: Introduction to AC Susceptibility. http://www.qdusa.com/sitedocs/appNotes/ppms/1078-201.pdf

(accessed March 2013).

(34) Miller, J. S. *Angew. Chem. Int. Ed.* **2006**, *45*, 2508-2525.

CHAPTER 2

PRESSURE DEPENDENT ENHANCED T_c AND MAGNETIC BEHAVIOR OF THE METAMAGNETIC AND FERROMAGNETIC POLYMORPHS OF $[Fe^{III}Cp^*_2]^{\bullet+}$ $[TCNQ]^{\bullet-}$ (Cp* = PENTAMETHYLCYCLOPENTADIENIDE; TCNQ = 7,7,8,8-TETRACYANO-*P*-QUINODIMETHANE)

Reprinted (adapted) with permission from: DaSilva, J. G.; Miller, J. S. *Inorg. Chem.* **2013**, *52*, 1108-1112.

Abstract

The magnetic behaviors of the metamagnetic and ferromagnetic polymorphs of $[Fe^{III}Cp_2^*]^{\bullet+}[TCNQ]^{\bullet-}$ (Cp* = pentamethylcyclopentadienide: TCNQ = 7,7,8,8-tetracyano-*p*-quinodimethane) were studied as a function of hydrostatic pressure. Both polymorphs exhibit a reversible enhancement of magnetic properties with increasing pressure. The T_c for the ferromagnetic polymorph increased by 70% from 2.95 to 5.01 K at 10.3 kbar at a rate of 0.21 K/kbar, which is similar to the 0.22 K/kbar reported for $[FeCp_2^*]^+[TCNE]^-$. The coercive field and remnant magnetization exhibit exponential-like growth upon application of external pressure, increasing from zero at ambient pressure to 550 Oe and 8880 emuOe/mol at 10.3 kbar, respectively. The T_c for the metamagnetic polymorph was determined to be 2.10 K from the maximum in the Fisher specific heat data, that is, $d(\chi T)/dT$, and it increases by 38% to 2.90 K at 2.9 kbar at a rate of 0.28 K/kbar, before vanishing in accord with a transition to a paramagnetic state. The metamagnetic critical field, H_c, determined from dM/dH increases linearly from 1300 Oe at ambient pressure to 1800 Oe at 2.9 kbar, but is not evident at and above 3.9 kbar, also in accord with a transition to a paramagnetic state.

Introduction

The $[Fe^{III}Cp_2^*]^{\bullet+}[TCNQ]^{\bullet-}$ (Cp* = pentamethylcyclopentadienide; TCNQ = 7,7,8,8-tetracyano-*p*-quinodimethane) electron-transfer salt was first synthesized in an attempt to create an organic-based conductor.[1] While not an organic-based metal, $[FeCp_2^*]^+[TCNQ]^-$ exhibited metamagnetic behavior.[2] This led to the synthesis of $[FeCp_2^*]^+[TCNE]^-$ (TCNE = tetracyanoethylene) as the first organic-based ferromagnet,[3,4,5] and subsequently the first organic-based room temperature magnet, $V[TCNE]_x$,[6,7] and evidence of their suitability for the discovery of multifunctional materials.[8]

$[Fe^{III}Cp_2^*]^+[TCNQ]^-$ is an electron transfer salt resulting from the reaction of TCNQ and $Fe^{II}Cp_2^*$ that crystallizes into three structurally and magnetically 1:1 distinct phases, namely:[5] paramagnetic,[9,10] metamagnetic (**MM**),[10] and ferromagnetic (**FO**) polymorphs.[11] The **MM** and **FO** polymorphs have the same structural motif of chains of alternating cations, $[FeCp_2^*]^+$, and anions, $[TCNQ]^-$. However, the 1-D chains in the **MM** phase possess $[TCNQ]^-$ planes that are approximately parallel to the plane of the Cp* ring, the centroids of both lie along the chain axis, and both planes are approximately orthogonal to the chain axis.[10] In contrast, the chains in the **FO** phase have the $[TCNQ]^-$ planes approximately parallel to the plane of the Cp* ring, the centroids are not aligned, and the planes of both are not orthogonal to the chain axis.[11]

The pentamethylcyclopentadienide ligand exerts a strong crystal field, causing the Fe^{III} to be low-spin. Thus, $S = 1/2$ $[FeCp_2^*]^+$ couples with the $S = 1/2$ $[TCNQ]^-$. A computational investigation of the similarly structured $[FeCp_2^*]^+[TCNE]^-$ indicates that the magnetic behavior arises from strong intrachain coupling and weak interchain coupling (2 orders of magnitude smaller).[12] Thus, although the inter- and intrachain interactions are necessary for magnetic order, the paramagnetic behavior above the ordering temperature, T_c, is appropriately modeled as 1-D chains.[13]

Ferromagnetic $[FeCp^*_2][TCNQ]$ (**FO**) has a magnetic ordering temperature, T_c, of 3.1 K from the maximum in the frequency-independent $\chi'(T)$ data and 3.0 K from the maximum in the specific heat, $C_p(T)$, data, and a saturation magnetization of 16,740 emu•Oe/mol,[14] but does not exhibit hysteresis at 2 K.[15] Aligned crystals of metamagnetic $[FeCp^*_2][TCNQ]$ (**MM**) saturate at 15,900 emu•Oe/mol, and have a 1300

Oe critical field, H_c, at 2 K that decreases with increasing temperature. The T_c is 2.5 K from the maximum in the frequency-independent $\chi'(T)$ data, and peak maximum in $C_p(T)$ data.[14]

The 0-D structural isolated-ion nature of $[FeCp_2^*]^+[TCNQ]^-$ suggests that application of hydrostatic pressure may lead to enhanced intra- and interchain couplings, and a higher magnetic ordering temperature, T_c, as observed for $[FeCp_2^*]^+[TCNE]^-$,[16] and $[FeCp_2^*]^+[DCNQ]^-$ (DCNQ = 2,3-dicyano-1,4-naphthoquinone).[17] Herein, we report the pressure dependence of magnetism for **MM** and **FO** due to their structural and electrochemical similarities to $[FeCp_2^*]^+[TCNE]^-$.

Experimental Section

FO and **MM** were prepared via the literature method.[14] IR spectroscopy and AC susceptibility were used to confirm purity. IR spectra were measured from 400 to 4000 cm^{-1} using a Bruker Tensor 37 spectrometer (± 1 cm^{-1}). A Quantum Design (QD) Physical Property Measurement System (PPMS 9 T) was used to measure the AC susceptibility at ambient pressure. Samples of **FO** and **MM** (3 - 15 mg) were loaded into gelatin capsules in inert atmosphere and sealed with silicon grease prior to removal from inert atmosphere. A QD Superconducting Quantum Interference Device (SQUID) Magnetic Property Measurement System (MPMS-5XL 5 T) (sensitivity = 10^{-8} emu or 10^{-12} emu/Oe at 1 T) was used to perform the DC pressure-dependent magnetization studies. Samples of **FO** and **MM** (~1 mg) were sealed into a cylindrical Teflon™ cell; the remaining volume of the cell was occupied by decalin (the hydrostatic pressure media) and capped with Teflon end caps. The loaded Teflon sample cell was housed in a beryllium-copper hydrostatic pressure cell, fabricated at the University of Utah from the Kyowa Seisakusho design, with zirconia pistons and rubber o-rings. Pressure was applied to the assembly using a Kyowa Seisakusho CR-PSC-KY05-1 apparatus with a WG-KY03-3 pressure sensor. An Aikoh Engineering model-0218B digital sensor readout was used as the pressure indicator. For the zero-field cooled magnetization, $M_{ZFC}(T)$, the sample was cooled in zero applied field, and the data were taken upon warming in a 5 Oe applied field, whereas, for the field cooled magnetization, $M_{FC}(T)$, the sample was cooled in a 5 Oe applied field, and the data were taken upon warming in

a 5 Oe applied field. The remnant magnetization, $M_r(T)$, was taken upon warming in a zero applied field after the sample was cooled in a 5 Oe applied field.

The Aikoh Engineering model-0218B digital sensor readout is an approximate method for determining pressure, and a superconductor with a known pressure-dependent transition temperature, $T_{sc}(P)$, for example, Pb,[18] was used to calibrate the pressure. Since the expected T_c for both **MM** and **FO** is in the range of 2 - 4 K,[14] no convenient superconducting pressure calibrant with a lower T_{sc} was available. Nonetheless, a statistical analysis of 159 individual pressure applications, Figure 2.1, from several previous studies using the identical digital sensor readout, and using a superconducting pressure calibrant, enabled the determination of the pressure, P, in kbar, from a least-squares linear regression fit, equation 2.1, where x is the readout from the digital sensor. The error associated with this correlated fit was assumed to be the standard deviation of the slope and intercept of the linear regression fit propagated through the pressure determination and is 0.048 kbar. The data were collected over several years to remove any technique-based bias, and χ^2 is 0.95301. As pointed out by a reviewer, the pressure dependence is never the same due to the difference in volume, tightness of joints, etc., and this accounts for the scatter of the data.

$$P = 0.025x - 0.7 \qquad (2.1)$$

The T_c of **FO** was determined through the extrapolation of the most linear portion of the remnant magnetization, $M_r(T)$, near zero magnetization to zero magnetization. The bifurcation temperature was taken as the temperature at which the divergence of zero-field cooled, $M_{ZFC}(T)$, and field cooled, $M_{FC}(T)$, magnetizations occur. The T_c of **MM** was determined from the maximum in the $d(\chi T)/dT$, that is, the Fisher specific heat.[19,20] Isothermal field-dependent magnetization measurements, $M(H)$, were performed for both phases at 2 K, and the coercive field, H_{cr}, of **FO** was determined from the extrapolation of the field intercept at zero magnetization upon reduction of an applied field of ± 50 kOe. The $M_r(H)$ for **FO** was determined from the extrapolation of the magnetization intercept at zero applied field upon reduction of an

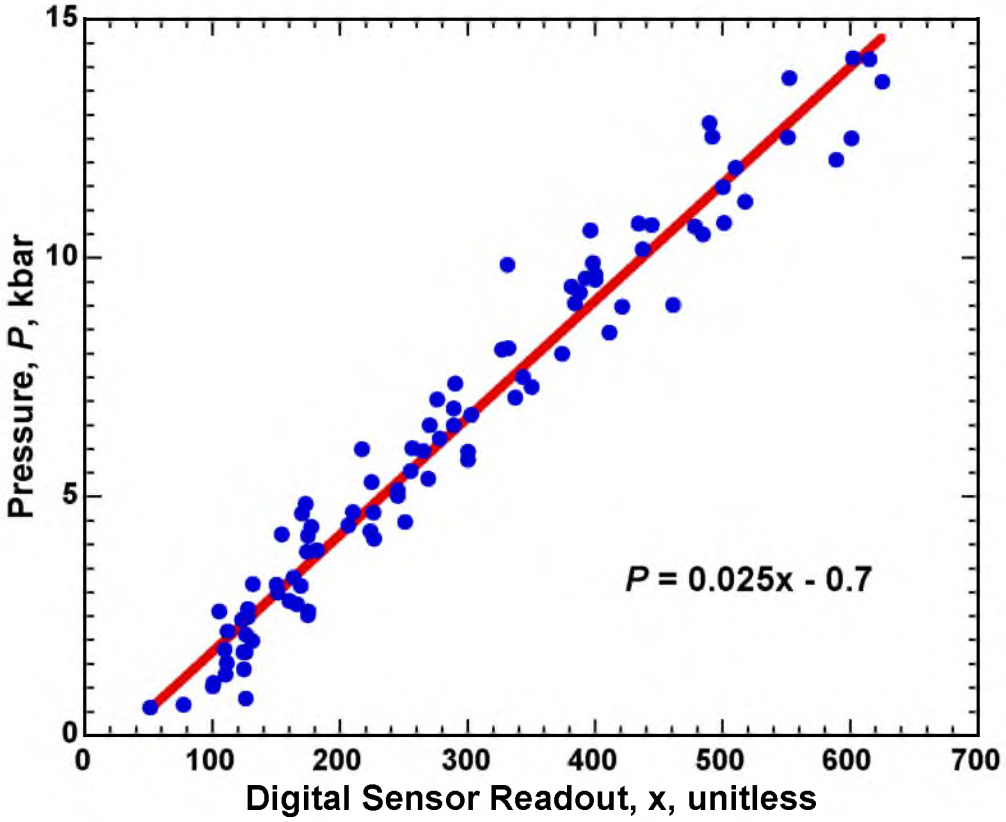

Figure 2.1. Correlation of 159 calibrated pressures (●) as a function of the digital sensor readout, *x*. The red line is the least squares linear regression fit, equation 2.1.

applied field of ± 50 kOe, and the critical field, H_c, of **MM** was defined as the maximum in dM/dH of the virgin curve.

Results and Discussion

The pressure-dependent magnetization as a function of applied field, $M(H,P)$, at 2 K, as well as the remnant magnetization, $M_r(T,P)$, zero-field cooled and field cooled magnetizations, $M_{ZFC}(T,P)$ and $M_{FC}(T,P)$, for **FO**, and as a function of applied field, $M(H,P)$ at 2 K, as a function of temperature, $M(T,P)$ at 500 Oe for **MM** were measured.

The **FO** polymorph of [FeCp*$_2$][TCNQ] was previously analyzed through AC and DC magnetometry and was found to have a T_c(AC) [from the maximum in $\chi'(T)$] of 3.1 K, a $T_c(M_{FC}(T))$ [from the extrapolation of the most linear portion of $M_{FC}(T)$] to zero magnetization] of 3.0 K, a $T_c(M_r(T))$ [from the extrapolation of the most linear portion of $M_r(T)$ to zero magnetization] of 3.3 K, a bifurcation temperature, T_b [from the divergence of the $M_{ZFC}(T)$, and $M_{FC}(T)$ magnetizations] of 3.0 K, and no coercive field, H_{cr}.[11,15] These values were reproduced through similar measurements at ambient pressure: $T_c(M_r(T))$ = 2.95 ± 0.05 K, T_b = 2.92 ± 0.05 K, and coercivity, H_{cr}, of 0 ± 2.5 Oe. The H_{cr} is consistent with an initial report of no coercivity, and within the sensitivity of measurements is zero.[11] Polycrystalline samples were used to be consistent with those used in the pressure cell.

The $M_r(T)$, $M_{ZFC}(T)$, and $M_{FC}(T)$ for **FO** decrease with increasing applied pressure by ~25% at 10.3 kbar, Figure 2.2. The rate of the magnetization suppression approaches zero above 7.7 kbar, which is most apparent in the low-temperature region of the $M_{FC}(T)$, Figure 2.2. The $T_c(M_r(T))$ and T_b increase by 0.21 and 0.25 K/kbar, respectively, Figure 2.2, which are similar to the reported trend from AC measurements of T_c for [FeCp$_2$*]$^+$[TCNE]$^-$ of 0.22 K/kbar.[16] The $T_c(M_r(T))$ and T_b increased by 70 and 87% from 2.95 and 2.92 K at ambient pressure to 5.01 and 5.46 K, respectively, at 10.3 kbar, Figure 2.3.

The magnetization at 50 kOe was somewhat reduced from 12,900 emuOe/mol at ambient pressure to 11,000 emuOe/mol at 10.3 kbar, Figure 2.4, in accord with that observed in the $M_r(T)$, $M_{ZFC}(T)$, and $M_{FC}(T)$ data. The H_{cr} and $M_r(P)$ exhibit exponential-like growth upon application of an external pressure, increasing from zero

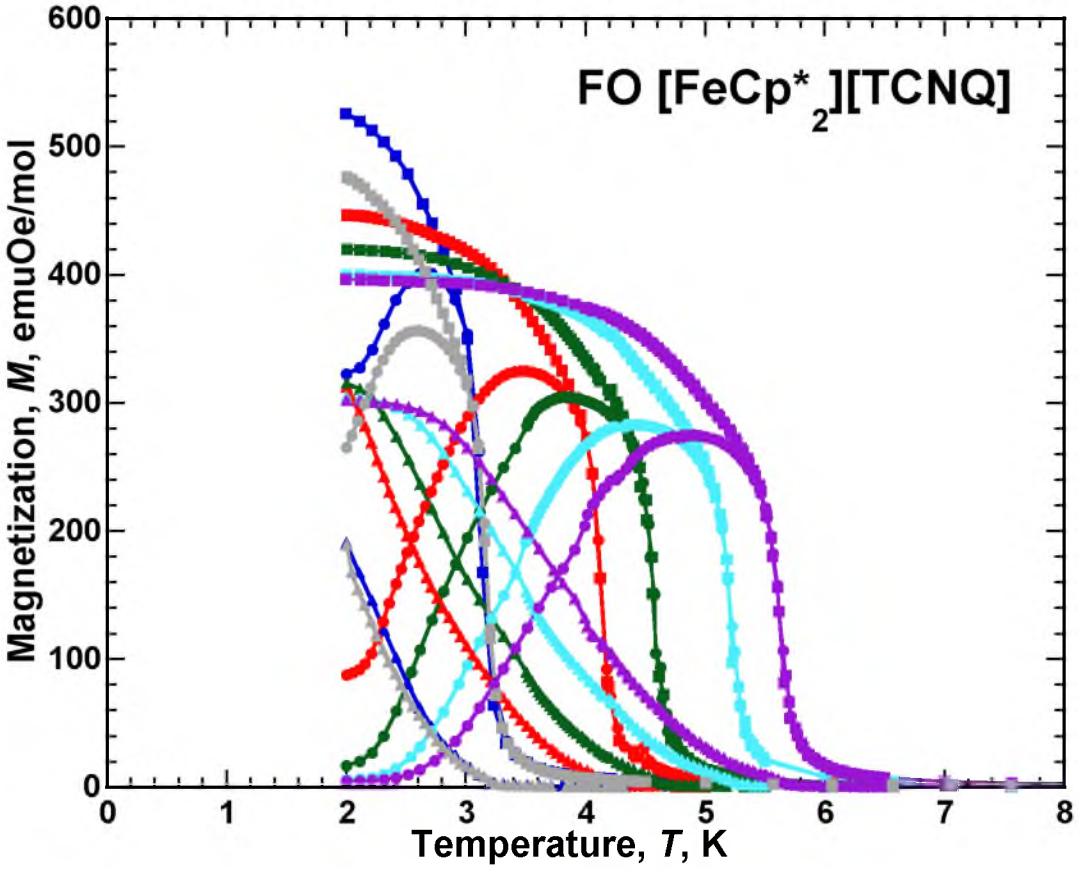

Figure 2.2. $M_r(T)$(▲), $M_{ZFC}(T)$(●), and $M_{FC}(T)$(■) of **FO** at 0.001 (●) (ambient pressure), 3.3 (●), 5.2 (●), 7.7 (●), 10.3 kbar (●), and upon returning to ambient pressure [0.001 kbar (●)]. The lines are guides for the eye.

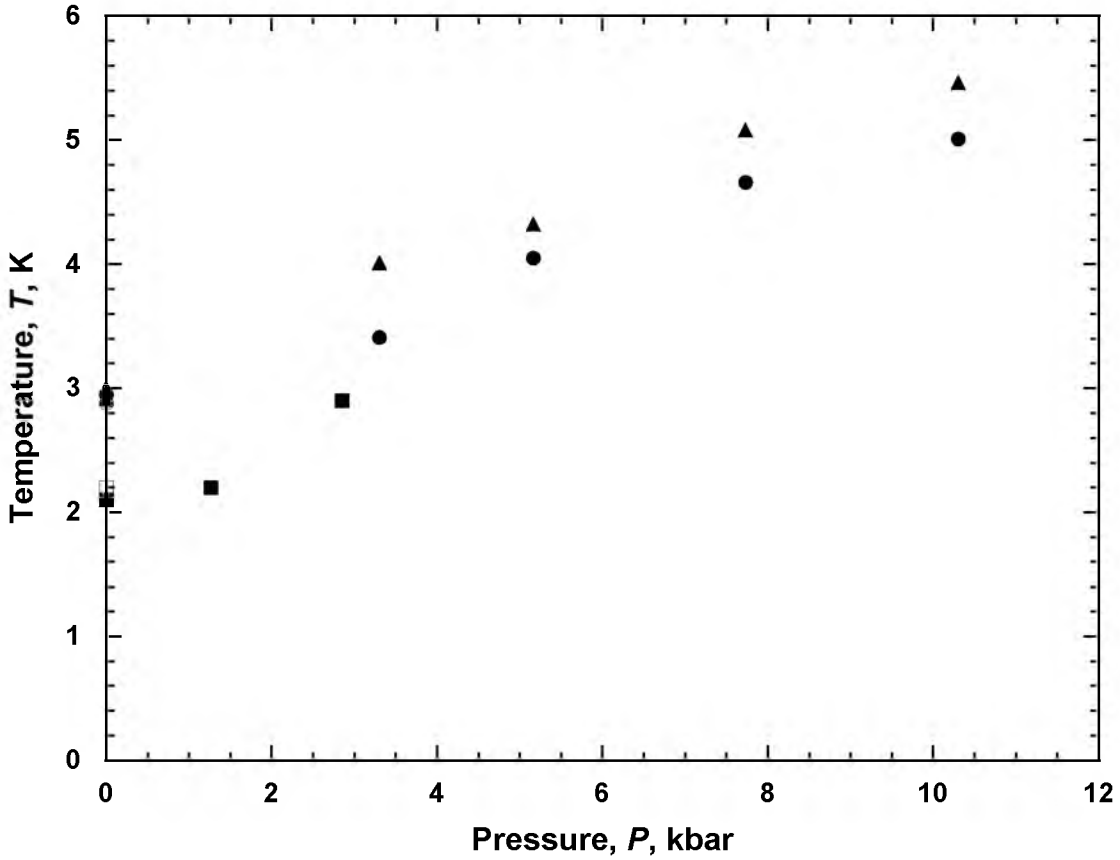

Figure 2.3. T_c(●) [from $M_r(T)$] and T_b(▲) of **FO**, and T_c (■) [from the temperature at which $d(\chi T)/dT$ is maximum] for **MM** as a function of pressure. Data for the released pressure measurements are hollow symbols (Δ, o, □). Error bars for pressure are approximately the size of the symbol.

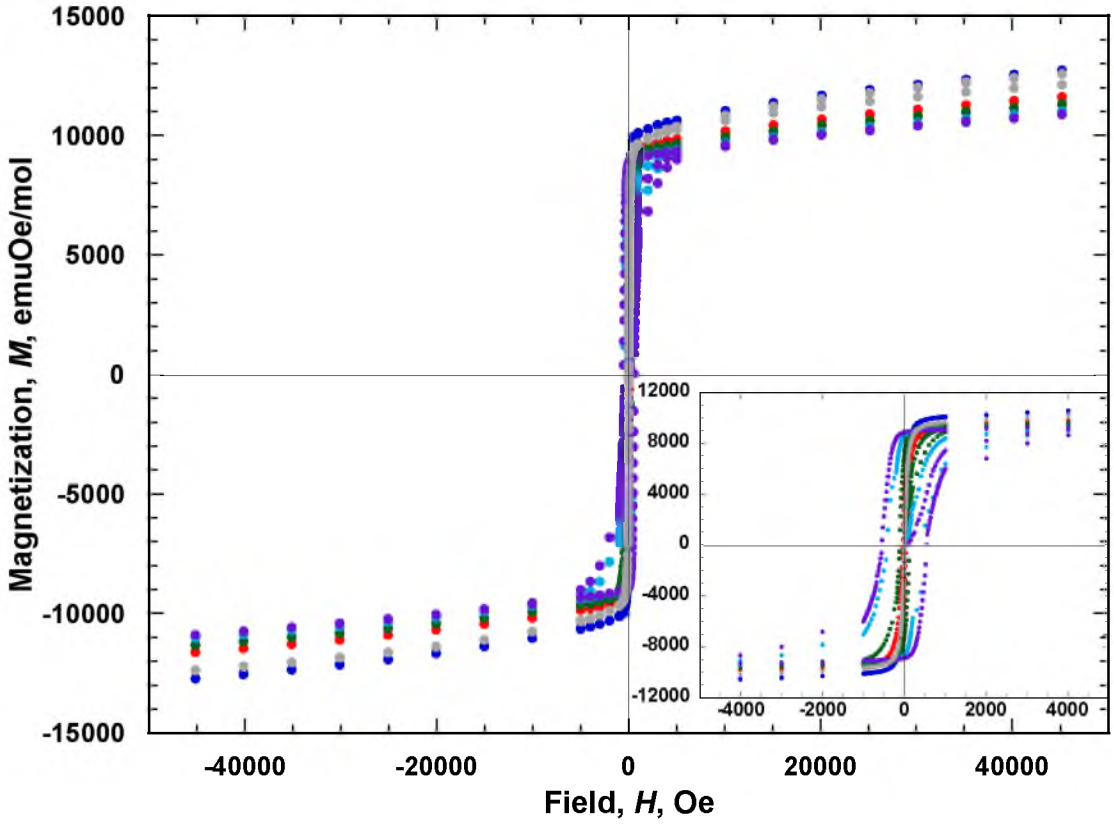

Figure 2.4. *M*(*H*) of **FO** at ambient pressure, 0.001 (●), 3.3 (●), 5.2 (●), 7.7 (●), 10.3 kbar (●), and upon returning to ambient pressure [0.001 kbar (●)]. Inset is an expansion of the hysteretic behavior.

at ambient pressure to 550 Oe and 8880 emuOe/mol at 10.3 kbar, respectively, Figure 2.5. The $M_r(H)$ approaches a constant value at ~7.7 kbar, while the rate of improvement in the H_{cr} decreases, which may indicate that the T_c has risen sufficiently above 2 K (the hysteresis measurement temperature) to prevent thermal disruption of the hysteresis as in the behavior of H_c in metamagnets.[21] The T_c, T_b, and H_{cr} were restored to their ambient pressure values, 2.88 ± 0.05 K, 3.00 ± 0.05 K, and 0 ± 2.5 Oe, respectively, upon returning to ambient pressure, indicating reversibility of the magnetic properties.

Under hydrostatic pressure, the intra- and interchain separations contract, leading to stronger couplings enhancing T_c and the bifurcation temperature, T_b. The increase in the magnetic irreversibility as evidenced by the appearance and growth of H_{cr} and, consequently, the M_r is more complex, as the lack of the coercivity at ambient pressure is at variance with the 1 kOe coercivity for [$FeCp_2$*][TCNE] at 2 K at ambient pressure.[7,13] A theoretical analysis in conjunction with a study of the pressure-dependent structure is needed to understand the genesis of these effects.

MM has been extensively studied through AC, and, to a lesser extent, DC magnetometry and was found to have a T_c [from the maximum in $\chi'(T)$] of 2.6 K,[14] T_c [from the maximum in $\chi(T)$] of 2.55 K,[2,14] and a critical field, H_c [from the maximum in dM/dH] of 1300 Oe at 2 K.[14] These values were reproduced at ambient pressure: T_c [$\chi'(T)$] = 2.55 ± 0.025 K, and H_c = 1300 ± 50 Oe. In addition, T_c was also determined from the maximum in $d(\chi T)/dT$ to be 2.10 ± 0.05 K, as this is a more accurate determination of T_c for an antiferromagnet.[19] This value correlates well with 2.35 ± 0.05 K.[14b] Polycrystalline samples were used to be consistent with those used in the pressure cell.

The 500 Oe $M(T)$ has a cusp at 2.42 ± 0.05 K at ambient pressure, in accord with antiferromagnetic ordering, Figure 2.6. The low-temperature magnetization decreases with increasing applied pressure, and the temperature at which the $\chi(T)$ displays a sharp maximum, or cusp, increases to 3.11 ± 0.05 K at 2.9 kbar. The T_c for an antiferromagnet is best determined from $d(\chi T)/dT$)[19] (Figure 2.3 and Figure 2.6 inset) and is 2.10 ± 0.05K at ambient pressure, and increases linearly to 2.90 ± 0.05 K at 2.9

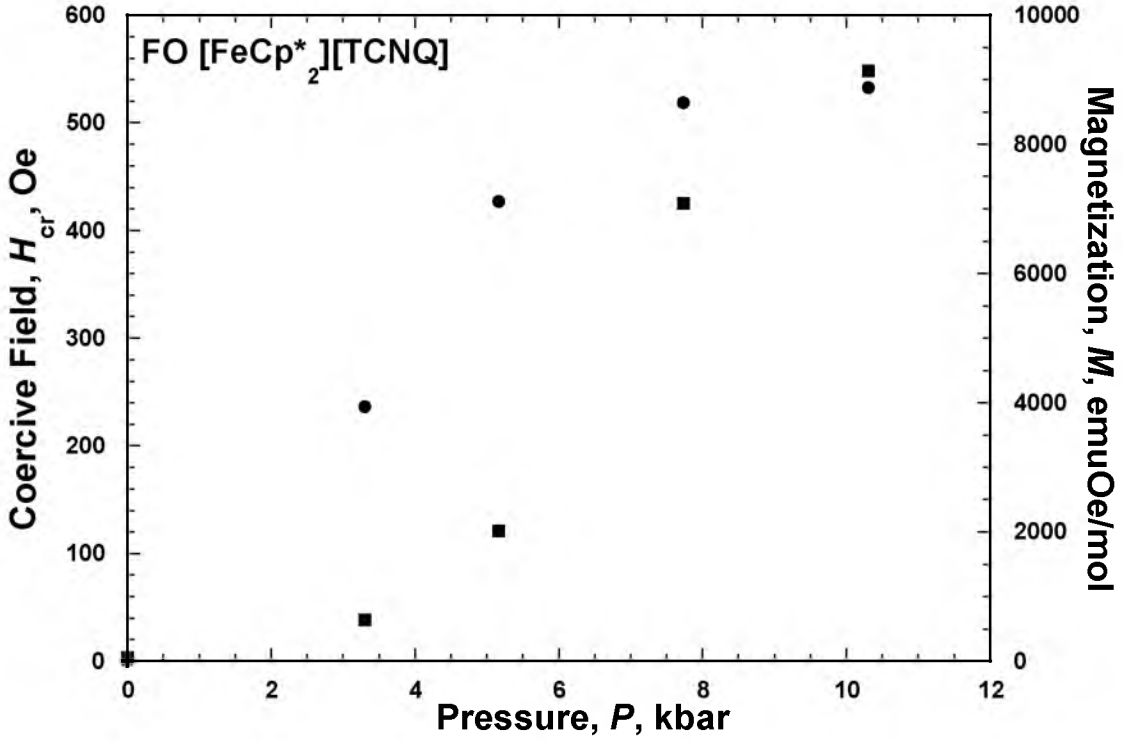

Figure 2.5. $H_{cr}(P)$ (■) and $M_r(P)$ (●) of **FO**; the released pressure measurements are hollow symbols (o, □). Error bars for H_{cr} and M_r are approximately the size of the symbol.

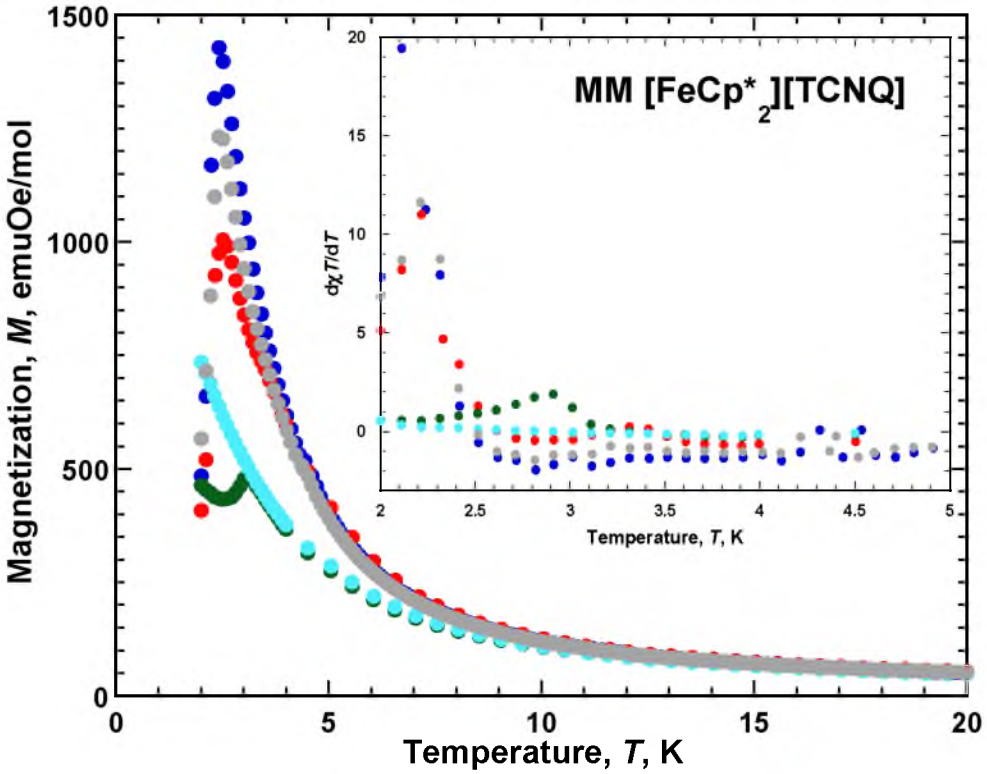

Figure 2.6. $M(T)$ at 500 Oe for **MM** as a function of pressure: 0.001 (●), 1.3 (●), 2.9 (●), 3.9 (●), and upon returning to ambient pressure [0.001 kbar (●)]. Inset is $d(\chi T)/dT$ (note: for $\geq$ 3.9 kbar the $d(\chi T)/dT$ plots are coincident).

kbar, and then abruptly decreases, consistent with a paramagnetic phase transition, Figure 2.3 and Figure 2.6 inset.

The magnetization is suppressed with increasing pressure, and this results in a significant decrease of the magnitude for the maximum in the $d(\chi T)/dT$ value with increasing pressure (<3.9 kbar), which is evidence of decreasing magnetization, as occurs for **FO** (vide supra), $[FeCp_2^*]^+[TCNE]^-$,[16] $[FeCp_2^*]^+[DCNQ]^-$,[17] and $Fe(pyrimidine)_2Cl_2$,[22] and $MnNi(NO_2)_4(ethylenediamine)_2$.[23] The T_c increases by 0.28 K/kbar below 2.9 kbar, Figure 2.3, which is consistent with the rate observed in $[FeCp_2^*]^+[TCNE]^-$ (0.22 K/kbar)[16] reaching a maximum of 2.90 ± 0.05 K at 2.9 kbar, and 0.33 K/kbar for $[FeCp_2^*]^+[DCNQ]^-$.[17]

The magnetization for **MM** increased by 6% from 13,700 emuOe/mol at ambient pressure to 14,600 emuOe/mol at 9.2 kbar at 50 kOe, which is in contrast to **FO**, Figure 2.7. The "S"-shaped $M(H)$ characteristic of metamagnetic behavior[24] is observed up to 3.9 kbar applied pressure, and a linear Brillouin-like $M(H)$ characteristic of paramagnetic behavior is observed at and above 3.9 kbar. The H_c determined from the maximum in dM/dH, Figure 2.8, increases linearly from 1300 ± 50 Oe at ambient pressure to 1800 ± 50 Oe at 2.9 kbar, Figure 2.9, but is not evident at and above 3.9 kbar. This is consistent with the absence of a maximum in the $d(\chi T)/dT$ value and paramagnetic behavior; hence, a transition to a paramagnetic state occurs at ~3.9 kbar. The T_c, and H_c were restored to their ambient pressure values: 2.20 ± 0.05 K, and 1200 ± 50 Oe respectively, upon release to ambient pressure, indicating reversibility. The increase in T_c and H_c with applied pressure has also been observed for $[FeCp_2^*]^+[DCNQ]^-$,[17] and $Mn^{II}(hfac)_2(BBA)$ (hfac = hexafluoroacetyacetonate; BBA =1,3-bis-*N*-*t*-butylaminoxyl).[25]

Under hydrostatic pressure, the intra- and interchain separations contract, leading to stronger couplings enhancing T_c and the metamagnetic critical field, H_c. However, above 2.9 kbar, a phase transition occurs, leading to paramagnetic behavior. This differs from $Mn^{II}(TCNE)[C_4(CN)_8]_{1/2}\bullet zCH_2Cl_2$ that exhibits a reversible pressure-induced piezomagnetic transition from an antiferromagnetic to a ferrimagnetic state above 0.50 kbar.[26] A study of the pressure dependent structure is needed to understand the genesis of these effects.

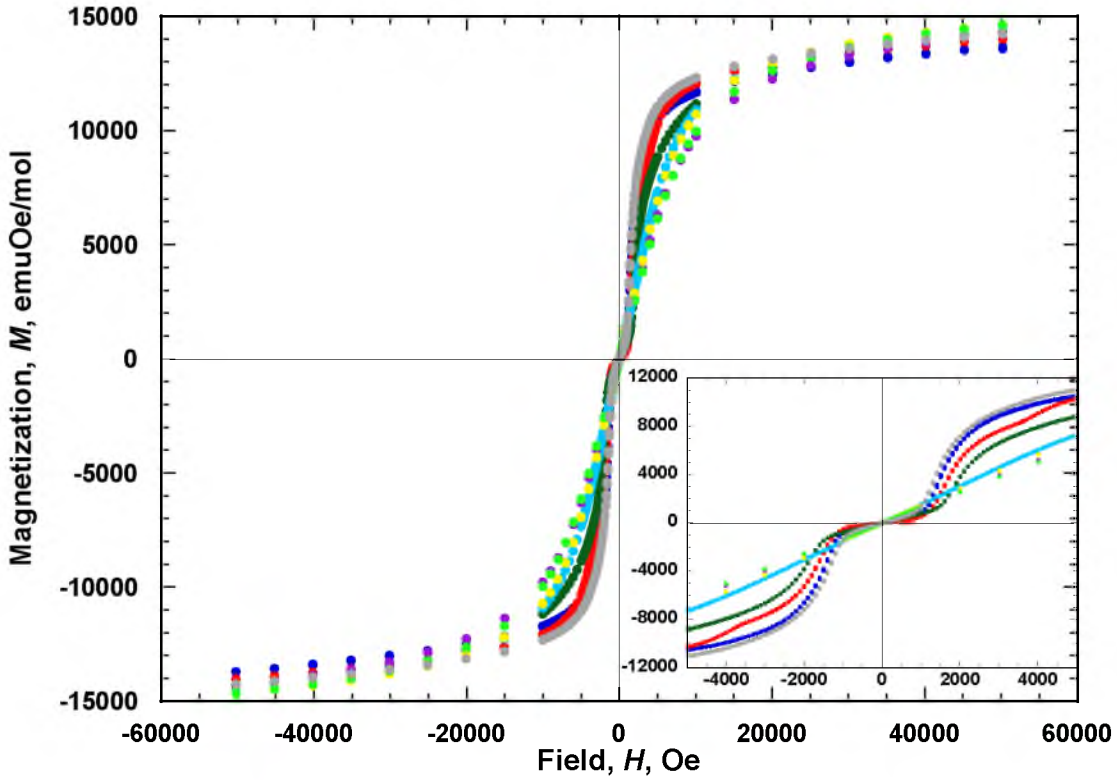

Figure 2.7. 2 K $M(H)$ of **MM** at ambient pressure 0.001 (●), 1.3 (●), 2.9 (●), 3.9 (●), 4.8 (●), 6.6 (●), 9.2 (●), and upon returning to ambient pressure [0.001 kbar (●)]. Inset is an expansion about the critical fields: at 1.3 kbar incomplete spin flop, as previously reported for eicosane-aligned samples, is evident.[14]

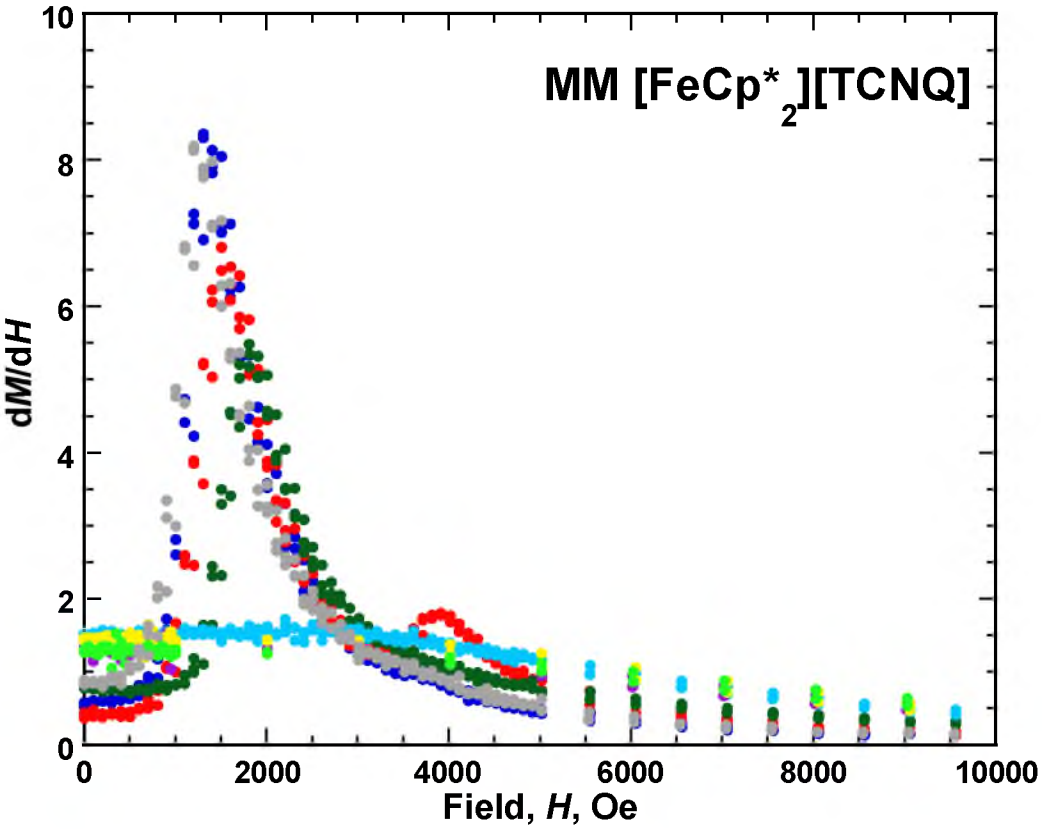

Figure 2.8. *dM/dH* of **MM** at several applied pressures: 0.001 (●), 1.3 (●), 2.9 (●), 3.9 (●), 4.8 (●), 6.6 (●), 9.2 kbar (●), and upon returning to ambient pressure [0.001 kbar (●)].

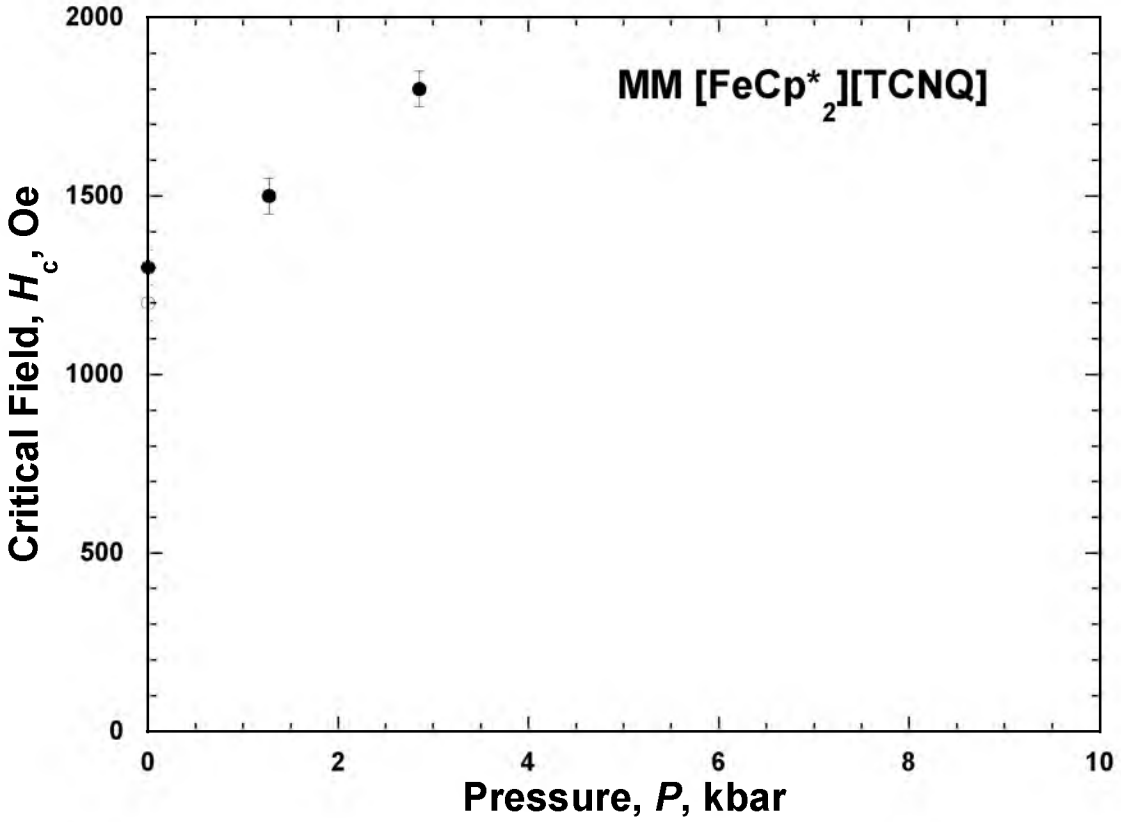

Figure 2.9. H_c (●) of **MM** for several applied pressures [released pressure (○)].

Conclusion

Temperature- and field-dependent magnetic studies of the **FO** and **MM** polymorphs of [FeCp*$_2$][TCNQ] at several applied pressures revealed similar enhancement to the $T_c(M_r(T))$ for ferromagnetic **FO** and $T_c[d(\chi T)/dT]$ for metamagnetic **MM** with an antiferromagnetic ground state, respectively, as the pressure was increased. The enhancement rates of 0.21 and 0.28 K/kbar, respectively, are similar to the structurally related electron-transfer salt [$FeCp_2$*]$^+$[TCNE]$^-$, which displayed an enhancement rate of 0.22 K/kbar $T_c(\chi')$.[16] **FO** was determined to exhibit no H_{cr} at ambient pressure, but H_{cr} and $M_r(H)$ increase to 550 Oe and 8880 emuOe/mol at 2 K and 10.3 kbar. **MM** exhibits a linear increase of H_c with pressure, reaching 1800 Oe at 2.9 kbar. Both the H_c and the T_c are absent at and above 3.9 kbar for the **MM** polymorph, indicative of a pressure-induced transition to a paramagnetic. Studies of the pressure-dependent structures are needed to understand the genesis of these effects.

References

(1) Miller, J. S.; Reis, A. H. Jr.; Gebert, E.; Ritsko, J. J.; Salaneck, W. R.; Kovnat, L.; Cape, T. W.; Van Duyne, R. P. *J. Am. Chem. Soc.* **1979**, *101*, 7111.

(2) Candela, G. A.; Swartzendruber, L. J.; Miller, J. S.; Rice, M. J. *J. Am. Chem. Soc.* **1979**, *101*, 2755-2756.

(3) Miller, J. S.; Calabrese, J. C.; Epstein, A. J.; Bigelow, R. W.; Zhang, J. H.; Reiff, W. M. *J. Chem. Soc., Chem. Commun.* **1986**, 1026.

(4) Miller, J. S.; Calabrese, J. C.; Rommelmann, H.; Chittipeddi, S. R.; Zhang, J. H.; Reiff, W. M.; Epstein, A. J. *J. Am. Chem. Soc.* **1987**, *109,* 769.

(5) Miller, J. S. *J. Mater. Chem.* **2010**, *20*, 1846.

(6) Miller, J. S.; Epstein, A. J.; Reiff, W. M. *Science* **1988**, *240*, 40.

(7) Miller, J. S. *Polyhed.* **2009**, *28*, 1596.

(8) (a) Blundell, S. J.; Pratt, F. L. *J. Phys.: Condens. Matter* **2004**, *16*, R771. Ovcharenko, V. I.; Sagdeev, R. Z. *Russ. Chem. Rev.* **1999**, *68*, 345. Kinoshita, M. *Phil. Trans. R. Soc. Lond. (A)* **1999**, *357*, 2855. (b) Miller, J. S.; Epstein, A. J. *Chem. Commun.* **1998**, 1319. Miller, J. S.; Epstein, A. J. *Angew. Chem. Int. Ed. Engl.* **1994**, *33*, 385. Miller, J. S. *Chem. Soc. Rev.* **2011**, *40*, 3266.

(9) Reis, H.; Preston, L. D.; Williams, J. M.; Peterson, S. W.; Miller, J. S. *J. Am. Chem. Soc.* **1979**, *101,* 2756.

(10) Miller, J. S.; Zhang, J. H.; Reiff, W. M.; Dixon, D. A.; Preston, L. D.; Reis, Jr., A. H.; Gerbert, E.; Extine, M.; Troup, J.; Ward, M. D. *J. Phys. Chem.* **1987**, *91,* 4344-4360.

(11) Broderick, W. E.; Eichhorn, D. M.; Liu, X.; Toscano, P. J.; Owens, S. M.; Hoffman, B. M. *J. Am. Chem. Soc.* **1995**, *117*, 3641-3642.

(12) Her, J.-H.; Stephens, P. W.; Ribas-Ariño, J.; Novoa, J. J.; Shum, W. W.; Miller, J. S. *Inorg. Chem.* **2009**, *48*, 3296.

(13) Chittipeddi, S.; Cromack, K. R.; Miller, J. S.; Epstein, A. J. *Phys. Rev. Lett.* **1987**, *58*, 2695.

(14) a) Taliaferro, M. L.; Palacio, F.; Miller, J. S. *J. Mater. Chem.* **2006**, *16*, 2677-2684. b) T_c from the maximum in $d(\chi T)/dT$ for the data reported in reference 14.

(15) Upon further detailed investigation, **FO** does not exhibit hysteresis, as initially reported.[11]

(16) Huang, Z. J.; Chen, F.; Ren, Y. T.; Xue, Y. Y.; Chu, C. W.; Miller, J. S. *J. Appl. Phys.* **1993**, *10*, 6563.

(17) Hamlin, J. J.; Beckett, B. R.; Tomita, T.; Schilling, J. S.; Tyree, W. S.; Yee, G. T. *Polyhedron* **2003**, *22*, 2249.

(18) Shum, W. W.; Her, J.-H.; Stephens, P. W.; Lee, Y.; Miller, J. S. *Adv. Mater.* **2007**, *19*, 2910.

(19) Fisher, M. E. *Philos. Mag.* **1962**, *7*, 17.

(20) (a) Aharen, T.; Greedan, J. E.; Ning, F.; Imai, T.; Michaelis, V.; Zhou, H.; Wiebe, C. R.; Cranswick, L. M. D. *Phys. Rev. B* **2009**, *80*, 134423. (b) Cage, B.; Nguyen, B.; Dalal, N. *Solid State Commun.* **2001**, *119*, 597.

(21) Carlin, R. L. *Magnetochemistry*, Springer, New York **1986**, pp. 202-206.

(22) Wolter, A. U. B.; Klauss, H.-H.; Litterst, F. J.; Burghardt, T.; Eichler, A.; Feyerherm, R.; Süllow, S. *Polyhed.* **2003**, *22*, 2139.

(23) Kreitlow, J.; Mathonière, C.; Feyerherm, R.; Süllow, S. *Polyhed.* **2005**, *24*, 2413.

(24) Stryjewski, E.; Giordano, N. *Adv. Phys.* **1977**, *26*, 487.

(25) Hosokoshi, Y.; Suzuki, K.; Inoue, K.; Iwamura, H. *Mol. Cryst. Liq. Cryst.* **1999**, *334*, 511.

(26) McConnell, A. C.; Bell, J. D.; Miller, J. S. *Inorg. Chem.* **2012**, *51*, 9978.

CHAPTER 3

PRESSURE DEPENDENT MAGNETIC BEHAVIOR OF FERROMAGNETIC [BIS(PENTAMETHYL-CYCLOPENTADIENYL)IRON(III)] [TETRACYANOETHENIDE], $[FeCp^*_2][TCNE]$

Abstract

The hydrostatical pressure-dependent DC magnetic behavior of ferromagnetic $[Fe^{III}Cp^*_2]^{\bullet+}[TCNQ]^{\bullet-}$ (Cp* = pentamethylcyclopentadienide; TCNE = tetracyanoethylene) up to 12.2 kbar was studied. A significant departure from the ambient pressure ferromagnetic behavior was observed at high pressures. The temperature dependent magnetization measurements were typical of a ferromagnet, but displayed extreme suppression of the magnetization intensity with increasing applied pressure, while anomalous metamagnetic-like behavior was evident in the field dependent magnetization data above 4.2 kbar. Hence, with increasing pressure the intermolecular separations decrease increasing the nearest neighbor ferromagnetic and antiferromagnetic couplings leading to an increase in magnetic ordering temperature, T_c. Furthermore, as the antiferromagnetic interchain interactions increase this may lead to canting that increases with pressure, and a transition to a canted antiferromagnet with a significant decrease in the magnetization. Additionally, the intrachain ferromagnetic coupling may cant with increasing pressure, and also contribute to the canted antiferromagnetic behavior.

Introduction

Organic-based magnets[1] were first realized through the synthesis and study of [bis(pentamethylcyclopentadienyl)iron(III)]$^+$[tetracyanoethenide]$^-$, $[Fe^{III}Cp^*_2]^+[TCNE]^-$, **1**, which magnetically orders below its critical temperature, T_c, of 4.8 K.[2,3,4,5] Ordering

as a ferromagnet was ascertained from the saturation magnetization,[4] and magnetic structure elucidated from neutron diffraction studies.[6] The discovery of ferromagnetic ordering in an organic-based magnet (OBM) has been of significant importance to theoretical solid-state physics and shows potential for accessing multifunctional materials.[7,8,9,10] $[FeCp^*_2]^{\bullet+}[TCNE]^{\bullet-}$ is an electron transfer salt possessing parallel linear chains of alternating S = 1/2 $[FeCp^*_2]^{\bullet+}$ cations and S = 1/2 $[TCNE]^{\bullet-}$ anions, with[11] and without solvent.[12,13] Several analogs of $[M^{III}Cp^*_2]^{+}[A]^{\bullet-}$ have been synthesized through the variation of the paramagnetic metal center (M = Fe, Mn, Cr) and/or the cyanocarbon [A = TCNE, 7,7,8,8-tetracyano-*p*-quinodimethane (TCNQ), hexacyanobutadiene (HCBD), 2,3-dichloro-5,6-dicyanobenzoquinone (DDQ), 2,3-dicyano-1,4-naphthoquinonide (DCNQ)].[5] This family of electron transfer salts has very similar structural motifs, which give rise to metamagnetic, ferromagnetic, and paramagnetic materials. For example, $[FeCp^*_2][TCNQ]$ has been isolated as three polymorphs, each having a different magnetic ground state, namely, one each with a metamagnetic, ferromagnetic, and paramagnetic ground state.[5]

This suggests that the magnetic properties are sensitive to the small variations in the nearest neighbor couplings arising from small structural differences arising within the family and perhaps the unique spin density of the various ligands, as computationally noted for $[FeCp^*_2]^{+}[TCNE]^{-}$.[11] The ten pairwise nearest neighbor interactions present for the 12 K structure of $[FeCp^*_2]^{+}[TCNE]^{-}$ were characterized by strong intrachain ferromagnetic coupling and weak (two orders of magnitude smaller) interchain ferro- and antiferromagnetic coupling, and proposed dipolar interactions. Thus, although the inter- and intrachain interactions are necessary for the existence of 3-D magnetic order, the paramagnetic behavior above T_c is appropriately modeled as 1-D chains.[4] The 0-D structural nature of this family of compounds presumably allows hydrostatic pressure to affect the crystal lattice in a manner more similar to a 3-D material than a 1-D material, and therefore enhance 3-D interchain interactions more readily than may be expected of a lower dimension compound.

Previous a hydrostatical pressure-dependent magnetic study of $[FeCp^*_2]^{\bullet+}[TCNE]^{\bullet-}$ based on AC susceptibility revealed low- and high-pressure regions of magnetic behavior, characterized by different rates of increase of the T_c. Above 5.30

kbar a new, higher temperature magnetic peak was observed at T_1. Upon release of the applied pressure the field dependent magnetization, $M(H)$, revealed complex hysteretic behavior, explained as an irreversible pressure-induced phase transition with incomplete conversion.[14] This was reinvestigated in order to clarify the origin of pressure-induced formation of a metamagnetic-like behavior, as well as understand the increase in T_c with increasing pressure. In addition, the pressure dependence for $[FeCp^*_2][TCNQ]$ is compared with that recently reported for the 0-D ferromagnetic (**FO**) and metamagnetic (**MM**) polymorphs of $[FeCp^*_2][TCNQ]$,[15] as well as 2-D $Mn^{II}(TCNE)I(OH_2)$ and 3-D $Mn^{II}(TCNE)_{3/2}(I_3)_{1/2}\bullet zTHF$.[16]

Experimental

$[FeCp^*_2]^+[TCNE]^-$ was prepared via the literature method.[3] IR and AC susceptibility measurements were used to confirm the purity of the sample. IR spectra were measured from 400 to 4000 cm^{-1} on a Bruker Tensor 37 spectrometer (± 1 cm^{-1}). A Quantum Design Physical Property Measurement System QD PPMS 9 T was used to perform ambient pressure AC susceptibility magnetometry. Samples of **1** (3 - 15 mg) were loaded into gelatin capsules in glovebox atmosphere and sealed with silicone grease prior to PPMS measurements. A Quantum Design (QD) Superconducting Quantum Interference Device (SQUID) Magnetic Property Measurement System (MPMS-5XL 5 T) (sensitivity = 10^{-8} emu or 10^{-12} emu/Oe at 1 T) was used to perform dc pressure dependent measurements, as previously described.[17] Samples of **1** (~1 mg) were loaded into a Teflon^{TM} cell, the remaining volume of the Teflon cell was filled with decalin (the hydrostatic pressure media) and capped with Teflon plugs. The loaded Teflon sample cell was placed in a beryllium-copper hydrostatic pressure cell fabricated at the University of Utah based on the Kyowa Seisakusho design with zirconia pistons and rubber o-rings. Pressure was applied to the assemblage by using a Kyowa Seisakusho CR-PSC-KY05-1 apparatus with a WG-KY03-3 pressure sensor. An Aikoh Engineering Model-0218B digital sensor readout was used as a pressure guide during pressure application.

The T_c was determined from the extrapolation of the most linear portion of the remnant magnetization, $M_r(T)$, to zero magnetization. The bifurcation temperature, T_b,

was taken to be the divergence of the zero-field cooled, $M_{ZFC}(T)$, and field cooled, $M_{FC}(T)$, magnetizations. Isothermal field dependent measurements, $M(H)$, were performed at 2 K. The coercive field, H_{cr}, was determined from the extrapolation of the field intercept at zero magnetization upon reduction of an applied field of ±50 kOe. The M_r was determined from the extrapolation of the magnetization intercept at zero applied field upon reducing the applied field from 50 kOe.

The Aikoh Engineering Model-0218B digital sensor readout is an approximate method for determining pressure, and a superconductor with a known pressure dependent transition temperature was used to calibrate the pressure. Since the $4 < T_c < 8$ K is expected for **1**,[14] no convenient superconducting pressure calibrant was suitable. As reported for [FeCp*$_2$][TCNQ][15] calibration was achieved from a least squares linear regression fit, equation 4.1, where x is the readout from the digital sensor from previous pressure data. The error associated with this correlated fit was assumed to be the standard deviation of the slope and intercept of the linear regression fit propagated through the pressure determination and is 0.048 kbar ($\chi^2 = 0.953$).

$$P = 0.025x - 0.7 \tag{4.1}$$

Results and Discussion

Prior to the study the pressure dependence of the magnetic properties of [FeCp*$_2$][TCNE] the ambient pressure magnetic properties were redetermined and compared to that previously reported to confirm the sample purity. Randomly orientated polycrystalline samples were studied, as this was needed for the hydrostatic pressure studies. The T_c was determined to be 5.11 ± 0.025 K from DC remnant magnetization, $M_r(T)$, measurements and 5.00 ± 0.0125 K determined as the peak of $\chi'(T)$ at 10 Hz. This is in agreement with 4.8 K from $M_r(T)$,[4] 4.74[18] from neutron diffraction,[6] and 4.82 K[19] from adiabatic calorimetry utilizing the drift method.[20] The observed coercive field, H_{cr}, was 540 ± 10 of Oe, the saturation magnetization (M_s) was 12,700 emuOe/mol, and the remnant magnetization, M_r, was 10,500 emuOe/mol. The H_{cr}, M_r, and M_s were expectedly reduced from the values of 1,000 Oe, 10,500 emuOe/mol, and 16,300 emuOe/mol at 2 K, respectively,[4] which were obtained for

aligned large single crystals, which are very anisotropic,[3,4] not the randomly orientated polycrystalline samples that were studied herein.

The DC magnetization of [FeCp*$_2$][TCNE] as a function of temperature, field, and pressure was investigated to complement the previous pressure dependence of the AC susceptibility.[14] Overall, there is general agreement with the previous DC and AC susceptibility measurements as $T_c(P)$ increases with increasing pressure, Table 3.1.

The pressure dependences of the 5 Oe remnant, $M_r(T)$, zero field cooled, $M_{ZFC}(T)$, and field cooled, $M_{FC}(T)$, magnetizations show that the onset temperature at 5.11 K at ambient pressure increases with applied pressure to 7.48 K at 12.2 kbar, Figure 3.1 and Figure 3.2. Concomitantly the magnetization dramatically decreases by six orders of magnitude from 2,345 emuOe/mol at ambient pressure to 0.00644 emuOe/mol at 12.2 kbar (Figure 3.A1). The T_c from the $M_r(T)$ data, and bifurcation temperature, T_b, from the divergence of the $M_{ZFC}(T)$ and $M_{FC}(T)$ data increase to 7.48 and 7.80 K, respectively, at 12.2 ± 0.83 kbar, Figure 3.2, which corresponds to a 46.4 and 51.5% increase at an average rate of 0.21 ± 0.1 K/kbar for $T_c(P)$, which is in accord with ~0.22 K/kbar previously reported from AC data, Figure 3.2.[14] The two rates of T_c increase (0.27 and 0.17 K/kbar at low- and high-pressures regions, respectively) are noted as guides for the eye, based both on the previous AC data and the current study with the two regions bordering between ~4.2 and 5.3 kbar, Figure 3.2. This border region coincides with the onset of T_1, discussed later.

These data suggest that as the applied pressure increases the intermolecular separations decrease enhancing the nearest neighbor intra- and interchain couplings increasing T_c (and T_b). Also, as the antiferromagnetic interchain interactions increase this may lead to canting, which increases with increasing pressure. This leads to a transition from a ferromagnet to a canted antiferromagnet, and as the canting angle increases with pressure the magnetization dramatically decreases with applied pressure. Additionally, the intrachain collinear ferromagnetic coupling between the S = 1/2 $[Fe^{III}Cp^*_2]^{\bullet+}$ and $[TCNE]^{\bullet-}$ lattices[11] may cant with increasing pressure, and also contribute to the canted antiferromagnetic behavior.

Table 3.1. Summary of the ambient and pressure-dependent magnetic behavior for polycrystalline [FeCp*$_2$][TCNE] (1), and the ferromagnetic (FO) and metamagnetic (MM) polymorphs of [FeCp*$_2$][TCNQ].

	P, kbar	Method	T_c, K	Rate, K/kbar	ϕ	T_b, K	Rate, K/kbar	H_{cr}, Oe	M(5 T), emuOe/mol	M_r, emuOe/mol
1	Ambient	$M_r(T)$	4.8[4] 5.11	-		5.15	-	1,000[e,4] 540	16,300[e,4] 12,700	10,500
1	12.2	$M_r(T)$	7.48	0.20		7.80	0.22	3,450	11,000	1,840
1	Ambient	ND[a]	4.74[18]	-		-	-	-	-	-
1	Ambient	C_p[b]	4.82[19]	-		-	-	-	-	-
1	Ambient	AC	4.95[e,12]	-	0.008					
1	Ambient	AC	5.1[d,14]	-						
1	13.75[14]	AC	7.85[14]	0.22[14]	-	-	-	-	-	-
FO	Ambient	AC	3.1[21]	-		-	-	-	-	-
FO	Ambient	$M_r(T)$	2.95[15]	-		2.92[15]	-	-	16,740[21]	-
FO	10.3	$M_r(T)$	5.01[15]	0.21[15]		5.46[15]	0.25[15]	550[15]	11,000[15]	8,880[15]
MM	Ambient	AC	2.5[21]	-		-	-	-	-	-
MM	Ambient	d(χT)/d T	2.10[15]	-		-	-	-	15,900[21]	-
MM	2.9	d(χT)/d T	2.90[15]	0.28[15]		-	-	-	14,600[f,15]	-

[a] Neutron diffraction [b] Heat capacity [c] T_f (10 Hz) [d] T_f (16 Hz) [e] Aligned single crystal

[f] 9.2 kbar

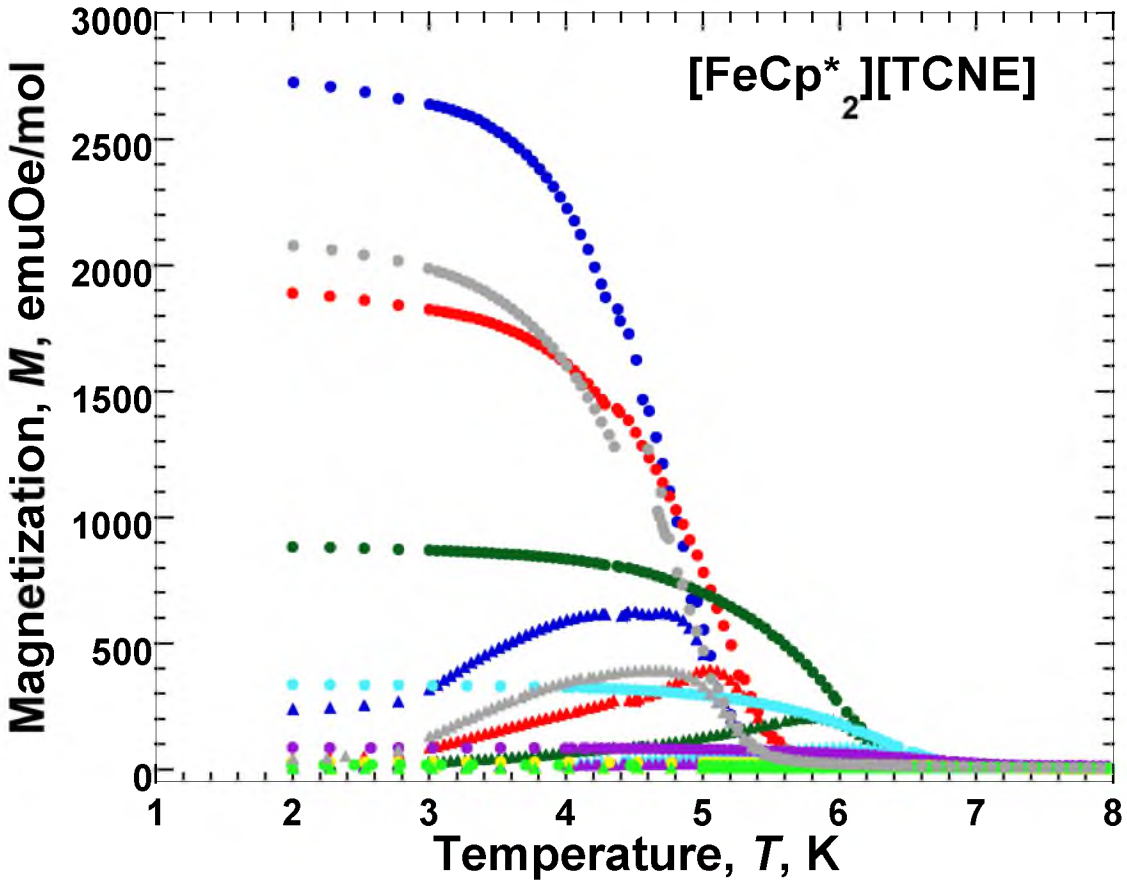

Figure 3.1. Pressure dependence of $M_r(T)$ (triangles), $M_{ZFC}(T)$ (circles), and $M_{FC}(T)$ (squares) of [FeCp*$_2$][TCNE] at 0.001 (●), 1.9 (●), 4.2 (●), 5.9 (●), 12.2 kbar (●), pressure released to 0.001 kbar (●).

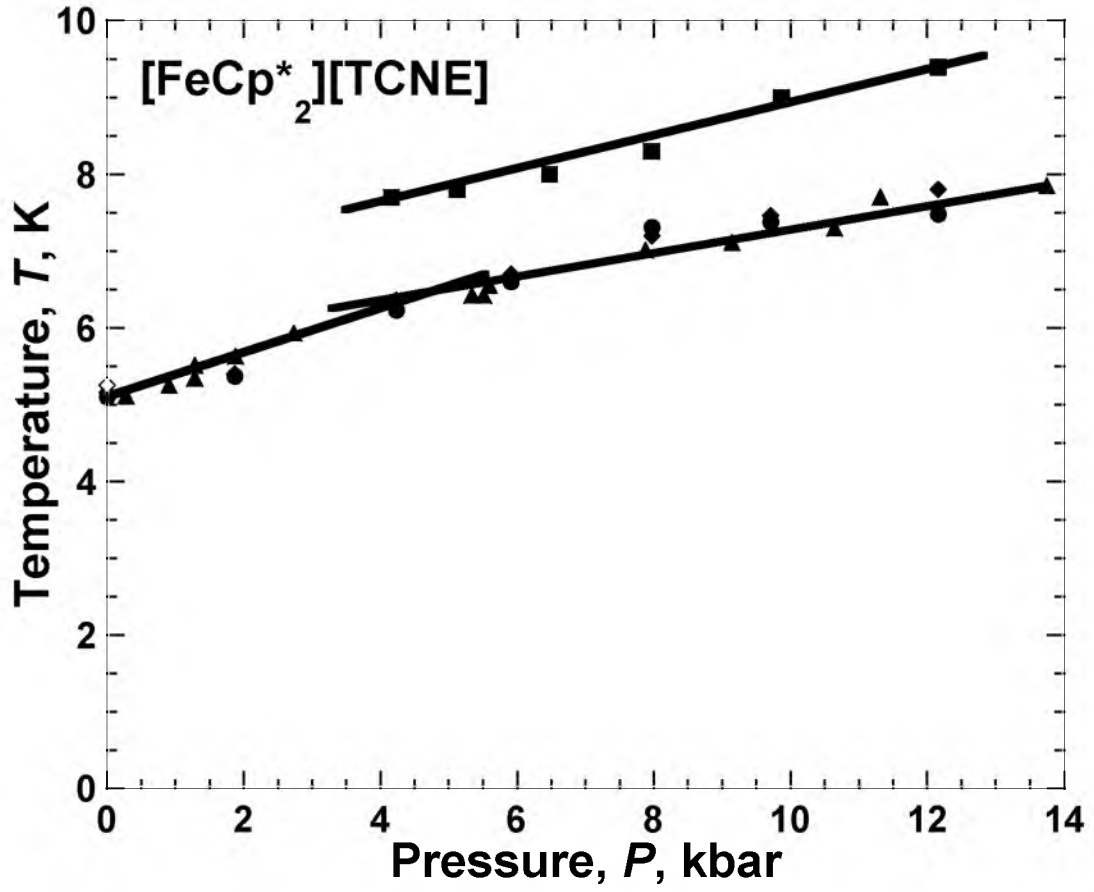

Figure 3.2. $T_c(P)$ (●), $T_b(P)$ (◆), and T_1 (■) (see text) determined from $M_{FC}(T,P,100$ Oe) (peaks were not observed below 4.2 kbar) for [FeCp*$_2$][TCNE] (the released pressure data are hollow symbols). The pressure error bars are approximately the size of the data points. $T_c(P)$ (▲) previously reported from AC susceptibility data.[14] The lines are guides for the eye.

The 2 K $M(H)$ has a H_{cr}, M_r, and M_s of 540 Oe, 10,500 emuOe/mol, and 12,700 emuOe/mol, respectively, at ambient pressure. With increasing applied pressure the H_{cr} gradually increases up to ~4.2 kbar, and then more steeply, but linearly to 3,450 Oe at 12.2 kbar, Figure 3.3 and Figure 3.4. The discontinuous increase of the H_{cr} coincides with an abrupt growth of the H_c, when the H_c is taken as a composite of the H_c and projected H_c of the low- and high-pressure data, Figure 3.4. The projected H_c was calculated from the virgin curve of $M(H)$ measurements performed below ~4.2 kbar and is not physically representative of H_c as the compound neither exhibits metamagnetic nor canted antiferromagnetic behavior at these pressures. In contrast, the M_r decreased by 82% to 1,840 emuOe/mol at 12.2 kbar, while the M_s decreases slightly to 11,000 emuOe/mol, Figure 3.3.

The shape of the hysteresis loop was qualitatively altered at 4.2 kbar, and became more constricted-like. At higher pressures the hysteresis resembles that of a canted antiferromagnet, with a large coercive field.[5,22] An *S*-shaped virgin curve occurs for all pressures, but was determined not to be indicative of a critical field, H_c, below ~4.2 kbar, Figure 3.3 and Figure 3.4, as a peak in dM/dH, i.e., H_c, was not evident. *S*-shaped virgin curves are suggestive of spin glass behavior in ferromagnetic materials.[23] Weak spin glass behavior has been observed for **1** from AC studies, for which the figure of merit, ϕ, is 0.008.[12,24] ϕ is a measure of the frequency shift of the freezing temperature, T_f, equation 4.1,

$$\phi = \frac{\Delta T_f}{\left[T_f \Delta(\log \omega)\right]},^{25} \tag{3.1}$$

where ω is the applied magnetic field frequency. The previous AC susceptibility pressure study revealed unexpected metamagnetic-like behavior above 5.30 kbar, which manifested as a second peak in the $\chi'(T)$ at higher temperature (with a peak at ~6.8 K at 5.49 kbar), while the ambient phase peak remained present.[14] The coexistence of these absorptions was interpreted as a partial conversion of the ferromagnetic phase to a high-pressure metamagnetic phase.[14] The discontinuities in the $H_{cr}(P)$ and $H_c(P)$ data, Figure 3.4, are consistent with the previously observed onset of the hypothesized metamagnetic

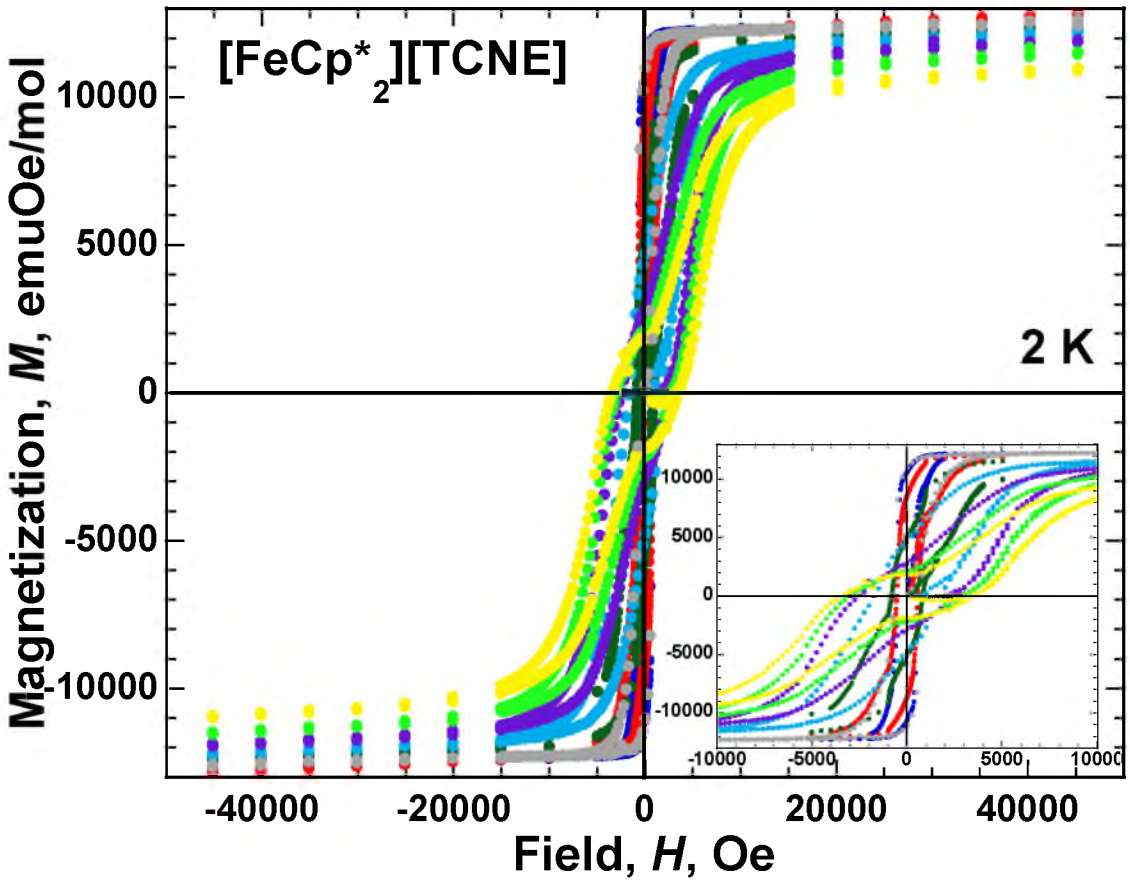

Figure 3.3. 2 K hysteretic $M(H,P)$ plots of $[FeCp^*_2]^+[TCNE]^-$ at 0.001 (●), 1.9 (●), 4.2 (●), 5.9 (●), 8.0 (●), 9.7 (●), 12.2 kbar (●), pressure released to 0.001 kbar (●).

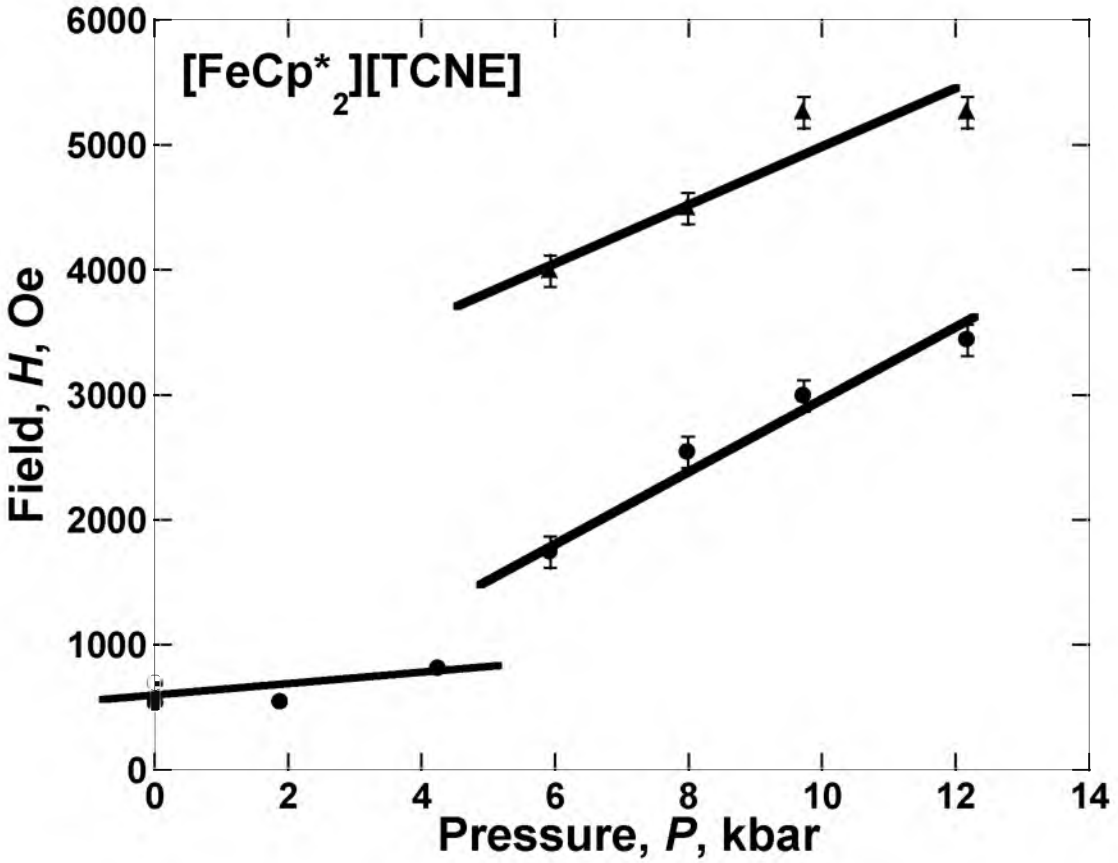

Figure 3.4. 2 K $H_{cr}(P)$ (●), and $H_c(P)$ (▲) of [FeCp*$_2$][TCNE]; released pressure data are hollow symbols. The lines are guides for the eye.

phase.[14]

The metamagnetic-like behavior was further investigated through the measurement of $M_{FC}(T,P)$ at several applied fields in order to track the temperature, pressure, and field dependences concurrently. The higher temperature peak attributed to metamagnetic-like behavior,[14] T_1, was observed only at and above 20 Oe applied fields and 4.2 kbar.[26] T_1 was identified from the $d(\chi T)/dT$ of the $M_{FC}(T,P,H)$ data as the local maximum, at intermediate pressures where the peak was weakly expressed, and the temperature intercept at high pressures where the peak was well resolved. From the 100 Oe $M_{FC}(T,P)$ data, T_1 increases from 7.7 K at 4.2 kbar to 9.4 K at 12.2 kbar at an average rate of ~0.23 K/kbar, Figure 3.5.

This rate of increase is 21% less than the AC determined rate of 0.29 K/kbar,[14] and may be explained from the poorly resolved peaks at intermediate pressures, which shift to lower temperature with increasing applied field, Figure 3.2 and Figure 3.6. The $M_{FC}(T,P,H)$ data exhibit the same trend as the reduced spontaneous magnetization with increasing pressure occurs for $M_r(T,P)$, $M_{ZFC}(T,P)$, and $M_{FC}(T,P)$, Figure 3.2. A unique field dependence of the spontaneous magnetization was observed at each applied pressure; first increasing with increasing field up to 200 Oe, then decreasing abruptly at 300 Oe and approximately maintaining the same value up to 1,000 Oe where another abrupt decrease was observed, then increasing significantly up to 3,000 Oe, and finally decreasing again at 5,000 Oe, Figure 3.6. While all of the data in Figure 3.6 is at 6.5 kbar, similar data were obtained at each pressure, but these are not shown in order to more easily display the trends of the compounds behavior (Figures 3.A12-3.A19). Additionally, plots of a single applied field and several pressures were prepared (Figures 3.A2-3.A11).

The $M_{FC}(T,P,H)$ data confirm the onset of complex magnetic behavior at ~4.2 kbar, and suggest that this behavior does not result from the formation of a pressure-induced phase. It was previously hypothesized that the secondary higher temperature peak in the $\chi'(T)$ data was indicative of incomplete conversion to a pressure-induced metamagnetic phase, as the primary peak remained and continued to shift to higher temperatures with additional pressure applications.[14] Thus, as expected this is observed in the $M_{FC}(T,P,H)$ data below the H_c, Figure 3.6, where the metamagnetic phase

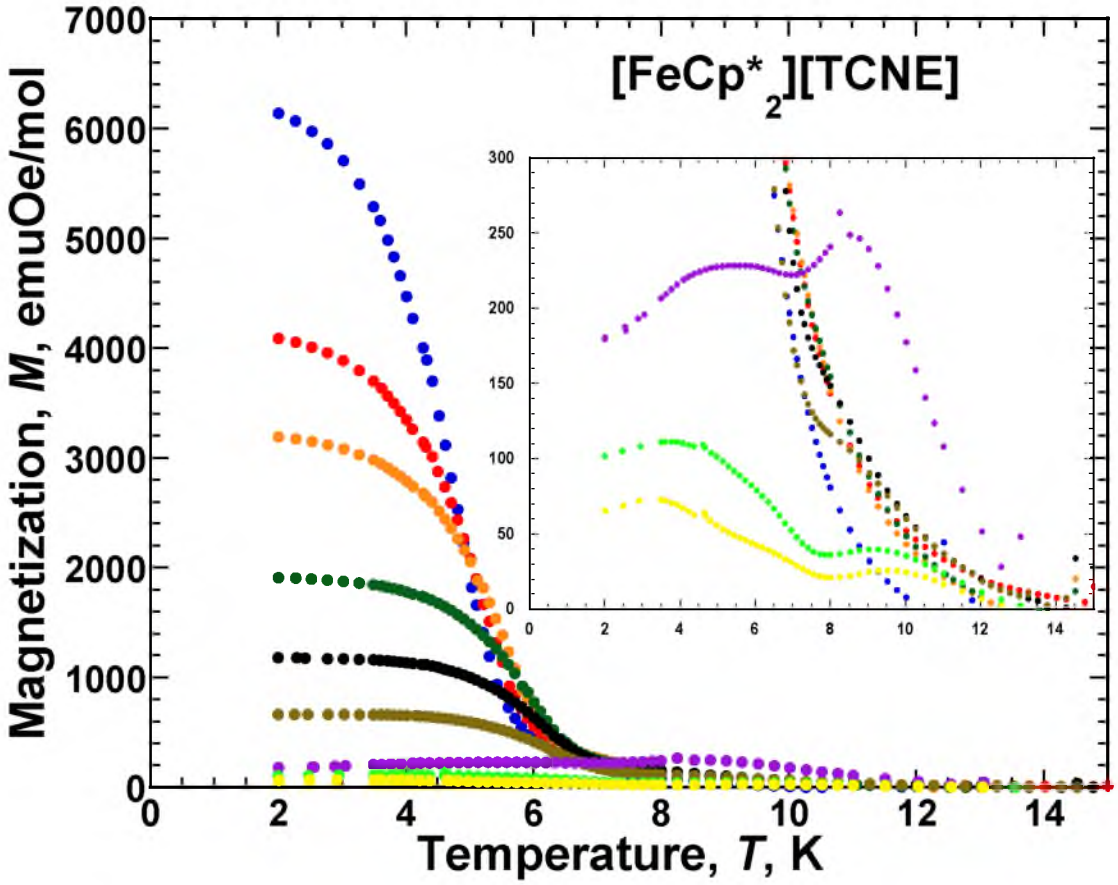

Figure 3.5. $M_{FC}(T,P,100\ Oe)$ at 0.4 (●), 2.2 (●), 3.1 (●), 4.2 (●), 5.1 (●), 6.5 (●), 8.0 (●), 9.9 (●), 12.2 kbar (●). Inset displays a zoomed view about the 8.0 kbar and greater applied pressure measurements. These data are representative of the data obtained at other applied fields (see Figures 3.A2-3.A11).

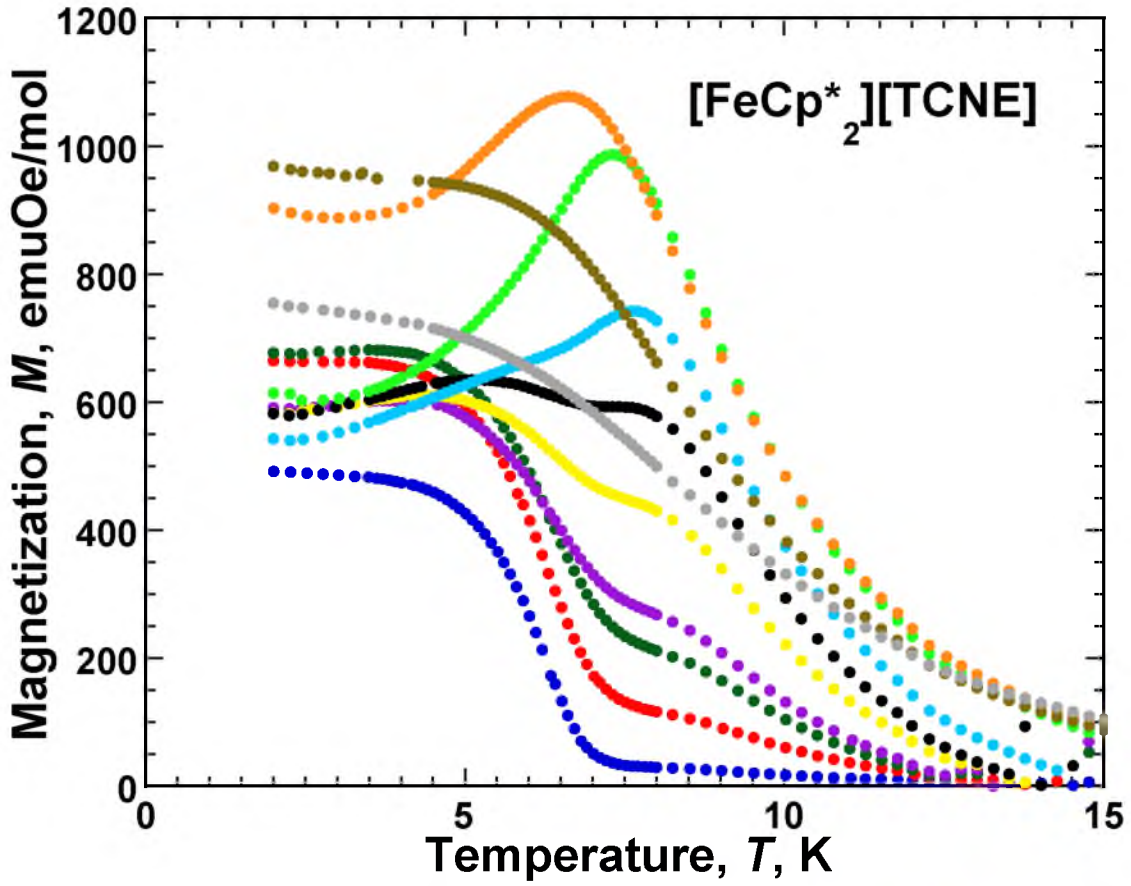

Figure 3.6. $M_{FC}(T,6.5\ \text{kbar},H)$ at 20 (●), 100 (●), 200 (●), 300 (●), 500 (●), 700 (●), 1,000 (●), 1,500 (●), 2,000 (●), 3,000 (●), and 5,000 Oe (●). These data are representative of the data obtained at other pressures (see Figures 3.A12-3.A19).

behaves as an antiferromagnet exhibiting a cusp in the in the $M_{FC}(T,P)$ data around the Néel temperature, T_N, for antiferromagnetic ordering. At successively higher applied fields approaching and exceeding the H_c when **1** is in the ferromagnetic-like state, the cusp in the $M_{FC}(T,P)$ data disappears as expected. However, below 20 Oe the antiferromagnetic cusp is not observed. Furthermore, the $M_{FC}(T,P)$ above H_c do not exhibit the low temperature behavior expected from a mixture of a metamagnet and a ferromagnet.

By contrast to the behavior of two distinct phases, vide supra, the $M_{FC}(T,P,H)$ data display the T_1 peak at intermediate fields between 100 and 3,000 Oe and pressures equal to or above 4.2 kbar. In the case of the multiphase hypothesis,[14] the field dependence of the metamagnetic phase suggests that the metamagnetic phase is dominant only at intermediate fields and that the ferromagnetic phase suppresses the metamagnetic phase at both low and high fields. This behavior is unprecedented, and, thus, the $M_{FC}(T,P)$ data suggest that complex monophasic magnetic behavior is pressure-induced.

Upon release of applied pressure the metamagnetic-like behavior was not observed and full reversibility was confirmed through the T_c, T_b, H_{cr}, and H_c, which were consistent with ambient pressure measurements. This was not the behavior expected from the previous AC study, where the metamagnetic-like behavior was evident in the released ambient pressure $M_{FC}(T)$ and $M(H)$ measurements.[14] The lack of reversibility in previous study is attributed to a portion of the sample cell remaining under applied pressure after release of applied pressure to the whole the pressure system. This was previously observed during experimentation, but not published, and arose from folding of the sample cell when pressurized.

Conclusion

The pressure dependent DC magnetic investigation of **1** yielded an enhancement of the T_c from 5.11 K at ambient pressure to 7.48 K at 12.2 kbar at an average rate of ~0.21 K/kbar, and the T_b from 5.15 to 7.80 K at an average rate of ~0.22 K/kbar in agreement with previous AC data under pressure.[14] The field dependent pressure measurements clearly displayed the onset of complex magnetic behavior at 4.2 kbar as a

distinct deviation from typically shaped hysteretic loops to a more constricted shape. The field dependent properties also revealed the onset of complex behavior through the discontinuous increase in H_{cr} from 540 to 3,450 Oe, and the onset of H_c, which grew to 5,270 Oe at 12.2 kbar. $M_{FC}(T,P,H)$ data suggest that the previous hypothesis of a pressure induced metamagnetic phase does not appropriately describe all of the observed magnetic behavior. The spin glass behavior and theoretical antiferromagnetic coupling pathways[11] support the hypothesis that **1** exhibits complex magnetic behavior arising from competing ferro- and antiferromagnetic coupling pathways, not a phase transition. Thus, at ambient pressure ferromagnetic behavior is dominant, as previously reported;[2,3,4,5,11] however, with increasing pressure the intermolecular separations decrease increasing the nearest neighbor ferromagnetic and antiferromagnetic couplings.[11] This, in turn, increases the T_c (and T_b), while these competing couplings can lead to canting that will increase with increasing pressure. Thus, the magnetization dramatically decreases with applied pressure. Structure determinations as a function of pressure and supporting theoretical and computational investigations enabling the prediction the pressure dependence of the couplings should identify the origins of the observed complex magnetic behavior.

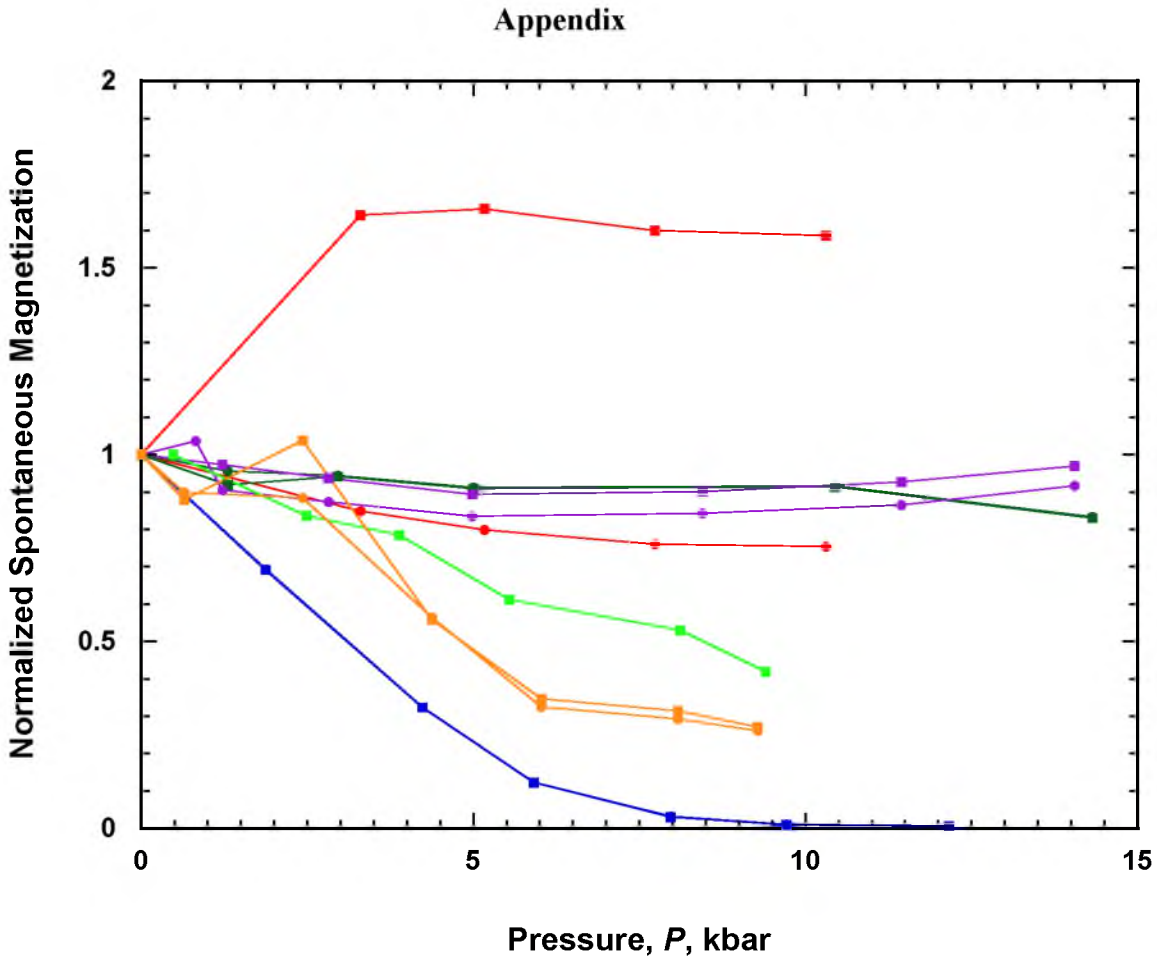

Figure 3.A1. The spontaneous magnetization taken from the M_{FC} (●) and $M_r(T)$ (▪) of $[FeCp^*_2]^{\bullet+}[TCNE]^{\bullet-}$ blue, ferromagnetic $[FeCp^*_2]^{\bullet+}[TCNQ]^{\bullet-}$ red, $[Ru_2(O_2CBu^t)_4]_3[Fe(CN)_6]\bullet 2H_2O$ orange, $[Ru_2(O_2CBu^t)_4]_3[Cr(CN)_6]\bullet 2H_2O$ bright green, $Mn(TCNE)I(OH_2)$ purple, and $Mn^{II}(TCNE)_{3/2}(I_3)_{1/2}\bullet zTHF$ green. All values have been normalized to the corresponding ambient pressure value.

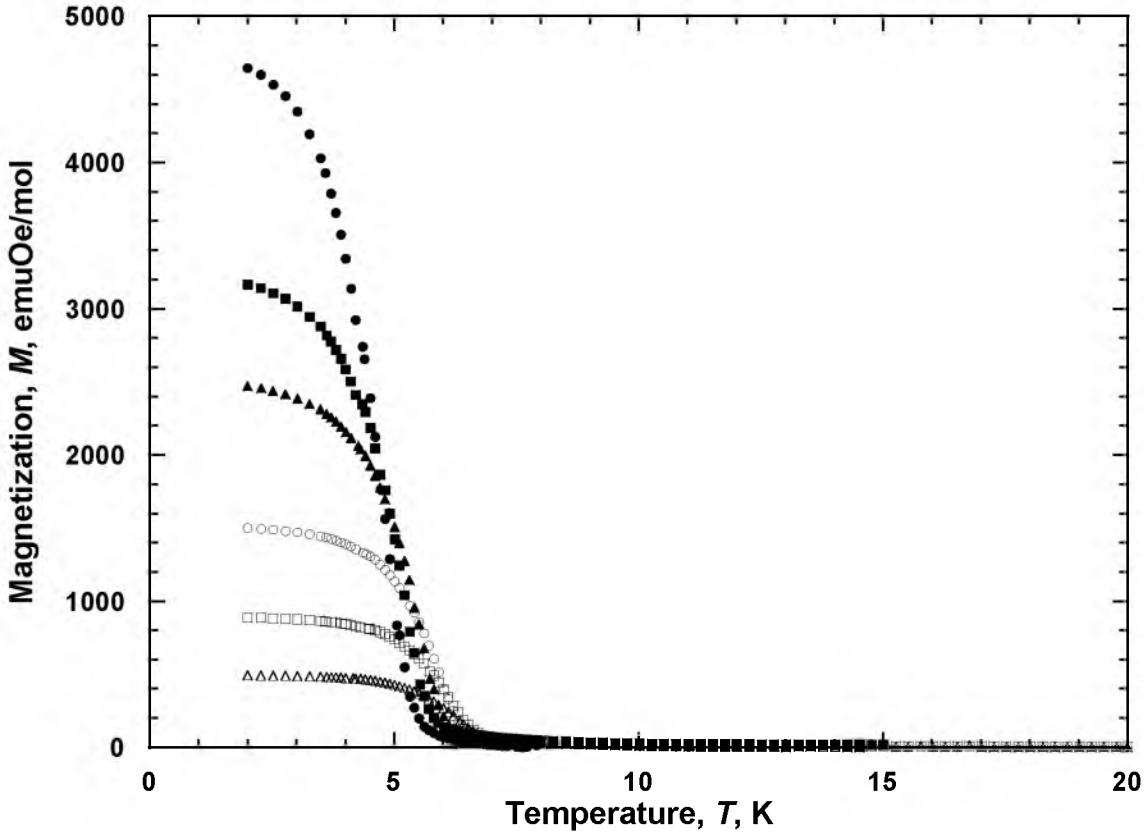

Figure 3.A2. $M_{FC}(T,P)$ at 20 Oe and 0.4 (●), 2.2 (■), 3.1 (▲), 4.2 (○), 5.1 (□), and 6.5 (Δ) kbar.

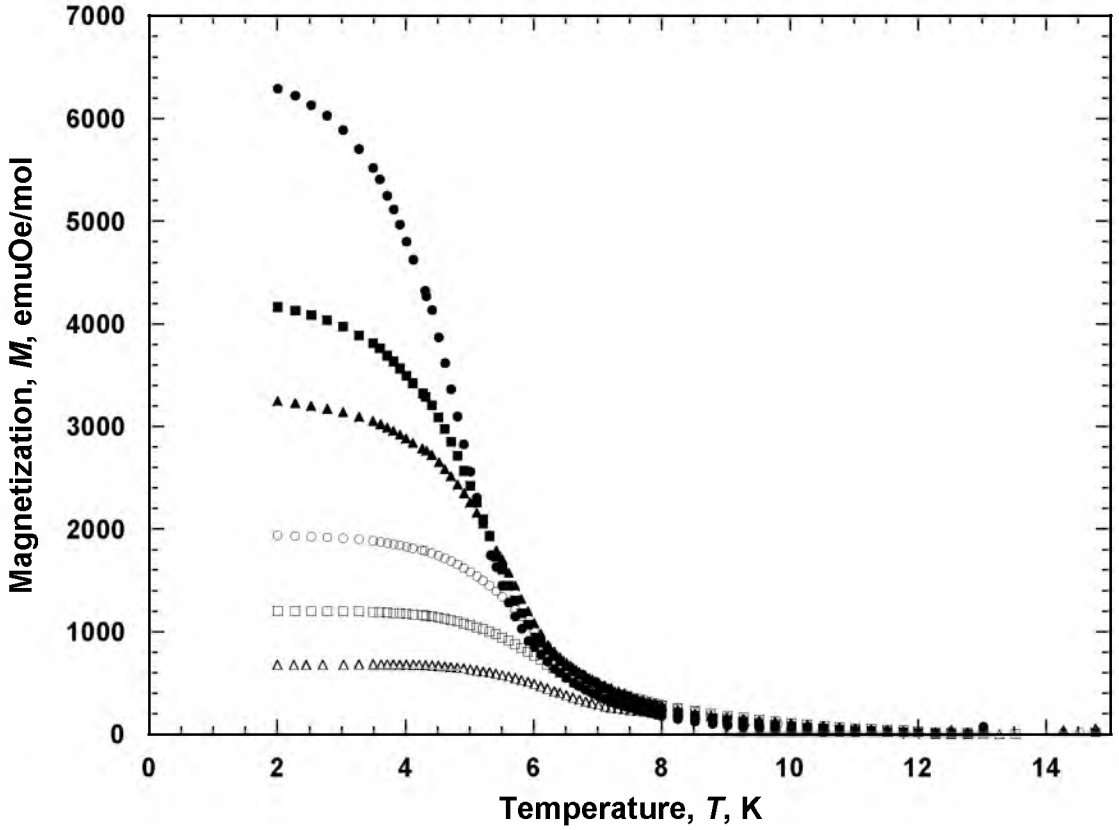

Figure 3.A3. $M_{FC}(T,P)$ at 200 Oe and 0.4 (●), 2.2 (■), 3.1 (▲), 4.2 (○), 5.1 (□), and 6.5 (Δ) kbar.

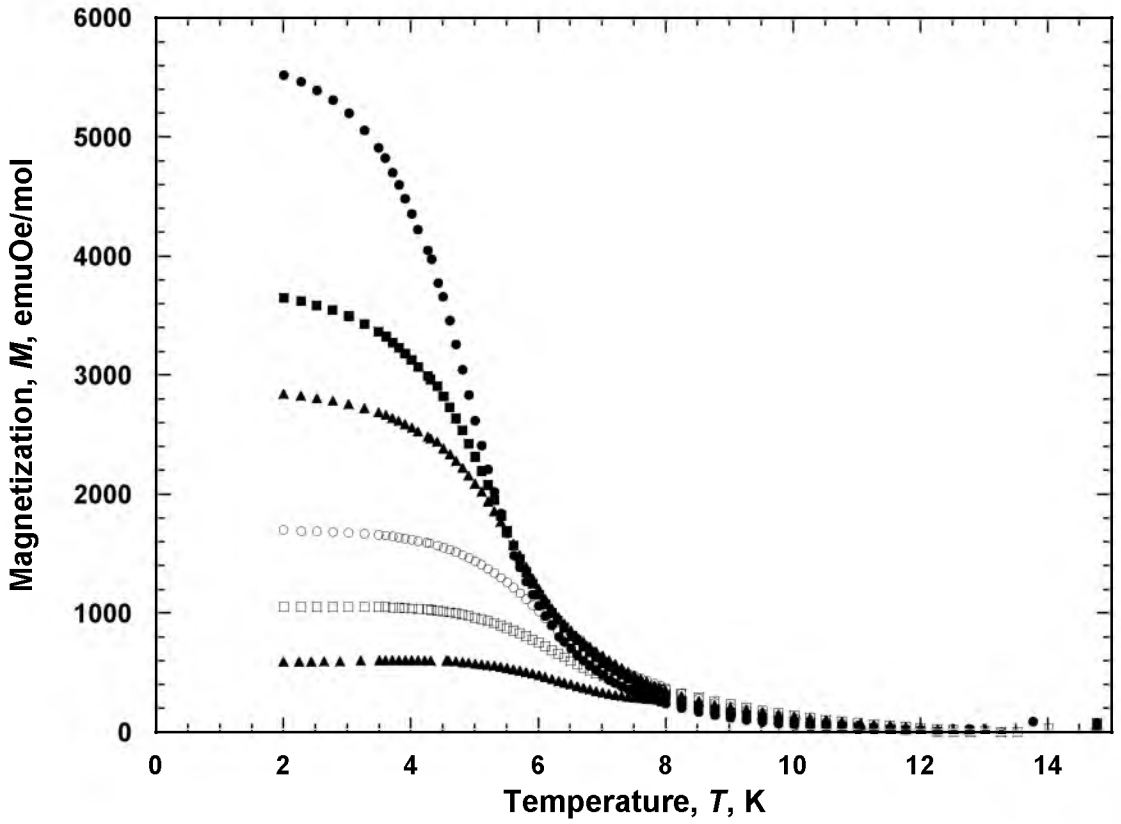

Figure 3.A4. $M_{FC}(T,P)$ at 300 Oe and 0.4 (●), 2.2 (■), 3.1 (▲), 4.2 (○), 5.1 (□), and 6.5 (Δ) kbar.

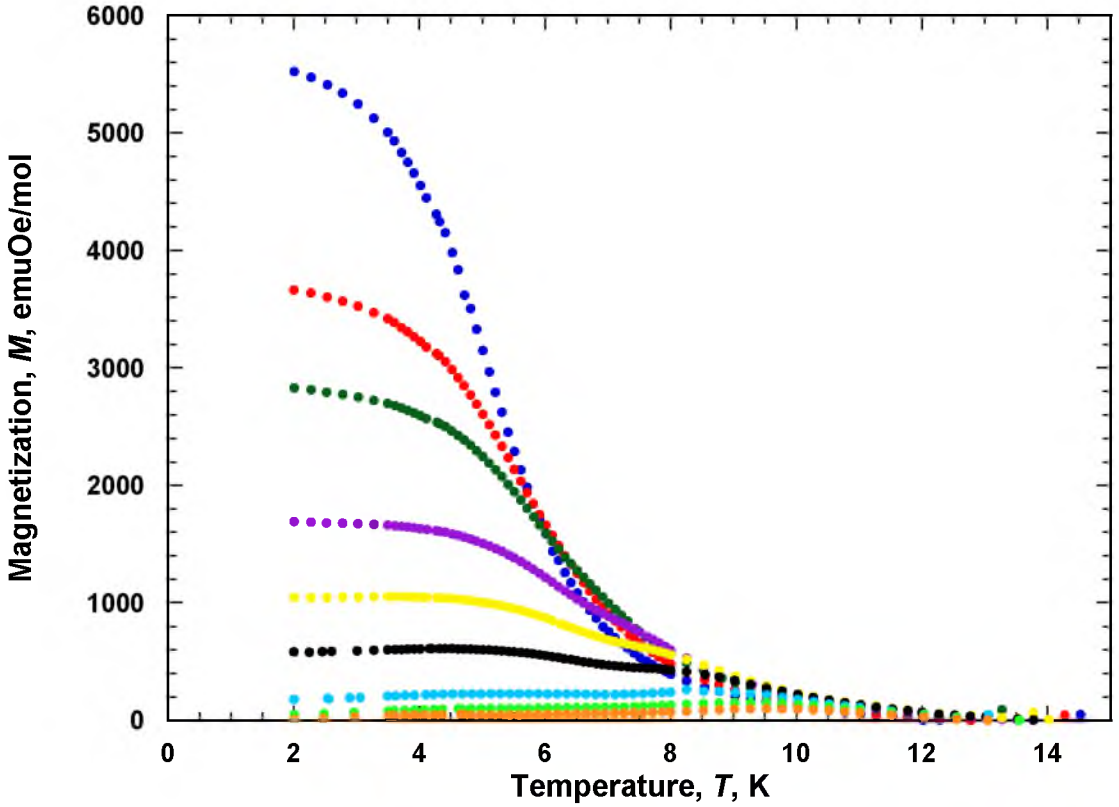

Figure 3.A5. $M_{FC}(T,P)$ at 500 Oe and 0.4 (●), 2.2 (●), 3.1 (●), 4.2 (●), 5.1 (●), 6.5 (●), 8.0 (●), 9.9 (●), and 12.2 (●) kbar.

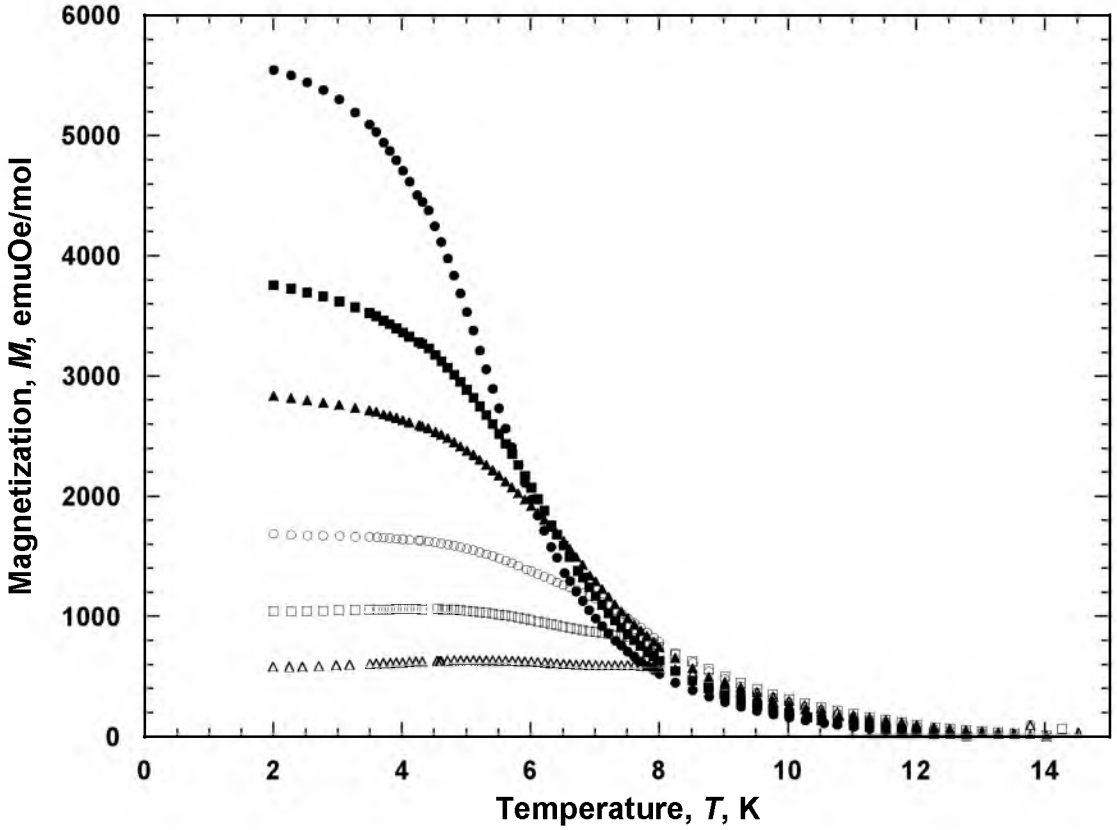

Figure 3.A6. $M_{FC}(T,P)$ at 700 Oe and 0.4 (●), 2.2 (■), 3.1 (▲), 4.2 (○), 5.1 (□), and 6.5 (Δ) kbar.

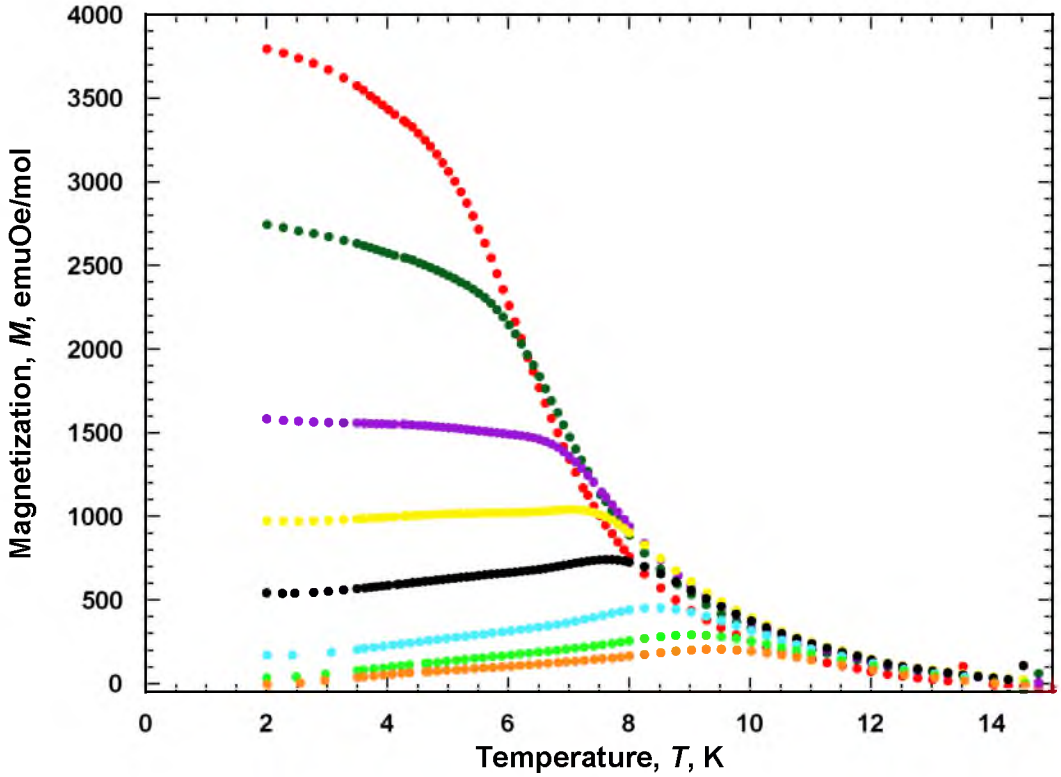

Figure 3.A7. $M_{FC}(T,P)$ at 1000 Oe and 2.2 (●), 3.1 (●), 4.2 (●), 5.1 (●), 6.5 (●), 8.0 (●), 9.9 (●), and 12.2 (●) kbar.

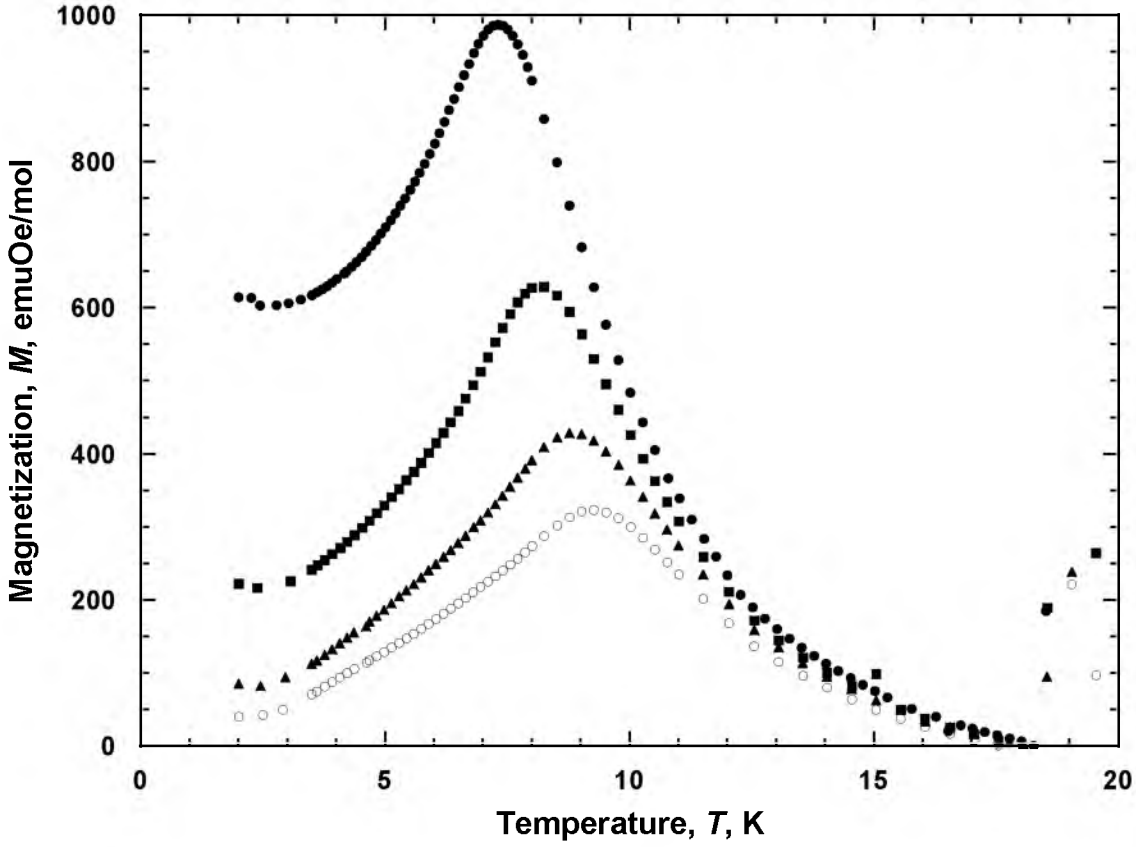

Figure 3.A8. $M_{FC}(T,P)$ at 1500 Oe and 6.5 (●), 8.0 (■), 9.9 (▲), and 12.2 (○) kbar.

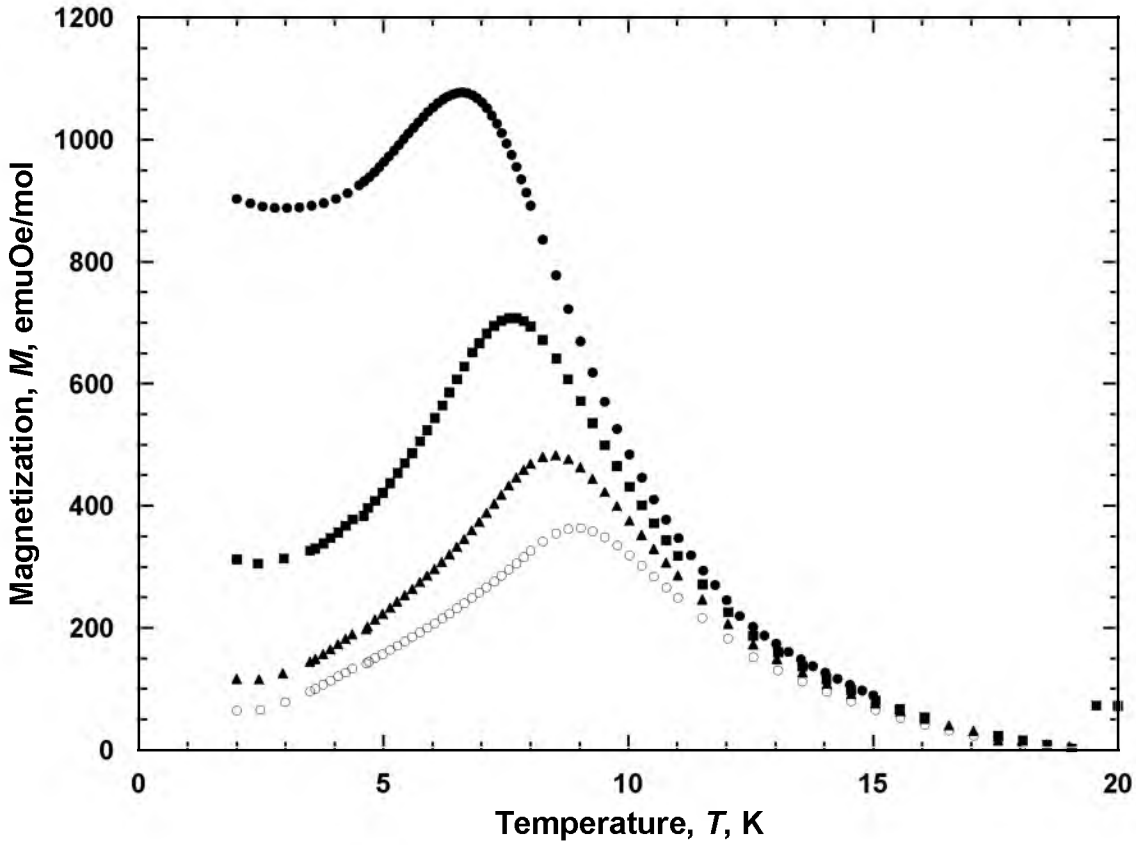

Figure 3.A9. $M_{FC}(T,P)$ at 2000 Oe and 6.5 (●), 8.0 (■), 9.9 (▲), and 12.2 (○) kbar.

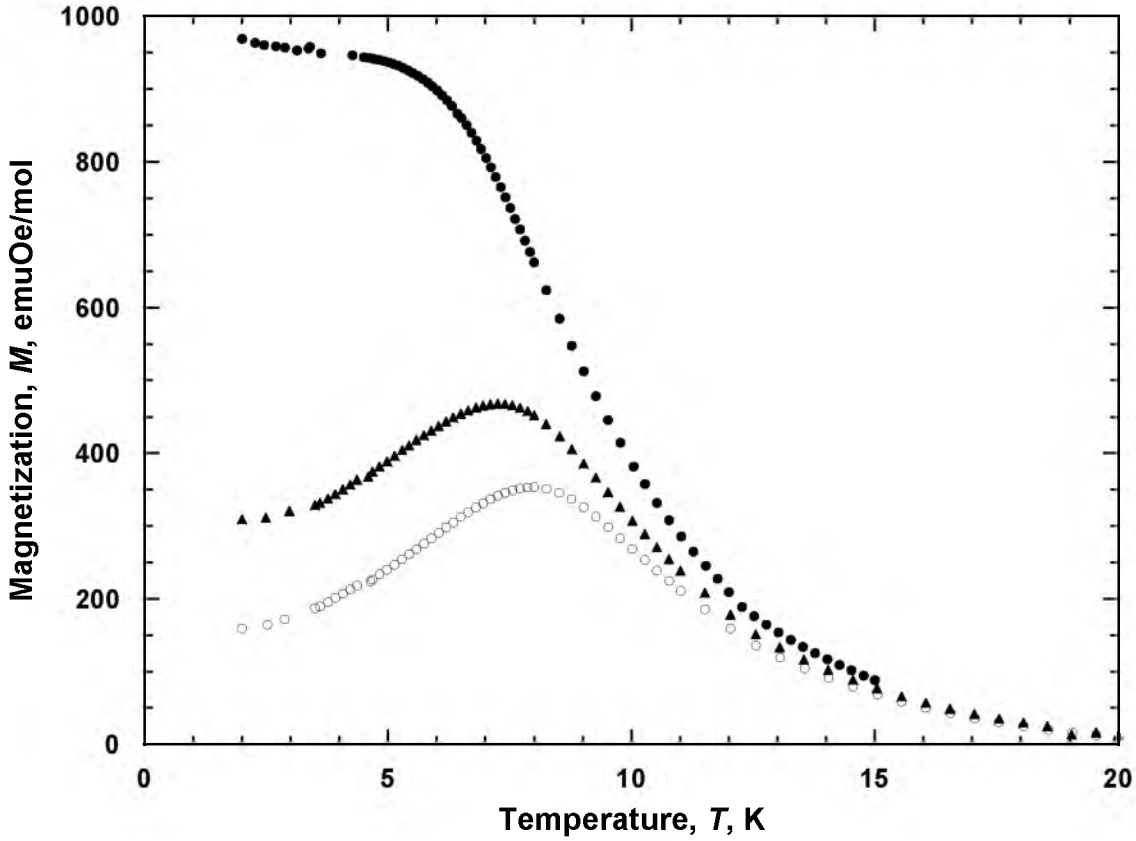

Figure 3.A10. $M_{FC}(T,P)$ at 3000 Oe and 6.5 (●), 9.9 (▲), and 12.2 (o) kbar.

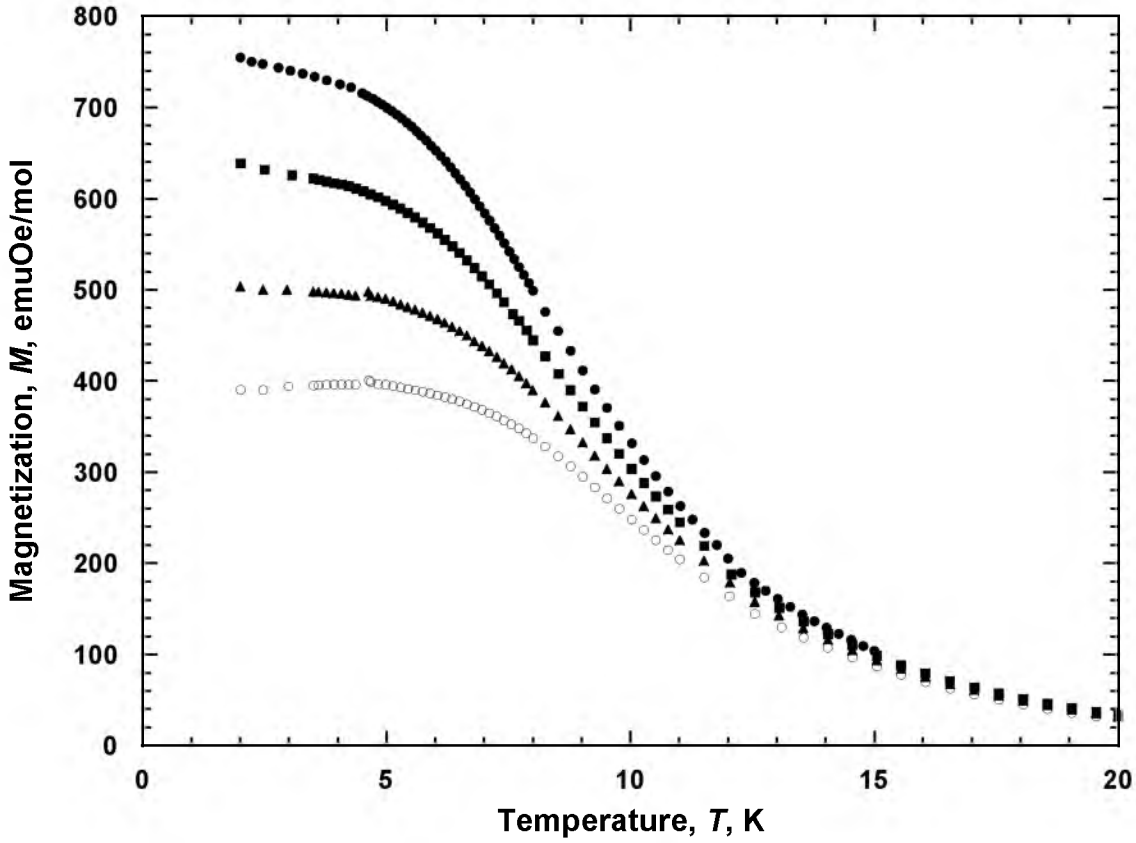

Figure 3.A11. $M_{FC}(T,P)$ at 5000 Oe and 6.5 (●), 8.0 (■), 9.9 (▲), and 12.2 (○) kbar.

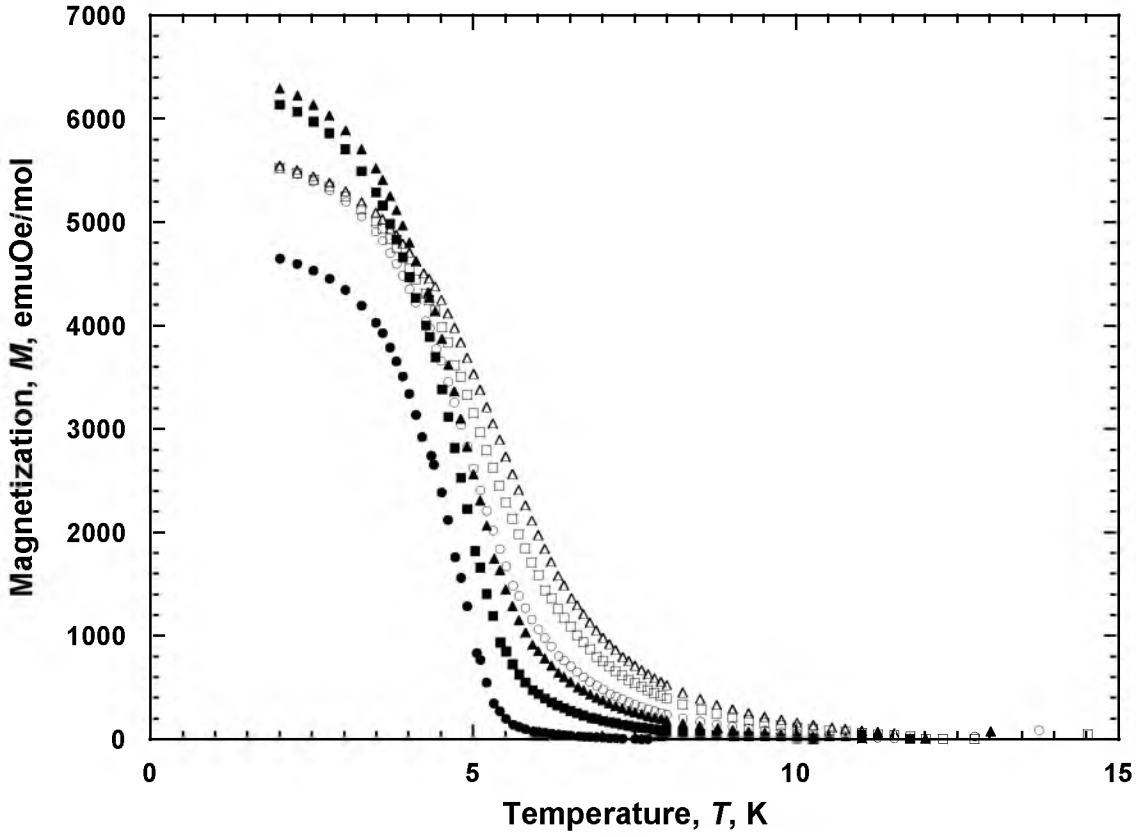

Figure 3.A12. $M_{FC}(T,P)$ at 0.4 kbar and 20 (●), 100 (■), 200 (▲), 300 (○), 500 (□), and 700 (Δ) Oe.

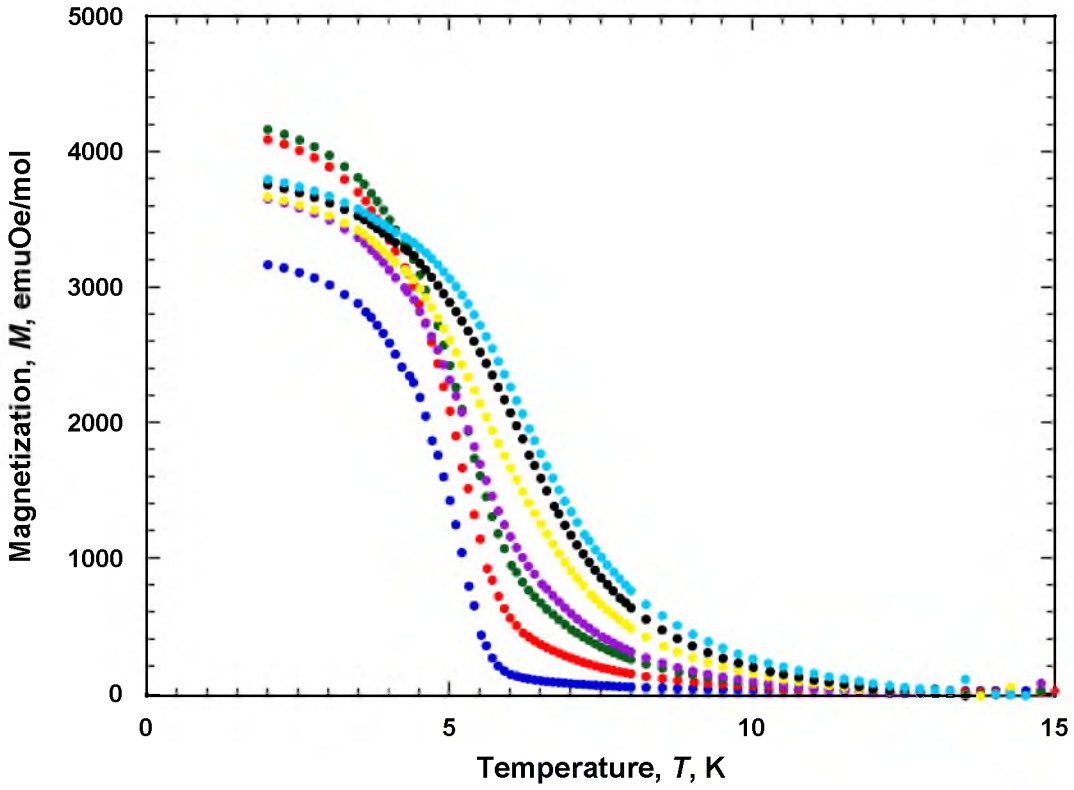

Figure 3.A13. $M_{FC}(T,P)$ at 2.2 kbar and 20 (●), 100 (●), 200 (●), 300 (●), 500 (●), 700 (●), and 1000 (●) Oe.

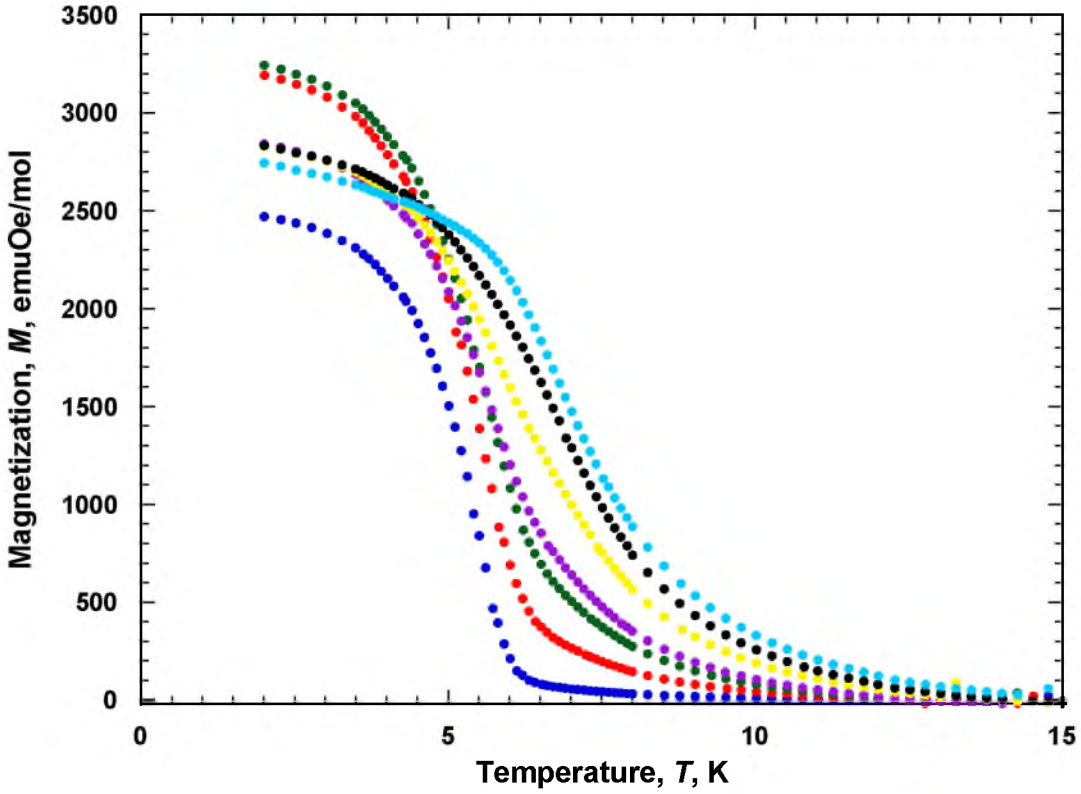

Figure 3.A14. $M_{FC}(T,P)$ at 3.1 kbar and 20 (●), 100 (●), 200 (●), 300 (●), 500 (●), 700 (●), and 1000 (●) Oe.

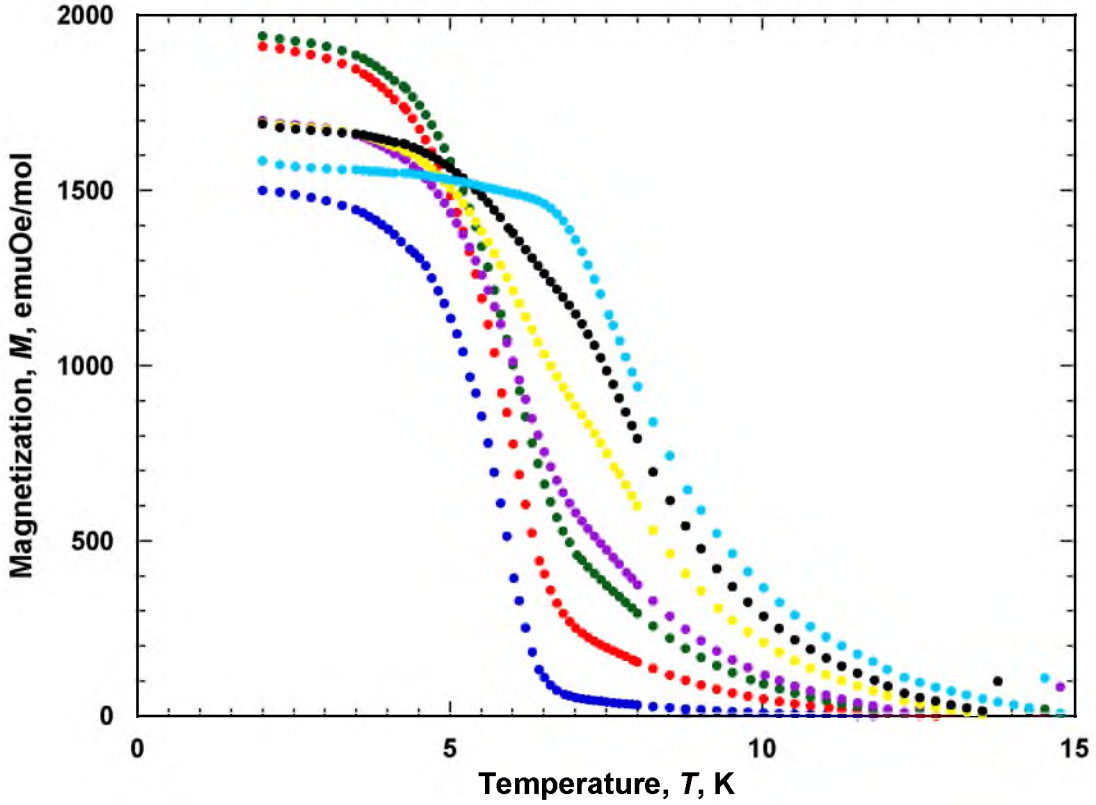

Figure 3.A15. $M_{FC}(T,P)$ at 4.2 kbar and 20 (●), 100 (●), 200 (●), 300 (●), 500 (●), 700 (●), and 1000 (●) Oe.

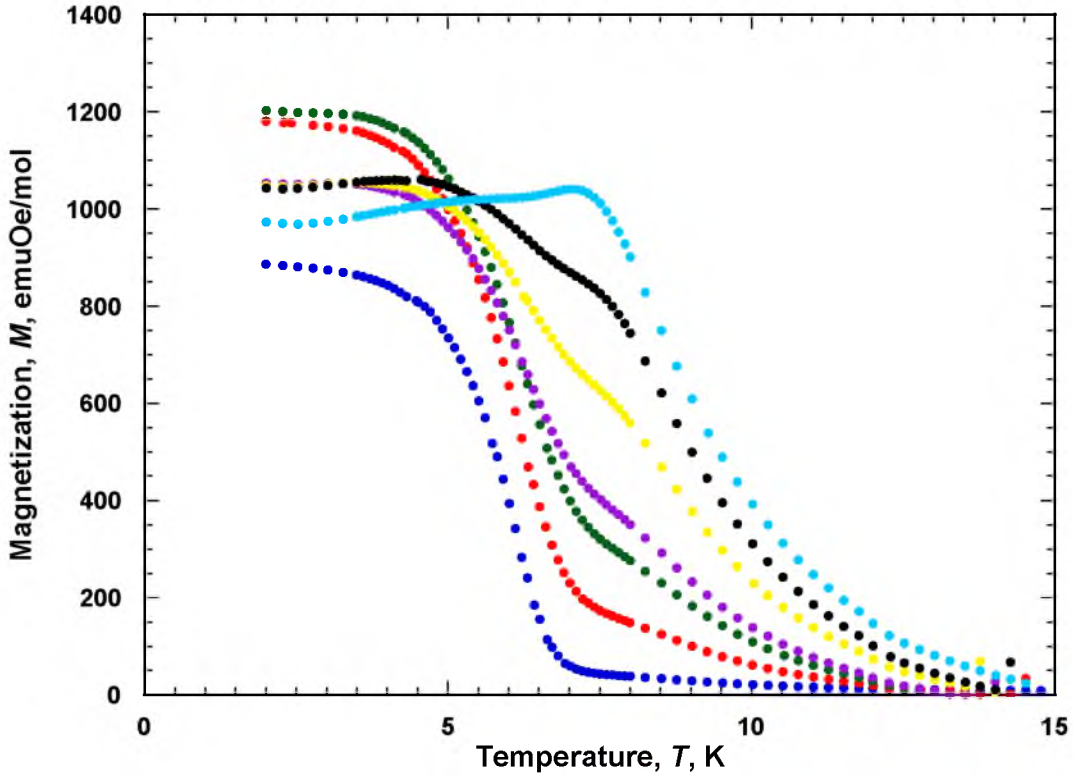

Figure 3.A16. $M_{FC}(T,P)$ at 5.1 kbar and 20 (●), 100 (●), 200 (●), 300 (●), 500 (●), 700 (●), and 1000 (●) Oe.

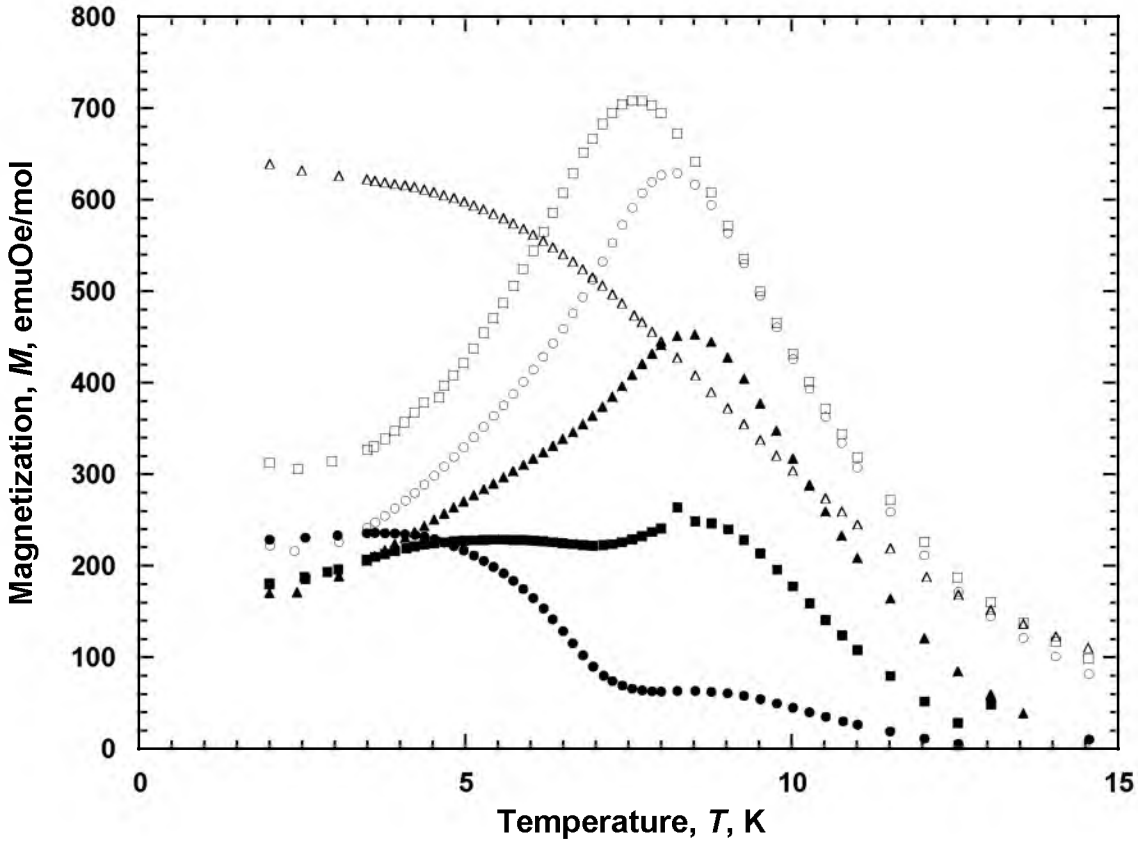

Figure 3.A17. $M_{FC}(T,P)$ at 8.0 kbar and 100 (●), 500 (■), 1000 (▲), 1500 (○), 2000 (□), and 5000 (Δ) Oe.

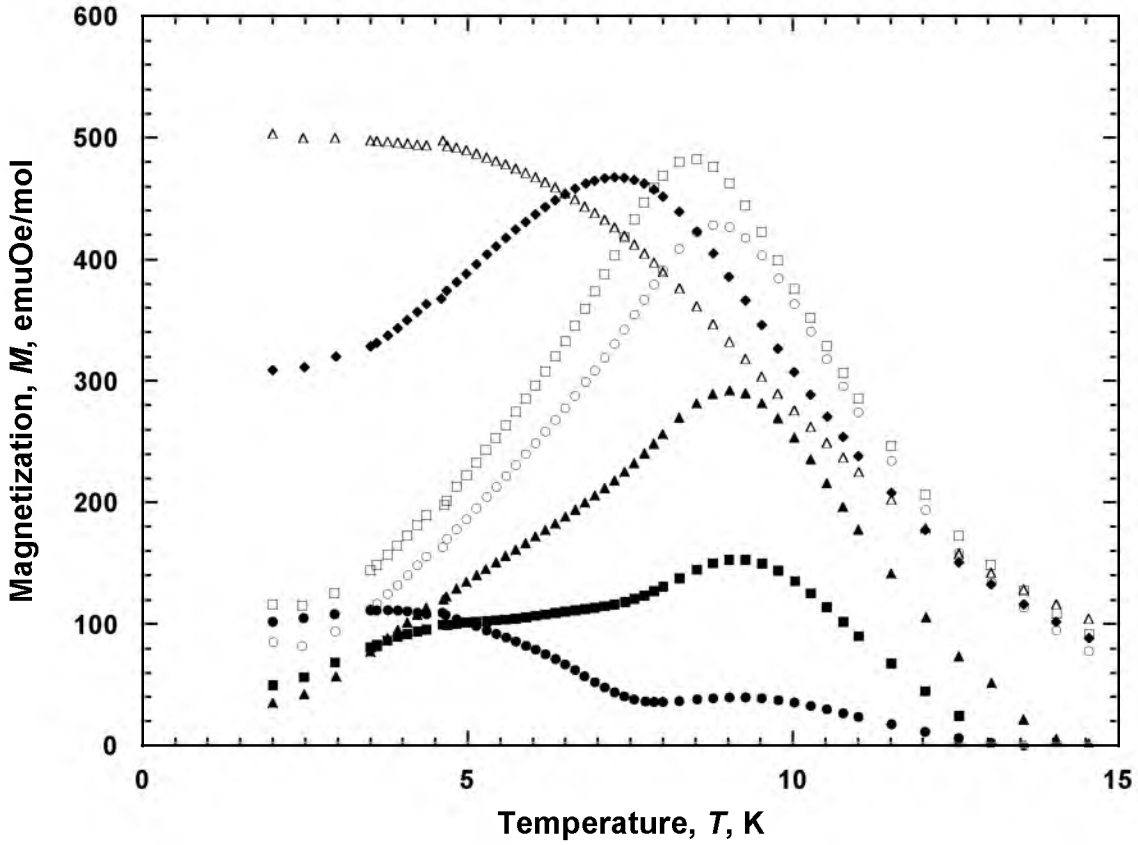

Figure 3.A18. $M_{FC}(T,P)$ at 9.9 kbar and 100 (●), 500 (■), 1000 (▲), 1500 (○), 2000 (□), 3000 (◆), and 5000 (Δ) Oe.

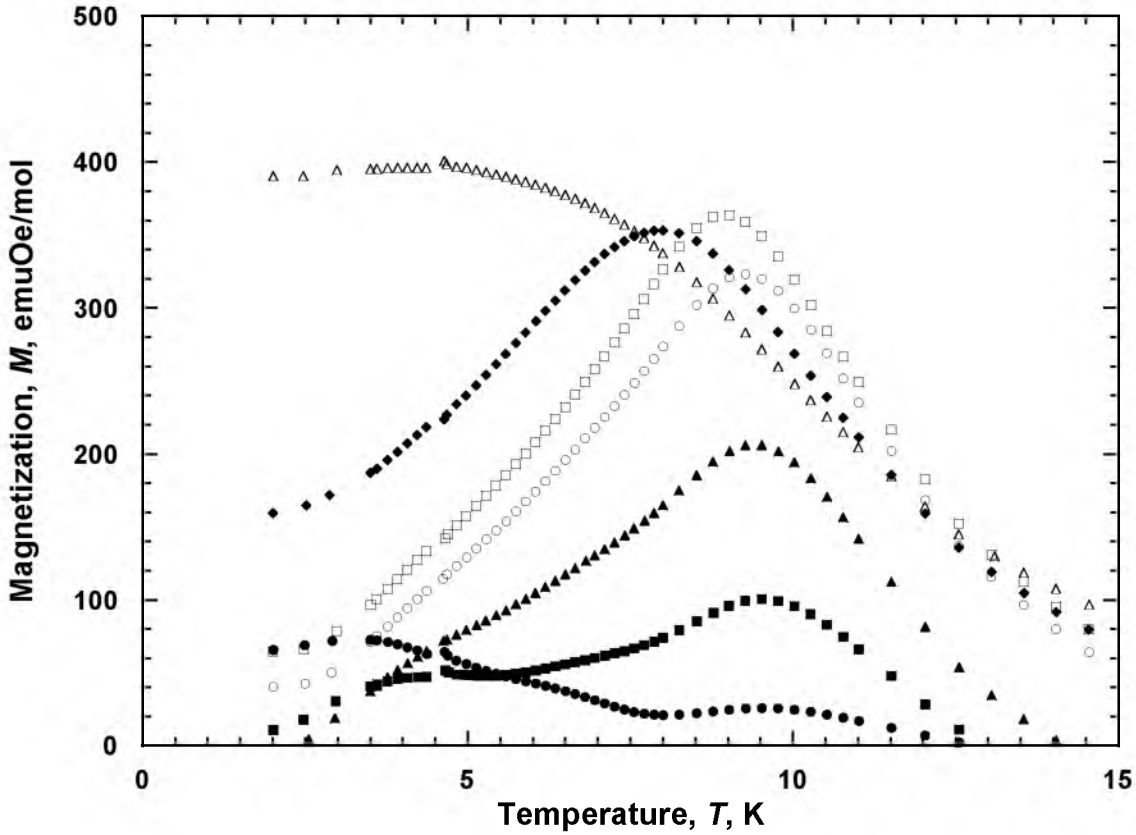

Figure 3.A19. $M_{FC}(T,P)$ at 12.2 kbar and 100 (●), 500 (■), 1000 (▲), 1500 (○), 2000 (□), 3000 (◆), and 5000 (Δ) Oe.

References

(1) (a) Blundell, S. J.; Pratt, F. L. *J. Phys.: Condens. Matter* **2004**, *16*, R771. (b) Ovcharenko, V. I.; Sagdeev, R. Z. *Russ. Chem. Rev.* **1999**, *68*, 345. (c) Kinoshita, M. *Phil. Trans. R. Soc. Lond. (A)* **1999**, *357*, 2855. (d) Miller, J. S.; Epstein, A. J. *Chem. Commun.* **1998**, *13*, 1319. (e) Miller, J. S.; Epstein, A. J. *Angew. Chem. Int. Ed. Engl.* **1994**, *33*, 385. (f) Miller, J. S. *Chem. Soc. Rev.* **2011**, *40*, 3266.

(2) Miller, J. S.; Calabrese, J. C.; Epstein, A. J.; Bigelow, R. W.; Zhang, J. H.; Reiff, W. M. *J. Chem. Soc., Chem. Commun.* **1986**, 1026-1028.

(3) Miller, J. S.; Calabrese, J. C.; Rommelmann, H.; Chittipeddi, S. R.; Zhang, J. H.; Reiff, W. M.; Epstein, A. J. *J. Am. Chem. Soc.* **1987**, *109,* 769-781.

(4) Chittipeddi, S.; Cromack, K. R.; Miller, J. S.; Epstein, A. J. *Phys. Rev. Lett.* **1987**, *58*, 2695-2698.

(5) Miller, J. S. *J. Mater. Chem.* **2010**, *20*, 1846.

(6) Chittappeddi, S.; Selover, M. A.; Epstein, A. J.; O'Hare, D. M.; Manriquez, J.; Miller, J. S. *Synth. Met.* **1989**, *27*, B417.

(7) Varret, F.; Nogues, M.; Goujon, A. In *Magnetism: Molecules to Materials*; Miller, J. S., Drillon, M., Eds.; Wiley-VCH: New York, 2000, Vol. 1, p 257.

(8) Kobayashi, H.; Kobayashi, A.; Cassoux, P. *Chem. Soc. Rev.* **2000**, *29*, 325.

(9) Ratera, I.; Veciana, J. *Chem. Soc. Rev.* **2012**, *41*, 303.

(10) Coronado, E.; Day, P. *Chem. Rev.* **2004**, *104*, 5419.

(11) Her, J.-H.; Stephens, P. W.; Ribas-Ariño, J.; Novoa, J. J.; Shum, W. W.; Miller, J. S. *Inorg. Chem.* **2009**, *48*, 3296-3307.

(12) Taliaferro, M. L.; Selby, T. D.; Miller, J. S. *Chem. Mater.* **2003**, *15*, 3602.

(13) Miller, J. S.; Gantzel, P. K.; Rheingold, A. L.; Taliaferro, M. L. *Inorg. Chem.* **2009**, *48*, 4201-4206.

(14) Huang, Z. J.; Chen, F.; Ren, Y. T.; Xue, Y. Y.; Chu, C. W.; Miller, J. S. *J. Appl. Phys.* **1993**, *10*, 6563-6565.

(15) DaSilva, J. G.; Miller, J. S. *Inorg. Chem.* **2013**, *52*, 1108.

(16) DaSilva, J. G.; McConnell, A.C.; Miller, J. S. *Inorg. Chem.* **2013**, *52*, 4629-4634.

(17) (a) Brandon, E. J.; Rittenberg, D. K.; Arif, A. M.; Miller, J. S. *Inorg. Chem.* **1998**, *37*, 3376. (b) Arthur, J. L.; Moore, C. E.; Rheingold, A. L.; Lapidus, S. H.; Stephens, P. W.; Miller, J. S. *Adv. Functional Mater.* **2012**, *22,* 1802.

(18) Nakano, M.; Sorai, M. *Mol. Cryst. Liq. Cryst.* **1993**, *233*, 161.

(19) Chakraborty, A.; Epstein, A. J.; Lawless, W. N.; Miller, J. S. *Phys. Rev. B* **1989**, *40*, 11422-11424.

(20) Lawless, W. N.; Clark, C. F.; renz, R. W. *Rev. Sci. Instrum.* **1982**, *53*, 1647.

(21) Taliaferro, M. L.; Palacio, F.; Miller, J. S. *J. Mater. Chem.* **2006**, *16*, 2677.

(22) Bhowmick, I.; Hillard, E. A.; Dechambenoit, P.; Coulon, C.; Harris, T. D.; Clérac, R. *Chem. Commun.* **2012**, *48*, 9717.

(23) (a) Binder, K.; Young, A. P. *Rev. Mod. Phys.* **1986**, *58*, 801. (b) Maryško, M.; Jirák, Z.; Hejtmánek, J.; Knížek, K. *J. Appl. Phys.* **2012**, *111*, 07E110. (c) Weng, D.-F.; Wang, Z.-M.; Gao, S. *Chem. Soc. Rev.* **2011**, *40*, 3157.

(24) (a) Mydosh, J. A. in *Spin Glasses: An Experimental Introduction*, Taylor and Francis: London, 1993, pg 67. (b) ϕ is a parameter indicative of the amount of spin disorder in a material is known as spin-glass behavior: $\phi = \Delta T_{max}/[T_{max}(\Delta \log \omega)]$, where ΔT_{max} = difference between peak maximum of the temperatures at the high and low frequencies, T_{max} = peak maximum of the temperature at low frequency, $\Delta \log \omega$ = difference in the logarithms of the high and low frequencies(ω).

(25) Mydosh, J. A. in *Spin Glasses: An Experimental Introduction*, Taylor and Francis: London, 1993, p 67.

(26) (a) Stryjewski, E.; Giordano, N. *Adv. Phys.* **1977**, *26*, 487. (b) Hysteresis is not an attribute of a metamagnet; however, several examples of metamagnets exhibit hysteresis, and this is ascribed to noncompensated canting leading to weak ferromagnetic (canted antiferromagnetic) behavior, e.g. (c) Zhang, D.; Wang, H.; Chen, Y.; Ni, Z-H.; Tian, L.; Jiang, J. *Inorg. Chem.* **2009**, *48*, 11215. (d) Sun, Q.; Cheng, A.; Wang, Y.-Q.; Ma, Y.; Gao, E.-Q. *Inorg. Chem.* **2011**, *50*, 8144. (e) Colacio, E.; Ghazi, M.; Stoeckli-Evans, H.; Lloret, F.; Moreno J.; Perez, C. *Inorg. Chem.* **2001**, *40*, 4876. (f) Yang, C.; Wang, Q.-L.; Qi, J.; Ma, Y.; Yan, S.-P.; Yang, G.-M.; Cheng P.; Liao, D.-Z *Inorg. Chem.* **2011**, *50*, 4006. (g) Keene, T.; Light, M.; Hursthouse, M.; Price, D. *Dalton Trans.* **2011**, *40*, 2983. (h) Numata, Y.; Inoue, K.; Baranov, N.; Kurmoo, M.; Koichi, K. *J. Am. Chem. Soc.* **2007**, *129*, 9902. (i) Weng, D.-F.; Wang, Z.-M.; Gao, S. *Chem. Soc.*

Rev. **2011**, *40*, 3157. (j) Rouco, A.; Obradors, X.; Tovar, M.; Pérez, F.; Chateigner, D.; Bordet, P. *Phys. Rev. B* **1994**, *50*, 9924. (k) Colacio, E.; Domínguez-Vera, J. M.; Ghazi, M.; Kivekäs, R.; Lloret, F.; Moreno, J. M.; Stoeckli-Evans, H. *Chem. Commun.* **1999**, 987. (l) Gao, E.-Q.; Wang, Z.-M.; Yan, C.-H. *Chem. Commun.* **2003**, 1748. (m) Yuan, A.-H.; Qian, S.-Y.; Liu, W.-Y.; Zhou, H.; Song, Y. *Dalton Trans.* **2011**, *40*, 5302. (n) Liu, D. S.; Sui, Y.; Wang, T. W.; Huang, C. C.; Chen, J. Z.; You, X. Z. *Dalton Trans.* **2012**, *41*, 5301. (o) Huang, Z.-L.; Drillon, M.; Masiocchi, N.; Sironi, A.; Zhao, J.-T.; Rabu, P.; Panissod, P. *Chem. Mater.* **2000**, *12*, 2805. (p) Zheng, Y.-Z.; Xue, W.; Tong, M.-L.; Chen, X.-M.; Grandjean, F.; Long, G. J. *Inorg. Chem.* **2008**, *47*, 4077. (q) Jia, Q.-X.; Tian, H.; Zhang, J.-Y.; Gao, E.-Q. *Chem. Eur. J.* **2011**, *17*, 1040.

CHAPTER 4

REVERSIBLE PRESSURE INDUCED TRANSITION FROM A SPIN GLASS TO METAMAGNET EXHIBITING WEAK FERROMAGNETISM OBSERVED FOR DECAMETHYLFERROCENIUM HEXACYANOBUTADIENIDE, $[FeCp^*_2]^{\bullet+}[HCBD]^{\bullet-}$

DaSilva, J. G.; Miller, J. S. *Dalton T.* **2013**, *42*, 8334-8338. Reproduced by permission of the Royal Chemistry Society.

Abstract

The magnetic properties of $[Fe^{III}Cp^*_2]^{\bullet+}[HCBD]^{\bullet-}$ (Cp* = pentamethylcyclopentadienide; HCBD = hexacyanobutadienide, $C_4(CN)_6$) and $[Fe^{III}Cp^*_2]^{\bullet+}[DDQ]^{\bullet-}$ (DDQ = 2,3-dichloro-5,6-dicyanoquinonide) were measured at ambient and applied hydrostatic pressures up to 11.4 and 9.2 kbar, respectively. At ambient pressure $[FeCp^*_2][HCBD]$ exhibits spin glass behavior with a freezing temperature, T_f, of 2.93 K from the peak in $\chi'(T)$ at 10 Hz, but magnetic ordering is not evident due to the lack of a remnant magnetization, bifurcation temperature, and hysteresis. Above 3.1 kbar, $[FeCp^*_2][HCBD]$ magnetically orders as a metamagnet with an antiferromagnetic ground state with an ordering temperature, T_c, of 2.46 K determined from the Fischer specific heat, which increases linearly to 4.80 K at 11.4 kbar at a rate of 0.28 K/kbar. Upon application of pressure metamagnetic-like behavior with hysteresis indicative of a weak ferromagnet (canted antiferromagnet) was observed at and above 3.1 kbar, with a coercive field, H_{cr}, of 25 Oe, and a critical field, H_c, of 2,200 Oe, which increase exponentially to 795 and 10,000 Oe, respectively, at 11.4 kbar. $[FeCp^*_2]^{\bullet+}[DDQ]^{\bullet-}$ did not magnetically order above 2 K, and magnetic order was not observed up to 9.2 kbar. The pressure dependencies are reversible.

Introduction

Strong, conjugated polynitrile organic electron acceptors have stabilized bulk magnetic ordering in molecule-based materials. Examples include: 0-D $[FeCp^*_2]^{\bullet+}[TCNE]^{\bullet-}$ (TCNE = tetracyanoethylene; Cp* = pentamethylcyclopentadienide),[1,2,3] 1-D $[Mn^{III}TPP][Me_2DCNQI]$ [$Mn^{III}TPP$ = tetraphenylporphyrinatomanganese(III); Me_2DCNQI = dimethyl-*N*,*N*'-dicyanoquinonediiminide],[4] 2-D $[Fe^{II}(TCNE)(NCMe)_2][Fe^{III}Cl_4]$,[5] and 3-D $Mn^{II}(TCNE)_{3/2}(I_3)_{1/2}\bullet zTHF$.[6] The successful synthesis of the first ferromagnetic molecule-based magnet, $[FeCp^*_2][TCNE]$,[1] motivated research into the utilization of conjugated electron accepting polynitrile compounds. Hexacyanobutadiene (HCBD) and 2,3-dichloro-5,6-dicyanoquinone (DDQ) were identified as promising electron accepting analogues on the basis of planarity, symmetry (HCBD = S_{2v} and DDQ = C_2), and electron affinity (HCBD: E_A = 3.24 eV;[7] DDQ: E_A ~ 3 eV[8]) compared to TCNQ (TCNQ = 7,7,8,8-tetracyano-*p*-quinodimethane: E_A = 2.8 eV[8,7] and TCNE: E_A = 2.88 eV.[7] However, neither $[FeCp^*_2]^{\bullet+}[HCBD]^{\bullet-}$ (**1**)[9] or $[FeCp^*_2]^{\bullet+}[DDQ]^{\bullet-}$ (**2**)[10] magnetically ordered. Nonetheless, several magnetic materials containing DDQ or HCBD have been reported: [MnOEP][HCBD][11] (MnOEP = octaethylporphyrinatomanganese(III)), $[MnCp^*_2][DDQ]$.[12] These examples and the previous hydrostatic pressure dependent magnetic investigation of the analogous compounds $[FeCp^*_2]^{\bullet+}[TCNQ]^{\bullet-}$ [13] and $[FeCp^*_2]^{\bullet+}[TCNE]^{\bullet-}$ [14] have prompted the pressure dependent magnetic study of **1** and **2**.

The structures of $[FeCp^*_2]^{\bullet+}[HCBD]^{\bullet-}$ (**1**)[9] and $[FeCp^*_2]^{\bullet+}[DDQ]^{\bullet-}$ (**2**)[10] possess a chain structure with alternating cations and anions with the Cp* ring plane and the anion plane are approximately parallel that are typical of this family of electron transfer complexes.[3,15] The structures of **1** and **2** are similar to the TCNE and TCNQ analogues, differing primarily in their interchain cyano-Fe nearest neighbor distances, due to the structure of the organic radical. **1** has Fe•••Fe, Fe•••N, and N•••N interchain distances of 8.719, 5.153, and 3.311 Å,[9] respectively, most closely resembling $[FeCp^*_2]^{\bullet+}[TCNE]^{\bullet-}$, at 8.205,[15] 5.145,[16] and 3.488 Å,[16] respectively. Only the ferromagnetic TCNQ analog has comparably small distances at 8.609, 5.020, and 4.337

Å, respectively.[17] Not surprisingly, the 5.209-Å Fe•••N intrachain distance is shortest for the TCNE analog, which displays the highest critical temperature, T_c,[15] while **1** is similar at 5.536 Å,[9] and is less than either the ferromagnetic polymorph of the TCNQ analog (5.858 Å)[17] or 6.120 Å for the metamagnetic polymorph.[18] **2** exhibits the largest separations in general, with interchain distances of 8.692, 5.369, and 6.529 Å, respectively, while the intrachain Fe•••N distance is also quite large for these compounds at 6.317 Å.[10]

1 exhibited paramagnetic behavior from DC magnetic measurements down to cryogenic temperatures with a broad, ill-resolved feature below 5 K,[9] although the high temperature susceptibility was modeled by Curie-Weiss law with θ = 35 K indicating significant ferromagnetic coupling. In contrast, the onset of hyperfine structure in the ^{57}Fe Mössbauer spectra at 7.5 K indicated that **2** was magnetically ordered with a critical temperature, T_c, of 7.5 K.[9] **2** exhibited paramagnetic behavior down to 2 K from DC magnetic measurements, with θ = 11.6 K from a fit to the Curie-Weiss law, also indicating significant ferromagnetic coupling.[10] **2** also exhibits hyperfine structure in the ^{57}Fe Mössbauer spectra, with onset at 22.1 K and fully resolved hyperfine structure at 2.68 K.[10]

Experimental Section

1[9] and **2**[10] were prepared via the literature methods. IR spectra were measured from 400 to 4000 cm^{-1} using a Bruker Tensor 37 spectrometer (±1 cm^{-1}), and were used to confirm purity through identification of characteristic nitrile absorptions. A Quantum Design (QD) Physical Property Measurement System PPMS 9 T was used to measure the AC susceptibility at ambient pressure at field oscillation frequencies of 10 to 1000 Hz (the instrument is capable of achieving 10,000 Hz) and field amplitude of 3 Oe. Samples of **1** and **2** (3 to 15 mg) were loaded into gelatin capsules in inert atmosphere and sealed with silicon grease prior to removal from inert atmosphere.

A QD Superconducting Quantum Interference Device (SQUID) Magnetic Property Measurement System (MPMS-5XL 5 T) (sensitivity = 10^{-8} emu or 10^{-12} emu/Oe at 1 T) was used to perform the DC pressure dependent magnetization studies. Samples of **1** and **2** (~1 mg) were sealed into a cylindrical Teflon™ cell; the remaining

volume of the cell was occupied by decalin (the hydrostatic pressure media) and capped with Teflon end-caps. The Teflon sample cell was then loaded into a beryllium-copper hydrostatic pressure cell, fabricated at the University of Utah from the Kyowa Seisakusho design, with zirconia pistons and rubber o-rings. Pressure was applied to the assembly using a Kyowa Seisakusho CR-PSC-KY05-1 apparatus with a WG-KY03-3 pressure sensor. An Aikoh Engineering Model-0218B digital sensor readout was used as the pressure indicator. The Aikoh Engineering Model-0218B digital sensor readout is an approximate method for determining pressure, and a superconductor with a known pressure dependent transition temperature was used to calibrate the pressure. Since the $2 < T_c < 5$ K is expected for **1**,[9] and $T_c < 2$ K for **2**[10] no convenient superconducting pressure calibrant was suitable. As reported for $[FeCp^*_2]^{\bullet+}[TCNQ]^{\bullet-}$,[13] calibration was achieved from a least squares linear regression fit, $P = 0.025x - 0.7$, where x is the readout from the digital sensor from previous pressure data. The error associated with this correlated fit was assumed to be the standard deviation of the slope and intercept of the linear regression fit propagated through the pressure determination and is 0.048 kbar ($\chi^2 = 0.953$).

For the temperature dependent DC magnetization, $M(T)$, the sample was cooled in zero applied field, and data were collected upon warming for **1** in a 5 Oe applied field, and in a 1000 Oe applied field for **2**. The T_c was determined from the Fischer specific heat, $d(\chi T)/dT$.[19] The field dependent DC magnetization, $M(H)$, was performed by cooling in zero applied field, and isothermally collecting data at 2 K as the field was applied to ± 50,000 Oe.

Results and Discussion

The isothermal magnetization, $M(H,P)$, was measured as a function of applied field and hydrostatic pressure at 2 K for **1** and **2**. The magnetization was also measured as a function of temperature and pressure, $M(T,P)$ at 5 Oe for **1**, and 1000 Oe for **2**. AC susceptibility measurements of **1** were performed at 10, 100, 333, and 1,000 Hz and 3 Oe amplitude from 2 to 10 K. Ambient pressure magnetic measurements confirmed the purity and reproducibility of the samples.

Complex **1** displayed Curie-Weiss behavior, $\chi \propto (T - \theta)^{-1}$, with θ = +8.8 K significantly decreased from the literature value of +35 K, at ambient pressure presumably due to differences in the average orientation, as the $[Fe^{III}Cp^*_2]^+$ cation is very anisotropic.[9,20] The $M(H)$ of **1** did not exhibit hysteresis or reach saturation, and has a magnetization at 50 kOe of 15,060 emuOe/mol (Figure 4.1), somewhat less than the literature value of 17,700 emuOe/mol.[10] The discrepancy is attributed to higher temperature data with respect to the literature value that was measured at 1.91 K,[9] and differences in orientation of the sample.

The ambient pressure AC susceptibility of **1** exhibited frequency dependent peaks in both the in-phase, real $\chi'(T)$ and out-of-phase, complex $\chi''(T)$, suggesting ferro- or ferrimagnetic order. A freezing temperature, T_f, was determined to be 2.93 K from the peak in $\chi'(T)$ at 10 Hz (3.30 K from the onset of $\chi''(T)$ at 10 Hz) (Figure 4.1). The lack of evidence of magnetic ordering from other studies, and its frequency dependence suggests spin glass behavior with the figure-of-merit, ϕ, of 0.094. This value of ϕ is significantly larger than those exhibited by all other desolvated $[FeCp^*_2]$[polynitrile] magnetic materials, as the TCNQ[21] and 2,3-dicyano-1,4-naphthoquinonide (DCNQ)[22] analogues display no frequency dependence, and the TCNE analogue exhibits a small ϕ of ~0.008; however, the solvated forms reach ~0.19.[23]

The zero field cooled, $M_{ZFC}(T)$, field cooled, $M_{FC}(T)$, and remnant, $M_r(T)$, magnetization measurements were performed at several applied pressures for **1**. The ambient pressure $M_{ZFC}(T)$ and $M_{FC}(T)$ were coincident at all temperatures and pressures, and, thus, a bifurcation of the data did not occur. The $M_r(T)$ was approximately one order of magnitude lower in intensity than the M_{ZFC} and M_{FC} suggestive of being extrinsic. Upon application of pressure the $M(T,P)$ data of **1** reversibly displayed a cusp-like feature in the susceptibility, $\chi(T)$, above 3.1 kbar, which shifted to higher temperature with increasing applied pressure (Figure 4.2a). However, a peak was not observed in the $d(\chi T)/dT$ until 3.1 kbar was applied; this peak also shifted to higher temperature with increasing applied pressure (Figure 4.2b). This indicates the onset of antiferromagnetic ordering above 1.8 kbar. The magnetic order temperature, T_c, was determined from the peak $d(\chi T)/dT$ (determined from the Fischer specific heat)[19] to be

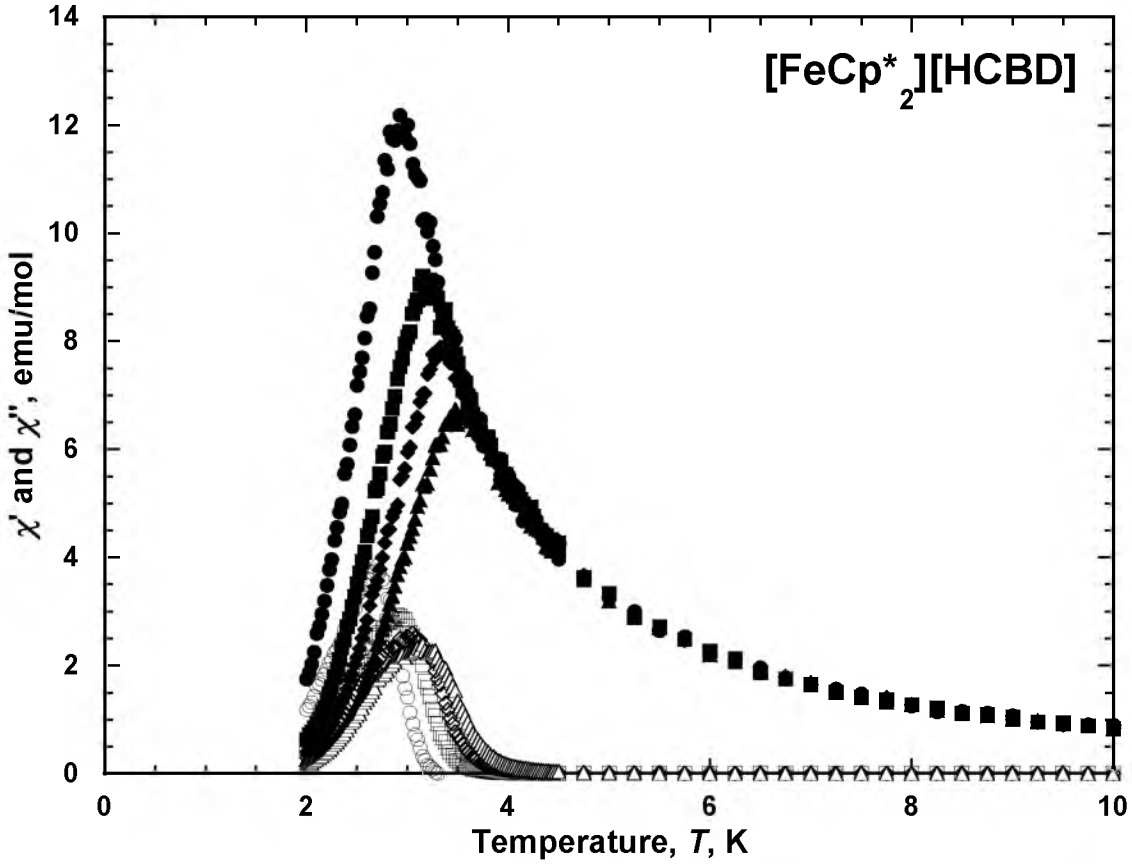

Figure 4.1. AC susceptibility of **1**: $\chi'(T)$ (solid symbols), $\chi''(T)$ (hollow symbols), at 10 (●), 100 (■), 333 (◆), 1000 Hz (▲).

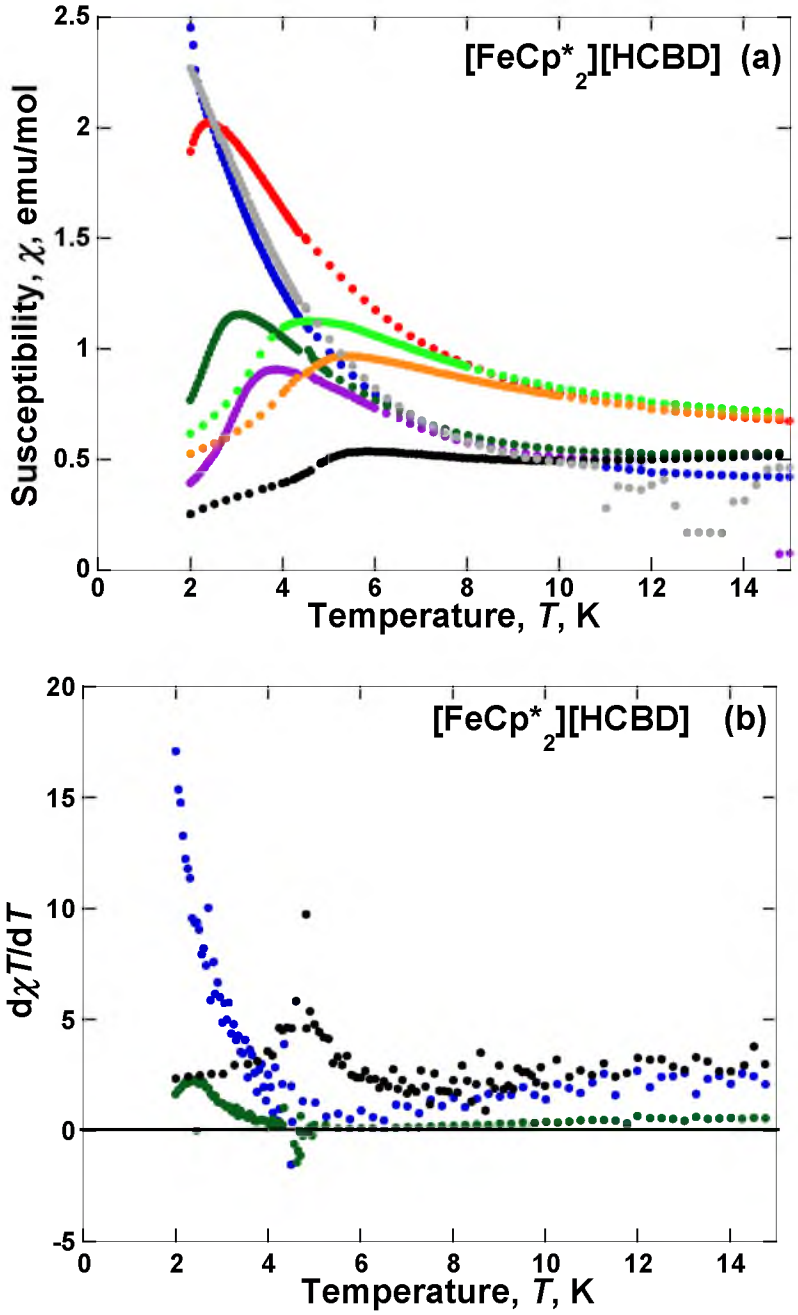

Figure 4.2. Temperature dependent magnetic measurements of **1**. (a) $\chi(T,P)$ of **1** at 0.001 (•), 1.8 (•), 3.1 (•), 4.2 (•), 6.5 (•), 9.3 (•), 11.4 kbar (•), and released to ambient pressure (•). (b) Representative d(χT)/dT data of 1 at 0.001 (•), 3.1 (•), and 11.4 kbar (•).

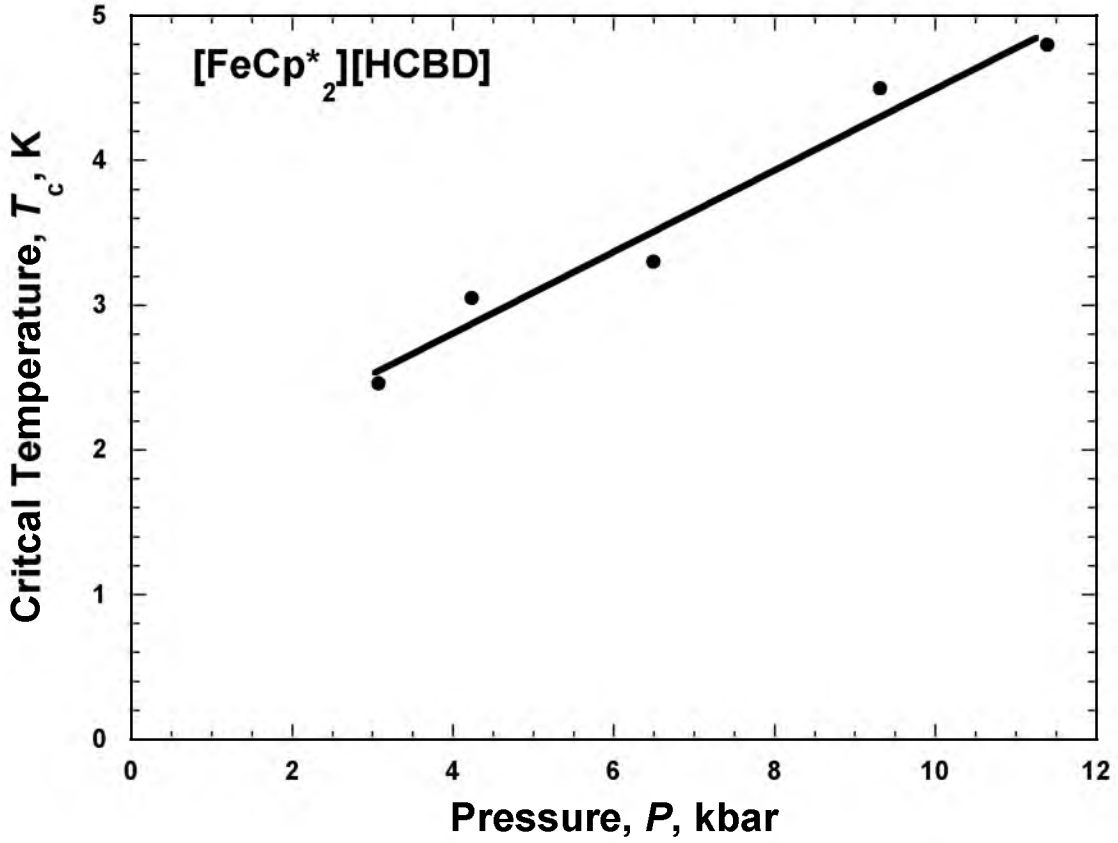

Figure 4.3. $T_c(P)$ of **1** at several pressures. The solid guide-for-the-eye line is a linear numerical fit to $T_c = 1.6771 + 0.28195P$; $R^2 = 96.7\%$. The error bars for pressure are approximately the size of the data points.

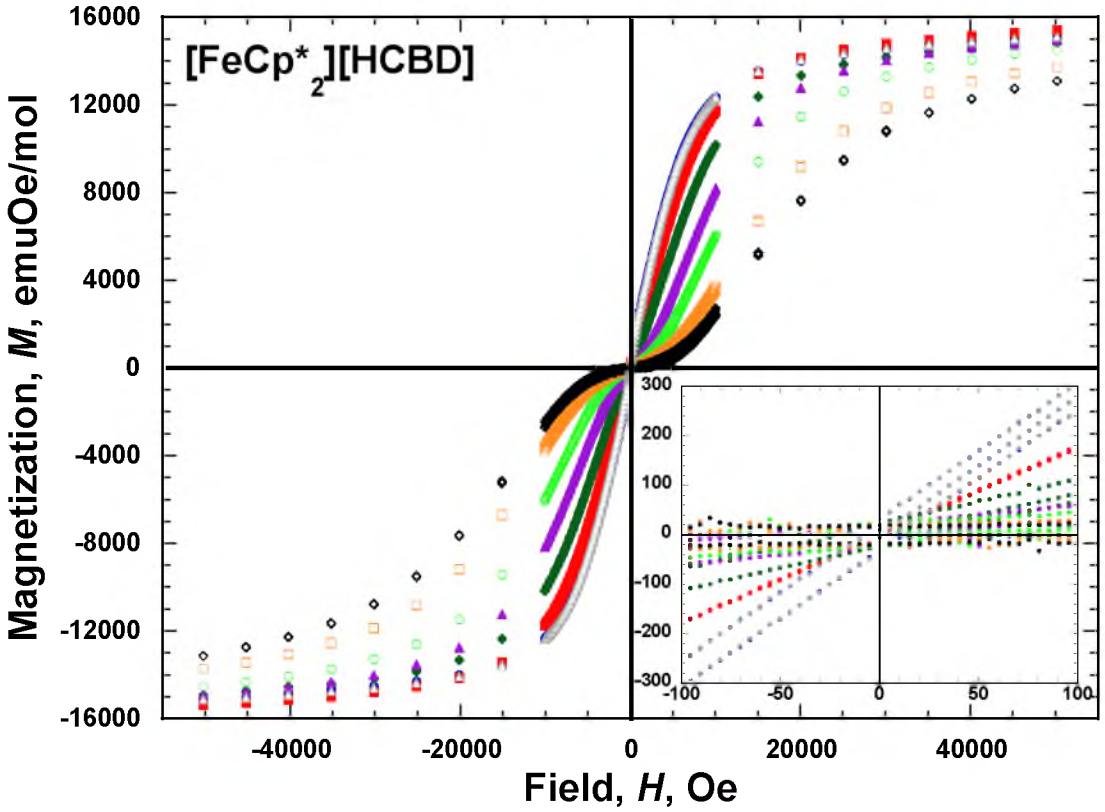

Figure 4.4. *M*(*H*,*P*) of **1** at 0.001 (•), 1.8 (•), 3.1 (•), 4.2 (•), 6.5 (•), 9.3 (•), 11.4 kbar (•), and released to ambient pressure (•).

2.46 K at 3.1 kbar, and it increased linearly (T_c = 1.6771 + 0.28195P) to 4.80 K at 11.4 kbar at a rate of 0.28 K/kbar (Figure 4.3).

The $M(H,P)$ of **1** displayed a slight decrease in magnetization at 50 kOe upon initial application of pressure, maintaining both the shape of the curve and the absence of hysteresis that is observed at ambient pressure. Further application of pressure led to the reversible evolution of metamagnetic-like behavior with hysteresis, with a continued decrease in the magnetization (Figure 4.4). Hysteretic behavior was observed at ~3.1 kbar with a coercive field, H_{cr}, critical field, H_c, and remnant magnetization, M_r, of 25 Oe, 2,200 Oe, and 25 emuOe/mol, respectively. The H_{cr} increased exponentially [H_{cr} = 9.8362exp(0.37616P); χ^2 = 98.1%] to 795 Oe, the H_c increased linearly to 10,000 Oe, while the M_r decreased to 20 emuOe/mol at the maximum achieved pressure of 11.4 kbar (Figure 4.5). Furthermore, at ambient pressure the presence of $\chi''(T)$ is inconsistent with an antiferromagnet.

The evolution of a metamagnetic-like behavior with hysteresis under applied pressure differs from the cusp in $\chi(T)$, the peak in d(χT)/dT, and the absence of bifurcation between the $M_{ZFC}(T)$ and $M_{FC}(T)$ data, which are suggestive of antiferromagnetic ordering, and not ferro- or ferrimagnetic behavior. Furthermore, hysteresis is attributed to a metamagnet,[24] although several examples of metamagnets have been reported to exhibit hysteresis, and this is ascribed to noncompensated canting leading to weak ferromagnetic (canted antiferromagnetic) behavior.[25] Hence, **1** appears to be a metamagnet with some canted antiferromagnetism as has been reported for [FeCp*$_2$][DCNQ],[22] as well as other molecule-based magnetic materials.[26]

Complex **2** exhibits Curie-Weiss behavior, but extrapolation of the 30 to 100 K data yielded a θ = +2.4 K that is significantly less than the literature value of + 11.6 K.[10] This discrepancy is attributed to differences in the average orientation, as the [FeCp*$_2$]$^+$ cation is very anisotropic.[9,20] The $M(H)$ of **2** did not saturate, and had a magnetization at 50,000 kOe of 10,740 emuOe/mol (Figure 4.6) in agreement with the literature value of ~20 emu/g (~11,060 emuOe/mol).[10] Hysteresis, in accord with earlier studies, was not observed at ambient pressure.

Upon application of pressure the $M(H,P)$ data for **2** maintained the qualitative shape of the curve without the onset of hysteresis, but did exhibit a slight 0.4%

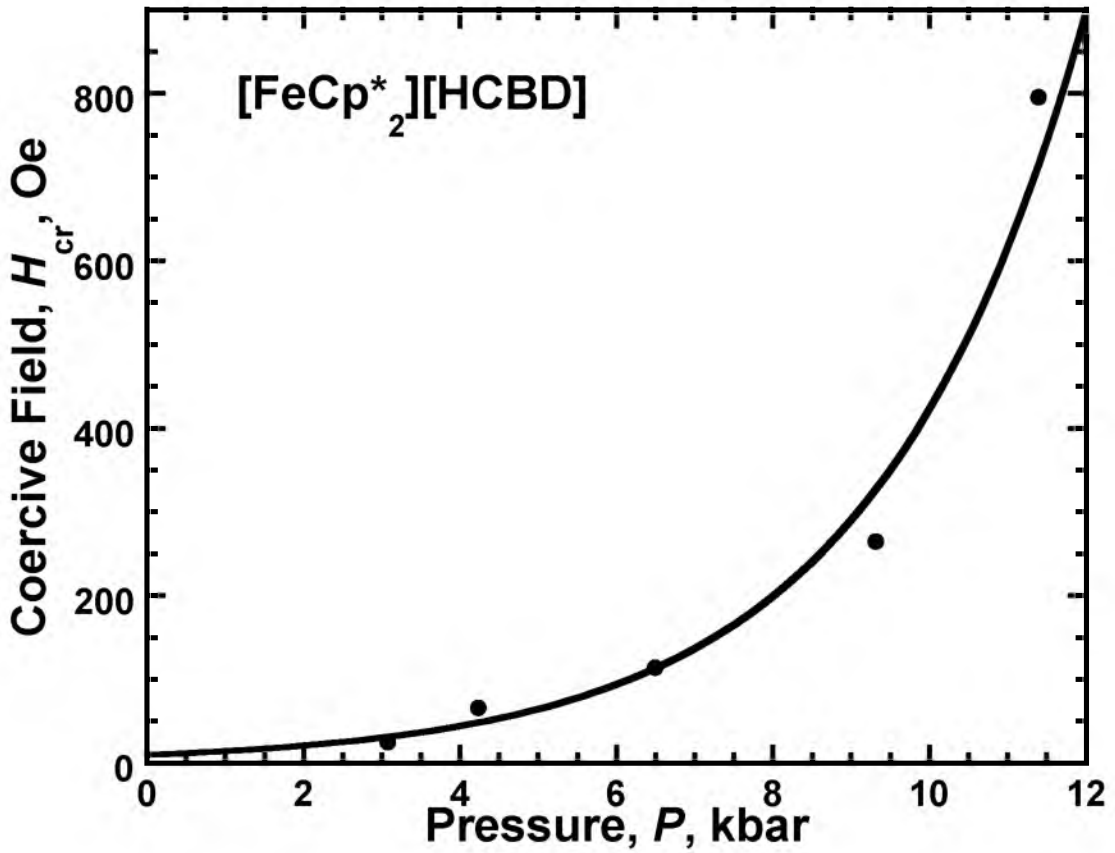

Figure 4.5. $H_{cr}(P)$ of **1** at several pressures. The solid guide-for-the-eye line is an exponential numerical fit to $H_{cr} = 9.8362\exp(0.37616P)$; $R^2 = 98.1\%$. The error bars for pressure are approximately the size of the data points.

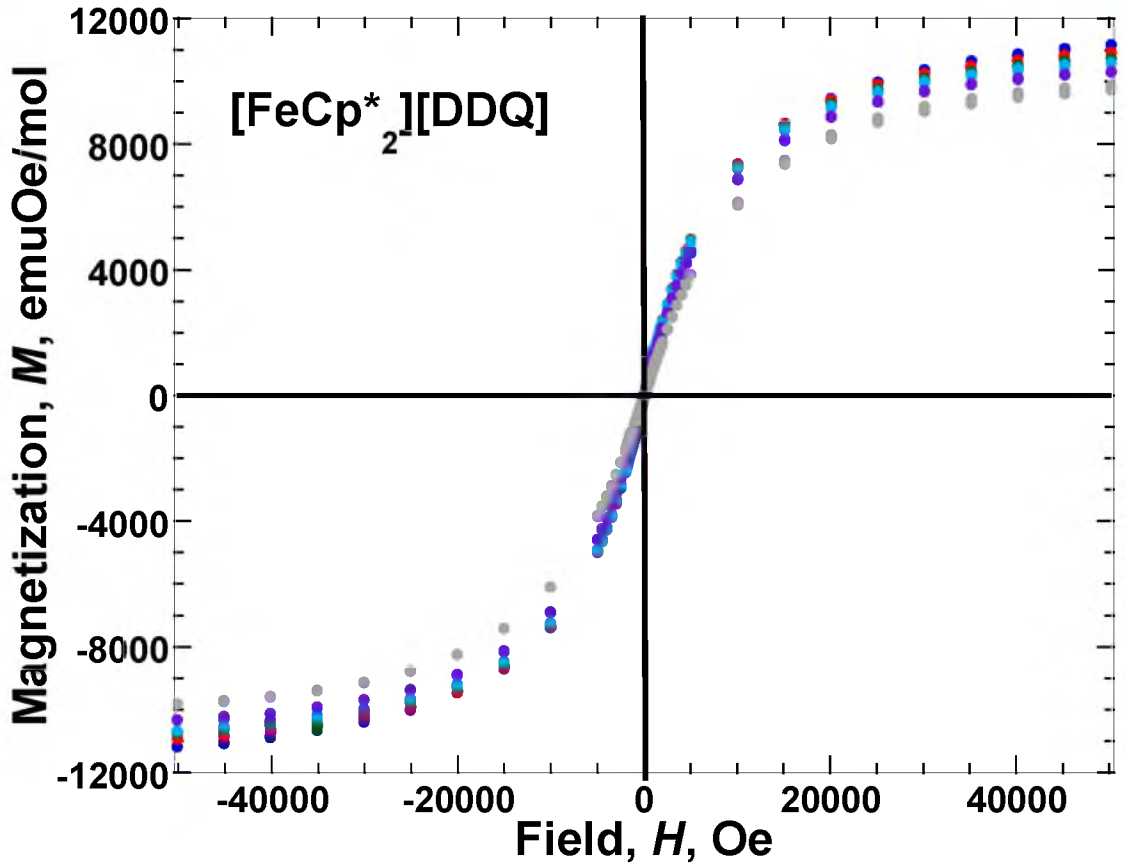

Figure 4.6. *M*(*H*,*P*) of **2** at 0.001 (•), 1.2 (•), 4.7 (•), 9.2 (•) kbar, and released to ambient pressure (•).

consistent decrease of the magnetization at 50 kOe from 10,740 emuOe/mol at ambient pressure to 10,320 emuOe/mol at 9.2 kbar. This loss was not reversible, as it decreased to 9,900 emuOe/mol for the pressure release measurement, Figure 4.6. The $M(T,P)$ of **2** did not exhibit a significant pressure dependent behavior, remaining paramagnetic up to 9.2 kbar, and does not magnetically order.

Conclusion

Both [FeCp*$_2$][HCBD], **1**, and [FeCp*$_2$][DDQ], **2**, exhibit different unexpected behaviors upon application of pressure. **1** appears to order from ^{57}Fe Mössbauer,[9] and AC susceptibility data, but not from the DC magnetization at ambient pressure, but exhibits hysteresis and apparent antiferromagnetic order under applied pressure. **2**, in contrast, neither magnetically orders at ambient or applied pressure. The onset of hysteresis, a metamagnetic-like $M(H)$, the absence of temperature dependent bifurcation, and a peak in the $\chi''(T)$ suggest **1** is a canted antiferromagnet above 3.1 kbar applied pressures. Similar behavior was observed for [FeCp*$_2$]$^{\bullet+}$[DCNQ]$^{\bullet-}$.[22] The absence of magnetic order under applied pressure for **2** suggests one of three possibilities: that the inter- and intrachain distances were not compressed significantly, that the π^* SOMO of [DDQ]$^{\bullet-}$ precludes sufficient overlap with the Fe d-orbitals, or that **2** exhibits similar behavior to high pressure [FeCp*$_2$]$^{\bullet+}$[TCNQ]$^{\bullet-}$ at all pressures.[13]

References

(1) Miller, J. S.; Calabrese, J. C.; Epstein, A. J.; Bigelow, R. W.; Zhang, J. H.; Reiff, W. M. *J. Chem. Soc. Chem. Commun.* **1986**, 1026.

(2) Miller, J. S.; Calabrese, J. C.; Rommelmann, H.; Chittipeddi, S. R.; Zhang, J. H.; Reiff, W. M.; Epstein, A. J. *J. Am. Chem. Soc.* **1987**, *109,* 769.

(3) Miller, J. S. *J. Mater. Chem.* **2010**, *20*, 1846.

(4) Arthur, J. L.; Lapidus, S. H.; Stephens P. W.; Miller, J. S. *Science China Chemistry* **2012**, *55*, 987.

(5) Pokhodnya, K. I.; Bonner, M.; Her, J.-H.; Stephens, P. W.; Miller, J. S. *J. Am. Chem. Soc.* **2006**, *128*, 15592.

(6) Lapidus, S. H.; McConnell, A. C.; Stephens, P. W.; Miller, J. S. *Chem. Commun.* **2011**, *47*, 7602.

(7) Chen, E. M. C.; Wentworth, W. E. *Mol. Cryst. Liq. Cryst.* **1989**, *171*, 271.

(8) Kampars, V.; Neiland, O. *Russ. Chem. Rev.*, **1977**, *46*, 503.

(9) Miller, J. S.; Zhang, J. H.; Reiff, W. M. *J. Am. Chem. Soc.* **1987**, *109*, 4584.

(10) (a) Gerbert, E.; Reis, A. H.; Miller, J. S.; Rommelmann, H.; Epstein, A. J. *J. Am. Chem. Soc.* **1982**, *104*, 4403. (b) Miller, J. S.; Krusic, P. J.; Dixon, D. A.; Reiff, W. M.; Zhang, J. H.; Anderson, E. C.; Epstein, A. J. *J. Am. Chem. Soc.* **1986**, *108*, 4459.

(11) Wynn, C. M.; Gîrtu, M. A.; Epstein, A. J.; Miller, J. S. *Phys. Rev. B* **1997**, *56*, 315.

(12) Miller, J. S.; McLean, R. S.; Vazquez, C.; Yee, G. T.; Narayan, K. S.; Epstein, A. J. *J. Mater. Chem.* **1991**, *1*, 479.

(13) DaSilva, J. G.; Miller, J. S. *Inorg. Chem.* **2013**, *52*, 1108.

(14) Huang, Z. J.; Cheng, F.; Ren, Y. T.; Xue, Y. Y.; Chu, C. W.; Miller, J. S. *J. Appl. Phys.* **1993**, *10*, 6563.

(15) Her, J.-H.; Stephens, P. W.; Ribas-Ariño, J.; Novoa, J. J.; Shum, W. W.; Miller, J. S. *Inorg. Chem.* **2009**, *48*, 3296.

(16) Miller, J. S.; Gantzel, P. K.; Rheingold, A. L.; Taliaferro, M. L. *Inorg. Chem.* **2009**, *48*, 4201.

(17) Broderick, W. E.; Eichhorn, D. M.; Liu, X.; Toscano, P. J.; Owens, S. M.; Hoffman, B. M. *J. Am. Chem. Soc.* **1995**, *117*, 3641.

(18) Miller, J. S.; Zhang, J. H.; Reiff, W. M.; Dixon, D. A.; Preston, L. D.; Reis, A. H., Jr.; Gerbert, E.; Extine, M.; Troup, J.; Ward, M. D. *J. Phys. Chem.* **1987**, *91*, 4344-4360.

(19) (a) Fisher, M. E. *Philos. Mag.* **1962**, *7*, 17. (b) Aharen, T.; Greedan, J. E.; Ning, F.; Imai, T.; Michaelis, V.; Zhou, H.; Wiebe, C. R.; Cranswick, L. M. D. *Phys. Rev. B.* **2009**, *80*, 134423. (c) Cage, B.; Nguyen, B.; Dalal, N. *Sol. State Commun.* **2001**, *119*, 597.

(20) Duggan, D. M.; Hendrickson, D. N. *Inorg. Chem.* **1975**, *14*, 955.

(21) Taliaferro, M. L.; Palacio, F.; Miller, J. S. *J. Mater. Chem.* **2006**, *16*, 2677.

(22) Yee, G. T.; Whitton, M. J.; Sommer, R. D.; Frommen, C. M.; Reiff, W. M. *Inorg. Chem.* **2000**, *39*, 1874.

(23) Taliaferro, M. L.; Selby, T. D.; Miller, J. S. *Chem. Mater.* **2003**, *15*, 3602.

(24) Stryjewski, E.; Giordano, N. *Adv. Phys.* **1977**, *26*, 487.

(25) (a) Zhang, D.; Wang, H.; Chen, Y.; Ni, Z.-H.; Tian, L.; Jiang, J. *Inorg. Chem.* **2009**, *48*, 11215. (b) Sun, Q.; Cheng, A.; Wang, Y.-Q.; Ma, Y.; Gao, E.-Q. *Inorg. Chem.* **2011**, *50*, 8144. (c) Colacio, E.; Ghazi, M.; Stoeckli-Evans, H.; Lloret, F.; Moreno, J.; Perez, C. *Inorg. Chem.* **2001**, *40*, 4876. (d) Yang, C.; Wang, Q.-L.; Qi, J.; Ma, Y.; Yan, S.-P.; Yang, G.-M.; Cheng, P.; Liao, D.-Z *Inorg. Chem.* **2011**, *50*, 4006. (e) Keene, T.; Light, M.; Hursthouse, M.; Price, D. *Dalton Trans.* **2011**, *40*, 2983. (f) Numata, Y.; Inoue, K.; Baranov, N.; Kurmoo, M.; Koichi, K. *J. Am. Chem. Soc.* **2007**, *129*, 9902.

(26) (a) Weng, D.-F.; Wang Z.-M.; Gao, S. *Chem. Soc. Rev.* **2011**, *40*, 3157-3181. (b) Rouco, A.; Obradors, X.; Tovar, M.; Pérez, F.; Chateigner, D.; Bordet, P. *Phys. Rev. B* **1994**, *50*, 9924. (c) Colacio, E.; Domínguez-Vera, J. M.; Ghazi, M.; Kivekäs, R.; Lloret, F.; Moreno, J. M.; Stoeckli-Evans, H. *Chem. Commun.* **1999**, 987. (d) Gao, E.-Q.; Wang, Z.-M.; Yan, C.-H. *Chem. Commun.* **2003**, 1748. (e) Yuan, A.-H.; Qian, S.-Y.; Liu, W.-Y.; Zhou, H.; Song, Y. *Dalton Trans.* **2011**, *40*, 5302. (f) Liu, D. S.; Sui, Y.; Wang, T. W.; Huang, C. C.; Chen, J. Z.; You, X. Z. *Dalton Trans.* **2012**, *41*, 5301. (g) Huang, Z.-L.; Drillon, M.; Masiocchi, N.; Sironi, A.; Zhao, J.-T.; Rabu, P.; Panissod, P. *Chem. Mater.* **2000**, *12*, 2805. (h) Zheng, Y.-Z.; Xue, W.; Tong, M.-L.; Chen, X.-M.; Grandjean, F.; Long, G. J. *Inorg. Chem.* **2008**, *47*, 4077.

CHAPTER 5

PRESSURE DEPENDENT REVERSIBLE INCREASE IN T_c FOR THE FERRIMAGNETIC 2-D $Mn^{II}(TCNE)I(OH_2)$ AND 3-D $Mn^{II}(TCNE)_{3/2}(I_3)_{1/2}$•zTHF ORGANIC-BASED MAGNETS

Reprinted (adapted) with permission from: DaSilva, J. G.; McConnell, A. C.; Miller, J. S. *Inorg. Chem.* **2013**, *52*, 4629-4634.

Abstract

The pressure dependence of the magnetic properties of ferrimagnetic $Mn^{II}(TCNE)I(OH_2)$ up to 14.05 kbar and $Mn^{II}(TCNE)_{3/2}(I_3)_{1/2}$•zTHF up to 14.32 kbar were studied. For $Mn^{II}(TCNE)I(OH_2)$ two distinct pressure regions separated at ~1 kbar were evident in both the temperature and field dependent magnetic measurements. No increase of the magnetic properties was observed in the low-pressure region, while significant increases to the magnetic ordering temperature, T_c, bifurcation temperature, T_b, coercive field, H_{cr}, and remnant magnetization, M_r, were evident in the high-pressure region. The T_c, T_b, H_{cr}, M_r, and M(5 T) reversibly increased from ambient pressure values of 169 K, 169 K, 690 Oe, 620 emuOe/mol, and 13,800 emuOe/mol to 257 K, 261 K, 1,460 Oe, 2,300 emuOe/mol, and 17,100 emuOe/mol at 14.05 kbar, respectively. For $Mn^{II}(TCNE)_{3/2}(I_3)_{1/2}$•zTHF the T_c and T_b were nearly coincident and increased linearly from 173 and 173 K, respectively, at ambient pressure to 273 and 272 K, respectively, at 14.32 kbar. Thus, the T_c increased at an average rate of 6.25 and 7.18 K/kbar for $Mn^{II}(TCNE)I(OH_2)$ and $Mn^{II}(TCNE)_{3/2}(I_3)_{1/2}$•zTHF, respectively. The remnant magnetization and saturation magnetization did not significantly change with applied pressure. The H_{cr} exhibited a linear increase from ambient pressure to 5.00 kbar, reaching 860 Oe, but only achieving 880 Oe at 14.32 kbar.

Introduction

In recent years much research has centered about the discovery and manipulation of organic-based analogs of metallic and metalloid functional materials.[1] Organic-based magnets (OBM) have advantages over traditional metal and metal oxide magnets.[2,3,4,5] OBMs frequently also exhibit photo[6] and piezo active properties.[7] Several OBMs have been synthesized containing $[TCNE]^{\bullet-}$ (TCNE = tetracyanoethylene) including $V(TCNE)_x$, which has a critical temperature (T_c) as high as 400 K.[2,3,4,5,8] The inability to structurally resolve this amorphous room temperature OBM has served to fuel the synthesis and structural determination of TCNE containing OBMs.

$M^{II}(TCNE)[C_4(CN)_8]_{1/2}\bullet zCH_2Cl_2$ (M = Fe,[9] Mn,[10]) and $[Fe^{II}(TCNE)(NCMe)_2][Fe^{III}Cl_4]$[11] have provided insight into possible structural features of high T_c TCNE containing magnets.[8] The former M = Fe and Mn isostructural compounds possess 3-D connectivity, and all three compounds contain μ_4-$[TCNE]^{\bullet-}$ bound to four M^{II} ions forming corrugated layers. The layers of $M^{II}(TCNE)[C_4(CN)_8]_{1/2}\bullet zCH_2Cl_2$ are connected by diamagnetic $[C_4(CN)_8]^{2-}$ with an average layer separation of 8.71 and 8.77 Å for M = Fe and Mn, respectively. This results in antiferromagnetic ordering with a T_c at ambient pressure of 84 and 69 K for M = Fe and Mn, respectively. $[Fe^{II}(TCNE)(NCMe)_2][Fe^{III}Cl_4]$ consists of 2-D layers with no interlayer connectivity, but has an 8.24 Å interlayer separation, and magnetically orders as a ferrimagnet below 90 K at ambient pressure.[11] $Mn^{II}(TCNE)I(OH_2)$,[12] **1**, and $Mn^{II}(TCNE)_{3/2}(I_3)_{1/2}\bullet zTHF$,[10] **2**, extend this family of structurally related $[TCNE]^{\bullet-}$ containing compounds.

$Mn^{II}(TCNE)_{3/2}(I_3)_{1/2}\bullet zTHF$, **2**, consists of layers separated by 7.96 Å that are interconnected by μ_4-$[TCNE]^{\bullet-}$, Figure 5.1, which results in ordering as a 3-D ferrimagnet with a T_c and T_b at ambient pressure of 171 and 171 K, respectively.[10] **1** likewise possesses Mn^{II} ions bonded to four μ_4-$[TCNE]^{\bullet-}$ forming 2-D layers, but does not display interconnectivity between layers. The axial positions of the Mn^{II} ions are capped by I^- and H_2O preventing 3-D connectivity and limiting the network structure to 2-D layers, Figure 5.2.[12] Although $Mn^{II}(TCNE)I(OH_2)$ is 2-D, the interlayer separation is smaller than the other structurally related compounds at 5.00 Å, which yields a

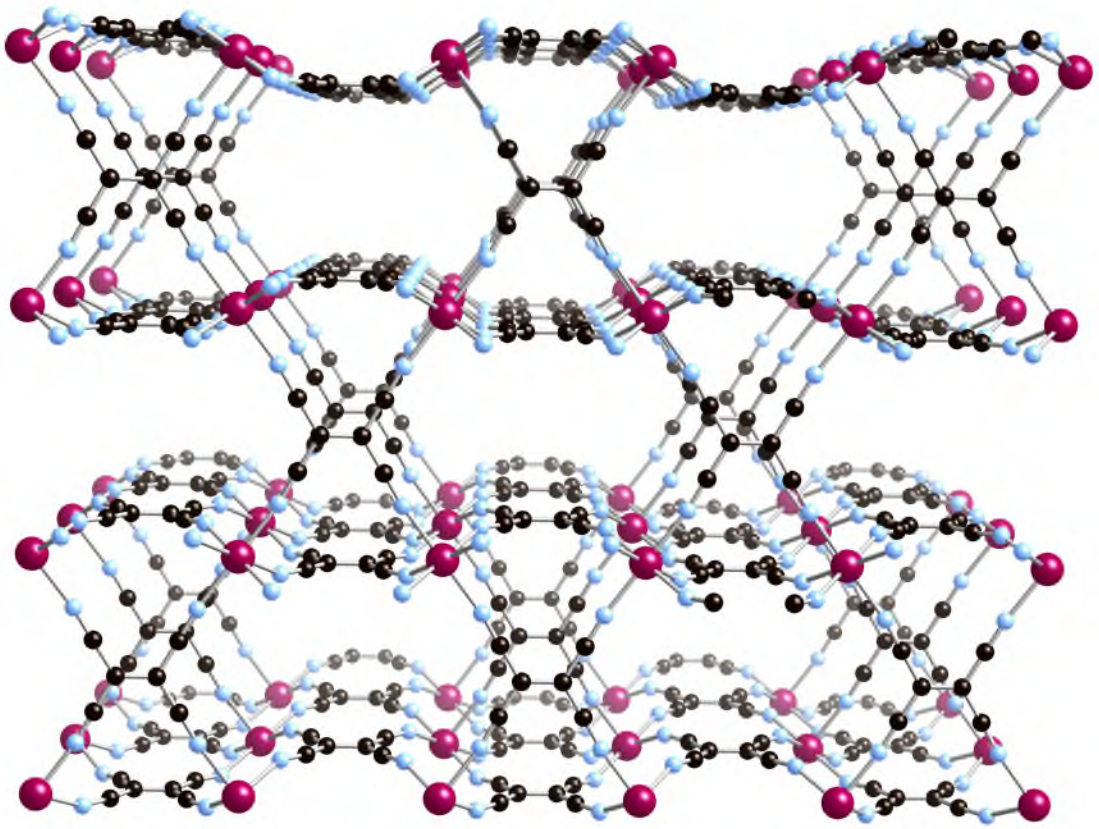

Figure 5.1. Extended network bonding via μ_4-[TCNE]$^{\bullet-}$ in 3-D present for $Mn^{II}(TCNE)_{3/2}(I_3)_{1/2}\bullet z$THF (Mn = maroon; C = black, N = blue).[10] The ordered solvent and ordered I_3^- anion reside in the channels.

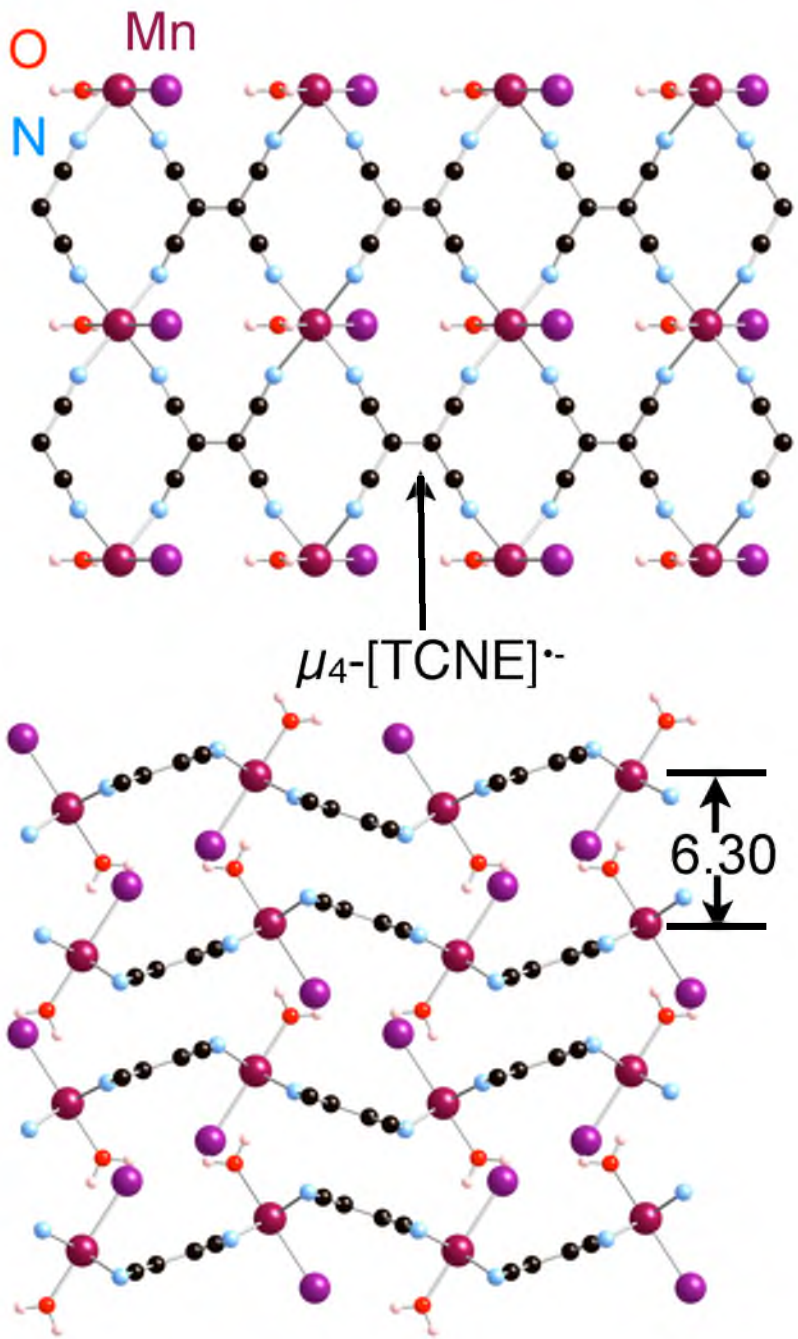

Figure 5.2. Single layer of the $Mn^{II}(TCNE)I(OH_2)$ structure (top). Side view of multiple layers of the structure of $Mn^{II}(TCNE)I(OH_2)$ (Mn = maroon; C = black, N = blue; O = red, I = purple; H = white) (bottom).[12]

correspondingly large T_c of 171 K,[12] similar to the 3-D analog $Mn^{II}(TCNE)_{3/2}(I_3)_{1/2}\bullet zTHF$.[10]

Detailed magnetic measurements under hydrostatically applied pressure have previously been performed on $Mn^{II}(TCNE)[C_4(CN)_8]_{1/2}\bullet zCH_2Cl_2$[13] and preliminary magnetic measurements were reported for $Mn^{II}(TCNE)_{3/2}(I_3)_{1/2}\bullet zTHF$.[12] $Mn^{II}(TCNE)[C_4(CN)_8]_{1/2}\bullet zCH_2Cl_2$ exhibited a magnetic transition from antiferromagnetic to ferrimagnetic behavior at 0.50 kbar, which resulted in an initial decrease in the T_c from 69 to ~20 K, followed by an increase to ~97 K at 12.6 kbar.[13] There is no hysteresis at ambient pressure. However, an onset was observed above 3.88 kbar, with the coercive field, H_{cr}, increasing with increased pressure, reaching a maximum of 280 Oe. While the ambient pressure magnetic behavior of these structurally related TCNE-based OBMs are similar [suggesting structural features of $V(TCNE)_x$], the pressure dependent magnetic behavior was evident of the subtle structural dependence of magnetic characteristics. The 2- and 3-D structural motifs and resulting magnetic properties have prompted the investigation of the pressure dependent magnetic behavior of **1** and **2**, and to compare these results with that observed for other materials.

Experimental

$Mn^{II}(TCNE)I(OH_2)$ (**1**)[12] and $Mn^{II}(TCNE)_{3/2}(I_3)_{1/2}\bullet zTHF$ (**2**)[10] were prepared similar to previously described. **1** was prepared in a glove box under N_2 atmosphere via the dropwise addition of a filtered solution of 35.6 mg of TCNE (0.28 mmol) to 145.8 mg of $MnI_2(THF)_3$ (0.28 mmol) in CH_2Cl_2. The latter solution had 6 mg of distilled H_2O added to it and it was stirred for 1 hr before it was added to the TCNE solution. This reaction was stirred for 10 days. The resulting precipitate was collected by vacuum filtration. **2** was prepared by the above route, using 50.3 mg of TCNE (0.39 mmol) to 198.3 mg of $MnI_2(THF)_3$ (0.38 mmol), except that water was not added.

Infrared spectroscopy (IR) and AC susceptibility measurements were used to confirm purity, as low temperature magnetic phases exist for each compound that have similar empirical formulas due to the limited degrees of freedom in the preparation method. The IR spectra were measured from 400 to 4,000 cm^{-1} on a Bruker Tensor 37

spectrometer (±1 cm^{-1}) as KBr pellets. A Quantum Design (QD) Physical Property Measurement System, PPMS 9 T, was used to perform AC susceptibility measurements as previously described.[14] Samples of **1** and **2** (3 - 15 mg) were loaded into gelatin capsules, to which 10 - 15 mg of decalin that freezes in the temperature range of the $M(H)$ measurements was added, in an inert atmosphere glovebox and sealed with silicone grease prior to measurement. A QD Superconducting Quantum Interference Device (SQUID) Magnetic Property Measurement System (MPMS-5XL 5 T) (sensitivity = 10^{-8} emu or 10^{-12} emu/Oe at 1 T) was used to perform the pressure dependent measurements. Samples of **1** (~ 1 mg) were loaded into a Teflon™ cell with ~1 mg tin (Mallinckrodt, 99.9769%), while samples of **2** were loaded with ~1 mg of Pb.[15] The remaining volume of the Teflon cell was filled with decalin (the hydrostatic pressure media) that is frozen at the temperatures utilized for $M(H)$ measurements, and capped with Teflon plugs. The Teflon sample cell was placed in a Be-Cu hydrostatic pressure cell based on the Kyowa Seisakusho design with zirconia pistons and rubber o-rings. Pressure was applied to the assemblage using a Kyowa Seisakusho CR-PSC-KY05-1 apparatus and a WG-KY03-3 pressure sensor. An Aikoh Engineering Model-0218B digital sensor readout was used as an approximate pressure guide during pressure application. The applied pressure was determined in situ by measuring the superconducting critical temperature, T_{sc}, of Sn[16a] for **1** and Pb[16b] for **2**, which have a known dependency of T_{sc} as a function of pressure. The estimated error for the pressure is ±0.05 kbar.

The zero-field cooled, $M_{ZFC}(T)$, and field cooled, $M_{FC}(T)$, magnetizations were measured in a 5 Oe applied magnetic field. The $M_{FC}(T)$ and remnant magnetization, $M_r(T)$, were cooled in a 5 Oe applied magnetic field. The T_c was determined as the temperature intercept of the extrapolation of the most linear portion of the remnant magnetization, $M_r(T)$. The bifurcation temperature, T_b, was taken to be the divergence of zero-field cooled, $M_{ZFC}(T)$, and field cooled, $M_{FC}(T)$, magnetizations. Isothermal field dependent measurements, $M(H)$, were performed at 4 K due to the inclusion of Sn (T_{sc} = 3.732 K).[16] The coercive field, H_{cr}, was determined from the extrapolation of the field intercept at zero magnetization upon reduction from an applied field of ±50 kOe, and the remnant magnetization, M_r, was determined from the extrapolation of the

magnetization intercept at zero applied field upon reduction of an applied field of ±50 kOe, and the saturation magnetization, M_s, was determined as the magnetization achieved at 5 T applied field.

Discussion

Prior to investigation of the pressure dependence of the magnetic properties of $Mn^{II}(TCNE)I(OH_2)$, **1**, the ambient pressure data were remeasured at 4 K for comparison to the literature values. The T_c and T_b were previously determined to be 171 and 172 K, from the $M_r(T)$ and the $M_{ZFC}(T)$ and $M_{FC}(T)$, respectively.[12] The H_{cr}, M_r, and M(9 T) were previously reported to be 400 Oe, 60 emuOe/mol, and 12,200 emuOe/mol at 5 K.[12] The immiscibility of water and CH_2Cl_2 makes it challenging to replicate reactions and isolate a pure product. This is illustrated by the previously published AC susceptibility, which displays two separate features at lower temperatures in addition to the major peak at 170 K.[12] The ambient pressure T_c, T_b, H_{cr}, and M_r of the sample used for pressure studies were 169 K, 169 K, 690 Oe, and 620 emuOe/mol, respectively. Due to instrumental limitations the maximum applied field was ±50 kOe, which was insufficient to saturate the magnetization of $Mn^{II}(TCNE)I(OH_2)$. The maximum observed magnetization was 13,800 emuOe/mol at 5 T. The T_c and T_b agreed within the error of the measurements, while the H_{cr}, M_r, and M(5 T) were significantly greater. This is attributed to the lower temperature of the measurement that has led to a larger H_{cr} in several related compounds.[17] In addition, isolation of a purer sample of $Mn^{II}(TCNE)I(OH_2)$ than has previously been measured could also be expected to yield a larger H_{cr}. Likewise, M_r and M(5 T) have been found to depend on purity and crystal alignment in some materials.[18,19]

The pressure dependence of $M_{ZFC}(T,P)$, $M_{FC}(T,P)$, and $M_r(T,P)$ had virtually no change below ~1 kbar for **1**, but both T_b, and T_c increase with increasing pressure above 1 kbar, Figure 5.3. Above ~1 kbar the T_c and T_b increase approximately linearly to 257 and 261 K at the maximum applied pressure of 14.05 kbar, at an average rate of 6.25

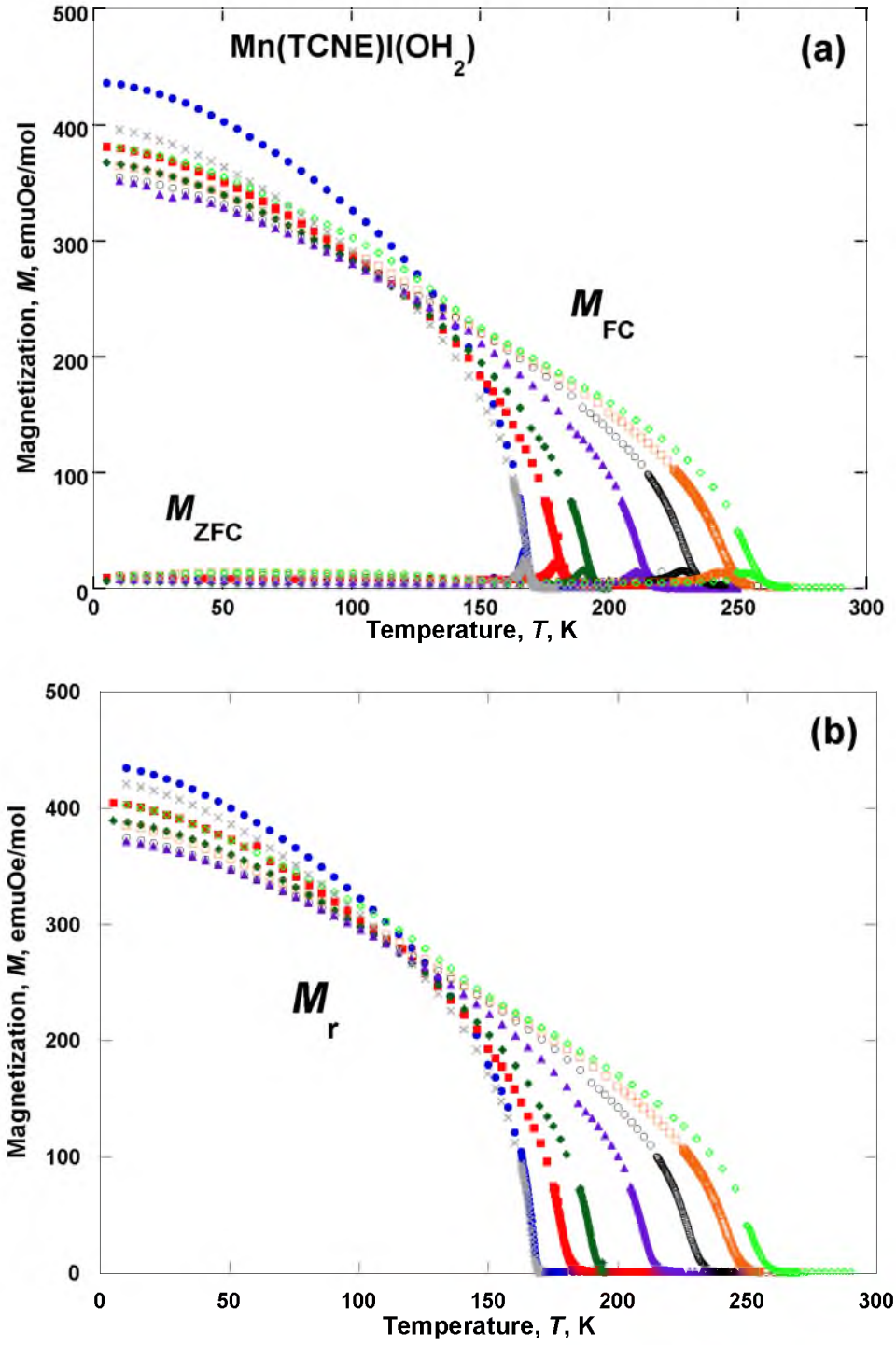

Figure 5.3. Pressure dependence of the $M_{ZFC}(T)$ and $M_{FC}(T)$ (a) and the $M_r(T)$ (b) for **1**: 0.82 (●), 1.22 (■), 2.82 (◆), 4.98 (▲), 8.45 (O), 11.44 (□), 14.05 kbar (◊), and upon returning to approximately ambient pressure [0.52 kbar (×)] for $Mn^{II}(TCNE)I(OH_2)$.

and 6.58 K/kbar, respectively, Figure 5.4. Upon release of the applied pressure the T_c and T_b were recovered, indicating reversibility. The decrease of $M_{ZFC}(T,P)$, $M_{FC}(T,P)$, and $M_r(T,P)$ is in agreement with previously reported studies,[15,20] up to 4.98 kbar, above which an anomalous increase in the magnetization was observed, Figure 5.3. The increase in the magnetization at intermediate to high pressures resembles that observed for $[Ru_2(O_2CMe)_4]_3[Cr(CN)_6]$ above 5.45 kbar,[15] even though not as pronounced for $Mn^{II}(TCNE)I(OH_2)$.

At ambient pressure and 4 K $Mn^{II}(TCNE)I(OH_2)$ has a H_{cr}, of 690 Oe, magnetization at 5 T of 13,800 emuOe/mol, and M_r, of 620 emuOe/mol, which are higher than the previously reported values of 400 Oe, 8,350 emuOe/mol at 5 T (12,200 emuOe/mol at 9 T), and 60 emuOe/mol, respectively.[12] With increasing pressure, the $M(H,P)$ at 4 K was similar to T_c and T_b with little change below ~1 kbar, followed by an approximately linear increase of the H_{cr} and M_r to 1460 Oe and 2300 emuOe/mol at 14.05 kbar, respectively, Figure 5.5 and Figure 5.6. The qualitative shape of the hysteresis loops transitioned between 2.82 and 4.98 kbar, from the complex ambient pressure behavior to a more standard shape, approaching saturation at 5 T instead of ~8 T, Figure 5.5, which was previously observed at ambient pressure.[12] The M_s above 2.82 kbar were as much as 40% greater than the literature value of 12,200 emuOe/mol, reaching 17,400 emuOe/mol at 11.44 kbar. This disparity is likely due in part to the enhanced purity with respect to previous samples (vide supra). Also, the M_s increased by 900 emuOe/mol with an increase of pressure from 4.98 to 11.44 kbar, which suggests that $Mn^{II}(TCNE)I(OH_2)$ does not saturate in ±5 T applied field until ~11.44 kbar. Upon release of the applied pressure the H_{cr}, M_r, and M(9 T) were recovered, indicating reversibility. The results are summarized in Table 5.1.

The ambient pressure magnetic properties of **2** were also reinvestigated prior to measurement of the pressure dependence for comparison to the literature values. The T_c and T_b were previously determined to be 171 and 171 K, from the $M_r(T)$ and the $M_{ZFC}(T)$ and $M_{FC}(T)$, respectively.[10] These values were reasonably reproduced with values of 173 and 173 K for the T_c and T_b, respectively. The H_{cr}, M_r, and M_s were previously reported to be 600 Oe, 8,000 emuOe/mol, and 21,800 emuOe/mol at 10 K.[10]

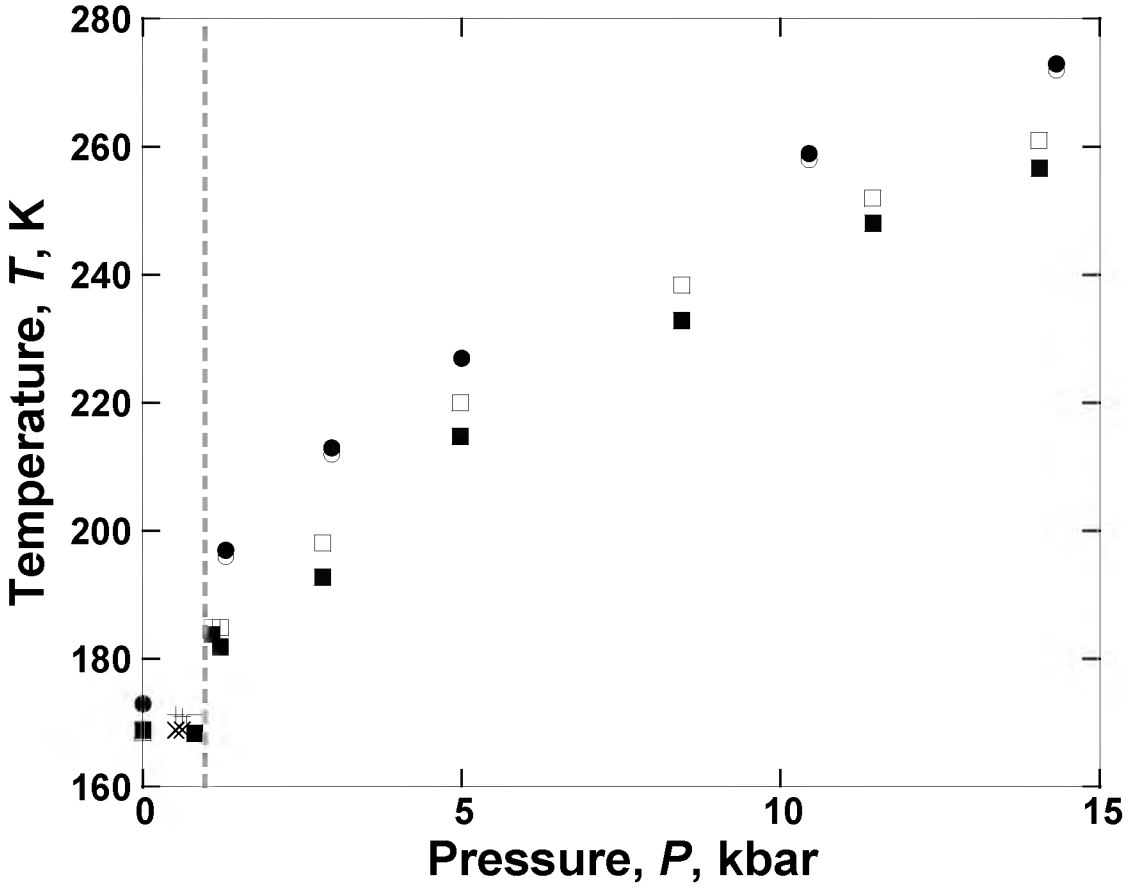

Figure 5.4. Pressure dependence of T_c (■) and T_b (□) for **1** and T_c (●), T_b (o) for **2**, released pressure data are + and x. The dashed line at ~1 kbar represents the separation of the high and low-pressure regions for **1**.

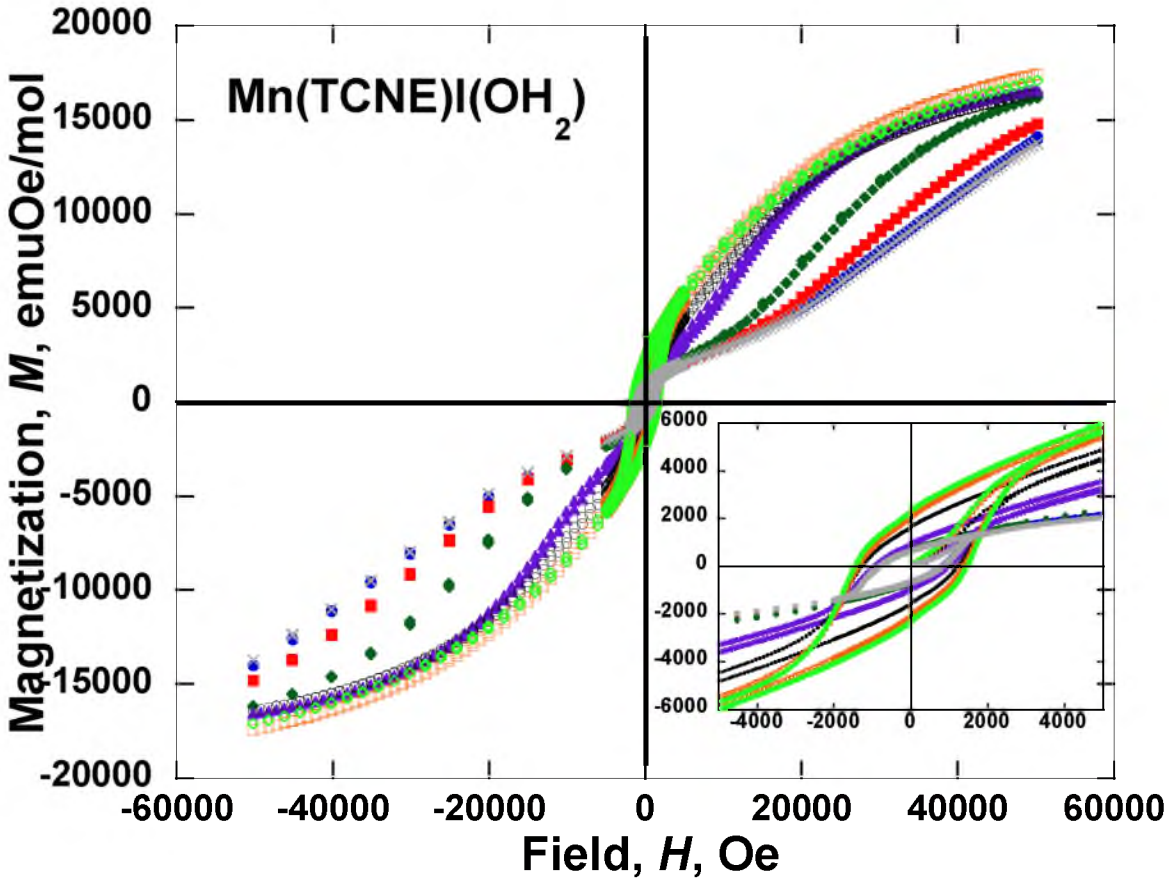

Figure 5.5. Pressure dependence of the $M(H)$ of **1** at 0.82 (●), 1.22 (■), 2.82 (◆), 4.98 (▲), 8.45 (O), 11.44 (□), 14.05 kbar (◊), and upon returning to approximately ambient pressure [0.52 kbar (×)]. Inset displays the hysteretic loop ± 5,000 Oe.

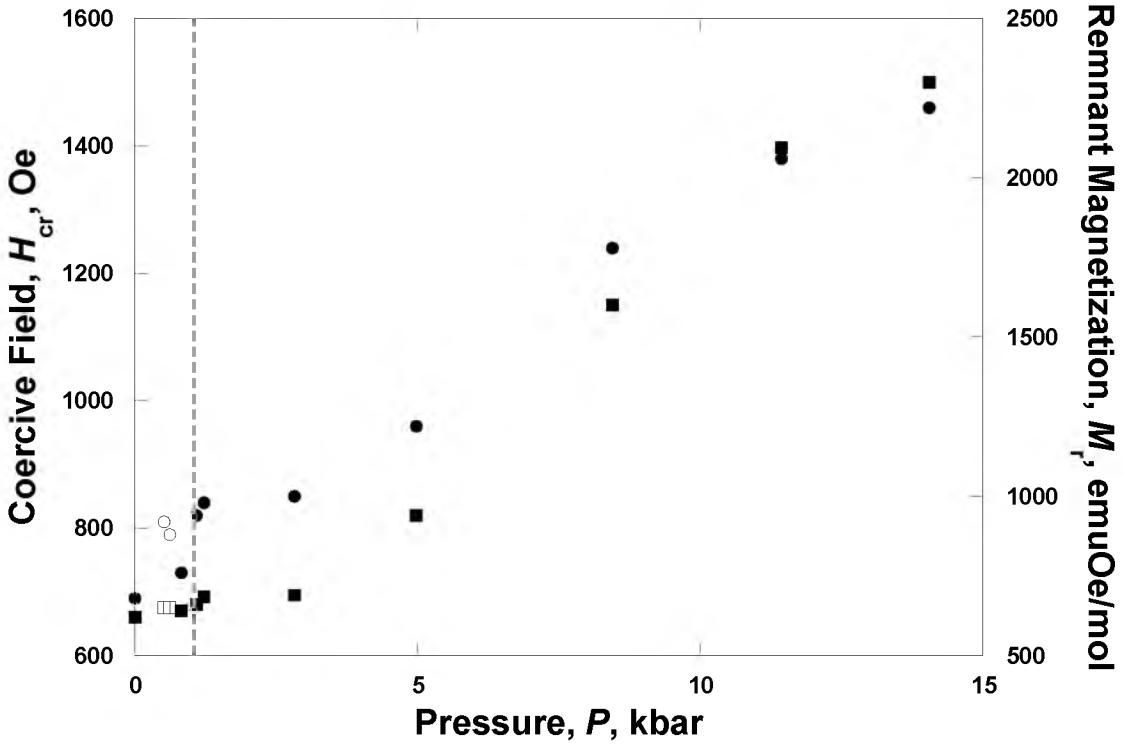

Figure 5.6. Pressure dependence of H_{cr} (●) and M_r (■) of **1**, released pressure measurements are hollow. The dashed line at approximately 1 kbar represents the separation of the high- and low-pressure regions.

Table 5.1. Summary of the ambient and pressure dependent magnetic behavior of magnetic behavior for **1** and **2**.

	P, kbar	T_c, K	Rate,[a] K/kbar	T_b, K	Rate,[a] K/kbar	H_{cr}, Oe	M(5 T), emuOe/mol	M_r, emuOe/mol
1	Ambient[12]	171	-	172	-	400	8,350	60
1	Ambient	169	-	169	-	690	13,800	620
1	14.05	257	6.25	261	6.58	1460	17,100	2300
2	Ambient[10]	171	-	171	-	600	18,200	8000
2	Ambient	173	-	173	-	860	18,200	5300
2	14.32	273	7.18[10]	272	7.06	880	17,100	5200

[a] Average

The field dependent properties were reproduced with less accuracy at 710 Oe, 5,300 emuOe/mol, and 18,200 emuOe/mol for the H_{cr}, M_r, and M_s, respectively. As for **1**, the field dependent properties of compound **2** appear to be significantly affected by the crystalline quality of a given sample.

The pressure dependence of the $M_{ZFC}(T,P)$, $M_{FC}(T,P)$, and $M_r(T,P)$ increase linearly with increasing pressure, Figure 5.7. The T_c from the $M_r(T,P)$ and T_b from the $M_{ZFC}(T,P)$ and $M_{FC}(T,P)$ increase to 273 and 272 K at 14.32 kbar (58 and 57%, respectively), Figure 5.4 and Figure 5.7. Similar to **1**, the low temperature $M_{ZFC}(T,P)$, $M_{FC}(T,P)$, and $M_r(T,P)$ magnetizations of **2** decrease with increasing pressure, as has been observed previously, but unlike **1** exhibits an anomalous improvement at intermediate pressures, Figure 5.7.[20] Upon release of the applied pressure the T_c and T_b were recovered, indicating reversibility. The results are summarized in Table 5.1.

The M_r and M(5 T) at 10 K decrease slightly with applied pressure, with values of 5,300 and 17,000 emuOe/mol at 14.32 kbar, Figure 5.8. The H_{cr} increased throughout the range of applied pressures, achieving a maximum of 880 Oe, but exhibited a greater rate of increase at low pressures than at high pressures; the division of the high and low-pressure regions for the H_{cr} increase occurring at ~5 kbar, Figure 5.9. The hysteretic behavior and shape remained consistent at all applied pressures, Figure 5.8. Upon release of the applied pressure the T_c and T_b were recovered, indicating reversibility.

The 2-D and 3-D structural motifs of **1** and **2** are responsible for the variation of their respective pressure dependencies: **1** exhibited an average rate of change for T_c and T_b of 6.25 and 6.58 K/kbar, respectively, while **2** exhibited rates of 7.18[10] and 7.06 K/kbar, respectively. The average values for **1** are skewed somewhat by the existence of a high and low-pressure region characterized by distinct rates of enhancement of T_c, T_b, and H_{cr}, Figure 5.4 and Figure 5.6. The rate of increase of the T_c and T_b is comparable to that observed for $M^{II}(TCNE)[C_4(CN)_8]_{1/2}\bullet zCH_2Cl_2$ (6.2 and 6.6 K/kbar, respectively),[13] and $Mn^{II}(TCNE)_{3/2}(I_3)_{1/2}\bullet zTHF$ (7.18 and 7.06 K/kbar, respectively).[10] The response of 2-D **1** to pressure was similar to the 3-D **2** when only the high pressure regime was considered, 6.67 and 6.88 K/kbar for the T_c and T_b, respectively, Figure 5.4.

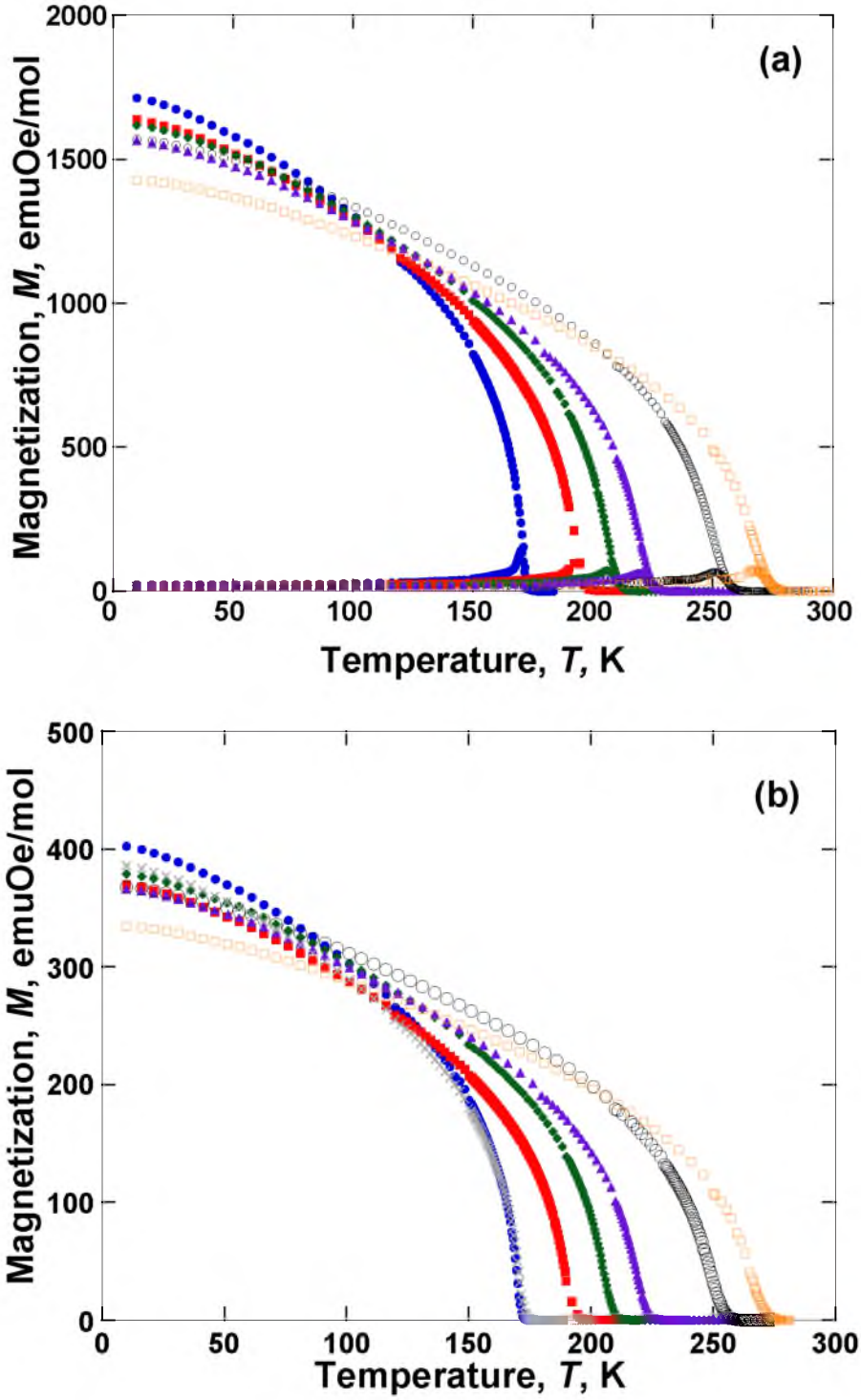

Figure 5.7. Pressure dependence of the $M_{ZFC}(T)$ and $M_{FC}(T)$ (a) and the $M_r(T)$ (b) for **2**: 0.001 (●), 1.30 (■), 2.96 (◆), 5.00 (▲), 10.44 (O), 14.32 (□), and upon returning to ambient pressure [0.001 kbar (×)] for $M_r(T)$ of **2**.

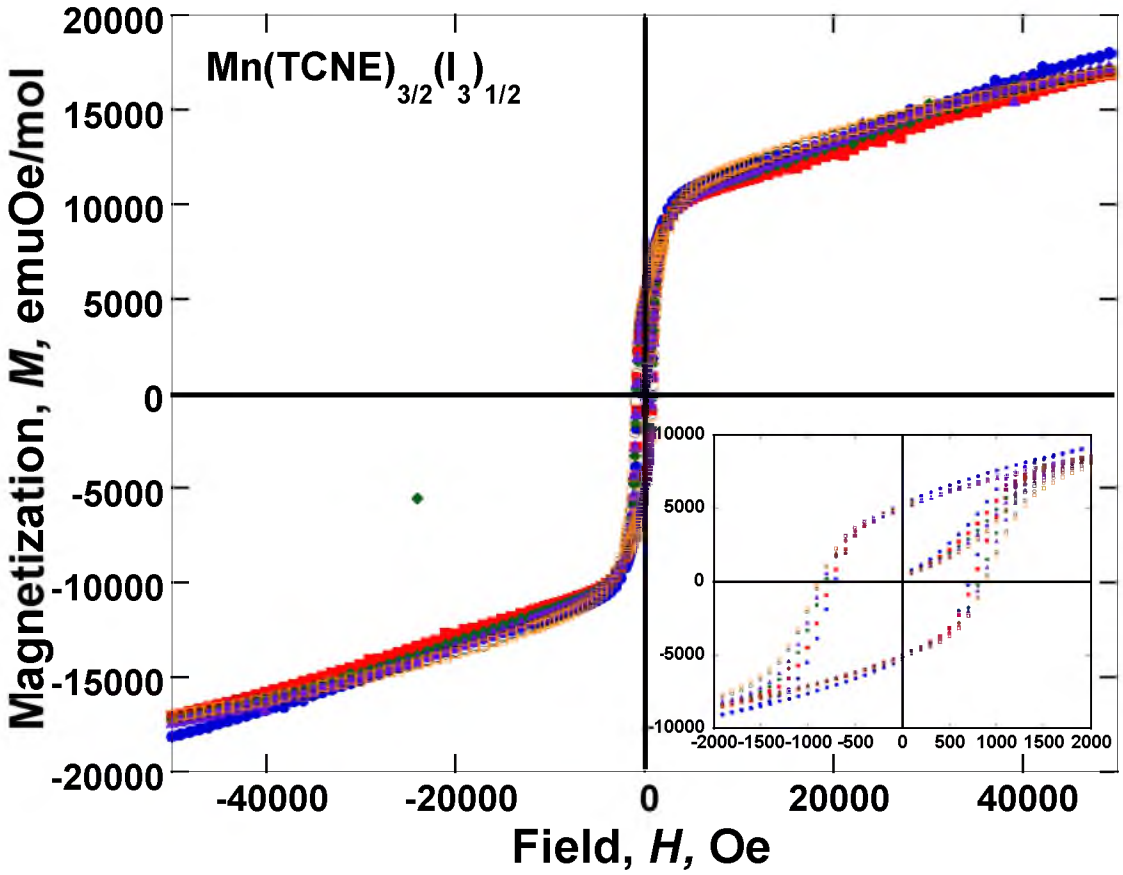

Figure 5.8. Pressure dependence of the $M(H)$ at 10 K: 0.001 (●), 1.30 (■), 2.96 (◆), 5.00 (▲), 10.44 (O), and 14.32 (□) for **2**. Inset displays the hysteretic loop ± 2000 Oe.

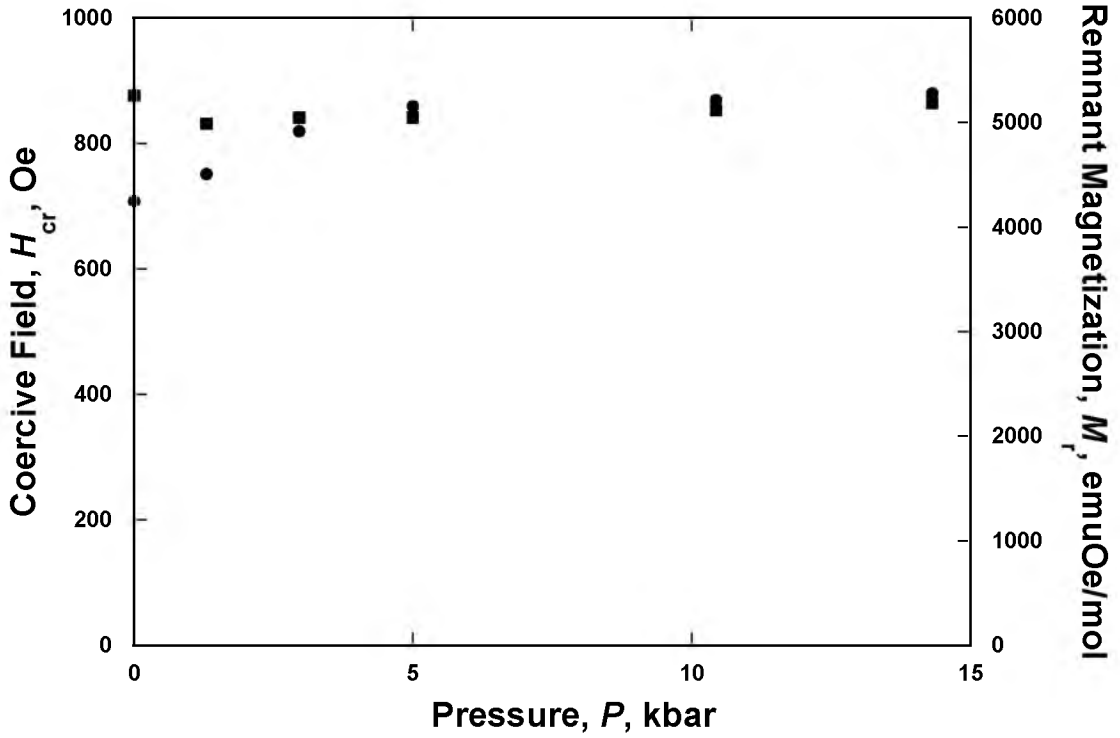

Figure 5.9. Pressure dependence of H_{cr} (●) and M_r (■) of **2**, released pressure measurements are concurrent with ambient pressure data points.

Presumably, these improvements are due to the contraction of interatomic distances, thereby increasing the coupling through increased overlap of the $[TCNE]^{\bullet-}$ π^* and Mn *d*-orbitals. Interestingly, though $Mn^{II}(TCNE)I(OH_2)$ is composed of 2-D layers, the trends observed in the magnetic data lack the complexity expected of improved interlayer coupling, namely the suppression of hysteretic behavior. This suggests that the interlayer interaction in $Mn^{II}(TCNE)I(OH_2)$ is either significantly weak, even with reduced interlayer separation, resulting in insufficient coupling to suppress the hysteretic behavior, or that the interaction is of quite a different nature than the expected through space antiferromagnetic coupling. The increased coercivity with applied pressure for **1** is qualitatively similar to that observed for **2** and $M^{II}(TCNE)[C_4(CN)_8]_{1/2}\bullet zCH_2Cl_2$, which increased from zero at ambient pressure to 280 Oe at 12.6 kbar,[13] which further suggests a unique interlayer interaction.

The existence of two distinct pressure regions is presumably due to the 2-D structural motif of $Mn^{II}(TCNE)I(OH_2)$, where the low pressure region is representative of interlayer compression over a distance insufficient to perturb the magnetic interaction between layers, thus resulting in a lack of significant increase in the T_c, T_b, H_{cr}, or M_r. The similarity of the pressure induced increase in T_c and T_b for **2** serves as a useful illustration of the macroscopic consequences of 3-D connectivity. **2** responds immediately and continually to applied pressure in contrast to the 2-D compound **1**, and, as the most significant structural difference between the two structures is the connectivity, it may be inferred that this quality is responsible for the varied behavior of the compounds.

Conclusion

The pressure dependent magnetic behavior of **1** was measured up to 14.05 kbar, with emphasis around ~1 kbar, which approximates a transition in the pressure dependent magnetic behavior, and was measured up to 14.32 kbar for **2**. Both compounds displayed pressure-induced enhancement of magnetic properties. Two-dimensional $Mn^{II}(TCNE)I(OH_2)$ exhibits a high T_c and substantial response to applied pressure up to 14.05 kbar, which more closely resembles the behavior of the related 3-D compounds, **2** and $Mn^{II}(TCNE)[C_4(CN)_8]_{1/2}\bullet zCH_2Cl_2$. This behavior suggests that the

initial pressurization reduces the interlayer separation of $Mn^{II}(TCNE)I(OH_2)$. Above ~1 kbar the interlayer separation has reduced sufficiently to allow significant or increased interlayer coupling. The nature of this unknown coupling mechanism makes further structural and spectroscopic studies of $Mn^{II}(TCNE)I(OH_2)$ under applied pressure important.

References

(1) Miller, J. S. *Adv. Mater.* **1990**, *2*, 98.

(2) Miller, J. S. *Chem. Soc. Rev.* **2011**, *40*, 3266.

(3) Ovcharenko, V. I.; Sagdeev, R. Z. *Russ. Chem. Rev.* **1999**, *68*, 345.

(4) Blundell, S. J.; Pratt F. L. *J. Phys.: Condens. Matter*, **2004**, *16*, R771.

(5) Miller, J. S.; Epstein, A. J. *Angew. Chem. Int. Ed. Engl.* **1994**, *33*, 385.

(6) Varret, F.; Nogues, M.; Goujon, A. in *Magnetism: Molecules to Materials*; Miller, J. S., Drillon, M., Eds.; Wiley-VCH: New York, 2000, Vol. 1, p 257.

(7) (a) Rabu, P.; Drillon, M.; Awaga, K.; Fujita, W.; Sekine, T. in *Magnetism: Molecules to Materials*, Vol. 2, Miller, J. S., Drillon, D., Eds.; Wiley-VCH: Weinheim, 2001; p 357. (b) Nakatsuji, S. *J. Synth. Org. Chem., Jpn.* **2003**, *61*, 670.

(8) Miller, J. S. *Polyhed.* **2009**, *28*, 1596.

(9) Her, J.-H.; Stephens, P. W.; Pokhodnya, K. I.; Bonner, M.; Miller, J. S. *Angew. Chem., Int. Ed.* **2007**, *46*, 1521.

(10) Stone, K. H.; Stephens, P. W.; McConnell, A. C.; Shurdha, E.; Pokhodnya, K. I.; Miller, J. S. *Adv. Mater.* **2010**, *22*, 2514.

(11) Pokhodnya, K. I.; Bonner, M.; Her, J.-H.; Stephens, P. W.; Miller, J. S. *J. Am. Chem. Soc.* **2006**, *128*, 15592.

(12) Lapidus, S. H.; McConnell, A. C.; Stephens, P. W.; Miller, J. S. *Chem. Commun.* **2011**, *47*, 7602.

(13) McConnell, A. C.; Bell, J. D.; Miller, J. S. *Inorg. Chem.* **2012**, *51*, 9978.

(14) Kareis C. M.; Her, J.-H.; Stephens, P. W.; Moore, J. G.; Miller, J. S. *Chem. Eur. J.* **2012**, *18*, 9281. Brandon, E. J.; Rittenberg, D. K.; Arif, A. M.; Miller, J. S. *Inorg. Chem.* **1998**, *37*, 3376.

(15) Shum, W. W.; Her, J.-H.; Stephens, P. W.; Lee, Y.; Miller, J. S. *Adv. Mater.* **2007**, *19*, 2910.

(16) (a) Jennings, L. D.; Swenson, C. A. *Phys. Rev.* **1958**, *112*, 31. (b) Clark, M. J.; Smith, T. F. *J. Low Temp. Phys.* **1978**, *32*, 495.

(17) (a) Chittipeddi, S.; Cromack, K. R.; Miller, J. S.; Epstein, A. J. *Phys. Rev. Lett.* **1987**, *58*, 2695. (b) Rittenberg, D. K.; Sugiura, K.-i.;Sakata, Y.; Mikami, S.; Epstein, A. J.; Miller, J. S. *Adv. Mater.* **2000**, *12*, 126. (c) Sun, H.-L.; Wang, Z.-M.; Gao, S. *Chem. Eur. J.* **2009**, *15*, 1757. (d) Sessoli, R. *Angew. Chem. Int. Ed.* **2008**, *47*, 5508. (e) Ishii, N.; Okamura, Y.; Chiba, S.; Nogami, T.; Ishida, T. *J. Am. Chem. Soc.* **2008**, *130*, 24.

(18) Taliaferro, M. L.; Palacio, F.; Miller, J. S. *J. Mater. Chem.* **2006**, *16*, 2677.

(19) Morrish, A. H. *The Physical Principles of Magnetism*; John Wiley & Sons, Inc.: New York, 1965, pp 340-60.

(20) DaSilva, J. G.; Miller, J. S. *Inorg. Chem.* **2013**, *52*, 1108.

CHAPTER 6

PRESSURE DEPENDENT INCREASE IN T_c AND MAGNETIC BEHAVIOR OF $[Ru_2(O_2CBu^t)_4]_3[M(CN)_6]\cdot 2H_2O$ (M = Cr, Fe)

Reprinted (adapted) with permission from: DaSilva, J. G.; Miller, J. S. *Inorg. Chem.* **2013**, *52*, 1418-1423.

Abstract

Magnetization as a function of applied pressure up to 10.16 kbar and magnetic field were obtained for layered $[Ru_2(O_2CBu^t)_4]_3[M(CN)_6]\cdot 2H_2O$ (M = Cr, Fe). For M = Fe the T_c increased by 13% from 6.1 to 6.9 K with a significant increase in the coercive field, H_{cr}, from 5 to 65 Oe, followed by a sharp decrease to less than 10 Oe at further applied pressure. A 32% increase in T_c from 37.8 to 50.0 K was observed for M = Cr as well as a linear decrease of H_{cr} upon increasing pressure from 6380 to 2380 Oe.

Introduction

The production excluding utilization of magnets is expected to reach $17.2 billion worldwide by 2020.[1] This has focused research toward the discovery, comprehension, and development of cheaper, more efficient and stronger magnets that have quantum characteristics coupled to their magnetic behavior. The discovery of the first ferromagnetic organic-based magnet,[2,3,4,5] $[Fe^{III}Cp^*_2][TCNE]$ (TCNE = tetracyanoethylene; Cp^* = pentmethylcyclopentadienide),[6,7] led to promising routes to photomagnetic,[8] optoelectronic,[9] and magnetoelectric materials.[9] While $[FeCp^*_2][TCNE]$ order magnetically at 4.8 K,[6,7] other organic-based magnets have higher critical temperatures (T_c), with some extending room temperature, e. g., $V(TCNE)_x$ (x ~ 2; T_c ~ 127 °C, 400 K)[10,11] and $V_x[Cr^{III}(CN)_6]$ (T_c ~ 100 °C, 373 K).[12,13,14]

Among the growing number of organic-based magnets is a family of compounds based upon diruthenium acetate paddlewheel (D_{4h}) structured materials. Most notably, diruthenium acetate $[Ru_2(O_2CMe)_4]^+$ when reacted with $[Cr(CN)_6]^{3-}$ forms $[Ru_2(O_2CMe)_4]_3[Cr(CN)_6]$, **1**, that possesses two interpenetrating sublattices that each have alternating $S = 3/2$ $[Ru_2(O_2CMe)_4]^+$ and $S = 3/2$ $[Cr(CN)_6]^{3-}$ ions.[15,16] Compound **1** exhibits an unusual pressure dependent magnetic behavior including a transition from a metamagnetic-like phase to a ferromagnetic-like phase with an 83% increase in T_c.[17] This is attributed to antiferromagnetic coupling between independent lattices[18] below 7 kbar.[19] Above 8 kbar the antiferromagnetic coupling between the interpenetrating lattices leads to bulk ferrimagnet behavior.[17] This is theorized to be the result of a high-to-low-spin transition in the paddlewheel moiety.[19] Similar pressure induced spin transition phenomena have been reported previously for compounds containing transition metals.[20]

The greater steric bulk arising from the terminal *t*-Bu groups causes the bulk structure of $[Ru_2(O_2CBu^t)_4]_3[M(CN)_6]\bullet 2H_2O$ to be 2-D layers with differing terminal and intralayer connectivity between the $[Ru_2(O_2CBu^t)_4]^+$ and $[M(CN)_6]^{3-}$ ions, Figure 6.1, with respect to the single position for **1**.[15,21] The terminal dimer position is similar to that observed for **1** with linear Ru-N-C bonds, while the intralayer position has a significantly nonlinear Ru-N-C bond angle of 149.8°.[21] The resulting magnetic properties of $[Ru_2(O_2CBu^t)_4]_3[M(CN)_6]\bullet 2H_2O$ [M = Cr (**2**), Fe, (**3**)] are significantly enhanced from **1**, Table 6.1.

Herein, the pressure dependent magnetic behavior of **2** and **3** are reported, and the results are compared to **1** and the iron analog $[Ru_2(O_2CMe)_4]_3[Fe(CN)_6]$ (**4**).

Experimental Section

Compounds **2** and **3** were prepared by a variation to the literature method,[21,22] as $[Ru_2(O_2CBu^t)_4]Cl$ was dissolved in 5 ± 2 mL MeOH. This solvent was selected due to its ability to readily dissolve $[Ru_2(O_2CBu^t)_4]Cl$ and its miscibility in H_2O. Infrared spectroscopy and ac susceptibility were used to confirm purity of **2** and **3**. IR spectra

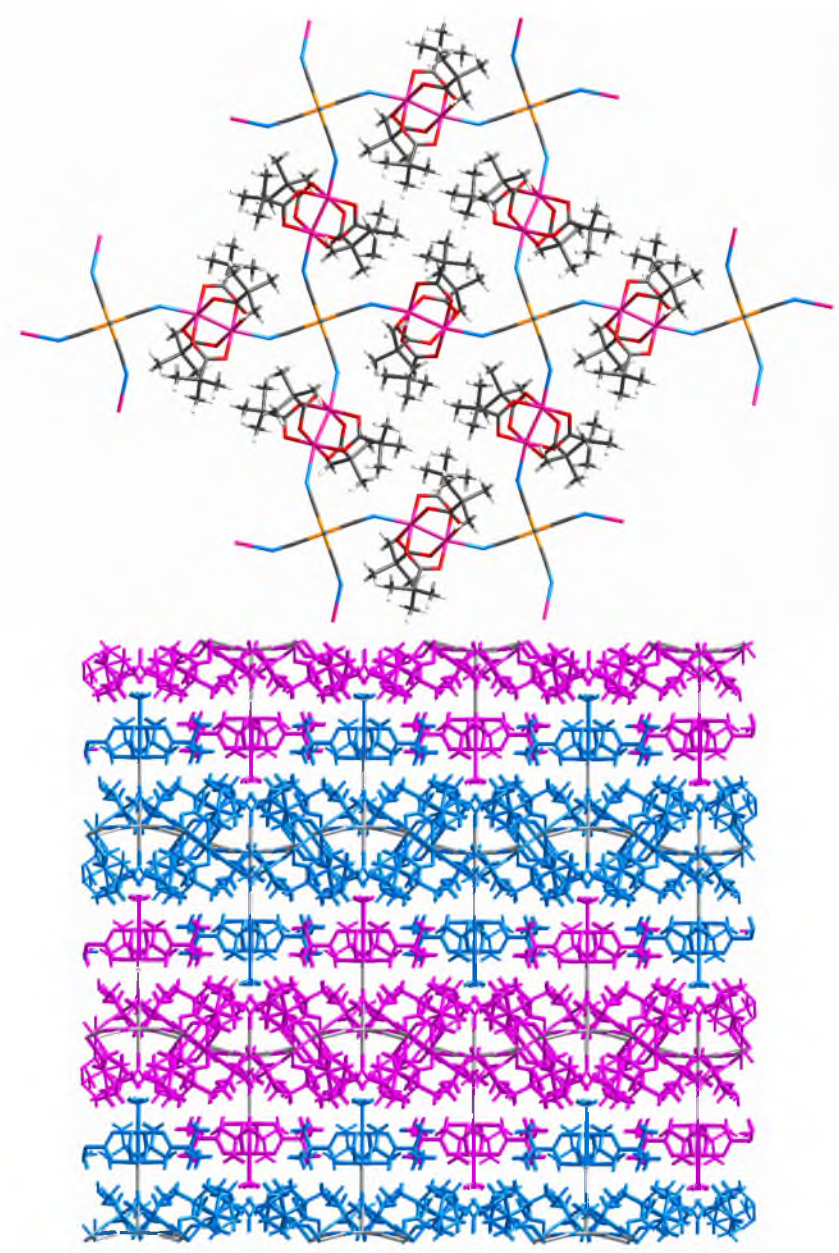

Figure 6.1. Layered structure of $[Ru_2(O_2CBu^t)_4]_3[M(CN)_6]\cdot 2H_2O$ [M = Cr, (**2**) and Fe, (**3**)]. View normal to one layer (top), and side view with adjacent layers being in different colors (bottom).[21]

Table 6.1. The T_c and H_{cr}, for **1 - 4.**

Compound	M	M_s (Oe)[b]	M_r (Oe)[b]	T_c (K)[a]	H_{cr} (Oe)[b]
2	Cr	16200	7500	37.5	20000
3	Fe	24400	3600	4.8	190
1	Cr	20800	3840	33.0	470
4	Fe	22700	40	2.1	10

[a] The T_c were reported as the peak in $\chi'(T)$ measured on a QD PPMS [b] 2 K

were measured from 400 to 4000 cm^{-1} on a Bruker Tensor 37 spectrometer (± 1 cm^{-1}) as KBr pellets. A Quantum Design (QD) Physical Property Measurement System, PPMS 9 T, was used to perform ac susceptibility measurements as previously described.[23] Samples of **2** and **3** (3-15 mg) were loaded into gelatin capsules in an inert atmosphere glovebox and sealed with silicon grease prior to PPMS measurements. A QD Superconducting Quantum Interference Device (SQUID) Magnetic Property Measurement System (MPMS-5XL 5 T) (sensitivity = 10^{-8} emu or 10^{-12} emu/Oe at 1 T) was used to perform pressure-dependent measurements.[17,23] Samples of **2** and **3** (~ 1 mg) were loaded into a Teflon^{TM} cell with ~ 1 mg tin (Mallinckrodt, 99.9769%). The remaining volume of the Teflon cell was filled with decalin (the hydrostatic pressure media) and capped with Teflon plugs. The Teflon^{TM} sample cell was placed in a beryllium-copper hydrostatic pressure cell based on the Kyowa Seisakusho design with zirconia pistons and rubber o-rings. Pressure was applied to the assemblage by using a Kyowa Seisakusho CR-PSC-KY05-1 apparatus with a WG-KY03-3 pressure sensor. An Aikoh Engineering model-0218B digital sensor readout was used as an approximate pressure guide during pressure application. The pressure was determined in situ by measuring the superconducting critical temperature, T_{sc}, of tin, which has been calibrated as function of pressure.[24]

Results and Discussion

Prior to studying the pressure dependence of magnetic properties of $[Ru_2(O_2CBu^t)_4]_3[M(CN)_6]$ [M = Cr (**2**), Fe (**3**)] the ambient pressure data were redetermined and compared to the literature values. The T_c of **2** and **3** were previously determined to be 37.5 and 4.8 K, respectively, from the peak in $\chi'(T)$.[22] Since AC measurements are not viable due to the bulk of the experimental apparatus used to maintain applied pressure on the magnetic samples, magnetization, $M(T)$, measurements were performed. The T_c was determined from the linear extrapolation of the region of most negative slope of the remnant magnetization, $M_r(T)$, and is 37.8 K for **2** and 6.1 K for **3**. Previously, irreversibility was demonstrated from the 39.5-K bifurcation temperature (T_b) of the zero-field cooled, $M_{ZFC}(T)$, and field cooled, $M_{FC}(T)$ data for **2**.[22] This is somewhat lower than 41.0 K as determined in this study. The hysteretic

behavior of **2** was determined from $M(H)$ measurements at 10 K. This is at a higher temperature than previously reported, due to the inclusion of superconducting Sn as a pressure indicator (T_{sc} = 3.728 K),[24] and to facilitate comparison with previous $M(H)$ studies that utilized superconducting Pb as a pressure indicator (T_{sc} = 7.203 K).[25] The H_{cr} of **2** was previously reported to be 20,000 Oe at 2 K,[22] is significantly reduced to 13,000 Oe at 5 K,[22] and is further reduced to 6380 Oe at 10 K. This inverse trend of $H_{cr}(T)$ has been previous reported.[26] The 5 T magnetization (M_s) and remnant magnetization (M_r) from the literature were, respectively, 16,200 and 7,500 emuOe/mol at 2 K and 15,800 and 7,500 emuOe/mol at 5 K.[22] The M_s and M_r also follow a similar trend of decreasing magnitude at elevated temperature, dropping to 14,950 and 6,590 emuOe/mol.

The pressure dependent magnetic properties of **2** reveal that the $M_r(T)$, $M_{ZFC}(T)$, and $M_{FC}(T)$ have an onset temperature that increases while the magnetization decreases with applied pressure, Figure 6.2. T_c measured by the method discussed above increases by 32.3% to 50.0 K at 10.16 kbar, and the T_b concomitantly increases by 25.6% to 51.5 K at 10.16 kbar, Figure 6.3.

Increasing applied pressure reduces the magnetization, M_s, at 5 T, the remnant magnetization, M_r, and the coercive fields, H_{cr}, while the hysteretic behavior remains consistent with the ambient pressure magnetic state, Figure 6.4. At 10.16 kbar the M_s decreases to 13,400 emuOe/mol, the M_r to 5,120 emuOe/mol, and the H_{cr} to 2,380 Oe, Figure 6.5. This is also consistent with the results of **3** at high pressures, vide infra. This is attributed to the interatomic separations decreasing as the interlayer separation of 2-D sheets decreases with pressure, thereby increasing the interlayer and intralayer couplings simultaneously. The $M_r(T)$, $M_{ZFC}(T)$, and $M_{FC}(T)$ exhibit some degradation through repetitive cycling of pressurization, but are nominally reversible, i.e., 6% reduction in T_b and a 9% reduction in T_c, Figure 6.2 and Figure 6.3. The hysteretic behavior was less reversible with further reductions in M_s, M_r, and H_{cr} upon release of the applied pressure.

This structural distortion and resultant coupling has been theorized to yield a phase transition to a canted antiferromagnetic state, CAF, where the net orientation of spin on the $S = 3/2$ $[Ru_2(O_2CBu^t)_4]^+$ is equal and opposite to the $S = 3/2$ Cr^{III} spin.[27]

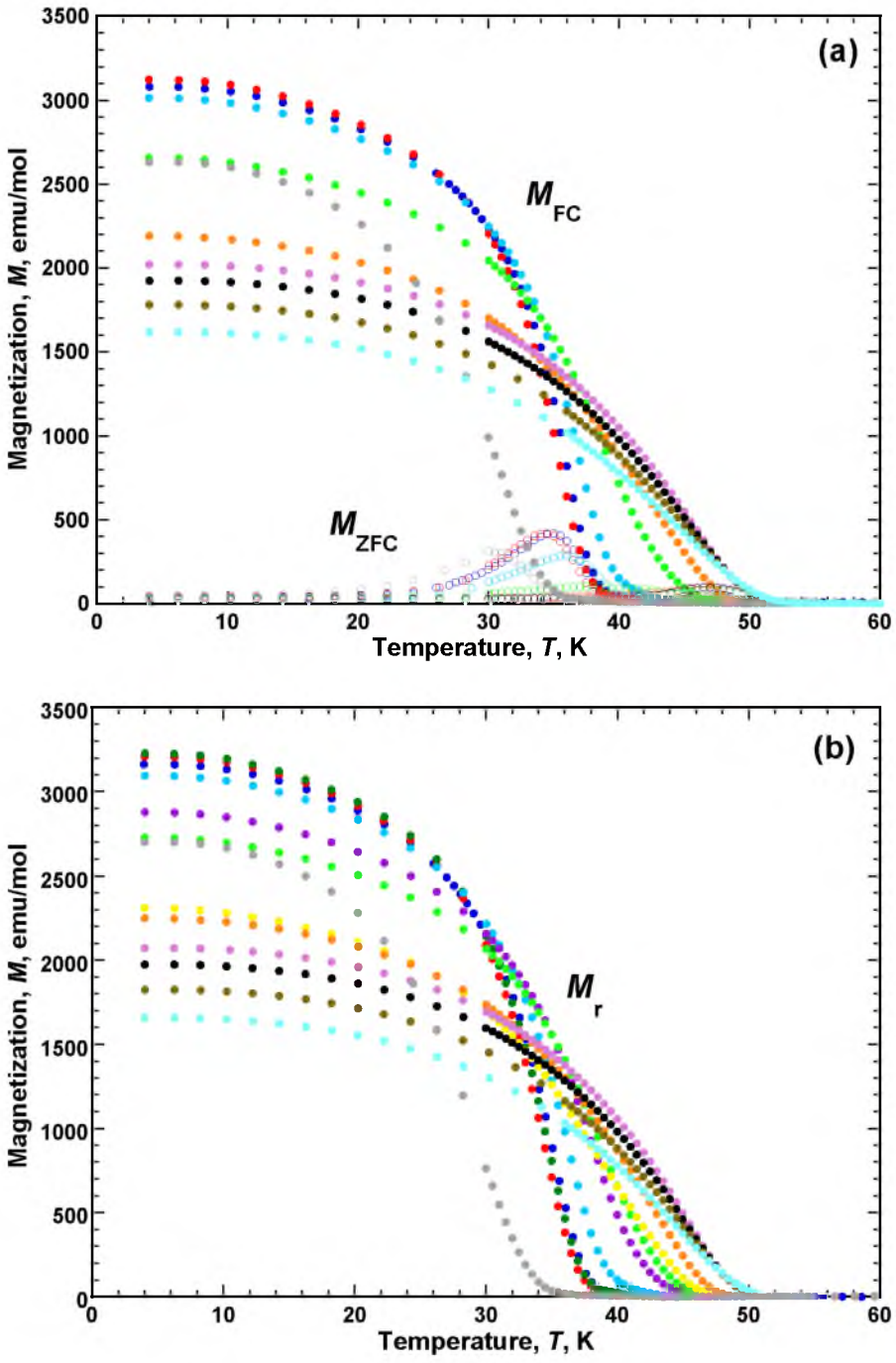

Figure 6.2. Pressure dependence for **2** of the M_{ZFC} and M_{FC} : 0.45 (◦•), 0.62 (◦•), 1.79 (◦•), 3.58 (◦•), 4.64 (◦•), 6.82 (◦•), 7.95 (◦•), 8.58 (◦•), 10.16 (◦•), and applied pressure released to 0.85 kbar (◦•) (a), and M_r : 0.45 (•), 0.52 (•), 0.62 (•), 1.79 (•), 2.73 (•), 3.58 (•), 4.19 (•), 4.64 (•), 6.82 (•), 7.95 (•), 8.58 (•), 10.16 (•), and applied pressure released to 0.85 kbar (•) (b).

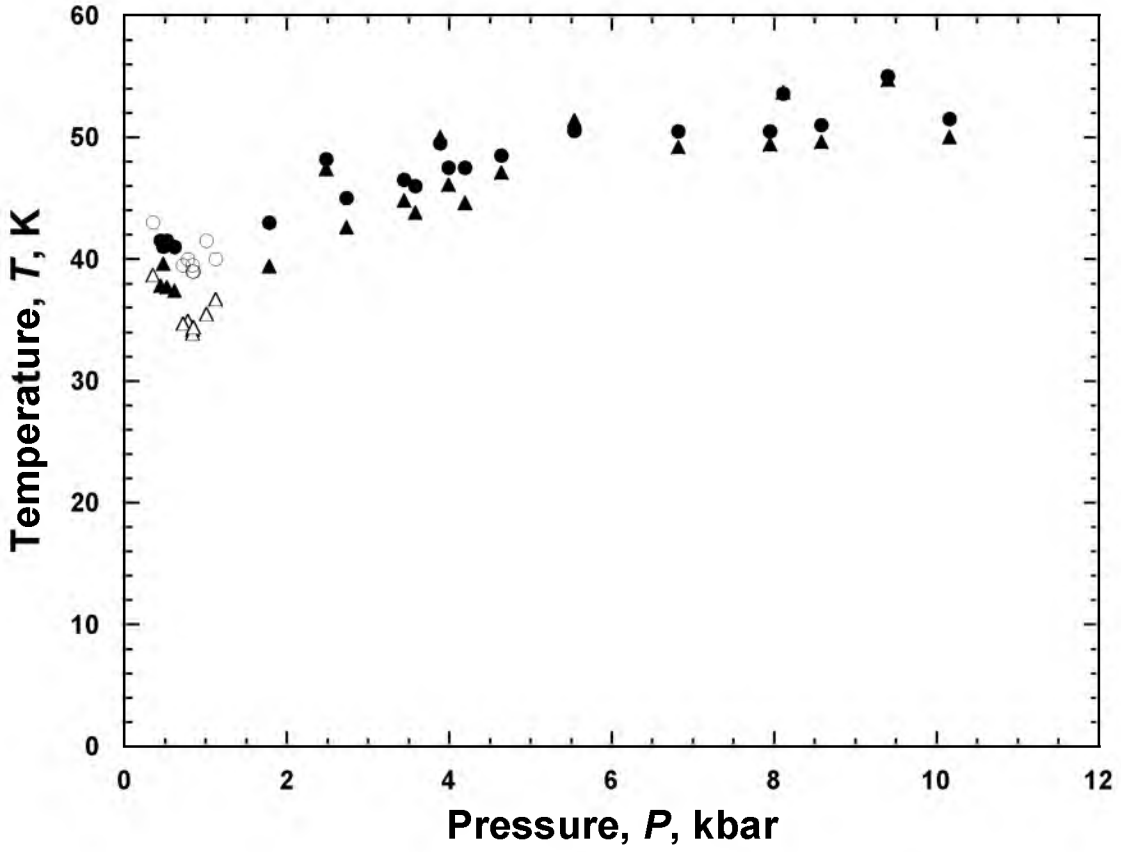

Figure 6.3. The $T_c(P)$ (▲) and $T_b(P)$ (•) (the released pressure measurements are hollow for **2** showing a linear increase with applied pressure, and reversibility with a slight decrease after successive pressure and release cycles).

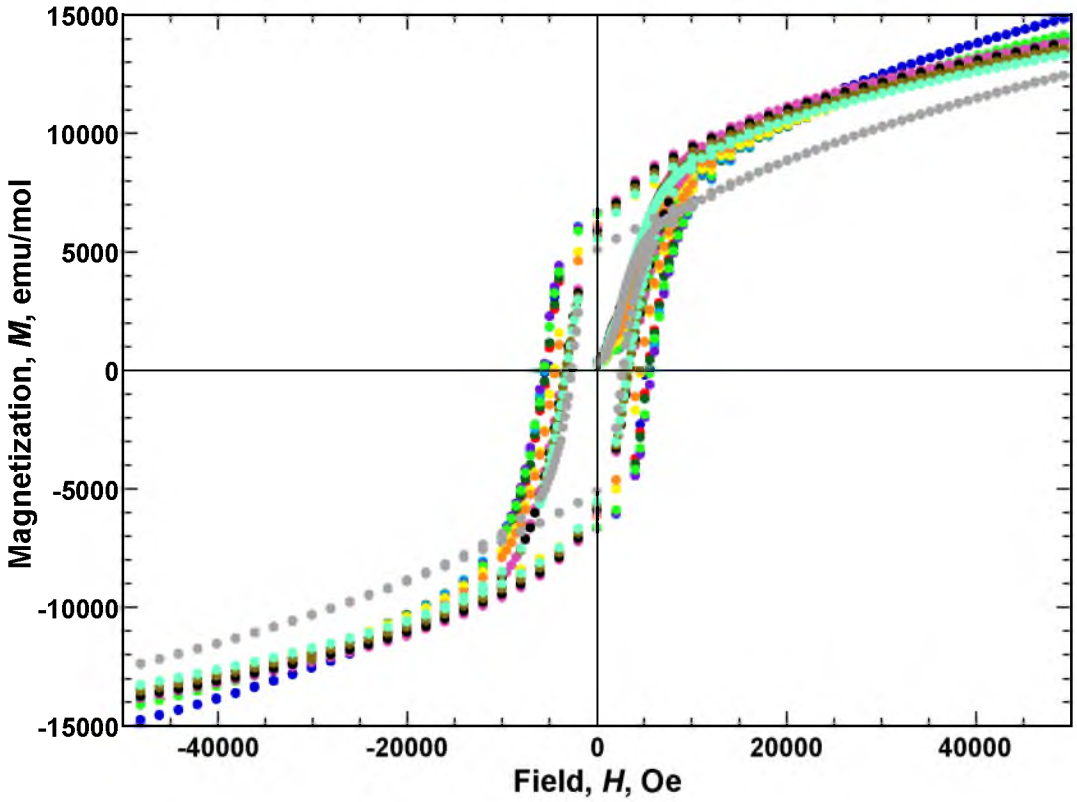

Figure 6.4. Field dependent magnetization at 10 K for **2**: 0.45 (•),0.52 (•), 0.62 (•), 1.79 (•), 2.73 (•), 3.58 (•), 4.19 (•), 4.64 (•), 6.82 (•), 7.95 (•), 8.58 (•), 10.16 (•), and applied pressure released to 0.85 kbar (•).

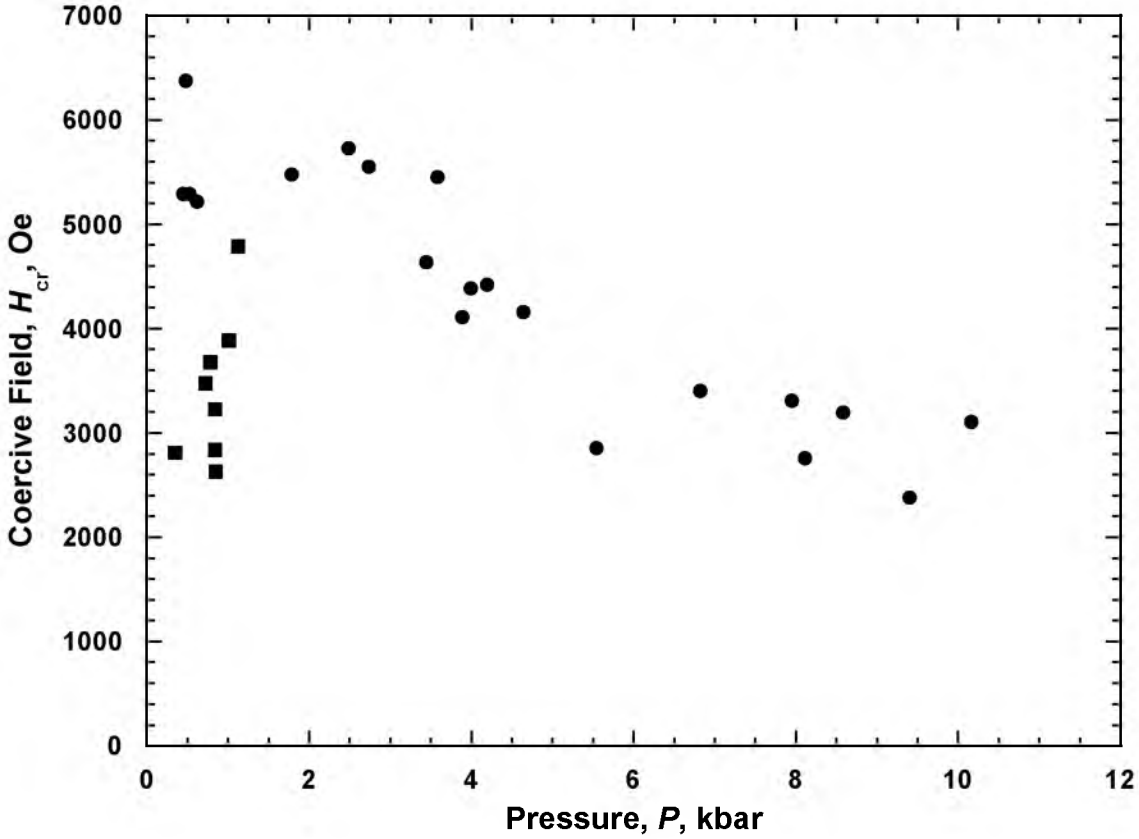

Figure 6.5. $H_{cr}(P)$ for **2** (•) released pressure measurements (■). The released measurements are shown from a series of increasing pressures, the largest H_{cr} values arising from the lowest released applied pressures. The released measurements indicate an irreversible hysteretic behavior.

Furthermore, the transition from the ambient pressure collinear ferrimagnetic phase to CAF would be evident as a "kink," or discontinuity, in $M(T)$ data.[27] Since this is not observed, higher pressure seems to be required.

Alternatively, the decreasing intralayer bond lengths increasing the intralayer coupling would account for the observed trend of both T_b and T_c increasing with applied pressure. The simultaneously decreasing interlayer separation would increase the interlayer coupling, likely antiferromagnetic, as occurs between sublattices in **1**.[19] Antiferromagnetic coupling between sublattices for **1** led to metamagnetic behavior and suppressed the H_{cr}.[17,19] Compounds **2** and **3** appear to have larger interlayer antiferromagnetic coupling as the pressure is increased suppressing H_{cr}, M_r, and to a lesser extent M_s. Complex pressure dependent suppression of the H_{cr}, M_r, and M_s was observed in the 2-D layered organic-based magnet, $[Fe^{II}(TCNE)(NCMe)_2][Fe^{III}Cl_4]$, and was hypothesized to arise from increasing antiferromagnetic interlayer coupling.[28]

$[Ru_2(O_2CBu^t)_4]_3[Fe(CN)_6]$ (**3**) magnetically orders below 4.8 K with a 5 T M_s of 24,400 emuOe/mol, a M_r of 3,600 emuOe/mol, and a H_{cr} of 190 Oe at 2 K and ambient pressure.[22] These properties were redetermined by measurements appropriate for pressurized studies. Similar measurement limitations arising from the inclusion of Sn as a pressure indicator occur for **3** as for **2**. The T_c from $M_r(T)$ was 6.1 K, the M_s was 22,810 emuOe/mol, the M_r was 180 emuOe/mol, and the H_{cr} was 5 Oe at 4 K at ambient pressure. These values are consistent with the corresponding decreases observed at 5 K for **2**.[26] The redetermined T_c, while significantly larger than the literature value of 4.8 K, is consistent with the value from the onset of $\chi''(T)$, ~ 6 K, which was not previously reported.[22]

Under increasing hydrostatic pressure, the $M_r(T)$, $M_{ZFC}(T)$, and $M_{FC}(T)$ decrease in both magnetization and onset temperature, Figure 6.6. The $M_{ZFC}(T)$ peak shifts to lower temperatures as pressure was increased, and was increasingly obscured due to the lower temperature limit of measurement. The T_c determined from $M_r(T)$ increases by 13% to 6.9 K at 9.28 kbar, but displays a plateau at intermediate pressures, Figure 6.7. Simultaneously, the T_b increase by 55% from 5.6 to 8.7 K at 9.28 kbar, but does not display a plateau, Figure 6.7.

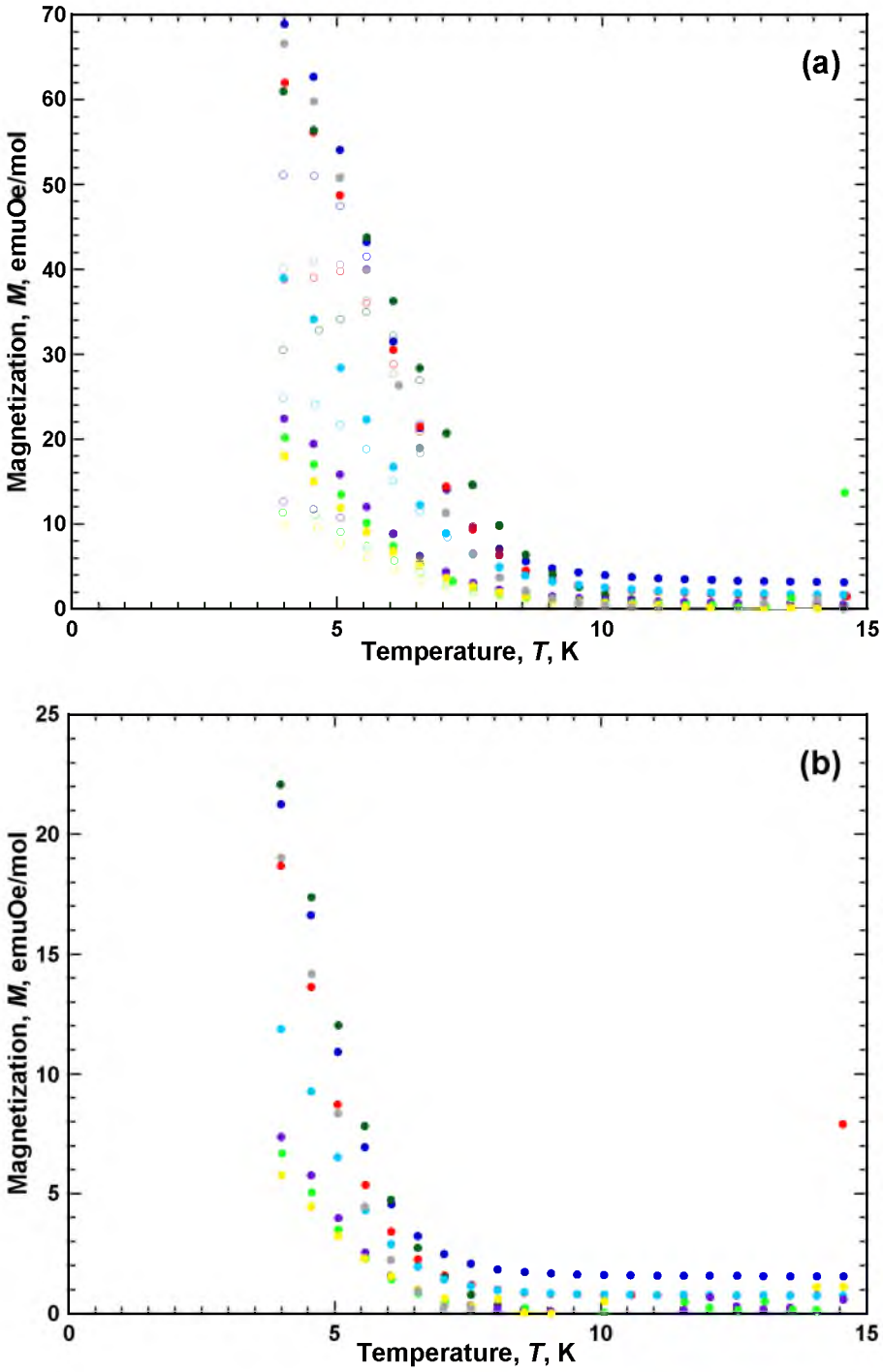

Figure 6.6. Pressure dependence for **3** of the M_{ZFC} and M_{FC} : 0.001 (◦•), 0.64 kbar (◦•), 2.43 (◦•), 4.37 (◦•), 6.02 (◦•), 8.08 (◦•), 9.28 (◦•), and applied pressure released to 0.58 kbar (◦•) (a), and M_r: 0.001 (•), 0.64 (•), 2.43 (•), 4.37 (•), 6.02 (•), 8.08 (•), 9.28 (•), and applied pressure released to 0.58 kbar (•) (b).

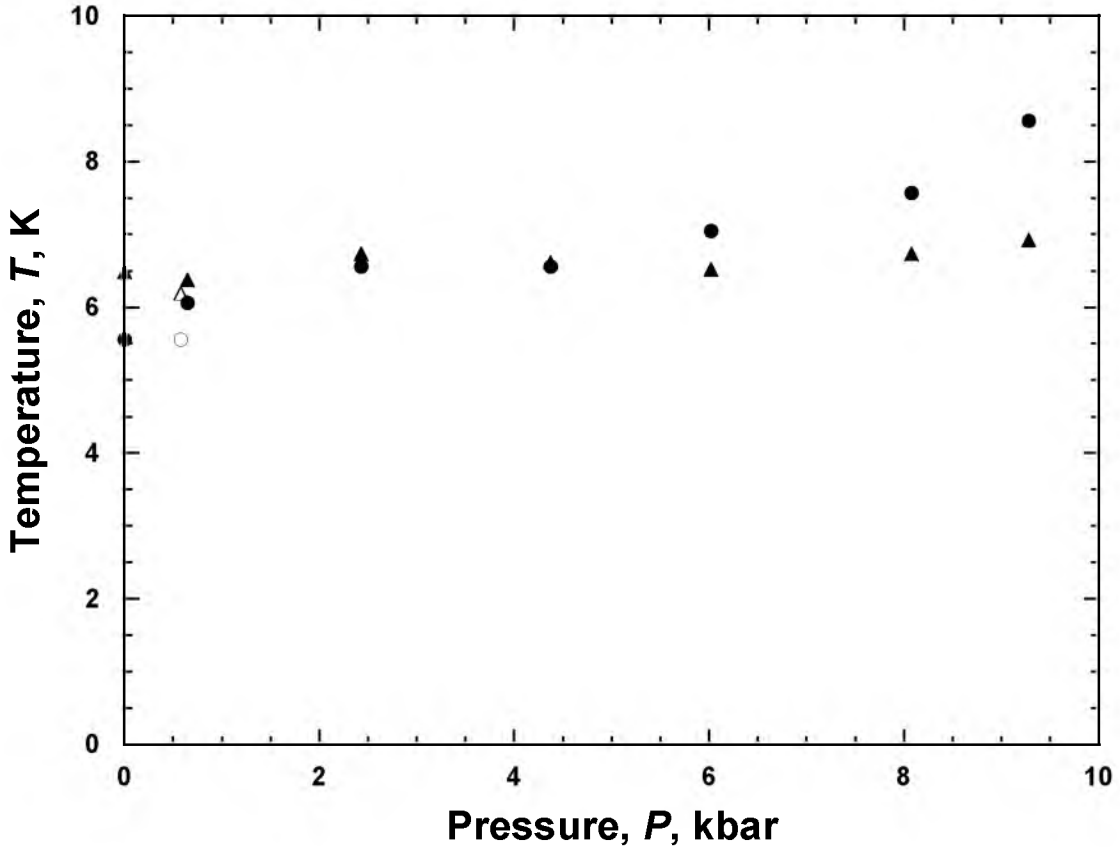

Figure 6.7. $T_c(P)$ (▲) and $T_b(P)$ (•) for **3**, the released pressure measurements are hollow.

Increasing applied pressure reduces the magnetization at 5 T, while both the M_r and the H_{cr} significantly increase. The hysteresis remains consistent with the ambient pressure magnetic state even though both M_r and H_{cr} increase, Figure 6.8. The H_{cr} increased 11-fold to 65 Oe at 2.43 kbar, but then decreased to zero as the pressure was increased to 9.28 kbar, Figure 6.9. Upon release of the applied pressure to near ambient conditions the $M_r(T)$, $M_{ZFC}(T)$, $M_{FC}(T)$, and $M(H)$ display reversibility with no apparent degradation as was observed for **2**. The large relative increase in H_{cr} upon pressurization is reasonable due to the proximity in temperature of the field dependent measurements to T_c. Quenching of the hysteretic behavior at higher applied pressures may suggest a phase transition to a metamagnetic state; however, this is inconsistent with theoretical prediction.[27] The observance of H_{cr} at intermediate pressures also does not support a phase transition. The suppression of H_{cr} above 2.43 kbar and the consistent increase of T_b with applied pressure suggests that **3** compresses similar to that proposed for **2**, resulting in simultaneous intra- and interlayer coupling increases. However, the ratio of intra/interlayer coupling for **3** differs from **2** likely due to the evidence of reversibility in the former. Finally, the reversibility of **3** suggests a structural difference from **2** under pressure, which is not yet understood.

The pressure dependences of H_{cr}, T_c, and T_b suggest a more complex behavior than observed for **2**. As pressure is increased below 2.4 kbar a similar structural change is expected for **2** and **3**. T_b and T_c would suggest this, while the precipitous increase in H_{cr} would at first seem contradictory. This can be explained by the proximity of the field-dependent measurements to the T_c. Proportionally the separation is quite small compared to the field-dependent measurement temperatures and T_c for **2**. Thus, a small increase in T_c or T_b through the application of pressure for **3** would result in a proportionally greater reduction in proximity of the field dependent measurement temperature than in **2**. H_c and H_{cr} have previously been shown to rely exponentially on the proximity of the measurement temperature to T_c in metamagnets and linearly in canted systems.[15,21,26] Above 2.4 kbar the plateau in T_c and T_b and the decrease in H_{cr} suggest a few possibilities. The plateau behavior is indicative of interlayer separation reaching a minimum, which the range of pressures utilized is incapable of surpassing, similar to the behavior of $[Fe^{II}(TCNE)(NCMe)_2][Fe^{III}Cl_4]$.[28]

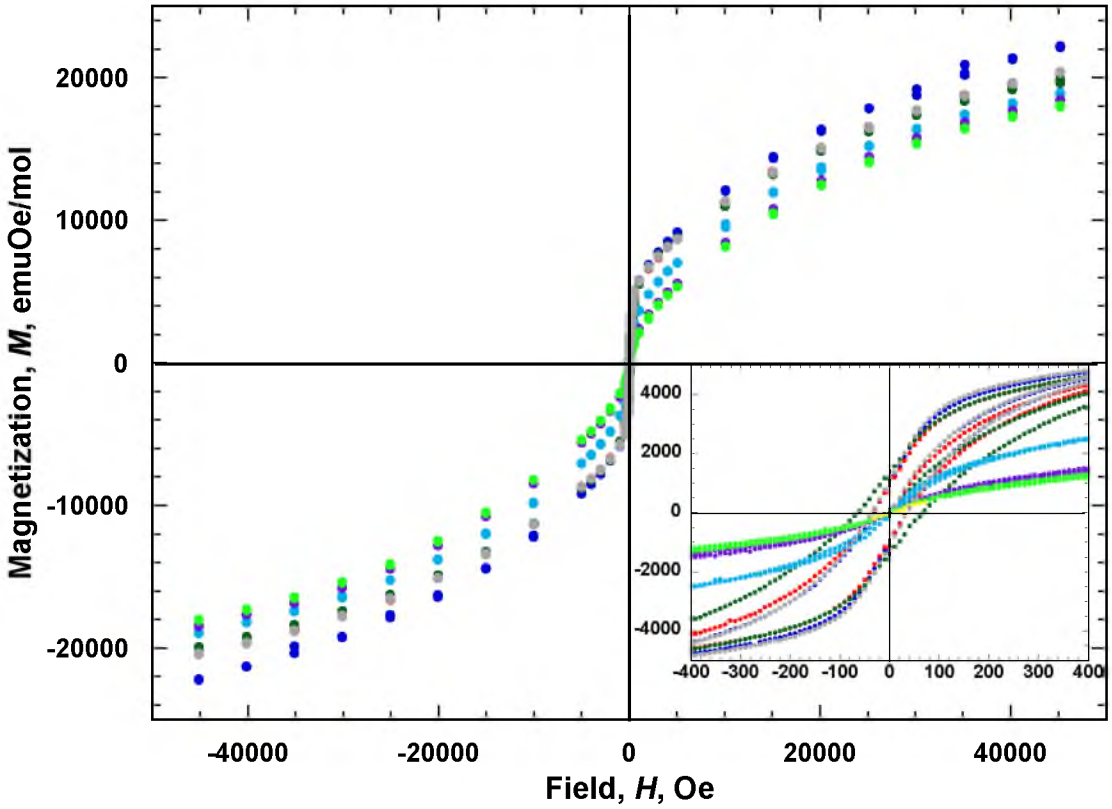

Figure 6.8. $M(T,P)$ at 4 K for **3**, displaying an increasing H_{cr} as pressure increased, then quenched at intermediate pressure and displayed reversibility as pressure was released: 0.001 (•), 0.64 kbar (•), 2.43 (•), 4.37 (•), 6.02 (•), 8.08 (•), 9.28 (•), and applied pressure released to 0.58 kbar (•).

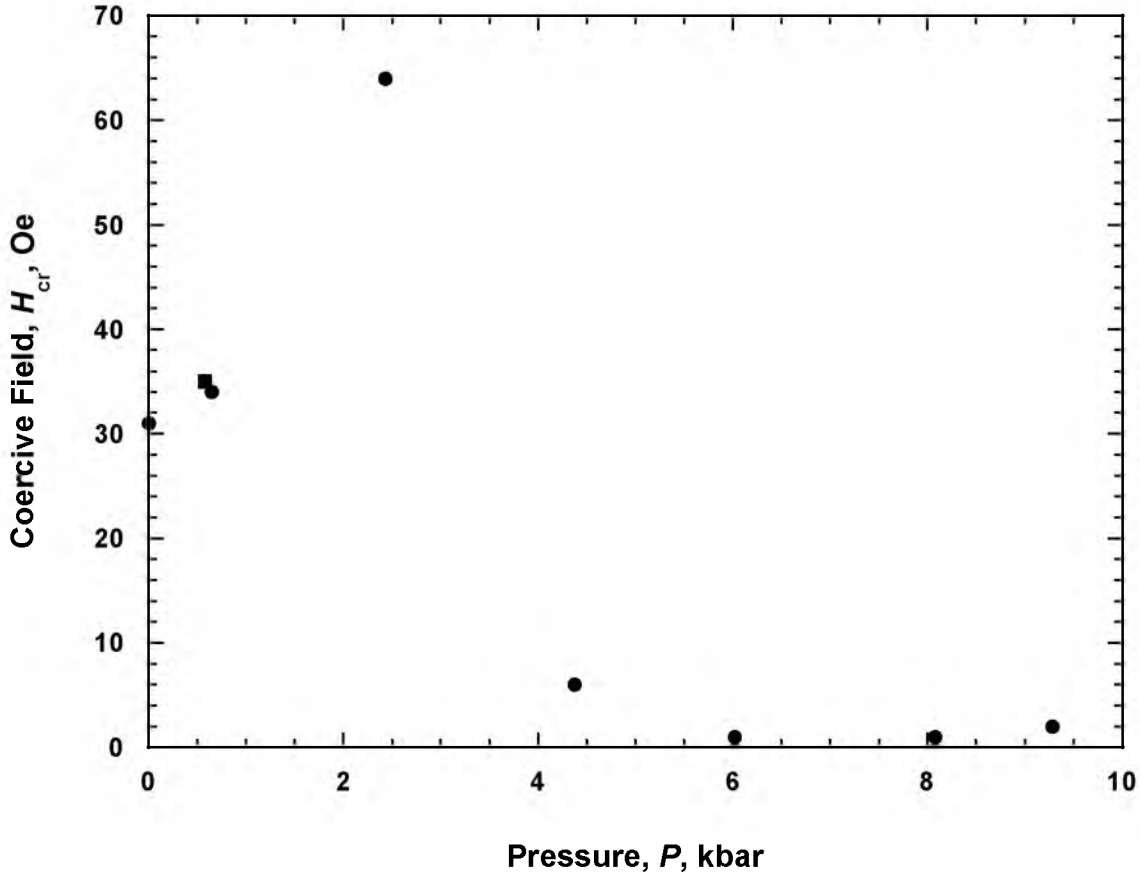

Figure 6.9. H_{cr} determined from field dependent hysteretic measurements of **3** are shown (•), released pressure measurement (■). The released measurements indicate a reversible hysteretic behavior. This is coincident with the T_b data, see text.

Conclusion

The layered structures **2** and **3** displayed increases in T_c and T_b with increased pressure and a propensity for the magnetic behavior to begin to quench at high pressure. **3** displayed a relatively large increase in H_{cr}, before quenching to antiferromagnetic behavior above 2.43 kbar. This is in agreement with the onset of a plateau in T_b and T_c above the same pressure. The quenching exhibited by **3** is in accord with the decrease in H_{cr} of **2** as pressure was applied. **2** displayed irreversibility of the hysteretic properties, H_{cr} and M_r, and to a lesser degree of the temperature dependent properties, T_c and T_b after the release of applied pressure. Similarly, complex behavior was investigated through pressure dependent IR spectroscopy coupled with computational simulations, which focused on the CN stretching frequencies. This technique could be adapted for **2** and **3** to determine the nature of bond compression, bending, or deformation upon pressure application and release. The computational simulation was previously used to support the hypothesis that pressure application induced stronger interlayer antiferromagnetic coupling and to explain the red or blue shift of the CN stretching frequency as either compression or bending.[28] Hypotheses in the absence of pressure dependent structural clues are necessarily limited.

References

(1) Benecki, W.; Clagett, T.; Trout, S. "Permanent magnets 2010–2020—A comprehensive overview of the Global Permanent Magnet Industry," Report No. 9-21,55, 2010.

(2) Miller, J. S. *Chem. Soc. Rev.* **2011**, *40*, 3266.

(3) Blundell, S. J.; Pratt F. L. *J. Phys.: Condens. Matter*, **2004**, *16*, R771.

(4) Ovcharenko, V. I.; Sagdeev, R. Z. *Russ. Chem. Rev.* **1999**, *68*, 345.

(5) Miller, J. S.; Epstein, A. J. *Angew. Chem. Int. Ed. Engl.* **1994**, *33*, 385.

(6) Miller, J. S.; Calabrese, J. C.; Rommelmann, H.; Chittipeddi, S. R.; Zhang, J. H.; Reiff, W. M.; Epstein, A. J. *J. Am. Chem. Soc.* **1987**, *109*, 769.

(7) Miller, J. S. *J. Mater. Chem.* **2010**, *20*, 1846.

(8) Varret, F.; Nogues, M.; Goujon, A. In *Magnetism: Molecules to Materials*; Miller, J. S., Drillon, M., Eds.; Wiley-VCH: New York, 2000, Vol. 1, p 257.

(9) Bozdag, K. D.; Yoo, J.-W.; Raju, N. P.; McConnell, A. C.; Miller, J. S.; Epstein, A. J. *Phys. Rev. B* **2010**, *82*, 094449.

(10) Manriquez, J. M.; Yee, G. T.; McLean, R. S.; Epstein, A. J.; Miller, J. S. *Science* **1991**, *252*, 1415.

(11) Miller, J. S. *Polyhed.* **2009**, *28*, 1596.

(12) (a) Ferlay, S.; Mallah, T.; Ouahes, R.; Veillet, P.; Verdaguer, M. *Nature* **1995**, *378*, 701. (b) Dujardin, E.; Ferlay, S.; Phan, X.; Desplanches, C.; Moulin, C. C. D.; Sainctavit, P.; Baudelet, F.; Dartyge, E.; Veillet, P.; Verdaguer, M. *J. Am. Chem. Soc.* **1998**, *120*, 11347. (c) Ferlay, S.; Mallah, T.; Ouahes, R.; Veillet, P.; Verdaguer, M. *Inorg. Chem.* **1999**, *38*, 229. (d) Verdaguer, M.; Bleuzen, A.; Train, C.; Garde, R.; Fabrizi de Biani, F.; Desplanches, C. *Phil. Trans. R. Soc. Lond. A* **1999**, *357*, 2959.

(13) Holmes, S. M.; Girolami, G. S. *J. Am. Chem. Soc.* **1999**, *121*, 5593.

(14) Hatlevik, Ø.; Buschmann, W. E.; Zhang, J.; Manson, J. L.; Miller, J. S. *Adv. Mater.* **1999**, *11*, 914.

(15) Liao, Y.; Shum, W. S.; Miller, J. S. *J. Am. Chem. Soc.* **2002**, *124*, 9336.

(16) Vos, T. E.; Liao, Y.; Shum, W. W.; Her, J.-H.; Stephens, P. W.; Reiff, W. M.; Miller, J. S. *J. Am. Chem. Soc.* **2004**, *126*, 11630.

(17) Shum, W. S.; Her, J.-H.; Stephens, W.; Lee, Y.; Miller, J. S. *Adv. Mater.* **2007**, *19*, 2910.

(18) Shum, W. W.; Liao, Y.; Miller, J. S. *J. Phys. Chem. A* **2004**, *108*, 7460.

(19) Fishman, R. S.; Shum, W. W.; Miller, J. S. *Phys. Rev. B* **2010**, *81*, 172407.

(20) (a) Takano, M.; Nasu, S.; Abe, T.; Yamamoto, K.; Endo, S.; Takeda, Y.; Goodenough, J. B. *Phys. Rev. Lett.* **1991**, *67*, 3267. (b) Rueff, J.-P.; Kao, C.-C.; Struzhkin, V. V.; Badro, J.; Shu, J.; Hemley, R. J.; Mao, H. K. *Phys. Rev. Lett.* **1999**, *82*, 3284. (c) Aguado, F.; Rodriquez, F.; Núñez, P. *Phys. Rev. B* **2007**, *76*, 094417. (d) Golosova, N. O.; Kozlenko, D. P.; Dubrovinsky, L. S.; Drozhzhin, O. A.; Istomin, S. Y.; Savenko, B. N. *Phys. Rev. B* **2009**, *79*, 104431.

(21) Yoshioka, D.; Mikuriya, M.; Handa, M. *Chem. Lett.* **2002**, 1044.

(22) Vos, T. E.; Miller, J. S. *Angew. Chem. Int. Ed.* **2005**, *44*, 2416.

(23) (a) Kareis C. M.; Her, J.-H.; Stephens, P. W.; Moore, J. G.; Miller, J. S. *Chem. Eur. J.* **2012**, *18*, 9281. (b) Brandon, E. J.; Rittenberg, D. K.; Arif, A. M.; Miller, J. S. *Inorg. Chem.* **1998**, *37*, 3376.

(24) Jennings, L. D.; Swenson, C. A *Phys. Rev.* **1958**, *112*, 31.

(25) Clark, M. J.; Smith, T. F. *J. Low Temp. Phys.* **1978**, *32*, 495.

(26) Rittenberg, D. K.; Sugiura, K.-I.; Sakata, Y.; Mikami, S.; Epstein, A. J.; Miller, J. S. *Adv. Mater.* **2000**, *12*, 126.

(27) Fishman, R. S.; Okamoto, S.; Miller, J. S. *Phys. Rev. B* **2009**, *80*, 140416.

(28) Shum, W. W.; Lee, Y.; Stephens, P. W.; Liu, Z.; Miller, J. S. unpublished results.

CHAPTER 7

A MEAN FIELD ANALYSIS OF THE EXCHANGE COUPLING (*J*) FOR NONCUBIC PRUSSIAN BLUE ANALOGUE MAGNETS

Reprinted (adapted) with permission from: DaSilva, J. G.; McConnell, A. C.; Fishman, R. S.; Miller, J. S. *J. Phys. Chem. C* **2012**, *116*, 24752-24756.

Abstract

Mean field expressions based on the simple Heisenberg model were derived to correlate the intra- and interlayer exchange couplings to the critical temperatures, T_c, for three metallocyanide-based magnets with extended 2- and 3-D structure types. These expressions were used to estimate the exchange coupling, *J*, for 2-D ferrimagnetic $[NEt_4]_2Mn^{II}_3(CN)_8$, 3-D antiferromagnetic $[NEt_4]Mn^{II}_3(CN)_7$, and 3-D antiferromagnetic interpenetrating 3-D $Mn^{II}(CN)_2$. The type and magnitude of the exchange coupling are in accord with the previously reported magnetic data.

Introduction

Many Prussian blue structured hexacyanometalates have been reported,[1,2,3,4] with members of this structure type having several compositions, for example, $M'^{III}_4[M^{II}(CN)_6]_3$, $C^+M'^{II}[M^{III}(CN)_6]$, $M'^{II}_3[M^{III}(CN)_6]_2$, $A^+M'^{III}[M^{II}(CN)_6]$, $A^+_2M'^{II}[M^{II}(CN)_6]$, and $M'^{III}[M^{III}(CN)_6]$ (A^+ = alkali cation) that are frequently solvated. They all share the common features of (i) being face centered cubic (*fcc*) ($a \sim 10.5$ Å), (ii) having the C-bonded M being low-spin and surrounded by high-spin M' that is bonded to six cyanide nitrogens, and (iii) having linear -M'-N≡C-M-C≡N-M'- linkages along the three unit cell axes, except where defect sites occur.

Recently several noncubic PBAs of $A_2Mn^{II}[Mn^{II}(CN)_6]$ (A = Na, K, Rb) composition have been reported.[5,6] More interesting, when A = NEt_4^+ a layered (2-D) ferrimagnet of $[NEt_4]_2Mn^{II}_3(CN)_8$ [7, 8] (Figure 7.1), and 3-D bridged-layered antiferromagnet of $[NEt_4]Mn^{II}_3(CN)_7$ (Figure 7.2) are formed.[8] Furthermore, thermolysis of either $[NEt_4]_2Mn^{II}_3(CN)_8$ or $[NEt_4]Mn^{II}_3(CN)_7$ forms $Mn^{II}(CN)_2$,[9] which possesses an interpenetrating extended 3-D sphalerite (diamonoid) structure (Figure 7.3). $[NEt_4]_2Mn^{II}_3(CN)_8$ is a ferrimagnet while $[NEt_4]Mn^{II}_3(CN)_7$ and $Mn^{II}(CN)_2$ are antiferromagnets. All have M-C≡N-M' (M = M' = Mn^{II}) linkages. However, the Mn-CN-Mn separation is longer by ~0.2 Å when both Mn^{II} sites are tetrahedral and high spin (HS), with respect to when the Mn^{II}-C site is octahedral and low spin (LS) (Table 7.1), as high-spin M sites have larger radii with respect to low-spin M sites due to the presence of antibonding electrons.[10]

The key to understanding PBA-based magnets is the determination of the nearest neighbor exchange coupling, J, for these magnetic materials. The Mean Field (MF) analysis based on the Heisenberg model [$\hat{H} = -\Sigma J_{ij} S_i \bullet S_j$ $(i > j)$][11] has been applied to cubic PBAs,[1] and equation 7.1 has been used extensively to relate T_c with an average J. This expression is applicable for materials with one type of spin site of total spin, S, where z is the number of nearest neighbors, and k_B is Boltzmann's constant. Antiferromagnetic PBAs have yet to be reported, as PBAs have differing M, M', S_M, and/or $S_{M'}$ yielding either ferrimagnets or less commonly ferromagnets.[1] Hence, an MF expression for a system possessing two different adjacent spin sites, i and j, was developed, equation 7.2,[1c,12] where z_i and z_j are the number of nearest neighbors, and S_i and S_j are the total spin on spin sites i and j, respectively, and the Landè g values for each spin site are the same. Note that the MF expressions for T_c with a single exchange interaction are the same for ferromagnetic ($J > 0$) or antiferromagnetic ($J < 0$) interactions.

$$T_c = \frac{|J| z S(S+1)}{3k_B} \tag{7.1}$$

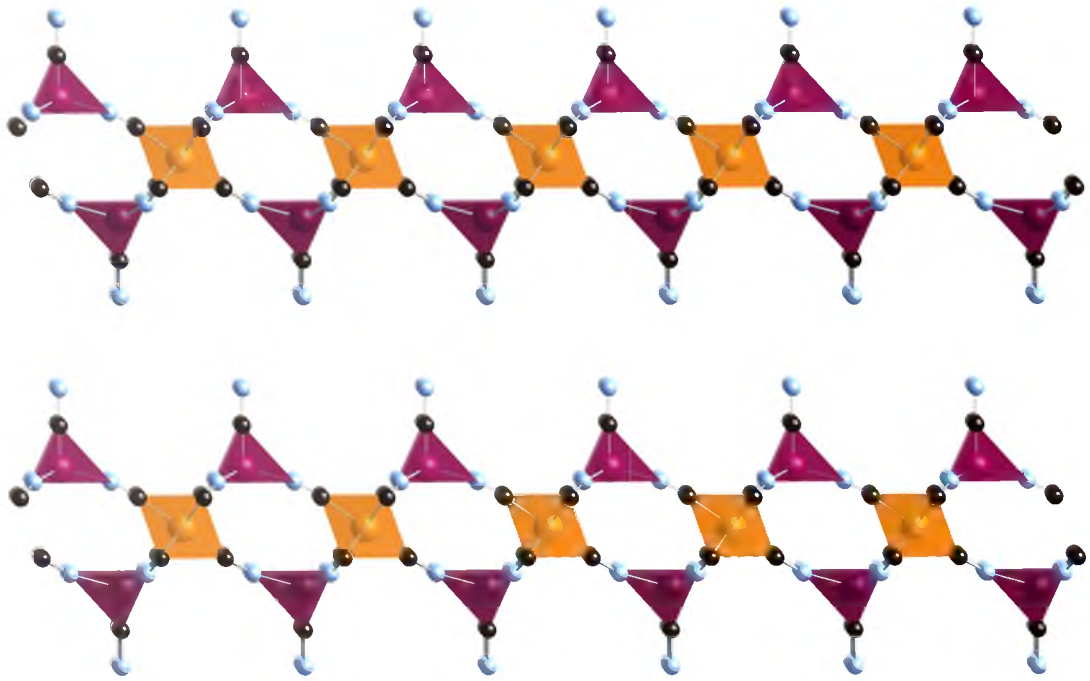

Figure 7.1. Extended 2-D network bonding observed for $[NEt_4]_2Mn^{II}_3(CN)_8$ (**1**) (high spin Mn is maroon, low spin Mn is orange, C is black, and N is blue).[7] The disordered anions and solvent reside between the layers.

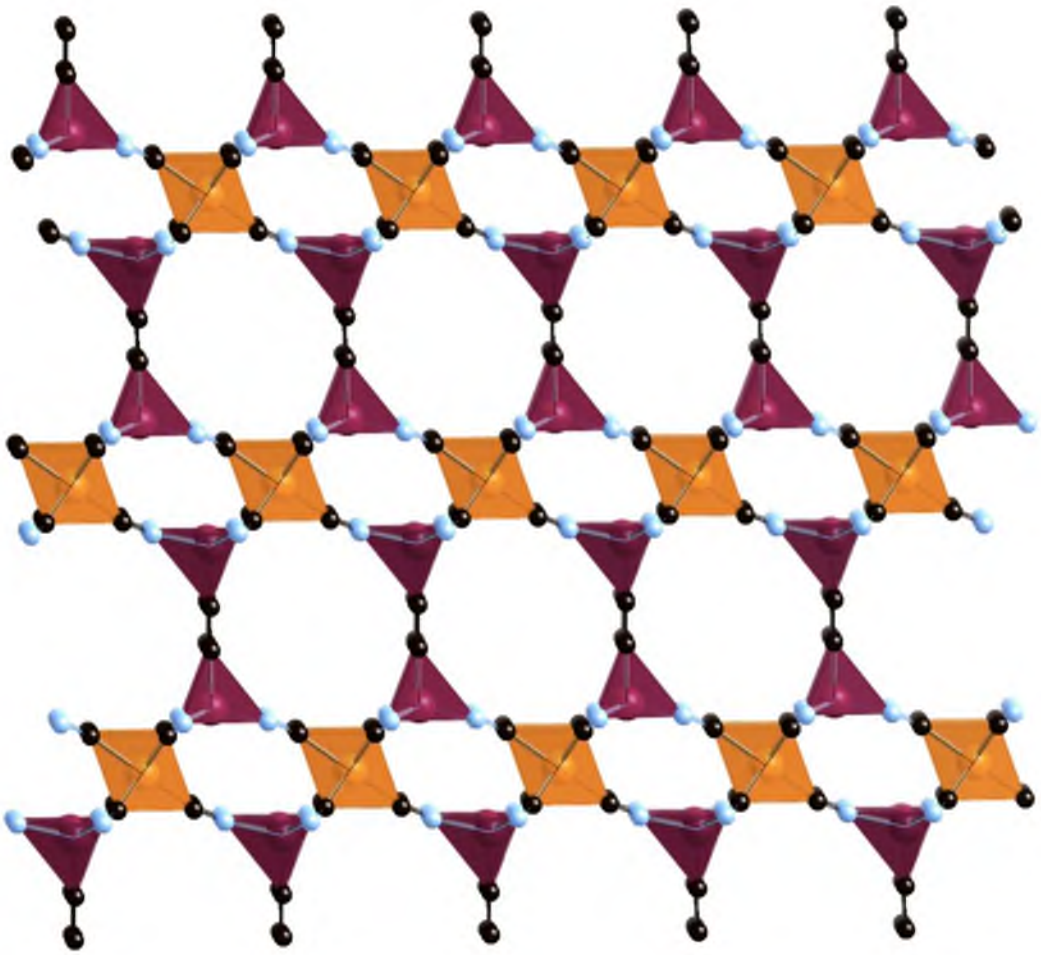

Figure 7.2. Extended bridged layer 3-D network bonding observed for $[NEt_4]Mn^{II}_3(CN)_7$ (**2**) (high spin Mn is maroon, low spin Mn is orange, C is black, and N is blue).[8] The disordered anions and solvent reside between the layers.

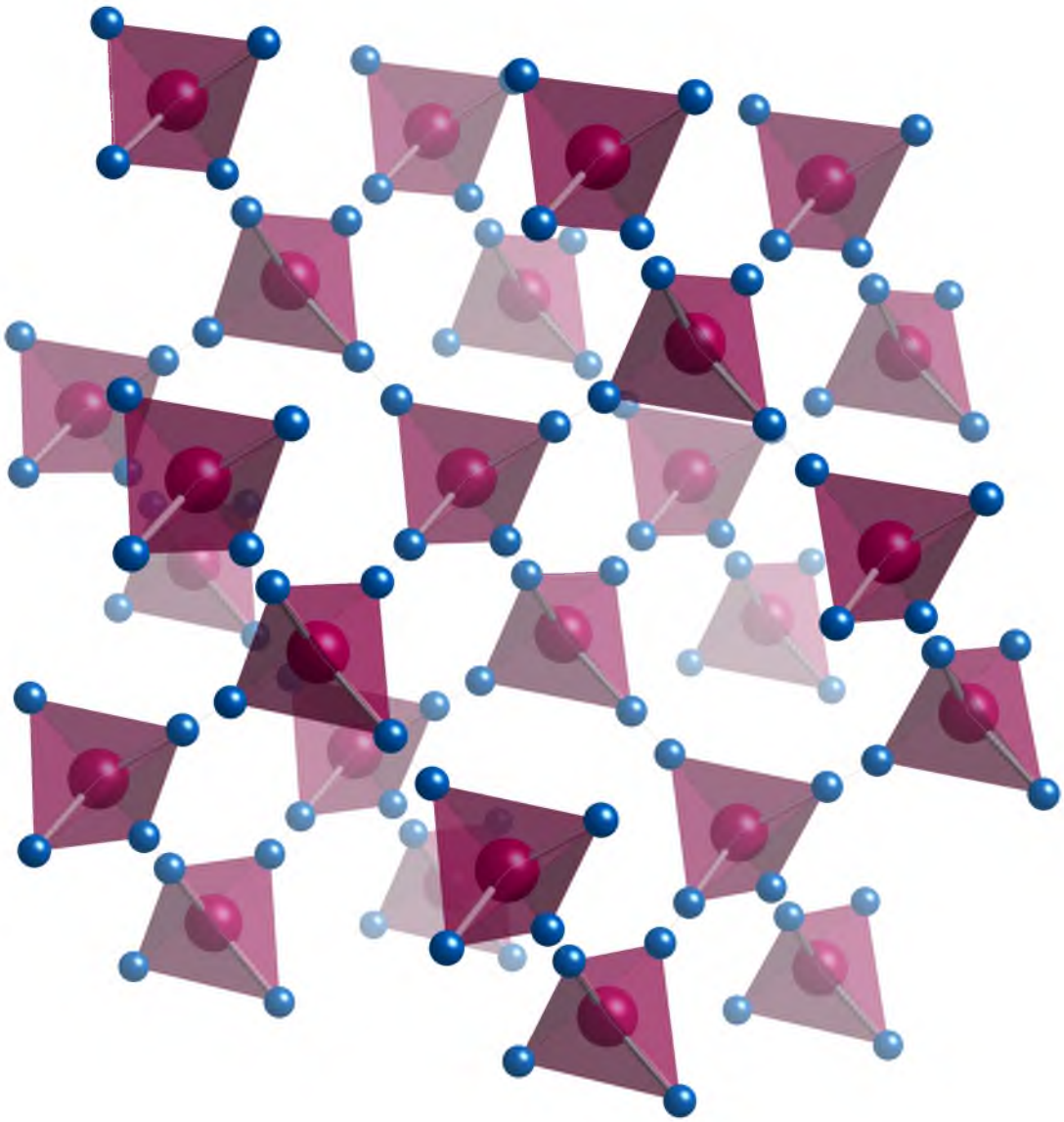

Figure 7.3. Single extended network bonding for 3-D $Mn^{II}(CN)_2$ (**3**) (high spin Mn = maroon; the disordered C and N are blue).[9] The second, interpenetrating lattice is not shown.

Table 7.1. Summary of structurally characterized 2- and 3-D non-cubic PBAs and their T_cs.

Magnet		Interlayer Separation, Å	Mn-CN-Mn, Å	Bonding Dimensionality	T_c,[d] K	Type[e]	ref
$[NEt_4]_2Mn^{II}_3(CN)_8$	**1**	8.074	5.144[a]	2-D	25.7	FI	7,8
$[NEt_4]Mn^{II}_3(CN)_7$	**2**	14.543	5.116[a] 5.482[b]	3-D	28.5	AF	8
$Mn^{II}(CN)_2$	**3**	--	5.325[b,c]	3-D	78	AF	9

[a] Low spin Mn^{II}-CN-high spin Mn^{II} [b] High spin Mn^{II}-CN-high spin Mn^{II}

[c] Intra- and interlattice Mn•••Mn separation [d] From the peak in $\chi'(T)$

[e] FI = Ferrimagnet; AF = Antiferromagnet

$$T_c = \frac{|J|\sqrt{z_i z_j S_i(S_i+1)S_j(S_j+1)}}{3k_B} \quad (7.2)$$

As MF theory ignores the effect of topology (i.e., dimensionality) on T_c, it provides the same result for any material with the same spin (S), exchange (J), and bonding, regardless of structural dimensionality. Furthermore, MF theory also gives the same result for either Heisenberg or Ising spins. In the absence of anisotropy, however, long-range spin fluctuations destroy the magnetic order of a 1- or 2-D system (Mermin-Wagner theorem).[11] Via evaluation of the spin excitation spectrum for a 2-D system with exchange, J, the T_c rises very rapidly with anisotropy D as $T_c \propto J/\log(J/D)$.[13] Thus, MF theory provides an adequate approximation for an anisotropic 2-D material when $D/J >> 1$. For $D \sim J$, the T_c of a 2-D material will be suppressed by long-range fluctuations, and higher T_c values will occur when the effect of those fluctuations is diminished by 3-D magnetic order. Nonetheless, for a 3-D system, MF theory may still overestimate the transition temperature by as much as 40%. Hence, MF theory is best used to estimate the ratios of exchange constants either for different materials or within the same material.

Equation 7.2 should work well for cubic and distorted cubic[5] PBAs with M:M'::1:1 and the free-electron isotropic Landè g value for each spin site,[1,2] as none have a single spin site that is needed for equation. 7.1. The aforementioned noncubic PBAs **1** and **2**, however, are inappropriate for equation 7.2, and an MF analysis was performed for these structures to develop appropriate expressions, which are reported herein. Note that $Mn(CN)_2$ (**3**) does have a single spin site for which equation 7.1 is appropriate.

Although $[NEt_4]_2Mn^{II}_3(CN)_8$ (**2**) is a 2-D ferrimagnet with very weak interlayer interactions, the anisotropy on the low-spin Mn^{II} ions with $S' = 1/2$ produces long-range magnetic order and justifies the application of MF theory for this compound.

The T_c values for the ferrimagnet $[NEt_4]_2Mn^{II}_3(CN)_8$ and the antiferromagnet $[NEt_4]Mn^{II}_3(CN)_7$ and $Mn^{II}(CN)_2$ were determined in several ways with some variation between methods.[8,9,14] To be self-consistent with our MF analysis, the same method,

namely, the temperature at which the maximum in the frequency independent $\chi'(T)$ occurs, will be used as T_c. These values are 25.7, 28.5, and 78 K for $[NEt_4]_2Mn^{II}_3(CN)_8$, $[NEt_4]Mn^{II}_3(CN)_7$, and $Mn^{II}(CN)_2$, respectively (Table 7.1).

Although MF theory can overestimate T_c by as much as 40%, it predicts trends and estimates of exchange constants,[12] and it provides better estimates for the ratios of exchange couplings in different materials. Herein, MF theory estimates the ratios of the interlayer and intralayer couplings.

Mean Field Expressions

The MF expressions for T_c, using $\hat{H} = -\Sigma J_{ij} S_i \cdot S_j$ ($i > j$), are determined for the noncubic layered (2-D) structure associated with $[NEt_4]_2Mn^{II}_3(CN)_8$ (**1**), and the 3-D bridged layer structure associated with $[NEt_4]Mn^{II}_3(CN)_7$ (**2**). The former 2-D layered system has two spin sites in a 1:2 ratio, and a single intralayer coupling J, while the latter 3-D system also has two spin sites in a 1:2 ratio, a single intralayer coupling, J, and single interlayer coupling, K. This paper adopts the sign convention that J or $K > 0$ corresponds to ferromagnetic coupling.

Compound 1. The MF solution for the general spin case of 2-D compound 1 of [NEt4]2MnII3(CN)8 composition, Figure 7.1, was constructed (see the Appendix). MF theory predicts

$$T_c = \frac{|J|}{k_B}\sqrt{2S(S+1)S'(S'+1)} \tag{7.3}$$

where J is the coupling between the low spin Mn^{II} ($z = 6$) with spin S, and the high spin Mn^{II} ($z = 3$) within the layers with S'.

Compound 2. The MF expression for the general spin case for 3-D **2** of $[NEt_4]Mn^{II}_3(CN)_7$ composition, Figure 7.2, was constructed (see the Appendix), and is

$$T_c = \frac{KS(S+1)+\sqrt{K^2\left[S(S+1)\right]^2+72J^2S(S+1)S'(S'+1)}}{6k_B}, \tag{7.4}$$

where J is the coupling within the layers between the low spin Mn^{II} (z = 6 for the six high-spin nearest neighbors) with spin S, and the high-spin Mn^{II} (z = 4 for the three high-spin and one low-spin nearest neighbors) with S', and K is the interlayer coupling between adjacent high-spin Mn^{II} (z = 4) sites.

A summary of the MF equations for general spin for the aforementioned cases **1** to **3** is contained in Table 7.2.

Estimation of Exchange Coupling, *J*

Based on a T_c of 78 K, the exchange coupling, J, for $M(CN)_2$ (**3**) is estimated from equation 7.1 as J/k_B is -6.7 K that is in accord with antiferromagnetic coupling. For the layered ferrimagnet $[NEt_4]_2Mn^{II}_3(CN)_8$, equation 7.3 gives an antiferromagnetic coupling between adjacent Mn^{II} sites of J/k_B = -7.1 K. The -6.7 and -7.1 K agree well, as expected for the same Mn^{II}-C≡N-Mn^{II} linkages, albeit for $[NEt_4]_2Mn^{II}_3(CN)_8$ the C-bonded Mn^{II} is low spin (S = 1/2), while it is high spin (S = 5/2) for $M(CN)_2$.[9,15] The slightly reduced J for $Mn^{II}CNMn^{II}$ when both Mn^{II} sites are tetrahedral and high spin with respect to when the Mn^{II}-C site is octahedral and low spin is in accord with the slightly longer (~0.2 Å) Mn^{II}•••Mn^{II} separation (Table 7.1).[10]

The intralayer, J, and interlayer, K, exchange coupling for $[NEt_4]Mn^{II}_3(CN)_7$ (**2**) can be estimated from equation 7.4. However, only T_c is known. Thus, J and K cannot be independently determined. Since $[NEt_4]Mn^{II}_3(CN)_7$ and $[NEt_4]_2Mn^{II}_3(CN)_8$ possess virtually identical 2-D layers, the interlayer coupling constant, K, can be estimated by assuming the value for J calculated for $[NEt_4]_2Mn^{II}_3(CN)_8$ using equation 7.3, that is, -7.1 K. This is a good assumption, as both $[NEt_4]Mn^{II}_3(CN)_7$ and $[NEt_4]_2Mn^{II}_3(CN)_8$ have identical layers with the same linkages and the identical spin states for each Mn^{II} ion, but due to the terminal cyanides, cations, and solvents separating the layers for $[NEt_4]_2Mn^{II}_3(CN)_8$, the isolated layers are nonbridging. Thus, its intralayer coupling K is negligible and is assumed to be zero. Using the estimated value J/k_B = -7.1 K and T_c = 28.5 K, the interlayer coupling, K/k_B, between the tetrahedral high-spin Mn^{II} ions via superexchange in $[NEt_4]Mn^{II}_3(CN)_7$ is estimated as -1.8 K. Alternatively, the interlayer

Table 7.2. Summary of the MF expressions [$\hat{H} = -\Sigma J_{ij} S_i \bullet S_j$ ($i > j$)] for general S for 2-D and 3-D compounds **1**, **2**, and **3**, and computed inter- and intralayer couplings (vide infra).

Composition (compound)	Mean Field (MF) Expression for T_c [a]	interlayer coupling, K/k_B, K	intralayer coupling, J/k_B, K
2-D			
$[NEt_4]_2Mn^{II}_3(CN)_8$ (**1**)	$T_c = \frac{\lvert J \rvert}{k_B}\sqrt{2S(S+1)S'(S'+1)}$	0[a]	-7.1
3-D			
$[NEt_4]Mn^{II}_3(CN)_7$ (**2**)	$T_c = \frac{KS(S+1)+\sqrt{K^2[S(S+1)]^2+72J^2S(S+1)S'(S'+1)}}{6k_B}$	-1.8 -6.7[a]	-7.1[b] -4.4
$M(CN)_2$ (**3**)	$T_c = \frac{\lvert J \rvert zS(S+1)}{3k_B}$	0[a]	-6.7

[a] J = intralayer coupling; K = interlayer coupling [b] Assumed

coupling, K, between the tetrahedral high-spin Mn^{II} ions can also be assumed to be similar to the intralattice coupling calculated for $Mn(CN)_2$, that is, -6.7 K, and based on this and the T_c, J/k_B is -4.4 K. The negative K indicates antiferromagnetic coupling between the ferrimagnetic layers, which is observed.

Note that K can be estimated from the critical field, $H_c = \{|K|S^2/[\mu_B(S - S')]\}$, for the spin-flop transition.[16] Since the spin flop transition is not observed[8] up to 9 T, $|K|/k_B > 3.8$ K, which is consistent with the estimate of $K/k_B = -6.7$ K above. The spin-flop field for that value of K would be ~14 T.

The value of K should be comparable to both J for $[NEt_4]_2Mn^{II}_3(CN)_8$ as well as $Mn(CN)_2$, as the linkages are comparable. This is observed as $K/J_{Mn3(CN)8} = 0.25$, and $K/J_{Mn(CN)2} = 0.66$. The disparity in these ratios is within reason, as MF Theory does not attempt to incorporate any interlattice coupling for $Mn(CN)_2$ due to the absence of interlattice bonding.

Similar to tetrahedral $Mn(CN)_2$, cubic PBAs have only one type of exchange coupling, J, and thus $Mn(CN)_2$ can be compared to J values estimated from an MF analysis of PBAs based on octahedral metal ion sites. Cubic and distorted cubic PBAs have one J; however, the M bound to the cyanide carbon may differ from the M' bound to the cyanide nitrogen. Equation 7.2 is the result of the MF analysis for this structure. For a similar reason the J values for $[NEt_4]_2Mn^{II}_3(CN)_8$ and $[NEt_4]Mn^{II}_3(CN)_7$ can be assessed. Hence, a comparison of J values, which are independent of both S and z, can be made. MF Theory applied to the known cubic $AMn^x[Mn^y(CN)_6]$ PBA materials yield J/k_B between 3.5 $\{CsMn^{II}[Mn^{III}(CN)_6]\}$[17] and 8.7 K $\{Mn^{III}_3[Mn^{II}(CN)_6]_2\}$[18] using equation 7.2. Likewise, equation 7.2 can be used for the distorted cubic $A_2Mn[Mn(CN)_6]$ (A = Na, K, Rb),[5,6] as the lattice connectivity is the same, and J/k_B ranges from 6.05 to 11.1 K (Table 7.2). The couplings for these Mn-CN-Mn systems are an order of magnitude lower than those for PBs containing V, Ni, and Cr, which have T_c values an order of magnitude larger, Table 7.3.[2c,19]

Conclusion

General spin, S, MF expressions for several 2- and 3-D noncubic Prussian Blue analogues were presented that relate the exchange constants and the critical temperature,

T_c, and the inter- and intralayer coupling constants for various noncubic PBA compounds using these expressions were evaluated. The sign of the inter- and intralayer coupling constants for compounds studied indicate antiferromagnetic coupling, as observed. The $K/J_{Mn3(CN)8}$ = 0.25, and $K/J_{Mn(CN)2}$ = 0.66 ratios match reasonably, but not quantitatively. Application of MF Theory to several cubic PBAs produced coupling values with a smaller deviation in coupling value, as expected for changing only spin states. Examination of noncubic PBAs found the expected inverse relationship between coupling strength and spin site distance, and MFT proves to be most useful in the comparative analysis of magnetic coupling in structurally related compounds.

Table 7.3. Summary of representative coupling constants, J, for Mn-based PBAs etc. possessing M-CN-M' linkages, using equation 7.2.

PBA	MCNM, Å	T_c, K	S_M	$S_{M'}$	J/k_B, K	ref
$CsMn^{II}[Mn^{III}(CN)_6]\bullet 1/2H_2O$	5.33[b] 5.35[b]	29 31	1	5/2	3.47 3.71	18 15
$Mn^{II}[Mn^{IV}(CN)_6]$	5.37[b]	48.7	3/2	5/2	4.28	19
$Mn^{III}[Mn^{III}(CN)_6]$	5.33[b]	31	1	2	4.47	20
$Mn^{III}_3[Mn^{II}(CN)_6]_2\bullet 2H_2O$	5.31[b]	37	1/2	2	8.72	16
$CsNi^{II}[Cr^{III}(CN)_6]\bullet 2H_2O$	5.29[b]	90	3/2	1	16.4	21
$Na_2Mn^{II}[Mn^{II}(CN)_6]\bullet 2H_2O$	5.33	31	5/2	1/2	6.05	6
$Na_2Mn^{II}[Mn^{II}(CN)_6]$	4.99	57	5/2	1/2	11.1	6
$K_2Mn^{II}[Mn^{II}(CN)_6]$	5.09	41	5/2	1/2	8.00	5,16
$Rb_2Mn^{II}[Mn^{II}(CN)_6]$	5.19	34.6	5/2	1/2	6.75	5
$Cs_2Mn^{II}[Mn^{II}(CN)_6]$	5.31[b]	21	5/2	1/2	4.10	5
$KV^{II}Cr^{III}(CN)_6]$	5.28[b]	376	3/2	3/2	50.1	3
$Cs_2Mn^{II}[V^{II}(CN)_6]$	5.33[b]	125	5/2	3/2	10.9	22
$CsMn^{II}[Cr^{III}(CN)_6]$	5.41[b]	90	5/2	3/2	7.86	23
$CsNi^{II}[Cr^{III}(CN)_6]\bullet zH_2O$ ($z = 3\pm1$)	5.29	42	1	1	10.5	16
$V^{III}[Mn^{III}(CN)_6]$	4.65	28	3/2	1	5.11	20
$Cr^{III}[Mn^{III}(CN)_6]$	5.29[b]	22	3/2	1	4.02	20

[a] $z_M = z_{M'} = 6$ [b] $a/2$

Appendix

Compound 1. Let $M1$ equal the average spin on the high-spin manganese ion (Mn^{HS}) in the effective field, H_{eff}, and $M2$ equal the average spin on the low-spin manganese ion (Mn^{LS}) in the effective field, H'_{eff}. Mn^{HS} experiences an effective field,

$$H_{eff} = 3JM2 \quad (7.1A)$$

where the factor of 3 arises from the coordination number. Mn^{LS} experiences an effective field,

$$H'_{eff} = 6JM1 \quad (7.2A)$$

where the factor of 6 arises from the coordination number, z. The effective Hamiltonian, $\hat{H}$, on the Mn^{HS} is given by

$$\hat{H} = -H_{eff}S, \quad (7.3A)$$

and the effective Hamiltonian, $\hat{H}'$, on the Mn^{LS} is

$$\hat{H}' = -H'_{eff}S'. \quad (7.4A)$$

J is the exchange coupling and the total spin is $-S \leq m \leq +S$. The self-consistent equation for $M1$ and $M2$ would then be

$$M1 = \frac{\sum_{m=-S}^{S} me^{\frac{mH_{eff}}{T}}}{\sum_{m=-S}^{S} e^{\frac{mH_{eff}}{T}}} \quad (7.5A)$$

and

$$M2 = \frac{\sum_{m=-S'}^{S'} me^{\frac{mH'_{eff}}{T}}}{\sum_{m=-S'}^{S'} e^{\frac{mH'_{eff}}{T}}} \tag{7.6A}$$

Since H_{eff} and H'_{eff} are small approaching T_c, the exponential expression can be expanded according to the identity exp(x) = 1+x. $M1$ reduces to

$$M1 = \frac{\sum_{m=-S}^{S} m(1+\frac{mH_{eff}}{T_c})}{\sum_{m=-S}^{S} (1+\frac{mH_{eff}}{T_c})} = \frac{\sum_{m=-S}^{S} m + \frac{H_{eff}}{T_c}\sum_{m=-S}^{S} m^2}{\sum_{m=-S}^{S} 1 + \frac{H_{eff}}{T_c}\sum_{m=-S}^{S} m}. \tag{7.7A}$$

Next, because the summation is $-S < m < +S$, the term $\sum_{m=-S}^{S} m = 0$. Applying this, reduces $M1$ to

$$M1 = \frac{\frac{H_{eff}}{T_c}\sum_{m=-S}^{S} m^2}{\sum_{m=-S}^{S} 1}. \tag{7.8A}$$

Identities 7.9A and 7.10A can be applied to equation 7.8A, resulting in equation 7.11A,

$$\sum_{m=-S}^{S} m^2 = \frac{1}{3}(2S^3 + 3S^2 + S), \tag{7.9A}$$

$$\sum_{m=-S}^{S} 1 = 2S + 1, \text{ and} \tag{7.10A}$$

$$M1 = \frac{\frac{H_{eff}}{T_c}\left[\frac{1}{3}(2S^3 + 3S^2 + S)\right]}{2S+1} = \frac{H_{eff}S(S+1)}{3T_c} . \quad (7.11A)$$

The same methodology applied to $M2$ yields

$$M2 = \frac{H'_{eff}\,S'(S'+1)}{3T_c} . \quad (7.12A)$$

Substituting equations 7.1A and 7.2A (effective field for $M1$ and $M2$) into 7.11A and 7.12A results in a system of linear equations which may be used to solve for T_c,

$$M1 = \frac{(3JM2)S(S+1)}{3k_B T_c} , \text{ and} \quad (7.13A)$$

$$M2 = \frac{(6JM1)S'(S'+1)}{3k_B T_c} . \quad (7.14A)$$

The two linear equations (7.13A and 7.14A) can be solved for the two unknowns using the following matrix representations,

$$Av = 0 \quad , \quad (7.15A)$$

where v is a two component vector,

$$v = (M1, M2), \quad (7.16A)$$

and A is a 2 x 2 matrix,

$$A = \begin{pmatrix} a-1 & b \\ c & d-1 \end{pmatrix}. \quad (7.17A)$$

A solution to equation 2.15A exists if Det(A) = 0:

$$(a-1)(d-1)-bc=0\,. \tag{7.18A}$$

Therefore, the coefficients from equations 7.13A and 7.14A are substituted into equation 7.18A as,

$$\begin{aligned} a &= 0 \\ b &= \frac{3JS(S+1)}{3k_BT_c} \\ c &= \frac{6JS'(S'+1)}{3k_BT_c} \\ d &= 0 \end{aligned}, \tag{7.19A}$$

and yield

$$(0-1)(0-1)-(\frac{3JS(S+1)}{3k_BT_c})(\frac{6JS'(S'+1)}{3k_BT_c})=0\,. \tag{7.20A}$$

Solving for T_c gives

$$T_c=\frac{|J|}{k_B}\sqrt{2S(S+1)S'(S'+1)}\,. \tag{7.21A}$$

Compound 2. Let $M1$ equal the average spin on the Mn^{HS} in the effective field, H_{eff}, and $M2$ equal the average spin on the Mn^{LS} in the effective field, H'_{eff}, J/k_B equal the coupling between Mn^{HS} and Mn^{LS}, and K/k_B equal the coupling between Mn^{LS} and Mn^{LS}. Mn^{HS} experiences an effective field

$$H_{eff} = 3JM2 + KM1 \quad , \tag{7.22A}$$

where the factor of 3 arises from the 3 Mn^{LS} nearest neighbors, and the factor of one arises from the single Mn^{HS} nearest neighbor. Mn^{LS} experiences an effective field

$$H'_{eff} = 6JM2 \quad , \tag{7.23A}$$

where the factor of 6 results from the 6 Mn^{HS} nearest neighbors. The effective Hamiltonians for Mn^{HS} and Mn^{LS} are the same as compound **1**, equations 7.3A and 7.4A.

Following the same procedure as compound **1**, equations 7.22A and 7.23A are substituted into equations 7.11A and 7.12A, respectively, yielding

$$M1 = \frac{(3JM2 + KM1)S(S+1)}{3k_B T_c} \text{, and} \tag{7.24A}$$

$$M2 = \frac{(6JM1)S'(S'+1)}{3k_B T_c} \quad . \tag{7.25A}$$

The same procedure used to solve the analogous system of equations for compound **1** is used for compound **2**. Beginning with equation 7.15A, the coefficients from equations 7.24A and 7.25A are organized for substitution into equation 7.18A yielding

$$\begin{aligned} a &= \frac{KS(S+1)}{3k_B T_c} \\ b &= \frac{3JS(S+1)}{3k_B T_c} \\ c &= \frac{6JS'(S'+1)}{3k_B T_c} \\ d &= 0 \end{aligned} \quad , \tag{7.26A}$$

which gives 7.27A when substituted into 7.18A,

$$(\frac{KS(S+1)}{3k_BT_c}-1)(0-1)-[(\frac{3JS(S+1)}{3k_BT_c})(\frac{6JS'(S'+1)}{3k_BT_c})]=0 \quad (7.27A)$$

Solving for T_c gives:

$$T_c=\frac{KS(S+1)+\sqrt{K^2\left[S(S+1)\right]^2+72J^2S(S+1)S'(S'+1)}}{6k_B} \quad (7.28A)$$

References

(1) (a) Verdaguer, M.; Girolami, G. S. in *Magnetism - Molecules to Materials*; J. S. Miller, M. Drillon, Eds.; Wiley-VCH: Weinheim, 2005, Vol. 5, pp. 283. (b) Hashimoto, K.; Ohkoshi, S. *Phil. Trans. R. Soc. Lond. A* **1999**, *357*, 2977. (c) Verdaguer, M.; Bleuzen, A.; Marvaud, V.; Vaissermann, J.; Seuleiman, M.; Desplanches, C.; Scuiller, A.; Train, C.; Garde, R.; Gelly, G.; Lomenech, C.; Rosenman, I.; Veillet, P.; Cartier, C.; Villain, F. *Coord. Chem. Rev.* **1999**, *190-192*, 1023.

(2) (a) Ferlay, S.; Mallah, T.; Ouahes, R.; Veillet, P.; Verdaguer, M. *Nature* **1995**, *378*, 701. (b) Dujardin, E.; Ferlay, S.; Phan, X.; Desplanches, C.; Moulin, C. C. D.; Sainctavit, P.; Baudelet, F.; Dartyge, E.; Veillet, P.; Verdaguer, M. *J. Am. Chem. Soc.* **1998**, *120*, 11347. (c) Ferlay, S.; Mallah, T.; Ouahes, R.; Veillet, P.; Verdaguer, M. *Inorg. Chem.* **1999**, *38*, 229. (d) Verdaguer, M.; Bleuzen, A.; Train, C.; Garde, R.; Fabrizi de Biani, F.; Desplanches, C. *Phil. Trans. R. Soc. Lond. A* **1999**, *357*, 2959.

(3) Holmes, S. M.; Girolami, G. S. *J. Am. Chem. Soc.* **1999**, *121*, 5593.

(4) Hatlevik, Ø.; Buschmann, W. E.; Zhang, J.; Manson, J. L.; Miller, J. S. *Adv. Mater.* **1999**, *11*, 914.

(5) Her, J.-H.; Stephens. P. W.; Kareis, C. M.; Moore, J. G.; Min, K. S.; Park, J.-W.; Bali, G.; Kennon, B. S.; Miller, J. S. *Inorg. Chem.* **2010**, *49*, 1524.

(6) Kareis C. M.; Lapidus, S. H.; Her, J.-H.; Stephens, P. W.; Miller, J. S. *J. Am. Chem. Soc.* **2012**, *134*, 2246.

(7) Her, J.-H.; Stephens, P. W.; Kareis, C. M.; Moore, J. G.; Miller, J. S. *Angew. Chem. internat. Ed.* **2010**, *49*, 7773.

(8) Kareis, C. M.; Her, J.-H.; Stephens, P. W.; Moore, J. G.; Miller, J. S. *Chem. Eur.-J.* **2012**, *18*, 9281.

(9) Kareis C. M.; Lapidus, S. H.; Stephens, P. W.; Miller, J. S. *Inorg. Chem.* **2012**, *51*, 3046.

(10) Mingos, D. M. P. *Essential Trends in Inorganic Chemistry*, Oxford University Press, 1998, p. 336.

(11) Smart J. S. *Am. J. Phys.* **1955**, *23*, 356. White, R. M. *Quantum Theory of Magnetism*; Springer: Berlin, 2007, pp. 149-153.

(12) (a) Verdaguer, M.; Bleuzen, A.; Marvaud, V.; Vaissermann, J.; Seuleiman, M.; Desplanches, C.; Scuiller, A.; Train, C.; Garde, R.; Gelly, G.; Lomenech, C.;

Rosenman, I.; Veillet, P.; Cartier, C.; Villain, F. *Coord. Chem. Rev.* **1999**, *190-192*, 1023. (b) Tanaka, H.; Okawa, N.; Kawai, T. *Solid State Commun.* **1999**, *110*, 191. (c) Greedan, J. E.; Chien, C.-L.; Johnston, R. G. J. *Solid State Chem.* **1976**, 19, 155. (d) Greedan, J. E. *J. Phys. Chem. Solids* **1971**, 32, 819. (e) Kimishima, Y.; Ichiyanagi, Y.; Shimizu, K.; Mizuno, T. *J. Magn. Magn. Mater.* **2000**, 210, 244.

(13) Erickson, R. P.; Mills, D. L. *Phys. Rev. B* **1991**, *43*, 11527.

(14) Miller, J. S. *Chem. Soc. Rev.* **2011**, *40*, 3266.

(15) Buschmann, W. E.; Arif, A. M.; Miller, J. S. *Angew. Chem. Internat. Ed.* **1998**, *37*, 781.

(16) McConnell, A. C.; Fishman, R. F.; Miller, J. S. *J. Phys. Chem. C* **2012**, *116*, 18952.

(17) Ziegler, B.; Witzel, M.; Schwarten, M.; Babel, D. *Z. Naturforsch.* **1999**, *54b*, 870.

(18) Entley, W. R.; Girolami, G. S. *Inorg. Chem.* **1994**, *33*, 5165.

(19) Klenze, R.; Kanellakopulos, B.; Trageser, G.; Eysel, H. H. *J. Chem. Phys.* **1980**, *72*, 5819.

(20) Buschmann, W. E.; Miller, J. S. *Inorg. Chem.* **2000**, *39*, 2411.

(21) Gadet, V.; Mallah, T.; Castro, I.; Verdaguer, M.; Veillet, P. *J. Am. Chem. Soc.* **1992**, *114*, 9213.

(22) Entley, W. R.; Girolami, G. S. *Science* **1995**, *268*, 397.

(23) Griebler, W. D.; Babel, D. *Z. Naturforsch. B* **1982**, *37*, 832.

CHAPTER 8

CONCLUSION AND FUTURE RESEARCH

An array of MBMs was presented and investigated through experimental and theoretical methods in this dissertation. Special attention was placed on reduced TCNE (TCNE = tetracyanoethylene) containing compounds, which highlighted the diversity of the ligand as a radical, a scaffold, and a counterion. Numerous bonding schemes and extended network structures of TCNE were not addressed, which further implies the utility and diversity of the ligand as an MBM component. The MBMs studied included ferromagnets (whose coupling was more complex than ambient pressure experiments would suggest), metamagnets, antiferromagnets, and ferrimagnets. Further, these MBMs coupled through direct exchange, superexchange, and indirect exchange. Despite this variety of magnetic behavior, or likely because of it, it has been difficult to arrive at any overarching conclusion and several avenues of research remain unfinished to date.

With regard to the compounds discussed in this dissertation, [$FeCp_2^*$][TCNE] had previously been investigated through the most numerous and diverse array of techniques: ambient pressure AC[1] and DC[2,3,4]magnetometry, solvated and desolvated synthetic products,[1] powder X-ray diffraction as a function of temperature, PXRD(T),[5] Mössbauer spectroscopy,[2,3] neutron diffraction,[6] AC susceptometry as a function of pressure, AC(P),[7] adiabatic heat capacity, $C_p(T)$,[8] and multiple theoretical studies.[5,6,9] These past studies served to accurately describe the ambient pressure structure and the predominant coupling pathways. However, the AC(P)[7] and in this dissertation the DC(P) magnetic studies suggest that the known coupling pathways do not sufficiently describe the magnetic behavior above ~4.2 kbar. Further theoretical investigation of [$FeCp_2^*$][TCNE] aided by powder X-ray diffraction as a function of pressure, PXRD(P), would allow an evaluation of the ferro- and antiferromagnetic couplings that give rise to

weak ferromagnetism with such large H_{cr}. In fact, it is perplexing that the H_{cr} increases as the spin canting increases, as the H_{cr} of [$FeCp_2$*][TCNE] arises from ferromagnetically aligned spins and canting would reduce this alignment, thereby imparting antiferromagnetic character. In the absence of PXRD(*P*) to yield structural data for a theoretical investigation of the coupling pathways under pressure, an assessment of the coupling pathways may be estimated through evaluation of the six principal pathways as a function of intermolecular separation.[5]

The ferromagnetic, **FO**, and metamagnetic, **MM**, polymorphs of [$FeCp_2$*][TCNQ] (TCNQ = 7,7,8,8-tetracyano-*p*-quinodimethane) have been the focus of nearly the same degree of experimentation[10,11,12,13] as [FeCp2*][TCNE] and as such further understanding of the systems would benefit from PXRD(*P*) and the corresponding theoretical studies, vide supra. However, the ferromagnetic and metamagnetic polymorphs offer a unique opportunity to quantitatively evaluate coupling pathways as a function of angle as well as distance due to the disparity in their ambient pressure crystal structures. While the effect of orbital orthogonality has been theoretically investigated previously,[14] there has yet to be a simultaneous experimental analogue for such an indirect exchange mechanism.

[FeCp2*][HCBD] (HCBD = hexacyanobutadiene) presents a fortunate opportunity due to the similarity of its crystal structure and molecular components to [$FeCp_2$*][TCNE]. Upon ordering at ~3.1 kbar, [$FeCp_2$*][HCBD] behaves as a weak ferromagnet without displaying the ferromagnetic behavior exhibited by [$FeCp_2$*][TCNE]. A comparison of the coupling pathways of the analogous compounds may serve to elucidate a coupling pathway critical to the exhibition of ferromagnetism/weak ferromagnetism. However, [$FeCp_2$*][HCBD] should be theoretically assessed at ambient pressure prior to PXRD(*P*) and associated theoretical investigation of high pressure structures.

Mn^{II}(TCNE)I(OH_2) and $Mn^{II}(TCNE)_{3/2}(I_3)_{1/2}\cdot$zTHF displayed remarkably similar DC(*P*) behavior, with the exception of the low pressure region of Mn^{II}(TCNE)I(OH_2), considering the structures have different bonding dimensionality. Theoretical investigation of the electronic structure may be accomplished through application of the L(S)DA+*U* method.[15] PXRD(*P*) would be most useful in

highlighting the similarities or dissimilarities that persist or arise as pressure is applied, especially when coupled with the L(S)DA+U method applied to the high pressure structure. Infra red spectroscopy as a function of applied pressure, IR(P), has proven useful in the structural determination of MBM's,[16] purely organic compounds,[17] and minerals.[18] The complexity of the IR spectra of TCNE relative to other compounds studied in such a fashion would likely result in a correspondingly complex IR(P) spectra. However, this would likely result in a more fully understood compressed structure when coupling with theoretical modeling of TCNE bond distortion and the resulting IR spectra.

$[Ru_2(O_2CBu^t)_4]_3[M(CN)_6]\bullet 2H_2O$ (M =Fe, Cr) present the intriguing property of H_{cr} suppression with increasing applied pressure and varying degrees of irreversibility with regard to the DC(P) measurements. PXRD(P) and/or IR(P) in tandem with theory may serve to explain the magnetic phenomena observed. IR(P) of the ν_{CN} coupled with theoretical modeling of the Ru-NC-M linkage may be capable of resolving the characteristics of compression along these bonds.[16]

References

(1) Taliaferro, M. L.; Selby, T. D.; Miller, J. S. *Chem. Mater.* **2003**, *15*, 3602-3606.

(2) Miller, J. S.; Calabrese, J. C.; Epstein, A. J.; Bigelow, R. W.; Zhang, J. H.; Reiff, W. M. *J. Chem. Soc., Chem. Commun.* **1986**, 1026-1028.

(3) Miller, J. S.; Calabrese, J. C.; Rommelmann, H.; Chittipeddi, S. R.; Zhang, J. H.; Reiff, W. M.; Epstein, A. J. *J. Am. Chem. Soc.* **1987**, *109*, 769-781.

(4) Chakraborty, A.; Epstein, A. J.; Lawless, W. N.; Miller, J. S. *Phys. Rev. B* **1989**, *40*, 11422-11424.

(5) Her, J.-H.; Stephens, P. W.; Ribas-Ariño, J.; Novoa, J. J.; Shum, W. W.; Miller, J. S. *Inorg. Chem.* **2009**, *48*, 3296-3307.

(6) Schweizer, J.; Bencini, A.; Carbonera, C.; Epstein, A. J.; Golhen, S.; Lelièvre-Berna, E.; Miller, J. S.; Ouahab, L.; Pontillon, Y.; Ressouche, E.; Zheludev, A. *Polyhedron* **2001**, *20*, 1771-1778.

(7) Huang, Z. J.; Chen, F.; Ren, Y. T.; Xue, Y. Y.; Chu, C. W.; Miller, J. S. *J. Appl. Phys.* **1993**, *10*, 6563-6565.

(8) Chittipeddi, S.; Cromack, K. R.; Miller, J. S.; Epstein, A. J. *Phys. Rev. Lett.* **1987**, *58*, 2695-2698.

(9) Miller, J. S.; Gantzel, P. K.; Rheingold, A. L.; Taliaferro, M. L. *Inorg. Chem.* **2009**, *48*, 4201-4206.

(10) Candela, G. A.; Swartzendruber, L. J.; Miller, J. S.; Rice, M. J. *J. Am. Chem. Soc.* **1979**, *101*, 2755-2756.

(11) Miller, J. S.; Zhang, J. H.; Reiff, W. M.; Dixon, D. A.; Preston, L. D.; Reis, Jr., A. H.; Gerbert, E.; Extine, M.; Troup, J.; Ward, M. D. *J. Phys. Chem.* **1987**, *91*, 4344-4360.

(12) Broderick, W. E.; Eichhorn, D. M.; Liu, X.; Toscano, P. J.; Owens, S. M.; Hoffman, B. M. *J. Am. Chem. Soc.* **1995**, *117*, 3641-3642.

(13) Taliaferro, M. L.; Palacio, F.; Miller, J. S. *J. Mater. Chem.* **2006**, *16*, 2677-2684.

(14) Rota, J.-B.; Le Guennic, B.; Robert, V. *Inorg. Chem.* **2010**, *49*, 1230-1237.

(15) Shum, W. W.; Epstein, A. J.; Miller, J. S. *Phys. Rev. B* **2009**, *80*, 064403.

(16) Shum, W. S. Magnetic Interactions in Novel Molecule-Based Materials. Ph. D. Thesis, The University of Utah, Salt Lake City, UT, December 2008.

(17) Pravica, M.; Liu, Y.; Robinson, J.; Velisavljevic, N.; Liu, Z.; Galley, M. *J. Appl. Phys.* **2012**, *111*, 103534.

(18) Shieh, S. R.; Duffy, T. S.; Liu, Z.; Ohtani, E. *Phys. Earth Planet In.* **2009**, *175*, 106-114.